UNIVERSITY OF BIRMINGHAM

CONTROL ORIENTED ENGINE MODELLING AND ENGINE MULTI-OBJECTIVE OPTIMAL FEEDBACK CONTROL

BY

HE MA

A thesis submitted to the

College of Engineering and Physical Sciences of

The University of Birmingham for the degree of

DOCTOR OF PHILOSOPHY

School of Mechanical Engineering

College of Engineering and Physical Sciences

The University of Birmingham

December, 2012

Abstract

The real-time control oriented Spark Ignition (SI)/ Homogenous Charge Compression Ignition (HCCI) engine statistical models were developed to run cycle-to-cycle, which can be used for real-time model-based predictive control and real-time controller design. The simulation was implemented by Simulink. With the aim of designing future real-time control strategies, the throttle position, spark timing, injection timing, Intake Valves Opening (IVO) and Exhaust Valves Closing (EVC) are set as variable in the SI model, and the phase of the IVO, EVC and air/fuel ratio (AFR) were designated as variables in HCCI model. The models consist of four major parts: 1. the engine geometry model, 2. the gas exchange model, 3. the combustion and emissions model, 4. the performance evaluation model. In order to achieve real-time simulation capabilities, a compromise between the model accuracy and computational cost had to be adopted. The simplified single-zone SI/HCCI combustion model was developed. The model can predict the combustion duration, mass fraction burned, in-cylinder pressure, Indicated Mean Effective Pressure (IMEP), Indicated Specific Fuel Consumption (ISFC), Indicated Specific Particulate Matter by Number (ISPMN) and Indicated Specific Particulate Matter by Mass (ISPMM) for SI engine, and auto-ignition position (AIP), combustion duration (CD), mass fraction burned (MFB), in-cylinder pressure, IMEP, ISFC and ISHC (Indicated Specific Hydrocarbon emissions) for HCCI engine simultaneously in real-time. Simulation results were validated by comparison with the experimental data obtained from a Jaguar V6 HCCI/SI dual mode naturally aspirated engine. Good agreement was observed between the simulation results and the experimental data within a wide engine operating range.

Moreover, the model was able to simulate the transient response within HCCI mode in certain operating conditions. The transient response of In-cylinder pressure, F_{rg}, mass of intake air and mass of fuel injected per cycle are presented and discussed.

With increasing number of degrees of freedom for engine operations, conventional mapping based engine optimisation methods are reaching their limits. To take their place, automated, multi-objective engine optimisation approaches are desirable. In this study, it presents a model-based multi-objective optimisation algorithm using the Strength Pareto Evolutionary Algorithm (SPEA2). The validated SI/HCCI engine models are used as a virtual test bed to implement the co-simulation tests with a developed SPEA2 controller.

For the experiments reported here, the variable parameters for SI engine is throttle position, spark timing, injection timing and valve timing (IVO, EVC) with respect to optimal ISFC, ISPMN and ISPMM, and for HCCI engine is valve timing (IVO, EVC) and λ with respect to optimal (ISFC) and indicated specific hydrocarbon (ISHC), while achieving a predefined power output at a given engine speed. The validation showed the optimal controller is able to find optimal engine parameters with good accuracy and speed.

Moreover, as one of the most important features of HCCI combustion, the self-stabilisation features of HCCI combustion are experimentally studied. The experimental conclusions have

great guiding effects on the DoE of HCCI engine multi-objective optimal feedback control in the future.

List of Abbreviations

A/D	Analogue to Digital
AFBR	Apparent Fuel Burning Rate
AFR	Air-Fuel Ratio
AIP	Auto-Ignition Position
AMC	Accumulation Mode Concentration
ANN	Artificial Neural Networks
aTDC	After Top Dead Centre
BDC	Bottom Dead Centre
BSFC	Brake Specific Fuel Consumption
bTDC	Before Top Dead Centre
bTDCc	Before Top Dead Centre of Combustion Phase
CAD	Crank Angle Degree
CAM	Concentration Accumulation mode weighted by Mass
CD	Combustion Duration
CFD	Computational Fluid Dynamics
CLD	Chemiluminescence Detector
CO	Carbon Monoxide
COV	Coefficient Of Variations
CPS	Cam Profile Switch
D/A	Digital to Analogue
DMS	Differential Mobility Spectrometer
DoE	Design of Experiment
DPGA	Distance-based Pareto Genetic Algorithm
EA	Evolutionary Algorithms
EGR	Exhaust Gas Recirculation
EPP	Experimental Peak Pressure
EPPP	Experimental Peak Pressure Position
EVC	Exhaust Valve Closing
EVO	Exhaust Valve Opening

Exp.	Experimental
FC	Fuel Consumption per hour
FID	Flame Ionisation Detector
FIFO	Floating Input-Floating Output
FSD	Full Scale Deflection
FSO	Full Scale Output
GA	Genetic algorithm
GDI	Gasoline Direct-Injection
GUI	Graphical User Interfaces
HC	Hydrocarbons simulation results of hydrocarbon emissions in ppm
HCCI	Homogenous Charge Compression Ignition
HILS	Hardware-in-the-Loop Simulation
HRR	Heat Release Rate
I/O	Input/output
IC	Internal Combustion
IMEP	Indicated Mean Effective Pressure
ISFC	Indicated Specific Fuel Consumption
ISHC	Indicated Specific Hydrocarbon emissions
ISPMM	Indicated Specific Particulate Matter by Mass
ISPMN	Indicated Specific Particulate Matter by Number
IVC	Intake Valve Closing
IVO	Intake Valve Opening
JLR	Jaguar and Land Rover
KIM	Knock-Integral Method
MAF	Air Mass Flow rate
MDP	Markov Decision Process
MFB	Mass Fraction Burned
MFF	Fuel Mass Flow rate
MIMO	Multiple-Input and Multiple-Output
Mins	Minutes
MMEx	Molar Mass of Emissions
MOEA	Multi-Objective Evolutionary Algorithm
MOGA	Multi Objective Genetic Algorithm

MOP	Multi-objective Optimisation Problem
MPC	Model-based Predictive Control
MVE	Mean Value Engine
NCGA	Neighbourhood Cultivation Genetic Algorithm
NDIR	Non-Dispersive Infrared Detector
NOx	Oxides of Nitrogen
NPGA	Niched Pareto Genetic Algorithm
NSGA	Non-dominated Sorting Genetic Algorithm
NVO	Negative Valve Overlap
OBD	On-Board Diagnostic
Ode	Ordinary differential equation
PAES	Pareto Archive Evolutionary Strategy
PESA	Pareto Envelope-based Selection Algorithm
PFI	Port Fuel Injection
PID	Proportion Integration Differentiation
PM	Particulate Matter
PRFs	Primary Reference Fuels
PVO	Positive Valves Overlap
PWM	Pulse-Width Modulation
RAM	Random Access Memory
RCP	Rapid Control Prototyping
RPM	Revolutions per Minute
RTW	Real-Time Workshop
Sec	Second
SI	Spark Ignition
Sim.	Simulation
SIMO	Single-Input and Multiple-Output
SKM	Skeleton Kinetic Mechanism
SOP	Single-objective Optimisation Problem
SPEA	Strength Pareto Evolutionary Algorithm
SPP	Simulation Peak Pressure
SPPP	Simulation Peak Pressure Position
TTL	Transistor-Transistor Logic

ULG	Un-Leaded Gasoline
VEGA	Vector Evaluated Genetic Algorithms
VGT	Variable Geometry Turbo-charging
VVT	Variable Valve Timing

List of Symbols

$\dot{m}_t$	mass flow through the throttle	kg/s
$\dot{m}_v$	mass flow through the intake and exhaust valves	kg/s
h_i	the specific enthalpy	J
h_i	individual number	
A_0	empty external archive for SPEA2	
A_R	effective open area of the valves	m^2
A_{ij}, B_{ij}	correlation coefficients matrix	
A_t	external archive for SPEA2	
B_x , B_y , B_z	moles of carbon, hydrogen and oxygen per mole of fuel	
C_d	discharge coefficient	
C_{p1} , C_{p2}	shape factors	
C_r	charge amplifier	F
C_v	Specific heat at constant volume	J/kg·C^o
E_A	activation energy	J
F_{rg}	Fraction of residual gas	%
M_{P_t}	response peak value	
M_{air}	mass of air	kg
M_b	molecular weight of the burned mixture	g/mol
M_{fuel}	mass of fuel	kg
P_0	initial population for SPEA2 upstream air pressure	
P_i	indicated power	kW
P_t	population for SPEA2 downstream air pressure	bar
Q_n	net heat release	cal
Q_w	Heat loss from cylinder wall	cal
$\dot{T}$	heat release rate	cal/CAD
T_0	upstream air temperature	K
T_s	stable times	s
U_0	output voltage	V

V_c	clearance volume	m^3
V_d	displacement volume	m^3
W_{i_2}	reaction rates of moles of resultant specie i_2 per unit volume	mol/l·s
$W_{mx}i_1$	reaction rate of moles of total species i_1 per unit volume	mol/l·s
$W_v i_3$	reaction rates of moles of reactant specie i_3 per unit volume	mol/l·s
X_{i_1}	concentration of moles of specie i_1	mol/l·s
X_{MFB}	mass fraction burned	%
f_i	fitness value	
m_{RP}	mass of mixture (burned or unburned)	kg
n_b	number of moles of burned mixture	mole
n_{rg}	mole number of residual gas	mole
r_c	compression ratio	
s_i	strength value	
x_1	throttle position in degree	deg
x_2	spark timing bTDC	CAD
x_3	fuel injection timing bTDC	CAD
x_4	EVC position aTDC	CAD
x_5	IVO position bTDC	CAD
θ_0	the crank angle when the combustion starts	CAD
σ_i^k	space distance	
τ_{id}	total ignition delay time	CAD
χ_{O_2}	oxygen mole fraction	%
ϕ_0	angle of the throttle plate when it is closed	deg
ΔP_c	pressure change due to combustion	bar
$\Delta\theta_b$	combustion duration	CAD
ΔP	in-cylinder pressure change	bar
A	open loop gain The predicted optimal point for ISFC (SI cases)	
B	bore diameter The predicted optimal point for ISPMN (SI cases)	dm
C	cluster set specific heat The predicted optimal point for ISPMM (SI cases)	 J/kg·C^o
D	decision space	

	throttle diameter	dm
e	specific energy	J/kg
$h(\gamma_t)$	pressure influence in subsonic flow	
m	Mass	kg
	combustion characteristic exponent	
$Mrei_4$	EGR per unit volume of specie i_4	mol/l
p	Pressure	bar
	Curve fitting coefficient for SI engines	
P	initial population for SPEA	
P'	external archive for SPEA	
Q	Curve fitting coefficient for SI engines	
T	Temperature	K
V	Combustion chamber volume	m^3
Y	target space	
$A(\phi)$	efficient throttle open area	m^2
CH_y	formula of gasoline	
$D(i)$	density value	
L	rod	dm
N	population size	
	engine speed	rpm
$P.O.$	percent overshoot	
Q	output charge	
R	crank radius	dm
	gas constant	J/mol·K
	correlation coefficients	
$R(i)$	fitness value for SPEA2	
fv	response final-value	
x	burn fraction	%
y	atom number ratio of H and C of gasoline	
γ	heat capacity ratio	
	specific heat ratio	
θ	Crank angle	CAD
λ	Relative Air to Fuel Ratio	
τ	local ignition delay time	CAD
ϕ	Equivalence Ratio (Fuel-Air Ratio)	
	throttle angle	deg

In memory of my grandfather, Jufa Ma

Acknowledgements

I would like to express my sincerely appreciate to my supervisor Professor Hongming Xu for his guidance and helps both in academic and live throughout my Ph.D study. I also want to thank my current associate supervisor Dr. Oluremi Olatunbosun. I also want to give my sincerely thanks to my previous associate supervisor Professor Jihong Wang in Warwick University, she gave me many helpful suggestions and encouragement during my Ph.D study. Thanks Professor Miroslaw Lech Wyszynski and Dr. Athanasios Tsolakis for their helpful suggestions. I also appreciate the helps from Professor Akbar Ghafourian and Dr. Thorsten Schnier in the Computer Science department.

I acknowledge the support of AWM / EU ERDF (Advantage West Midlands / European Union European Regional Development Fund), EPSRC (EP/J00930X/1), Jaguar and Land Rover (JLR) and Shell Global Solutions. Without their equipments and financial supports, I could not finish my Ph.D study.

Great thanks go to the laboratory technicians - Peter Thornton, Carl Hingley, Simon Rowan and Lee Gauntlett - for their support with all test facility matters. I am also grateful to Dr. Jacek Misztal, Dr. Guohong Tian, Dr. Xiao Ma, Dr. Jun Zhang, Dr. Yanfei Li, Dr. Ritchie Daniel, Dr. Lixia Wei, Professor Fujun Zhang and Professor Shaohua Zhong for their generous help

and technical support. I also acknowledge the English writing support from Mrs. Janet Hingley and Mr. Thomas Lattimore.

Special thanks should go to my friends and colleagues at the University of Birmingham: Haiying Li, Fan Zhang, Changzhao Jiang, Dai Liu, Chongming Wang, Cheng Tan, Jianyi Tian, Wentao Wang and Mr. Vincent Manfredini for their great supports in my study and social life.

Finally, I would like to express my sincere gratitude to my parents, parents in law and other family members from the bottom of my heart for their unconditional support and encouragement. Last but not least, I want to give my most special thanks to my wife Ye Tian, I am so lucky to have her during my Ph.D study, without her understanding and supports I cannot finish my Ph.D study.

Table of Content

List of Figures

List of Tables

List of Publications

Journal

1. He Ma, Hong-Ming Xu, Ji-Hong Wang. Real-time Control Oriented HCCI Engine Cycle-to-cycle Dynamic Modelling. International Journal of Automation and Computing 8(3), August 2011, 317-325.

Conference Papers

1. HE MA, Hongming Xu, Thorsten Schnier, Jihong Wang, Guohong Tian. A Real-Time Control Oriented HCCI Combustion Model in 4-Stroke HCCI/SI GDI Engine and Model-Based Fast Calibration Development. SAE 2012-01-1123 (approved)
2. He Ma, Hong-Ming Xu, Ji-Hong Wang, Guohong Tian. Real-time Control Oriented HCCI Engine Cycle-to-cycle Dynamic Modelling. 16th International Conference on Automation & Computing. *IEEE*.11.Sep.2010.
3. He Ma, Hongming Xu, Thorsten Schnier, Jihong Wang. The Development of a Real-time Control Oriented HCCI Engine Model and SPEA2 based Fast Calibration. MEGS II Event, Loughborough, 13th December 2011.

Awards

1. "The Best Paper Prize" award in the 16th International Conference on Automation and Computing.

Chapter 1 Introduction

In 1860, French engineer Étienne Lenoir invented the first engine to come into general use (Suzuki 1997), since then energy conservation and emissions' reduction are two eternal themes of internal combustion (IC) engine research (Stone 1999). For that purpose, many generations of researchers and engineers from different disciplines, such as mechanics, electronics, mathematics, chemistry, material science and optics etc. (Jurgen 2004), have made a remarkable effort through their research.

1.1 Background

Although the research of electrical vehicles is under rapid development and they have the potential to provide alternatives for short distance and light duty transportation (Xu, Wang et al. 2012), the internal combustion engine will continue to be the main power for vehicles in the coming decades (Gieré and Stille 2004). The forecast of global road transport technology shares is shown in Figure 1.1 (Gurney, Ahammad et al. 2009).

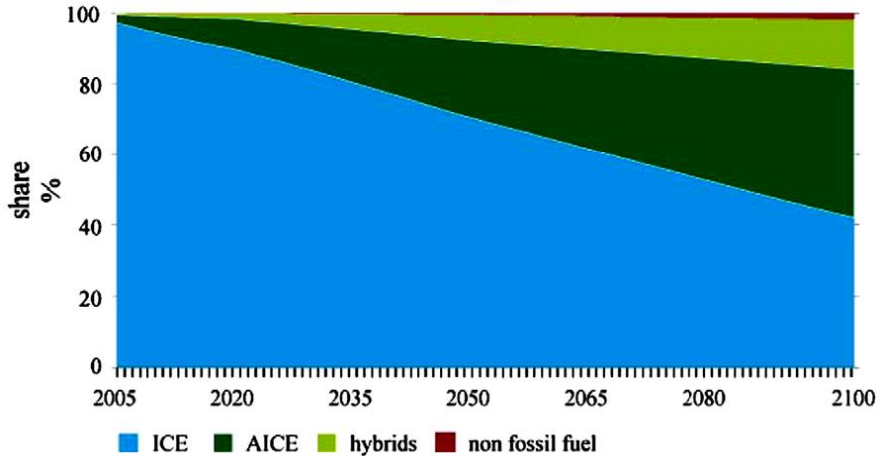

Figure 1.1 The Forecast of Global Road Transport Technology Shares

In order to improve the fuel consumption and emissions' performance, a lot of new technology is being developed and implemented on modern engines. However, compared with the extensive research on combustion and after-treatment systems, little work has been completed with respect to engine system control optimisation, leaving considerable space to improve fuel economy and emissions' performance (Xu, Wang et al. 2012). For engine multi-objective optimal control, the most common approach is conventional engine calibration. However, as the degrees of freedom for engine optimisation and the number of the calibration parameters are increasing, the classic off-board one-off manual test bench based dynamometer calibration mapping method is reaching its limit (Malikopoulos, Assanis et al. 2009). The classic calibration approach is becoming more complicated, expensive and time consuming, with the increasing complexity of engines and the combinatorial explosion of the parameter space (Malikopoulos, Assanis et al. 2008). Moreover, since the classic engine calibration cannot self-adapt as engines age, the fuel consumptions and emissions tend to increase (Obodeh and Ajuwa 2008).

1.2 SI and HCCI Engines and Modelling

Nowadays, diesel engines and gasoline engines are two of the most commonly used engines for vehicles. Compared with the conventional gasoline engine, the thermal efficiency of the diesel engine is relatively high, which is mainly due to the multi-points combustion and high compression ratio of diesel engines (Stone 1999). On the other hand, due to the advantages of their high rotational speed, simple structures, low emission, light weight, low cost of construction and smooth operation, gasoline engines are widely used in the world, especially for family use.

To improve the thermal efficiency of gasoline engines is one of the most important topics for engine researchers. There is much new technology which has been developed for that purpose, such as the intake air boost (Pfiffner, Weber et al. 1997), lean combustion (Ma, Ding et al. 2008), stratified combustion (Lu, Shen et al. 2011), HCCI combustion (Zhao 2003), GDI (Heywood 1988) and microwave ignition (Schoning and Li 2011). For the control of emissions in gasoline engines, although the three-way catalytic converter is able to convert 99% of HC, NO_x and CO emissions to N_2 and H_2O, the wide application of gasoline direct injection (GDI) technology results in PM emissions becoming more and more non-negligible (Maricq, Szente et al. 2012). With the concerns about fuel demand/consumption and the environment, the regulations on fuel economy and emissions, including HC, NOx, CO and PM are becoming increasingly stringent as shown in Table 1.1 (Wikipedia 2012).

Table 1.1 European Emissions Regulations for Passenger Cars (Category M*), g/km Petrol (Gasoline)

Tier	Date	CO	THC	NMHC	NOx	HC+NOx	PM
Euro 1	Jul-92	2.72 (3.16)	-	-	-	0.97 (1.13)	-
Euro 2	Jan-96	2.2	-	-	-	0.5	-
Euro 3	Jan-00	2.3	0.20	-	0.15	-	-
Euro 4	Jan-05	1.0	0.10	-	0.08	-	-
Euro 5	Sep-09	1.000	0.100	0.068	0.060	-	0.005
Euro 6 (future)	Sep-14	1.000	0.100	0.068	0.060	-	0.005

For engine multi-objective optimal feedback control purpose, a reliable and high speed SI engine model is desired. A simplified single-zone SI engine model was developed and will be demonstrated in chapter 5. The model can predict the combustion duration (CD), mass fraction burned (MFB), in-cylinder pressure, Indicated Mean Effective Pressure (IMEP), Indicated Specific Fuel Consumption (ISFC), Indicated Specific Particulate Matter by Number (ISPMN) and Indicated Specific Particulate Matter by Mass (ISPMM) simultaneously in real-time.

As a promising method to improve engine performance, Homogeneous Charge Compression Ignition (HCCI) has been attracting researchers' attention over the last few decades. Owing to low temperature combustion, multi-point combustion and throttle-free operation, HCCI engines are able to provide ultra-low NOx emissions and up to 30% improved fuel consumption (Zhao 2003). The main reasons for HCCI engines not being commercialized yet are: the difficulty of effectively controlling the HCCI combustion in steady state and transient conditions, the limitation of the HCCI operating window and high HC emissions (Zhao 2003).

The fast and efficient control of the auto-ignition timing is one of the major challenges of HCCI engines in manufacturing them for commercial use in the real world. Because there is no direct control approach for controlling the starting phase of combustion after the intake valve closes (IVC). A reliable high speed control-oriented HCCI engine virtual test bed model is desired, which should allow researchers to design the cycle-based real-time engine controller through adjusting engine input parameters for both steady and transient conditions. A simplified single-zone HCCI engine model was developed and will be demonstrated in chapter 4. The model can simulate the auto-ignition position (AIP), CD, MFB, in-cylinder pressure, IMEP, ISFC and ISHC simultaneously in real-time.

1.3 Engine Optimal Control Strategies

In order for vehicles to give their best performance in both steady status and transient status, the vehicle variables should be adjusted by the engineer step by step very carefully, and this procedure is defined as vehicle optimisation, i.e. calibration, one of the most important works of vehicle development. Figure 1.2 shows a conventional vehicle calibration process (International-Limited-of-China-Yuchai 2007).

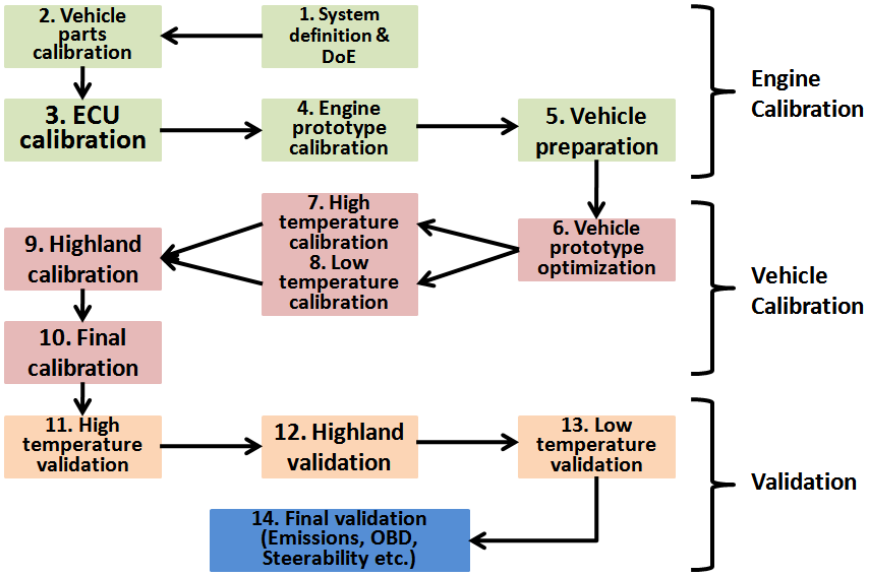

Figure 1.2 The Conventional Vehicle Calibration Flow Chart

It can be seen that the conventional calibration process of an IC engine is divided into three stages, i.e. engine calibration stage, vehicle calibration stage and validation stage. As the engine is the most important element of a vehicle, the engine calibration work is extremely important. Some extreme environmental conditions affect the vehicle's performance greatly. For instance, the density and viscosity of fuel and the density of intake air is very different from their regular conditions when the environmental temperature is very low (Li 2012). Therefore, in order to guarantee that the vehicles are able to work with these conditions, extreme environmental conditions (high temperature, low temperature, highland) should be considered during the engine calibration process. There are many commercial calibration tools which are developed for engine calibration works, such as INCA(ETAS 2012), TOPexpert (FEV 2012), CANape (Vector 2012) and CAMEO (AVL 2012).

However, the conventional engine calibration process is very time consuming and expensive work. For example, for a BOSCH system based engine calibration, the variables of the engine that need to be calibrated are over tens of thousands, and the pages of calibration documents are more than 1,500. Generally, it costs around £1,000,000 and takes 18 months to calibrate a new engine for commercial application (International-Limited-of-China-Yuchai 2007). The conventional engine calibration approach utilizes the test bench results to generate set-point maps for all variables that lead to a considerable amount of requested tests and cost. Thus, a fast and efficient engine optimisation method is desired.

As more new technology is applied to modern engines, such as VVT, GDI, multi-injection, two stages supercharger etc, the number of engine variables is increased consequently. On the other hand, due to the increasingly stringent emissions' regulations and the fierce competition between automotive industries, the control objectives (PM emissions, unregulated emissions, fuel consumption, noise, comfortability etc.) of modern engines are becoming more and more. Since the engine is a Multi-Input Multi-Output (MIMO) system, it is desirable to seek an efficient approach to find the best optimisation result, i.e. the compromise among different references.

On the other hand, a fast and MIMO engine optimisation is not only of benefit to off-board engine calibration work, but will also be very useful to on-board engine optimal control in the future. So-called on-board self-learning engine optimisation is a novel approach to

optimise engines in real-time intelligently. Unlike the conventional one-off engine calibration approach, the on-board engine calibration approach can continue to optimise the engine performance when the vehicles are being driven by customers. In other words, the engine is able to “learn” the steering habits, the surrounding environmental conditions and the aging speed of vehicles, based on some particular on-board diagnostic (OBD) instruments or sensors in real-time. Therefore, this technology allows the vehicles to be sold to customers without detailed calibration maps beforehand. The flow chart of the on-board calibration approach is shown in Figure 1.3.

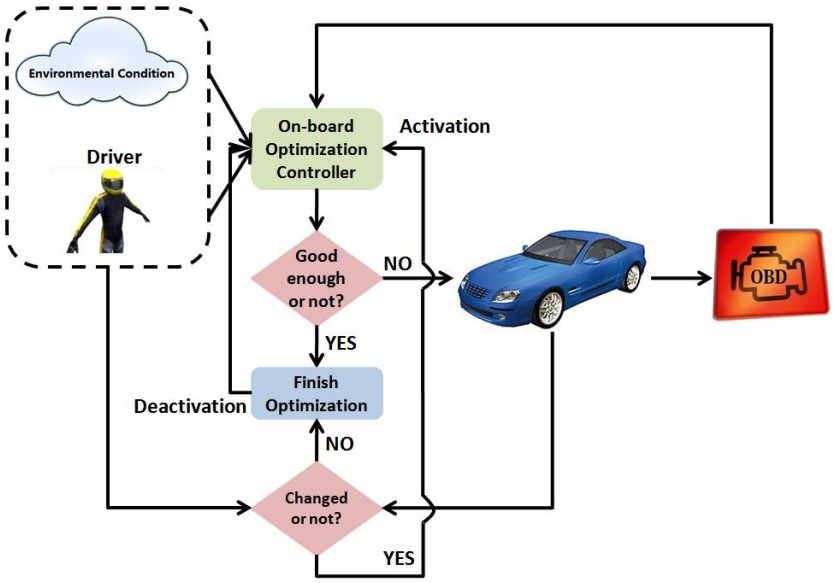

Figure 1.3 On-board Multi-objective Optimal Feedback Control Flow chart

This technology is able to ensure that the MIMO engine system can always be operated to produce its best performance, despite the aging of the engine. Meanwhile, it helps automotive companies to save huge amounts of money from vehicle calibration works. As the first stage in implementing this in the future, a self-learning automatic control strategy for optimising IC engines is desirable. In order to test and improve the whole control process,

it is necessary to couple the control strategy module with the engine model, and simulate the optimal control process. Because whether the control module is expected to be implemented in real vehicles or be model-based multi-objective optimal feedback control, the controller inputs and outputs should be received and processed in real-time. Therefore, the real-time based engine model is preferable for the simulation study. Figure 1.4 shows the flow chart of the development procedures of on-board engine optimisation strategy.

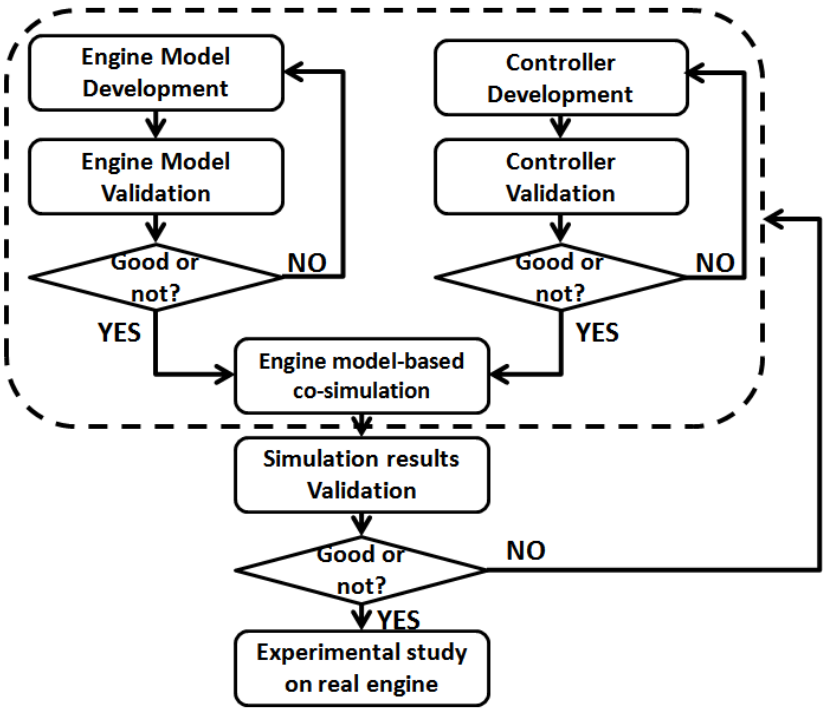

Figure 1.4 Flow Chart of On-board Optimisation Strategy Development

As a preliminary exploration of the on-board optimal control strategy, the studies in this thesis will cover steady states real-time engine modelling and multi-objective optimal feedback controller developments.

1.4 Objectives and Approaches

The main topic of this study can be summarized into two subtopics. First, the real-time control oriented SI/HCCI engine modelling. Second, the application of fast intelligent self-learning engine optimal control strategy for SI and HCCI engines. The objectives of these two subtopics can be described as following:

1. To find an approach to simulate SI/HCCI engine operating procedures cycle-to-cycle reliably in real-time. In order to achieve this aim, the combustion and gas exchange process modelling should be reasonably simple.
2. To build a real-time control oriented model for an SI engine by Simulink. The model variables are throttle position, spark timing, injection timing, IVO and EVC. The model should be able to simulate the SI engine working procedures cycle-to-cycle in real-time. Meanwhile, the model needs to predict the control objectives ISFC, IMPMN and IMPMM reliably. The model should be validated by the corresponding experimental data.
3. To build a real-time control oriented model for an HCCI engine by Simulink. The model variables are engine speed, IVO, EVC and lambda. The model should be able to simulate the HCCI engine working procedures cycle-to-cycle in real-time. Meanwhile, the model needs to predict the ISFC and ISHC reliably. Moreover, in order to utilize the model to implement real-time transient engine control, the model should be able to simulate the main features of the HCCI engine transient process when the engine speed and load are changed. The model should be validated by the corresponding experimental data.
4. To develop a multi-objective optimal feedback control module; the control module should be able to “self-learn” the comparison results between the current and previous

outputs, and find out the optimal engine performance outputs and the corresponding engine variable inputs loop by loop based on an evolutionary algorithm (EA) automatically.

5. In order to implement the co-simulation for the self-learning engine control strategy, it is necessary to find a way to link the engine model and optimal control module together. Therefore, an I/O interface module should be developed.
6. To study the co-simulation results of the SI and HCCI engine's case and validate the optimal control results for different engine operating conditions with experimental data. The time consumption of each optimal control case should be recorded as evidences to prove the feature of "high speed and high efficiency" compared with conventional engine calibration procedures.
7. As one of the most important features of HCCI combustion, the self-stabilisation behaviour has useful guidance on the DoE of the HCCI engine multi-objective optimal feedback control. Therefore, the experimental study of this feature is essential.

1.5 Thesis Outline

The thesis is divided into 8 chapters, and summarized as follows:

Chapter 1, i.e. this chapter, intends to give the background and motivation of the research. In addition, it introduces the main objectives and approaches of this research. In chapter 2, the literature review on SI/HCCI engine modelling approaches, multi-objective optimal

feedback algorithms and some multi-objective engine optimal controllers which were developed by previous researchers, are presented. Some of the previous studies about the self-stabilisation feature of HCCI combustion are introduced. In chapter 3, the Jaguar SI/HCCI dual mode engine test bench is described, which includes the software configurations and hardware arrangement. In addition, the experimental data processing method is presented. Chapter 4 introduces the modelling approaches for both real-time control oriented SI and HCCI engines, which includes the model structure and detailed descriptions of each model module. The development of multi-objective engine optimal control strategy is presented in this chapter as well. Chapter 5 gives the validation results and analysis of SI and HCCI real-time engine models. Because the models are used for real-time control purpose and corresponding on-board self-learning control strategy development, the simulation speeds are given as well. Chapter 6 reports the validation results and discussions of the multi-objective optimal feedback control strategy for SI engines and HCCI engines respectively. In chapter 7, the experimental study on the self-stabilisation feature of HCCI combustion is presented. Chapter 8 summarises the achievements through this study, and future work is recommended.

Chapter 2 Literature Review

The aim of this chapter is to review the literature relevant to this thesis. The areas of discussion cover the major developments in the numerical simulation of SI and HCCI engines, the multi-objective optimal control methods, the applications of multi-objective optimisation approaches on engine control and the self-stabilisation features of HCCI engines.

2.1 The Numerical Simulation of SI Engines

The history of researchers utilizing a mathematical model to analyse the working process of internal combustion engines and guide the engine development or optimisation, is very long, and even could date back to the end of the 19th century. Since the 1960s, as a result of the rapid development of modern computers, the progress of engine numerical simulation has been very fast (Suzuki 1997). Three main categories of engine numerical simulation research, zero-dimensional model, quasi-dimensional model and multi-dimensional model will be introduced respectively.

2.1.1 Multi-dimensional CFD with Detailed Chemistry Models

The Computational Fluid Dynamics (CFD) multi-dimensional engine modelling method is always the best tool for accurately simulating SI engines. Furthermore, the CFD models are becoming a standard diagnostic tool for the engine optimisation process (Richard, Bougrine et al. 2009, Lee, Lee et al. 2010). Nevertheless, the high cost of computation and the complexity of model development are two main barriers to researchers. For instance, a typical period for simulating an IC engine can last many weeks (Jasak, Gosman et al. 1999). The main reasons for this can be attributed to the high complexity of engine mesh generation, the massive of cells sensible number of combustion and the large amount of data available from calculation.

In order to deal with these problems, many researchers made considerable efforts. There were some tools which were developed for reducing the time consumption of SI engine simulation (Jasak, Gosman et al. 1999). Although the approach is able to reduce the simulation time from months to less than a week, it is far away from the real-time controller development requirements.

2.1.2 Quasi-dimensional Multi-zone Models

The quasi-dimensional models and zero-dimensional models are all used for analyzing the combustion process by thermodynamic theory and regardless of the fluid dynamics process (Watson, Das et al. 1998, Ma, Wang et al. 2008, Perini, Paltrinieri et al. 2010). However, the combustion model of the zero-dimensional engine model is developed by empirical formulae or curve fitting. The quasi-dimensional combustion model introduced a chemistry based sub-model to describe the combustion process. On the other hand, the zero-dimensional models consider the in-cylinder mixture as homogeneous, and the quasi-dimensional models divide the cylinder into many zones and the parameters for the different zones are different (Stiesch 2003).

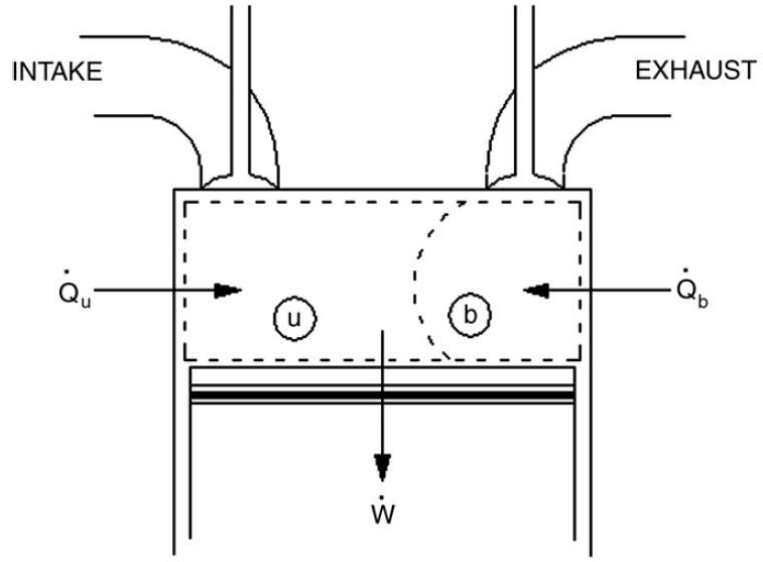

Figure 2.1 Schematic of the Two-Zone Combustion Modelling

The two-zone model is the simplest and commonest quasi-dimensional model. For a two-zone model, the in-cylinder mixture is divided into two zones, i.e. the burned zone and the unburned zone. As it shows in Figure 2.1, these two zones are separated by the flame front surface (Catania, Misul et al. 2003). Although the temperature and composition for these two zones are different, the in-cylinder pressure is homogeneous. It is necessary to stress

that it is reasonable to assume the temperature is homogeneous in the unburned zone. However, for the burned zone, due to combustion occurring at different times, the temperature gradient is remarkable. In order to solve this problem, it is possible to divide the burned zone into some more sub-zones; then it becomes a multi-zone model. However, this will lead to enhancing the simulation time consumption considerably, and the improvements on the simulation results are not very obvious. Therefore, it is seldom that the multi-zone SI engine model is used in engineering application.

2.1.3 Zero-dimensional Single-zone Wiebe Models

With respect to single-zone engine models, the space differences of every in-cylinder variable are completely ignored. In other words, the in-cylinder pressure, temperature and composition are considered as homogeneous (Ramos 1989). The model is based on thermodynamic conservation of mass and energy. The conservation of energy in the combustion chamber is able to be represented by the first law of thermodynamics as (Heywood 1988):

$$\frac{d(me)}{d\theta} = -p\frac{dV}{d\theta} - \frac{dQ_w}{d\theta} + \sum m_i h_i \quad ,$$

$$e = e^0 + \int_{T_0}^{T} C_V dT \quad ,$$

where p is the in-cylinder pressure; T is the in-cylinder temperature; e is the specific energy; m is the mass of in-cylinder mixture; V is the combustion chamber volume; C_v is the specific

heat at constant volume; T_0 is reference temperature; e^0 is the energy when the temperature is T_0; Q_w is the heat loss from cylinder wall; m_i and h_i are the mass of in-cylinder air amount and the specific enthalpy respectively; θ presents the crank angle.

For zero-dimensional single-zone models, the heat-release rate model is not given but is calculated by empirical sub-models. The Wiebe function is the most popular approach to simulate the heat release rate for SI combustion owing to its simplicity and versatility (Wiebe 1962). Ivan Wiebe was a Russian engineer and scientist from the Urals, of German descent, and he was one of the first people try to link the chain chemical reactions with the fuel reaction rate for internal combustion engines (Ghojel 2010). The original form of the Wiebe function is given by:

$$x = 1 - e^{C\left(\frac{\theta-\theta_0}{\Delta\theta_b}\right)^{m+1}},$$

$$C = \ln(1 - x_d),$$

here, x is the burn fraction; θ is the crank angle; θ_0 is the crank angle when the combustion starts; $\Delta\theta_b$ is the combustion duration; m is the combustion characteristic exponent; x_d is the burned fraction. The relationship between C and x_d at the end of combustion is shown in Table 2.1 (Ghojel 2010).

Table 2.1 The Relationship between C and the Burn Fraction x_d at the End of Combustion

x_d	0.990	0.992	0.994	0.996	0.998	0.999
C	-4.60517	-4.82831	-5.116	-5.52146	-6.21461	-6.90776

As the most popular function to simulate the zero-dimensional SI combustion, Wiebe function is used for many engineering applications, such as the prediction of performance and emissions of SI engines, transient process of HCCI engines and GA based engine optimisation etc.

2.2 The Numerical Simulation of HCCI Engines

The study about HCCI engines started in 1980s (Najt and Foster 1983), as a results, the numerical simulation study history is much shorter than SI engines. Generally, the numerical modelling of HCCI engines could be classified into three categories, the multi-dimensional CFD models, the quasi-dimensional models and the zero-dimensional single-zone models (Ma, Xu et al. 2011). In order to simplify the model for time saving or controller development purposes, many approaches were developed by researchers (Shahbakhti and Koch 2007). For different purposes, these approaches could be coupled with different modelling categories. Depending on the relevance to the research, some of the most important and representative modelling categories and approaches are introduced in this section, respectively.

2.2.1 Multi-dimensional CFD with Detailed Chemistry Models

The multi-dimensional CFD simulation of HCCI engines always has the highest accuracy and reliability to predict the performances of combustion and emissions (Embouazza, Haworth et al. 2002, Flowers, Aceves et al. 2002, Kong and Reitz 2003). It usually couples a detailed chemical kinetic mechanism with the multi-dimensional reacting flow code KIVA-3V (Kong and Reitz 2002). The reason for KIVA being used so widely is mainly thanks to its open source and free nature. It should be noted that there are also other CFD codes which have been used for modelling the combustion of HCCI engines, such as CFX, FIRE, IFP-C3D, Star-CD and VECTICS, however, all of them are commercial software and the ability to be modified is limited.

The multi-dimensional CFD models are usually used for engine optimal design. Due to the considerable time consumption and the high requirement of computational resources (Embouazza, Haworth et al. 2002), the CFD HCCI models are not suitable for high efficiency control strategy development.

2.2.2 Quasi-dimensional with Detailed Chemistry Models

A quasi-dimensional model is always used to link the gap between multi-dimensional models and zero-dimensional models as a compromise solution to predict engine performance and emissions.

The schematic of a comprehensive quasi-dimensional HCCI model is shown in Figure 2.2, which contains an adiabatic core, a boundary layer model and a crevice region, and which is able to predict the full-cycle engine performance and emissions (Fiveland and Assanis 2001).

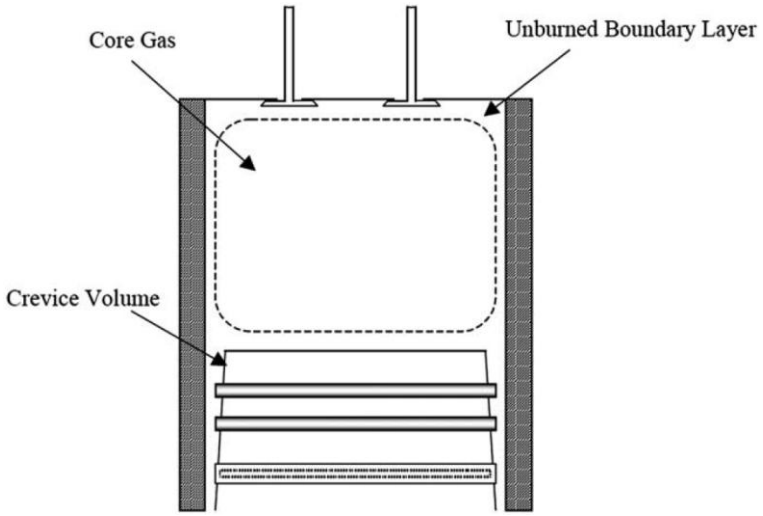

Figure 2.2 Schematic of the Two-zone HCCI Combustion Modelling

The quasi-dimensional HCCI model shows the potential to predict the engine performance and emissions in a relatively shorter time after good calibration. However, the simulation results fail to show good agreement with the inhomogeneous in-cylinder conditions.

2.2.3 Skeleton Kinetic Mechanism (SKM) Based Models

For reducing the simulation time consumption, the SKM method is usually used for simplified HCCI combustion modelling. The chemical kinetic mechanism of the combustion is

reduced to few reaction steps and species. This method is able to be coupled with a multi-dimensional CFD model or a zero-dimensional control-oriented model.

A skeleton kinetic mechanism for iso-octane fuelled HCCI combustion was developed and published in 'Fuel', which simplified the chemical reaction mechanism to only 69 reaction steps and 38 species (Jia and Xie 2006). The computed results show good agreement with experimental data on auto-ignition timing, combustion duration and pressure trace. The success of this model gives the researchers great confidence to develop the SKM for gasoline or diesel fuelled HCCI combustion.

Another SKM reduced chemical kinetic model for Primary Reference Fuels (PRFs) fuelled HCCI combustion was published in the journal of 'Combustion and Flame', which contains 55 reaction steps and 32 species (Tanaka, Ayala et al. 2003). The model is able to reproduce the pressure trace in a wide range remarkably well. It is suggested that the model has the potential to predict the knocking in SI engines and burning rate in HCCI engines.

A simplified control-oriented HCCI model for a propane fuelled engine was developed by simplifying the propane combustion reaction mechanism to one step:

$$\phi C_3H_8 + 5O_2 + 18.8N_2 \longrightarrow 3\phi CO_2 + 4\phi H_2O + 5(1-\phi)O_2 + 18.8N_2 \quad ,$$

the model was able to capture the importance of species concentration and temperature on the ignition process and predict the start of combustion cycle-to-cycle (Shaver, Gerdes et al. 2005). Many controllers have been designed based on this model (Shaver, Roelle et al. 2006) (Shaver, J.Christian et al. 2003).

Based on the research of Shaver, a propane fuelled cycle-to-cycle HCCI engine model was developed by Simulink (Jia, Wang et al. 2007). The model is able to run in real-time within some operating conditions. The description of the model is shown in Figure 2.3.

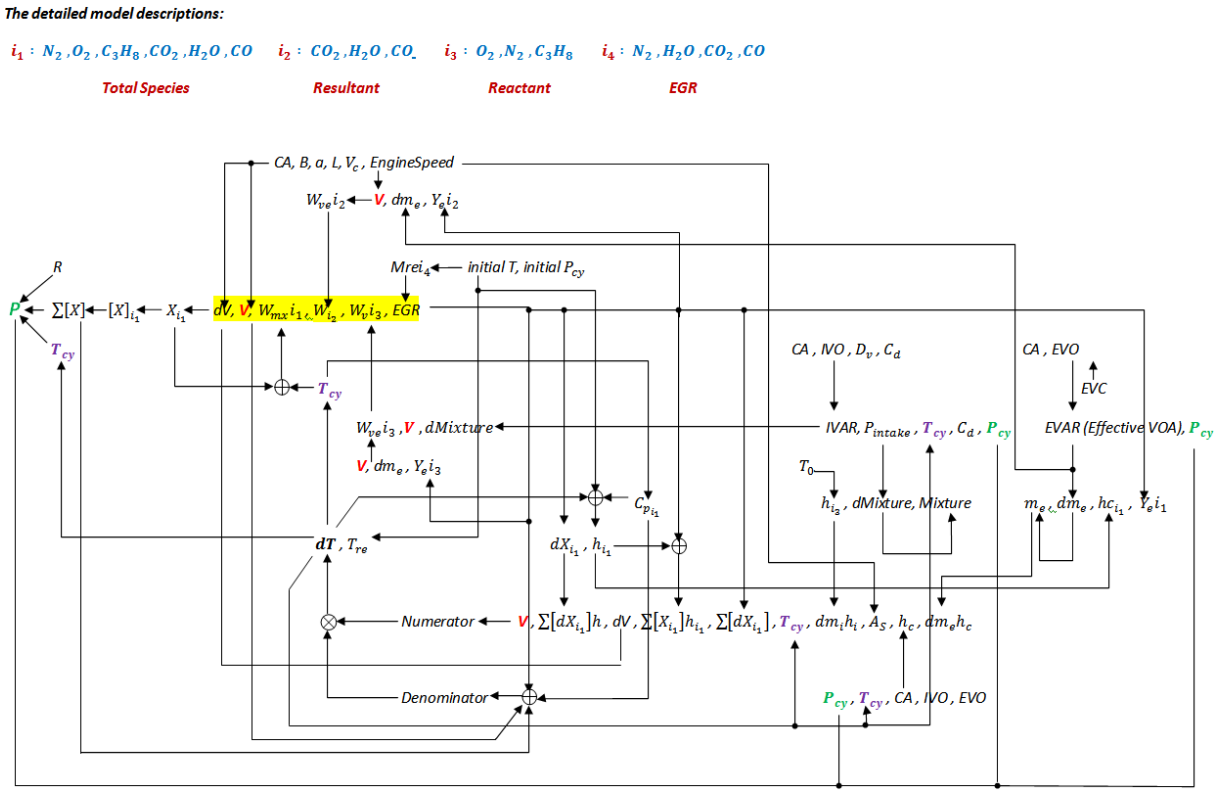

Figure 2.3 The Description of Jia's Real-time Control Oriented HCCI Model

Where $W_{mx}i_1$ is the reaction rate of moles of total species i_1 per unit volume; W_{i_2} is the reaction rates of moles of resultant specie i_2 per unit volume; $W_v i_3$ is the reaction rates of

moles of reactant specie i_3 per unit volume; X_{i_1} is the concentration of moles of specie i_1 (mol/L); $Mrei_4$ is the EGR per unit volume; dm_e is the derivative of exhaust mass; $dm_i h_i$ is the $\dot{m}_i h$ (intake); $dm_e h_i$ is the $\dot{m}_e h$ (exhaust) (Jia 2007).

Although the SKM can reduce the complexity of HCCI combustion chemical reaction steps and the requirements of computational resources remarkably, the simulation speed is still not satisfactory for the requirement of real-time HCCI controller development. Moreover, due to the much higher complexity of commercial fuels than the pure fuels (C_3H_8, *n*-heptane, *iso*-octane etc.), it is very difficult to develop SKM for gasoline or diesel, which constrains the possibility to implement the SKM in real-time controller development.

2.2.4 Zero-dimensional Single-zone Apparent Fuel Burning Rate (*AFBR*) Formulations Models

The apparent fuel burning rate formulations model (statistical model) is the simplified single zone combustion model, which assumes the in-cylinder mixtures are homogenous. Although this approach is not able to be used for fundamental combustion research, it gives the main features of the combustion process, which are good enough for controller designing (Yasar, Soyhan et al. 2008). The basic idea of this method is to utilize the experimental data of MFB which was derived from in-cylinder pressure, and fit the shape factors of MFB mathematic

model as close as possible to the experimental data, by curve fitting or other approaches (Watson and Pilley 1980).

A gasoline-fuelled *AFBR* based HCCI engine model was developed by GT-Power (Qin, Xie et al. 2005). The model can be used for real-time feedback control algorithms (Xie, Qin et al. 2004). The ignition position is defined as the crank angle where in-cylinder temperature reaches 1000K. The heat release rate correlations of pre-combustion and main combustion are given by:

$$X_{MFB-PreComb} = A + Bexp\left(-\frac{\theta}{C}\right) ,$$

$$X_{MFB-mainComb} = 1 - (1 - \tau^{c_{p1}})^{c_{p2}} ,$$

$$\tau = \frac{\theta - \theta_{10\%MFB}}{\Delta\theta} ,$$

A HCCI engine model using *AFBR* was developed by WAVE as an improvement work to Qin's model (Potrzebowski, Misztal et al. 2009). The model accounts for the AFR as an engine input variable, and uses the Knock-Integral Method (KIM) to predict the timing of auto-ignition. The equations are given by:

$$\int_{t_{IVC}}^{t_{IVC}+\tau_{id}} \frac{1}{\tau} dt = 1 ,$$

$$\tau = A_A \phi^{1.7} \chi_{O_2}^{-9.5} \frac{1}{Speed^{13.1}} \chi_{O_2}^{m \times speed} p^{-n} exp\left(\frac{E_A}{RT}\right) .$$

Where, τ is the local ignition delay time; τ_{id} is the total ignition delay time; t_{IVC} is the time of the inlet valve closure; ϕ is the equivalence ratio; χ_{O_2} is the oxygen mole fraction; E_A activation energy.

However, the computational cost for integral calculation of this model is still considerable. The model is unable to satisfy requirements of real-time simulation (Choi and Chen 2005).

2.3 Comparisons of Different Modelling Approaches

After good calibration and adjustment, the modelling approaches mentioned above are all able to provide the engine performance and emissions information with enough accuracy for controller development purposes. However, the time consumption of simulation is remarkably different for different approaches.

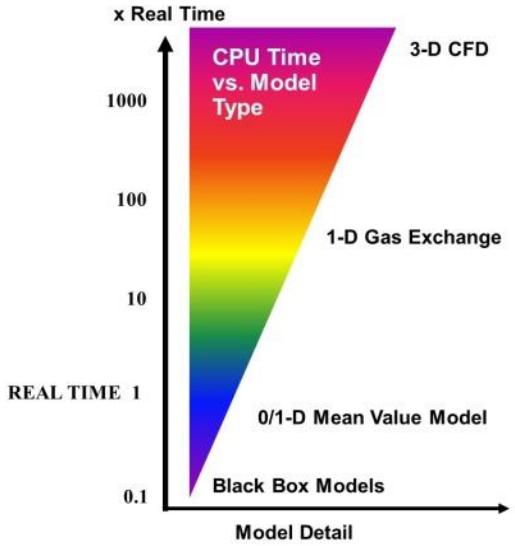

Figure 2.4 Flowchart of the Main Engine Modelling Methodologies, Showing Model Detail Vs. Computational Time (Millo, Rolando et al. 2011)

As Figure 2.4 shows, generally, the time consumption of the CFD model is thousands of times longer than the real-time based Mean Value Engine (MVE) model (Rausen, Stefanopoulou et al. 2005). The CFD and other detailed chemistry models display their advantages in the domain of engine geometry design, engine optimisation, engine diagnosis and theoretical research etc. For the development of the on-board engine real-time controller, only the main features of engine performance are desirable, such as in-cylinder pressure, peak pressure, IMEP and ISFC etc.

Although the MVE model is able to implement real-time based simulation for SI engines and HCCI engines, the time based nature and the lack of in-cylinder pressure trace is very unsatisfactory. As a result, the phenomenological crank angle resolved SI and HCCI models for real-time high efficiency controller development is desired. Through comparisons, the zero-dimensional single-zone model is adopted for this research. The Wiebe function is

applied to build the SI combustion model, and the *AFBR* method (statistical model) is used for developing the HCCI combustion model.

2.4 Multi-objective Optimisation Methods

For developing a novel multi-objective optimisation control strategy for engines as it has been mentioned in chapter 1, the evolutionary algorithm is adopted. Unlike the Single-objective Optimisation Problem (SOP), the Multi-objective Optimisation Problem (MOP) is much more widespread in applied disciplines (Lei and Yan 2009). It is because in most cases of practical applications, the objectives which need to be optimised are usually more than one.

Generally, the MOP is able to be defined mathematically as (Lei and Yan 2009):

$$\begin{cases} min/max\ y = f(x) = [f_1(x), \quad f_2(x), \quad \cdots, \quad f_M(x)] \\ g_i(x) \le 0, \quad i = 1,2,\cdots,p \\ h_i(x) = 0, \quad i = 1,2,\cdots,q \end{cases},$$

where $x = (x_1, \quad x_2, \quad \cdots, \quad x_n) \in D$ are decision vectors; $y = (f_1, \quad f_2, \quad \cdots, \quad f_M) \in Y$ are target vectors; D is the decision space which is constructed by decision vectors; Y is the target space which is constructed by target vectors.

In most cases, the improvement of one objective may lead to the reductions of other objectives' performances. It is impossible to have all objectives achieve the optimal performances simultaneously. Therefore, in order for the performances of all the objectives to be as good as possible, the best solution is to find an approach to make a compromise among them. Since Vector Evaluated Genetic Algorithms (VEGA) was developed in 1985 (Schaffer 1985), the Multi-Objective Evolutionary Algorithm (MOEA) became the most popular approach to deal with the MOP. There are three developing stages for MOEA researches, as follows (Lei and Yan 2009):

1. 1985-1994, the research progress of the MOEA experienced a slow period. The algorithms of this stage included non-Pareto algorithm (VEGA etc.) and Pareto algorithm. The representatives of the first generation MOEA contains: VEGA, Multi Objective Genetic Algorithm (MOGA) (Fonseca and Fleming 1993), Niched Pareto Genetic Algorithm (NPGA) (Horn, Nafpliotis et al. 1994) and Non-dominated Sorting Genetic Algorithm (NSGA) (Srinivas and Deb 1994).
2. 1994-2003, the MOEA research progress experienced a fast developing period. Since the Strength Pareto Evolutionary Algorithm (SPEA) was proposed (Zitzler and Thiele 1999), many researchers started to combine the external population with the MOEA. The elitism explicitly strategy became the basic process of the second generation MOEA design. NSGA2 (Deb, Pratap et al. 2002), Pareto Archive Evolutionary Strategy (PAES) (Knowles and Corne 2000), Pareto Envelope-based Selection Algorithm (PESA) and SPEA2 (Zitzler, Laumanns et al. 2001) are the representatives of the second generation MOEA.

3. 2003-now, the MOEA is going through a comprehensive developing stage nowadays. The research of the MOEA is reaching a new level. In order to achieve higher performance and efficiency, many new concepts, mechanisms and strategies are being developed, such as Memetic strategy, parallel strategy, co-evolutionary strategy and dynamic evolutionary strategy etc.

Although there are many available approaches to solve the MOP, the basic principles of these approaches are similar. Unlike the single-objective evolutionary algorithm, the MOEA needs to offer:

1. the greatest possible set of nondominated solutions,
2. the solutions set need to be very close to the global Pareto optimal front,
3. the solutions distribution should be as even as possible.

Most of the MOEA developments are focused on finding a way to implement the three objectives which were presented above.

An evolutionary search is a trial-based stochastic search process, inspired by the process of natural evolution. It maintains a population of potential solutions to the search problem (individuals), where each solution is typically represented in a predefined format, such as a vector of floating-point values (genotype). For each individual, the fitness is a measure of the performance of this solution with respect to one or more evaluation criteria. In an iterated

process, a set of new individuals (offspring) are created from the current population (parents) through a process of selecting the best performing individuals (parents), and forming new individuals through information exchange between the genotypes of two or more parents (crossover) and stochastic changes to individual genotypes (mutation). The process to form the population for the next iteration (generation) typically involves picking the better offspring and parents and discarding the worst performing parents, such that the population size remains constant.

Evolutionary algorithms are most useful in situations where no conventional optimisation knowledge exists. As they are population based, they are particularly well suited in applications with a trade-off between two or more fitness criteria. Multi-objective EAs can produce a whole set of solutions (Pareto front), allowing the user to analyse the trade-off and pick the preferred solution. Most multi-objective EAs are based on the notion of dominance: one solution is said to dominate another if it is as good or better in all fitness criteria, and better in at least one. Dominance establishes a partial ordering, where it is possible to establish a preference only for some pairs of individuals. A number of evolutionary algorithms have been designed based on this partial ordering, including the Non-sorting Genetic Algorithm (NSGA) and the Strength Pareto Evolutionary Algorithm (SPEA, SPEA2, SPEA2+).

2.4.2 The first generation MOEA

The characteristic of the first generation of MOEA emphasizes the simplicity of the algorithm. However, it lacks a validation approach and standard test function.

2.4.2.1 VEGA

The specific steps of VEGA are given as the following: suppose there are M objective functions, and apply the proportion selection method to each objective. Then, they will get M sub-population respectively, and the size of each sub-population is N/M. After the sub-population evolves, combine them into a new population with size N. Then, operate the selection, crossover and mutation etc until the end condition is reached. N is the population size (Schaffer 1985).

There are many disadvantages of VEGA, such as it cannot guarantee the good individuals can get into the next generation, and it seems like only the extreme points on the optimal front can be found (Schaffer 1985) (Fonsecay and Flemingz 1993).

2.4.2.2 MOGA

For MOGA, the order of individuals is equal to one plus the number of chromosomes which dominates itself in the current population, and the order of all the nondominated individuals are equal to one (Fonseca and Fleming 1993). The dominated individuals are punished depends on the population density of their own domain. The fitness assignment method is given by:

1. sort the population by the individual order,
2. apply the linear or nonlinear interpolation method to interpolate between the lowest ordinal and the highest ordinal,
3. the fitness value is shared for the individuals have the same ordinal.

It is very simple and highly efficient to execute MOGA, however, it is easily affected by the Niche size (Murata, Ishibuchi et al. 1996) (Ishibuchi 1998).

2.4.2.3 NPGA

The Pareto-based tournament selection mode is applied by NPGA (Horn, Nafpliotis et al. 1994). The principle is that, choose two individuals randomly and compare with a subset from the population, if one of the individuals dominates by the subset and the other individual dominates the subset, then the nondominated individual wins. If both of the two individuals are not dominated or dominated by the subset, then adopt the sharing mechanism to select one from them into the next generation. Owing to the selection of

nondominated solution of NPGA is based on portion of population but entire population, it is able to find some good Pareto optimal domain very fast and remain a longer population updating period. However, the disadvantages of NPGA are obvious as well. It not only needs to set the sharing parameters but also requires a proper tournament size, which constrains the practice application effects (Abido 2003) (Horn, Nafpliotis et al. 1994).

2.4.2.4 NSGA

The specific steps of NSGA are given as the following (Srinivas and Deb 1994): the individuals will be sorted based on the Pareto optimal theory before selection, the sharing function method is introduced to keep the population diversity. Ignore the sorted individuals afterwards, then consider the nondominated individuals who belong to another level, and this process will continue until all the individuals have been sorted. As the earlier obtained nondominated individual has the largest fitness value, the chance they are copied is higher.

The advantages of NSGA are: 1. the number of optimised objectives is variable; 2. the distribution of nondominated optimal solutions is even; 3. it is allowed to have many different equivalent solutions. However, due to the Pareto based sorting needs to be repeated many times, the calculation efficiency is relatively lower (Deb and Goel 2001) (Kuriakose and Shunmugam 2005) (Guriaa, Bhattacharyab et al. 2005).

2.4.3 The second generation MOEA

In the second generation of MOEA, researchers combined the external population and archive into the MOEA, and considered elitism explicitly strategy as one of the basic designing procedures. There are four representatives of the second generation MOEA which will be introduced afterwards.

2.4.3.1 NSGA2

The NSGA2 is different from other second generation MOEA, there is no external archive (Deb, Pratap et al. 2002). In instead of that, it apples the inherit operation to population P firstly to obtain the population Q, and after combine the two population implements, nondominated sorting and crowding distance sorting, to generate the new population P, the process will be repeated until the end. The NSGA2 is the updated version of NSGA and was proposed in 2002. The NSGA2 is very popular and will always be treated as a contrast for the other MOEA.

2.4.3.2 PAES

The PAES adopts an adaptive grid method to maintain the external archive (Knowles and Corne 2000). The fundamental principle of Adaptive Grid Algorithm utilizes the external archive to store all the nondominated solutions and then divides the objective space into many grids. If there are any individuals which are inserted in the achieve and located out of the boundary of current grids, then re-divide grids and calculate the individual number in each grid (Corne, Knowles et al. 2000).

2.4.3.3 SPEA

SPEA is a very important algorithm in the development history of MOEA. It is able to efficiently guide the search to the Pareto optimal front (Zitzler and Thiele 1999). Moreover, the experimental data showed SPEA can find the solutions which are even closer to the optimal front compared with the solutions which are derived from single-objective EAs. The specific steps are shown as follows:

1. generate an initial population *P* and an empty external nondominated solution set *P'* *(external archive)*,
2. copy the nondominated individuals from the initial population *P* to the nondominated solution set *P'*,
3. remove the solutions within *P'* which are dominated by any other solutions of *P'*,
4. if the number of nondominated in set *P'* is larger than a given maximum value, then reduce the Pareto front set by cluster analysis,

5. calculate the fitness of every individual in population *P* and set *P'*,
6. choose the individuals from $P \cup P'$ by binary tournament selection until the mating pool is filled, and put them in the next generation,
7. apply the crossover and mutation operator as usual,
8. if it reaches the maximum generation number, then stop, or else move to step 2.

The fitness assignment and cluster analysis are presented as follows.

Fitness Assignment: It is divided into two stages for the whole process. First, the individuals of set *P'* are ranked. Second, rank the individuals of P. The detailed description is shown as follows:

(1) For every solution $x^i \in P'$ is assigned a strength value $s_i \in [0, 1)$, $s_i = h_i/(N+1)$, where h_i stands for the individual number which is dominated by x^i, N is the size of P, the fitness value of individual x^i is f_i and equal to s_i.

(2) The fitness value f_j for each individual $x^j \in P$ is:

$$f_j = 1 + \sum_{i, i \succcurlyeq j} s_i \qquad , \ where \ \ f_j \in [1, N) \ ,$$

the reason for adding one is to guarantee that the individuals of *P'* have better fitness than the individuals of *P*.

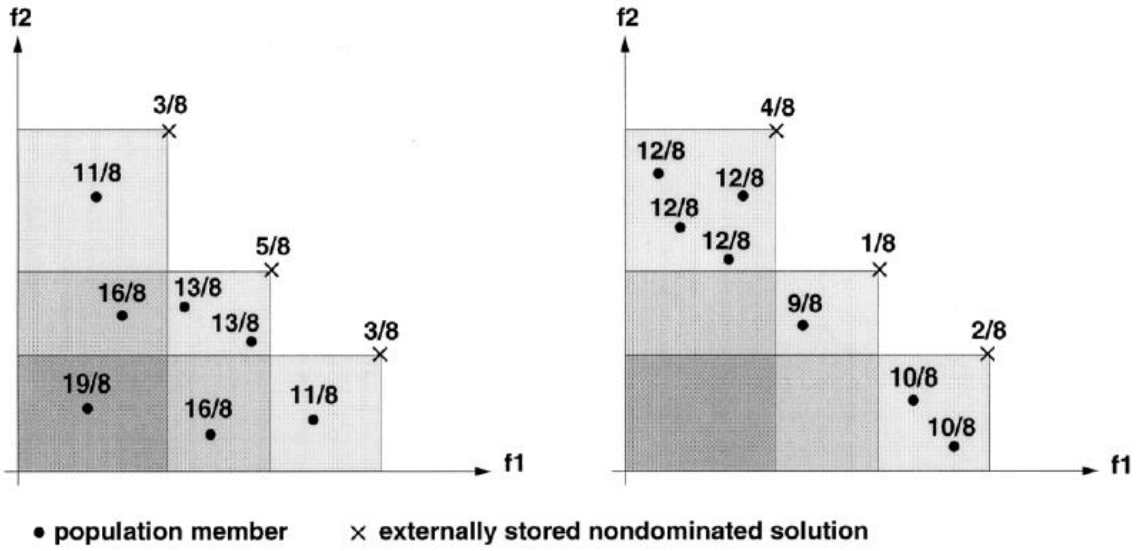

Figure 2.5 Two Scenarios for a Maximization Problem with Two Objectives. The Number Associated with Each Solution Gives the Fitness (and Strength in Case of Nondominated Points)

There are two examples shown in Figure 2.5. As we can see from this figure, the objective space which is covered by 3 nondominated solutions is divided into many different rectangles. The individuals in the dark-shaded area are dominated by all three nondominated solutions and the one in the bright-shaded area is only covered by one point.

Clustering analysis: Generally, the size of nondominated solutions should be limited. The reasons are:

(1) it is possible to have a huge set of nondominated solutions, even infinite,

(2) the calculation resources for applying the algorithm are limited,

(3) the complexity of archive maintenance will be greatly increased with the increasing of the archive size,

(4) the inheritance floating will possibly to appear.

The first three reasons indicate the necessity to restrain the archive size, and the fourth reason implies the possibility that the algorithm performance may benefit from archive truncation. The clustering analysis is implemented by the averaged linkage method to truncate the nondominated solution set and is able to be presented as the following:

(1) initialize the cluster set *C*, which is constructed by the individuals of *P'*. Each individual corresponding to a cluster,

(2) if $|C| \leq \overline{N}$, then move to step 5, else move to step 3,

(3) calculate the distances between all the clusters, the distance between cluster c_1 and c_2 (c_1 & $c_2 \in C$) is given by:

$$d = \frac{1}{|c_1||c_2|} \sum_{i_1 \in c_1 \, , \, i_2 \in c_2} \|i_1 - i_2\| \quad ,$$

(4) find two cluster c_1 & c_2 which has the minimal distance, and then let cluster set C equal to $C \backslash \{c_1 \, , c_2\} \cup \{c_1 \cup c_2\}$, and go to step 2,

(5) determine the representative individual for each cluster, it is usually the chosen individual which has the minimal average distance between others.

Although SPEA is able to guide the search towards to Pareto optimal front efficiently, it still has disadvantages as follows (M.A. Abido 2006) (Zitzler and Thiele 1998):

(1) According to the SPEA assignment process of fitness, the fitness values for the individuals who are dominated by the same external nondominated point are still the same as well. In other words, if there is only one nondominated individual in the

external archive, despite whether the domination relationships exist or not between individuals, the fitness values of all individuals are the same. The SPEA is similar to a random search under this situation.

(2) The cluster analysis is able to reduce the size of the nondominated solutions set. However, there is a possibility that it is able to delete some nondominated individuals by mistake and thereby affecting the diversity of the algorithm.

2.4.3.4 SPEA2

In order to compensate the shortages of SPEA, SPEA was updated to SPEA2, which improved the domains of fitness assignment, individual density estimation and environmental selection (Zitzler, Laumanns et al. 2001). The working process of SPEA2 is very different from SPEA as well. The specific working steps of SPEA2 are shown as following:

1. generate the initial population P_0 and an empty external archive A_0, and let $t = 0$,
2. calculate the fitness values of the individuals of population P_t and external archive A_t,
3. copy all the nondominated individuals in P_t and A_t to A_{t+1}. If the size of A_{t+1} larger than $\overline{N}$ (archive size), then reduce A_{t+1} by means of the truncation operator; else fill A_{t+1} by the dominated individuals in P_t and A_t until the size equals to $\overline{N}$,
4. if $t > T$, where T is the maximum number of generation, then output A to external archive A_{t+1} and stop search,

5. in order to fill the mating pool, apply the binary tournament selection with replacement in A_{t+1},
6. implement recombination and mutation operators to the mating pool and let $t = t + 1$, then go to step 2.

Unlike SPEA, SPEA2 utilizes a fine-grained fitness assignment method and cooperates with individual density. Moreover, the size of external archive is fixed. In addition, the clustering technology is replaced by an alternative truncation method, which will not lead to the missing of boundary points.

The fitness assignment and environmental selection are presented as follows:

Fitness assignment: in order to avoid the individuals who are dominated by external archive points, having the same fitness value, in SPEA2, the dominated solutions of every individual and the solutions which are dominated by every individual are considered. A strength value $S(i)$ is assigned for each individual of the population and external archive, which indicates the number of the solutions which are dominated by the individual. The equation to calculate the strength value is given in Equation 2.1.

$$S(i) = \left| \left\{ j \middle| x^j \in P_t + A_t, x^i \succ x^j \right\} \right|$$

Equation 2.1 The Equation to Calculate the Strength Value

The fitness value $R(i)$ of individual i is equal to the sum of the strength values of all the individuals which dominates the individual i, i.e.

$$R(i) = \sum_{x^j \in P_t + A_t, x^i \succ x^j} S(j)$$

Figure 2.6 shows the comparison results of the fitness assignment between SPEA and SPEA2. $f(1)$ and $f(2)$ are two objectives of this maximization problem.

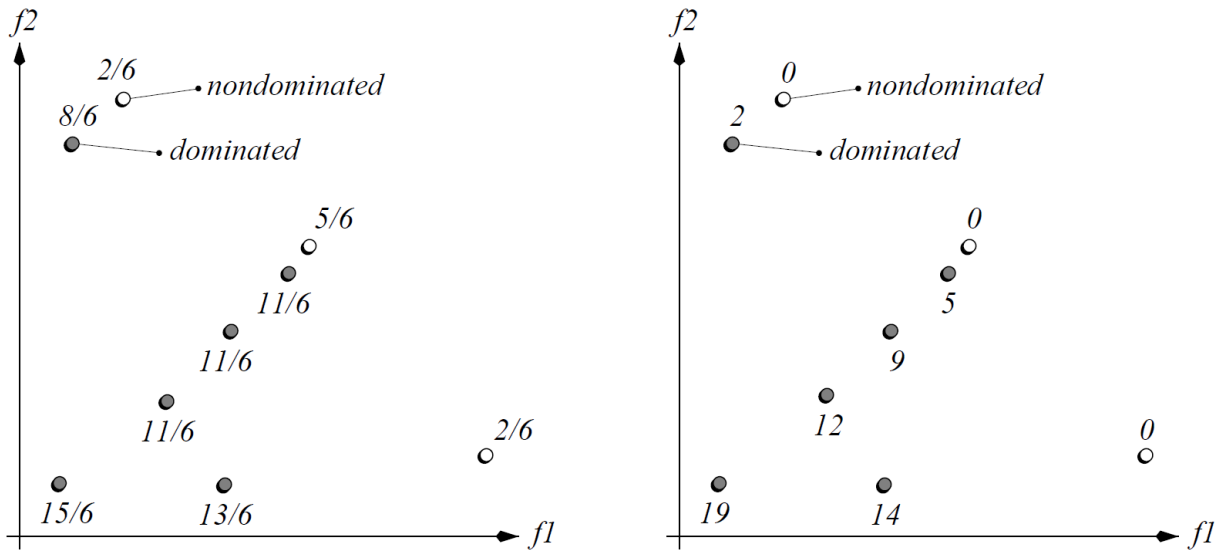

Figure 2.6 The Comparisons of Fitness Assignment Schemes between SPEA (left) and SPEA2 (right) for Optimising Two Objectives *f1* and *f2* Simultaneously

Unlike SPEA, when it calculates the fitness value $R(i)$, the individuals of the population and external archive are considered. Furthermore, the smaller the raw fitness value, the less the individuals who dominate the individual i. If $R(i) = 0$, then it indicates the individual i is a nondominated solution.

The raw fitness assignment process introduces a nondominated sorting. However, it is not enough; it is necessary to introduce the density information to distinguish the individuals who have the same raw fitness. The k^{th} nearest neighbour method is adopted to calculate the density value $D(i)$ of individual i, and which is given by:

$$D(i) = \frac{1}{\sigma_i^k + 2} ,$$

where σ_i^k indicates the space distance between the individual i and the k[th] nearby individual, and $k = \sqrt{N + \overline{N}}$. Finally, the fitness value $F(i)$ of individual i is the sum of raw fitness value and the density value, i.e.:

$$F(i) = R(i) + D(i) \quad .$$

Equation 2.2 The Equation to Calculate the Fitness Value of Individual i

Environmental selection: There are two differences between SPEA and SPEA2 concerning environmental selection. 1. The archive size is constant. 2. SPEA2 avoids the boundary solutions being removed from archive. The specific procedures are shown as follows:

1. copy all the nondominated solutions from population P_t and external archive A_t to A_{t+1}, if the size of A_{t+1} is equal to $\overline{N}$, then accepted,
2. if $|A_{t+1}| < \overline{N}$, then copy $\overline{N} - |A_{t+1}|$ best solutions from P_t and A_t to A_{t+1},
3. if $|A_{t+1}| > \overline{N}$, then constantly move the solutions from A_{t+1} until $|A_{t+1}| = \overline{N}$. The principle of deciding which solution will be moved is: for all the individual j, if $i \leq {}_d j$, and iff $\forall 0 < k < |A_{t+1}|$, $\sigma_i^k = \sigma_j^k$, or $\exists 0 < k < |A_{t+1}|$, $\sigma_i^k < \sigma_j^k$, and when $\forall 0 < l < k$, $\sigma_i^k = \sigma_j^k$.

SPEA2 has been shown, in comparison with other MOEA, to perform generally better. It is a good starting point to use it to explore the novel engine optimisation control strategy (Kim, Hiroyasu et al. 2004).

2.5 Engine Multi-objective Optimal Feedback Control Strategies

Depending on the different purposes, multi-objective engine optimisation is able to be classified into two categories generally. The first category is the transient multi-objective self-learning optimisation technology, which is used for learning the driver's driving style on-board to multi-objective optimise the transient engine performance, such as stop-start, acceleration, and braking (Malikopoulos, Papalambros et al. 2008). The second category is the steady status engine self-learning optimisation technology, which is used for learning the steady status performance of the engines when the engine is aging or environmental condition is changing (such as air temperature, humidity and pressure) (Kesgin 2004). Both of these two categories are based on the MOEA approach and are able to improve time consumption and cost on engine calibration works. The attention of this research is focused on the second multi-objective optimisation category.

2.5.1 Transient Multi-objective Self-learning Optimal Control

The current engine transient calibration relies on dynamometer static calibration and interpolation methods for steady state operating points. However, this method lacks the capability to capture the transient engine operating performances, such as stop-start, acceleration, brake, in terms of the different drivers' driving habits. In other words, although there is great potential to improve the current engine transient calibration results, the possibility to implement it based on the current conventional optimal control methods is very limited (Malikopoulos, Assanis et al. 2008). On the other hand, if there is a controller able to optimise the engine transient performance (fuel economy and emissions etc.) according to the particular driver's personal driving habits continuously in real-time, it will help people to get rid of the backbreaking and time consuming engine calibration work as well.

A controller was developed at the University of Michigan (Malikopoulos, Assanis et al. 2009), which is able to gradually learn the driving habits from drivers and optimise the specific engine performances consequently; it was applied to a four-cylinder 1.9L turbo-charged diesel engine. The learning process is shown in Figure 2.7. The decentralized learning control strategy was applied for this controller and the engine operation was modelled as a Markov Decision Process (MDP). Injection timing and Variable Geometry Turbo-charging (VGT) are variables to be optimised and thereby optimising the engine fuel consumption and NO_x concentration.

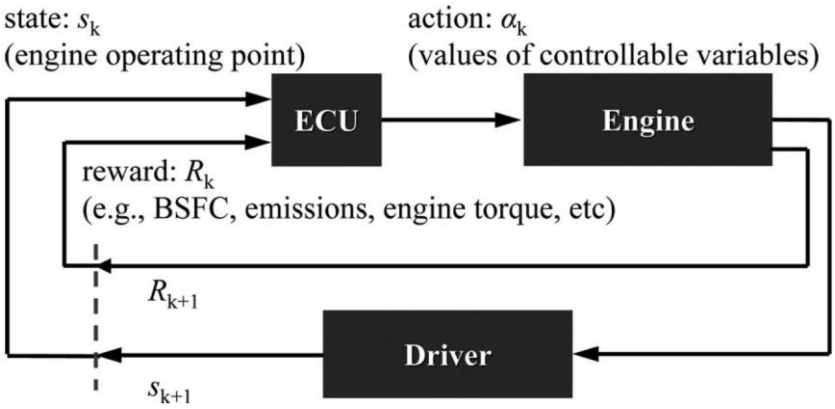

Figure 2.7 Learning Process during the Interaction between the Engine and the Driver (Malikopoulos, Assanis et al. 2009)

2.5.2 Steady Status Multi-objective Self-learning Optimal Control

As many new technologies are applied to modern engines, such as VVT, GDI (BOSCH 2006), multi-injection (Mancaruso, Merola et al. 2008), two stage supercharging (Woollenweber and Halimi 2000) etc, the number of adjustable variables for SI engines are increased considerably. As degrees of freedom for engine optimisation and the number of calibration parameters are increasing, the classic off-board manual engine-bed based dynamometer calibration mapping method is reaching its limit. The classic calibration approach is becoming more complicated, expensive and time consuming with the increasing complexity of engines, and the combinatorial explosion of the parameter space. Moreover, since the classic engine calibration cannot self-adapt as engines age, the fuel consumption and emissions tend to increase. Therefore, a multi-objective fast on-board engine optimal control strategy is desired.

Many researchers concentrate their work on the steady state multi-objective intelligent engine optimal control strategy. A multi-objective engine optimal controller was developed by Distance-based Pareto Genetic Algorithm (DPGA) and NSGA-EMOGA to improve fuel consumption and emissions of SI engines (Vossoughi and Rezazadeh 2-5 Sept. 2005). A neural-network model was applied as a virtual engine test bed. The inputs are requested engine speed and torque, and the adjustable objectives are λ and spark timing. The outputs are BSFC, emissions and torque etc. The schematic of Vossoughi's model is shown in Figure 2.8.

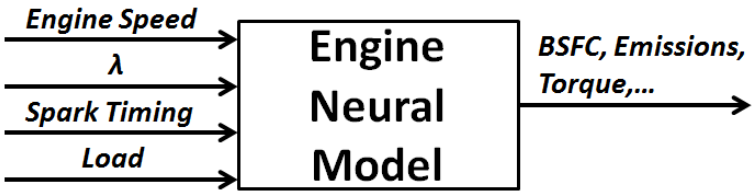

Figure 2.8 The Schematic of Vossoughi's Model

Figure 2.9 shows the Pareto optimal surfaces of fuel consumption against the sum of emissions ($HC + CO + NO_x$). It shows that DPGA has a better performance to find the lowest emissions and NSGA-EMOGA can provide better results on fuel consumption. The simulation was implemented on a single-processor Pentium IV computer, and each runs needed around 100 hours to complete.

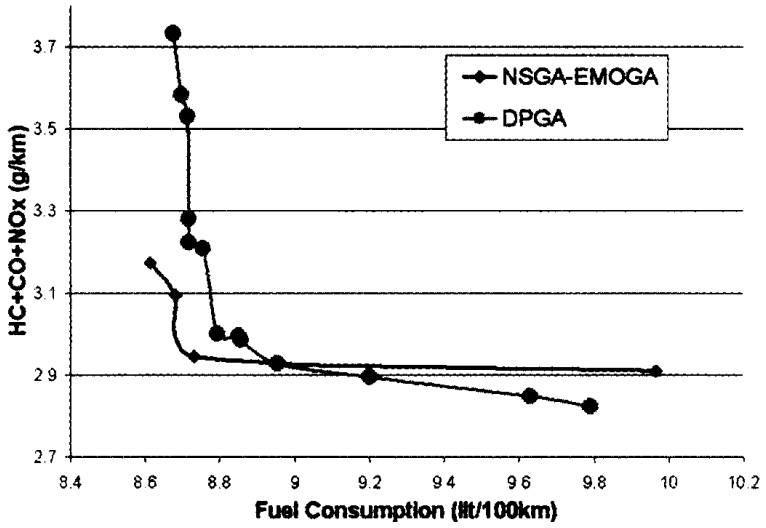

Figure 2.9 The Pareto Optimal Surfaces of Vossoughi's Controller

A genetic algorithm and artificial neural network for optimising engine efficiency and NO_x emissions was developed (Kesgin 2004). A zero-dimensional reaction kinetic model was used to predict the engine efficiency and NO_x emissions. A simple GA programme was applied to optimise the engine efficiency and NO_x emissions, and equivalence ratio, charge pressure, charge temperature, combustion duration, combustion start position and form factor are the input variables. The optimisation results are shown in Figure 2.10. However, the method of combustion duration control and the time consumption of one GA case were not given.

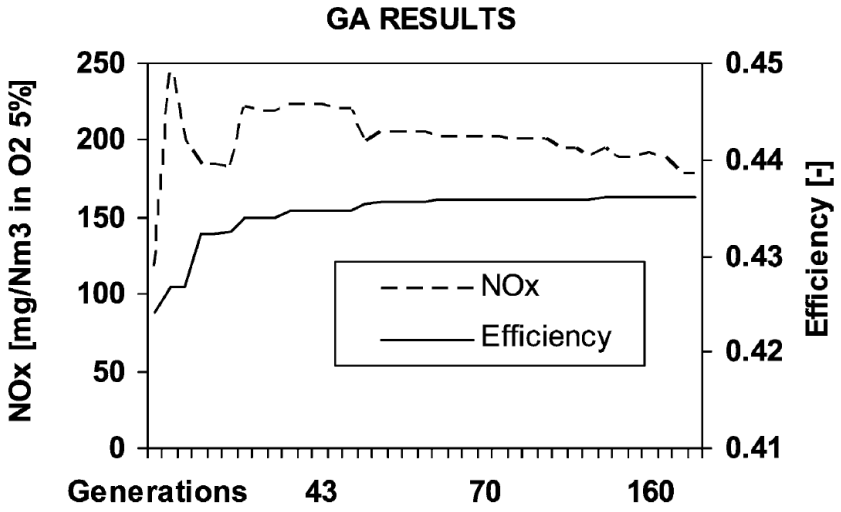

Figure 2.10 The GA Results of Kesgin's Controller Model

A penalty function based multi-objective optimal feedback controller for a DaimlerChrysler 2.4 Litre four-cylinder SI engine was proposed (Wu, Prucka et al. 2006). The method was able to improve fuel consumption and NOx emissions simultaneously by optimising cam-phasing. They developed an engine model with a one dimensional gas dynamics module and quasi-dimensional combustion module, and utilized the model to train an Artificial Neural Networks (ANN) to simulate the engine performance with high computationally-efficiency. The ANN model was considered as a benchmark to implement multi-objective optimal feedback control; the fuel consumption and NO_x emissions were outputs, and camshaft position and spark timing were adjustable variables. The model was developed to search the optimal value of engine fuel consumption firstly. In order to involve the NO_x emissions into the optimisation function, a penalty term was added to the objective function. The Pareto optimal fronts for different engine operating conditions (47NM, 2000 rpm & 119NM, 2200 rpm) are shown in Figure 2.11 respectively.

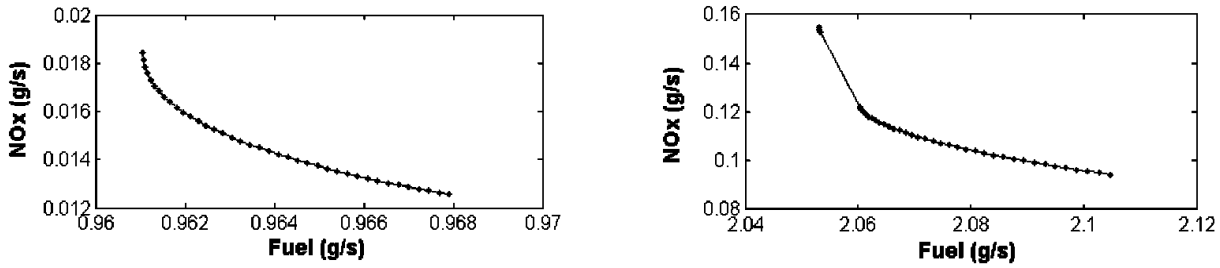

Figure 2.11 The Pareto Optimal Fronts for Different Engine Operating Conditions (47NM, 2000 rpm & 119NM, 2200 rpm) of Wu's Controller

An intelligent optimal control strategy to improve the NOx, PM and CO emissions for an aged four-cylinder diesel engine was built (Obodeh and Ajuwa 2008). An ANN model was used to predict the engine performance and emissions data, and utilize penalty terms to implement multi-objective optimal feedback control. The objectives of optimisation are fuel consumption, NO_x, PM and CO emissions. The objectives were improved very much through the control strategy; a reduction of 39.3% for NO_x, 69.2% for PM, 39.3% for CO and 2.5% for $ISFC$ were obtained.

A Pareto optimum solution based multi-objective optimal feedback control strategy was developed (Hiroyasu, Miki et al. 2002), which was able to optimise the indicated specific fuel consumption ($ISFC$), NO_x and soot simultaneously for a diesel engine. The control strategy is based on the Neighbourhood Cultivation Genetic Algorithm (NCGA), which is an extended algorithm of GA. The derived Pareto optimal solutions are shown in Figure 2.12. However, for their research, the injection rate is the unique variable, and it needs around 3 hours to obtain the Pareto optimal solutions. Therefore, there is plenty of room to improve their controller.

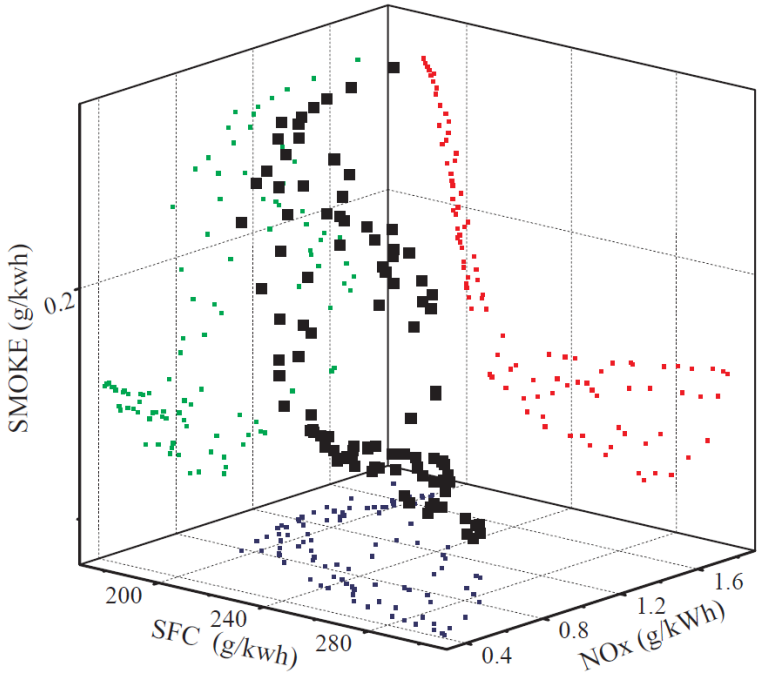

Figure 2.12 The Derived Pareto Solutions (SFC, NOx, Smoke) of Hiroyasu's Controller (Hiroyasu, Miki et al. 2002)

It can be found from the literature review above that most researchers choose ANN modelling to simulate the engine operation. Although the computational efficiency of ANN is very high, its black-box nature does not allow for explaining the processes of specific analysis and research, such as in-cylinder pressure trace, heat release rate and peak pressure.

In Chapter 4, the intelligent model-based multi-objective high speed self-learning optimal controllers for SI and HCCI engines are introduced. The simplified single-zone control oriented gasoline-fuelled SI and HCCI engine model was used as a virtual engine test-bed. For SI engines, the optimal control method was able to find the optimal engine parameters set (Throttle Position, Spark Timing, Injection Timing, IVO and EVC) for the optimal control

objectives ISFC, ISPMN and ISPMM. For HCCI engines, the optimal control method was able to find the optimal engine parameters set (IVO, EVC and λ) for the optimal ISFC and ISHC, i.e. multi-optimisation for multi-objective, with good accuracy. The validation results will be given in Chapter 5 and 6.

2.6 Control Oriented Engine Emissions Models

In general, the most trustworthy approach to simulate the engine emissions is the chemical kinetics emission calculation. However, the computational cost is too high to satisfy the real-time control requirement. There are two popular approaches to simulate the engine emissions for real-time controller development, i.e. experimental data based curve fitting and interpolation. Prabhakar et al. reported a least square curve fitting based emissions prediction model for optimal engine control. The model predicted the experimental data of engine emissions, NO_x, CO and HC, as a polynomial function of engine operating variables. The engine operating variables include engine speed, load, spark advance and EGR fraction (PRABHAKAR, CITRON et al. 1977 Jan 01). The map-based interpolation technique is one of the most popular approaches to predict the engine emissions.

With respect to this study, the simulation results of emissions' data are used for validating the multi-objective optimal feedback control strategy. The map-based interpolation method is used to simulate the PM emissions of the SI combustion, and the experimental data based

curve fitting is applied for the HC emissions prediction of HCCI combustion. Although it is time consuming for developing the emissions maps, the simulation is reliable and time saving.

2.7 The Self-stabilisation Feature of HCCI Engines Control

As one of the most important features of HCCI combustion, the self-stabilisation behaviour has great guiding effects on the DoE of HCCI engine multi-objective optimal feedback control strategy. The self-stabilisation features of HCCI combustion had been observed by many researchers and mentioned in some publications (Chiang and Stefanopoulou 2004, Chiang and Stefanopoulou 2007, Shaver 2009). However, there is no report to analyse this phenomenon from the view of system control individually (Chang, Babajimopoulos et al. 2006). Due to the fuel injection normally ending during the NVO process and the spark plug is turned off for HCCI engines; there is no direct control approach after the Intake Valve Close (IVC). The experimental proof or numerical validation of this feature will deliver great confidence to control engineers to control the HCCI combustion reliably and efficiently.

Shaver et al. mentioned the self-stabilisation feature of HCCI combustion as “an interesting characteristic of residual-affected HCCI”, since the combustion timing, work output and in-cylinder peak pressure often converge to a stable equilibrium point (Shaver 2009). They

supposed the behaviour is due to the competing residual-induced heating and dilution of the reactant gas. However, they could not prove this guess by any powerful evidence.

Jia presented a propane fuelled HCCI model for control strategy development. From his numerical simulation study, he found the combustion reaction rate tended to converge to a stable status without any external control signal. The simulation results are shown in Figure 2.13 with different valve timing.

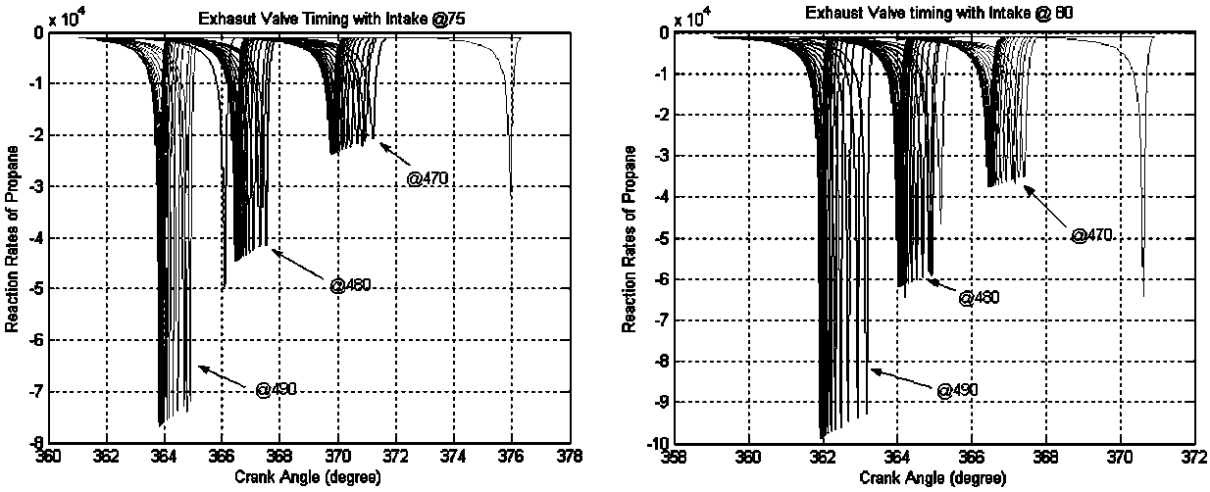

Figure 2.13 The Self-Stabilisation Behaviour of HCCI Combustion Reaction Rate in Jia's Simulation Study

2.8 Summary

In summary, the literature review places emphasis on the introduction of the development of SI and HCCI engine modelling, the multi-objective optimisation methods and the

application of multi-objective optimisation on engines. In addition, the background knowledge and research progress of the HCCI self-stabilisation feature is discussed as well.

From the literature review, it is possible to find that:

1. Modern internal combustion engine research and study is a complex and accurate interdisciplinary science. It includes mechanical engineering, chemical engineering, electrical engineering, computer science, automatic control, biological engineering and material engineering etc.
2. The numerical simulation study of engines is essential. Depending on the different purposes, the simulation theories, dimensions, approaches, tools and the combination of the items above should be determined carefully. For this research, the zero-dimensional single zone *AFBR* method was adopted to simulate the engine in-cylinder pressure, gas exchange process, IMEP and ISFC etc. The experimental data based curve fitting and interpolation technology were utilized to predict the emissions amount for SI and HCCI engines.
3. The developing speed of MOEA is very attractive; from the first MOEA generation to the second MOEA generation and the third MOEA generation in the future, the fast developing speed is impressive. Especially for engine optimisation, the advantages include speed, efficiency, economy and high compatibility. The potential of an online engine multi-objective optimal feedback controller is considerable.
4. The self-stabilisation feature of HCCI combustion is very interesting and lacks numerical simulation study and mathematical proof. If it can be proved in the future, then it will

deliver huge confidence and theory foundation to researchers for HCCI engine control research.

Chapter 3 Experimental System Setup

The aim of this chapter is to introduce the experimental test facilities, which includes the SI/HCCI dual model GDI V6 engine, Cam Profile Switch (CPS) system, dSPACE test bench control system, test cell arrangement and some engine performance test equipment. Additionally, the experimental data processing methods are presented.

3.1 Introduction

The test bench for this study was built for two former finished HCCI engine research projects, i.e. Controlled Homogeneous Auto-ignition Supercharged Engine (CHASE) and Controlled Homogeneous Auto-Ignition Reformed Gas Engine (CHARGE).

The test bench and control system was upgraded by Jaguar and Land Rover, dSPACE Ltd., university laboratory technicians and a previous PhD research student Dr. Jacek Misztal. However, as the test bench was unused for a quite long time before the author started to do the experimental tests, the engine test bench and dSPACE control system went through a

series of re-configuration, re-calibration, components' failure fixing and renovation works by the author with technical supports from Jacek.

Since the implementation of HCCI combustion in a real engine is much more complex than in SI mode, the author made a great effort to let the engine operate HCCI combustion with different operating conditions. The naturally aspirated HCCI operating window after the renovation works is shown in Figure 3.1.

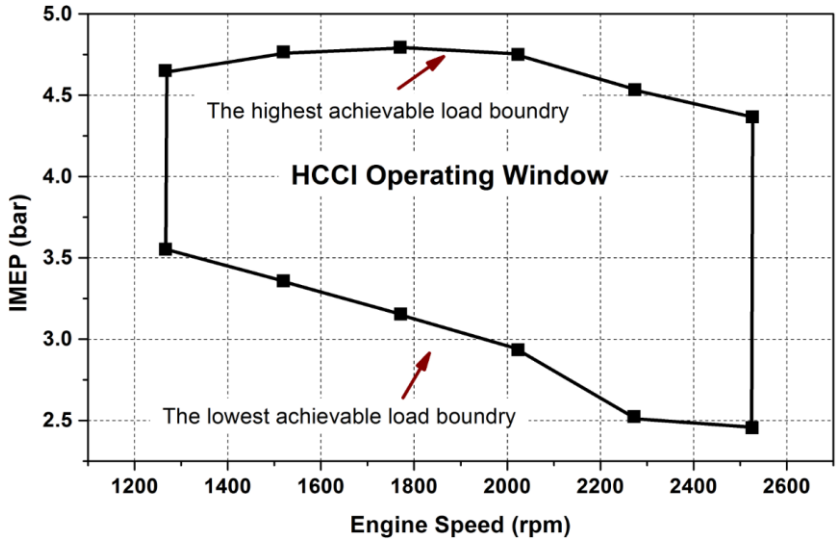

Figure 3.1 The Naturally Aspirated HCCI Operating Window of the Jaguar V6 Engine

3.2 The Jaguar SI/HCCI Dual Mode V6 Engine

The Jaguar SI/HCCI dual mode GDI V6 engine test bench is shown in Figure 3.2 and the engine specification summary is shown in Table 3.1 (Misztal 2008). Since the engine is able

to be operated in SI and HCCI modes, and is switched between each one online, the CPS system is applied to provide two sets of cam profiles in one cam shaft for operating different combustion modes. For better control flexibility and space, the Variable Valve Timing (VVT) system is supplied with the engine, which allows the engine to change the intake and exhaust cam position within 60 CAD. Additionally, the GDI technology is applied to the engine fuel supply system for better engine performance. Since the system was designed for HCCI research, the engine was equipped with a thermal management system to control the intake air temperature and a supercharger to boost the intake air pressure. A DSG Series 2000 test bench control system was used to control the Froude EC38 eddy current dynamometer. The accuracy of the speed indicator is within ±1 rev/min. The digital torque indicator has an accuracy of ±0.05% FSD (Full Scale Deflection).

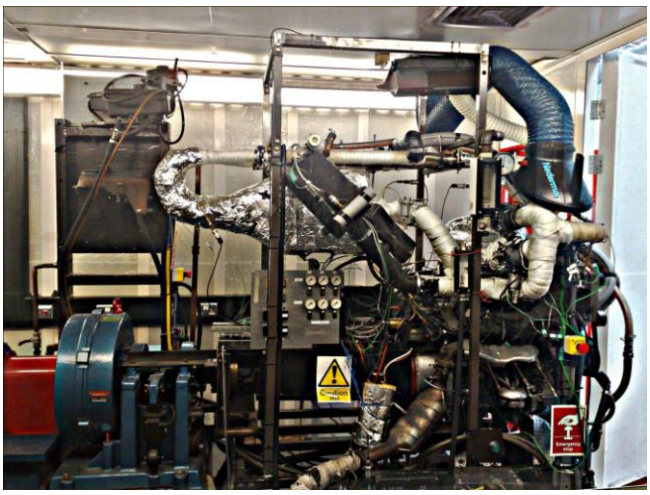

Figure 3.2 The Jaguar SI/HCCI Dual Mode V6 Research Engine

Table 3.1 Engine Specification Summary

Engine type	Jaguar V6 GDI	**Compression ratio**	11.3
Displacement Volume	3.0 Litres	**Max Valve Lift (SI/HCCI)**	9/3 mm
Engine speed	800~ 3500 rpm	**Valve Duration (SI/HCCI)**	260/160 CAD
Bore	89mm	**Intake valve timing**	Variable
Stroke	79.5mm	**Exhaust valve timing**	Variable
Rod	138mm	**Intake temperature**	Variable
Fuel	ULG95	**Air/Fuel ratio**	Variable

The schematic of the engine gas exchange system is shown in Figure 3.3.

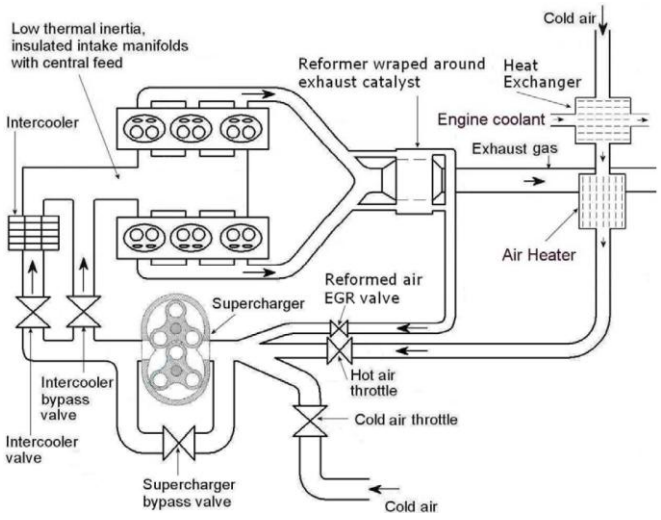

Figure 3.3 The Schematic of Engine Gas Exchange System

3.3 The Cam Profile Switching System

One of the most popular approaches for implementing the HCCI combustion is to utilize a NVO strategy to trap part of the internal EGR to promote the HCCI combustion for the upcoming cycle. In order to trap the internal EGR, the valve open duration should be much shorter than the conventional SI engine's valve open duration for both intake and exhaust

cams. However, the maximum valve lifts are constrained to a very small height for keeping the smoothness of the valve lift profile. It is one of the main reasons for the operating window of an HCCI engine being narrow, i.e. the fresh air intake amount is constrained by the HCCI valve lift profile. Therefore, most of the HCCI engines are coupled with an air boost system to increase the efficiency of the HCCI air intake system.

In order to operate SI and HCCI combustion mode in the same engine, a CPS system was installed into the engine to switch the valve lift profiles between the different combustion modes. The dual mode cam shaft for SI and HCCI combustion of this engine is shown in Figure 3.4.

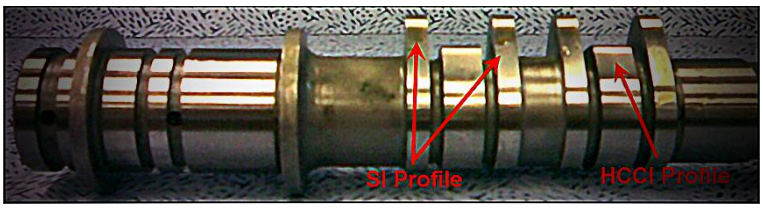

Figure 3.4 The Cam Profile Switching (CPS) System

The sectional drawing of the CPS system is shown in Figure 3.5. The hydraulic tappet is driven by tappet stem “5”. If the engine oil pressure is ordinary, the return spring “4” will push the lock pin “3” back to the tappet stem “5”, then the tappet stem “5” disconnects with the tappet sleeve “6”. The tappet sleeve “6” is driven by the SI cam “1” and decouples with tappet stem “5”; the valves are driven by the HCCI cam “2”. If the engine oil is given enough pressure, the lock pin “3” is pushed into the tappet sleeve “6” and they become an entirety. Meanwhile, the valves are driven by the SI cam “1” (Tian 2007).

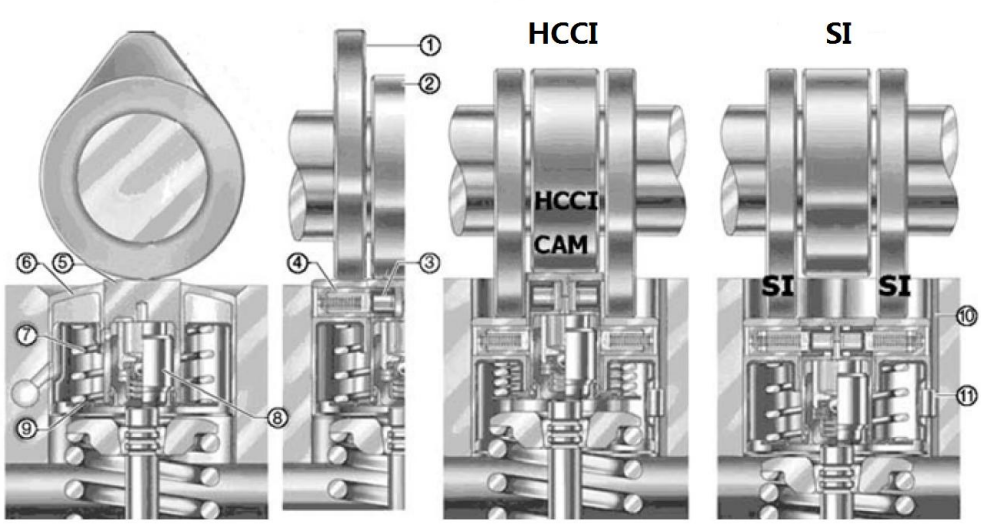

Figure 3.5 The Sectional Drawing of CPS System

1 – the SI cam, 2 – the HCCI cam, 3 – the lock pin, 4 – the return spring, 5 – the tappet stem, 6 – the tappet sleeve, 7 – the spring, 8 – the valve clearance adjustment, 9 – the shield, 10 – the tappet stem seat, 11 – the positioning pin

The intake and exhaust valves lift the profiles of the SI cam and HCCI cam as shown in Figure 3.6. The highest lifts of the SI and HCCI cams are 9mm and 3mm respectively. Moreover, in order to improve the charging efficiency, the valves' lift profiles of the intake valves are a little bit higher than the exhaust valves.

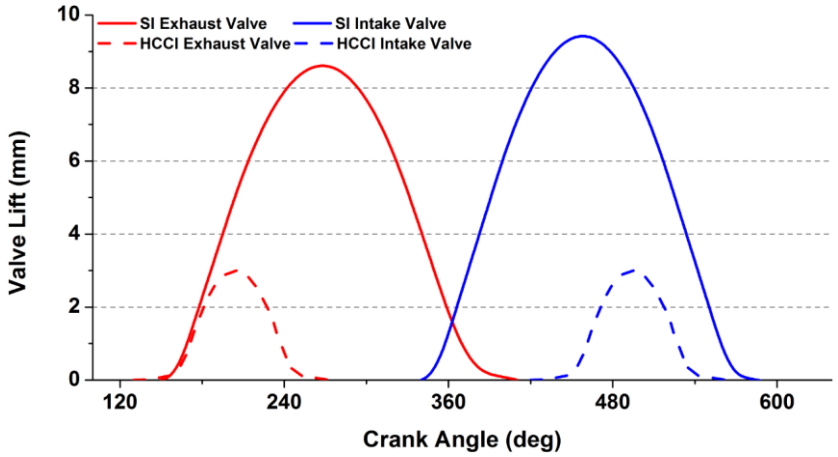

Figure 3.6 The Intake and Exhaust Valves Lift Profiles

The valves open duration is given in Table 3.2 in CAD.

Table 3.2 The Valves Open Duration of SI and HCCI Cams

	Intake Valves Duration	Exhaust Valves Duration
SI Cam	250	250
HCCI Cam	173	173

3.4 The dSPACE Engine Control System

The dSPACE real-time control system is developed by dSPACE Ltd. Germany. It is a MATLAB/Simulink based software-hardware working platform, which is able to implement Rapid Control Prototyping (RCP), Hardware-In-the-Loop Simulation (HILS) and the totally seamless connection with MATLAB/Simulink/RTW. The dSPACE is able to provide powerful real-time ability, high reliability and good extendibility.

The processor of the dSPACE hardware has very high computational capability and is assembled with many I/O supports, which help the customers with configuration depending on their needs. Furthermore, the dSPACE software is very powerful and convenient; it includes the whole tools package of automatic code generation, downloading, testing and debugging processes. The dSPACE control tower of this test bench is shown in Figure 3.7.

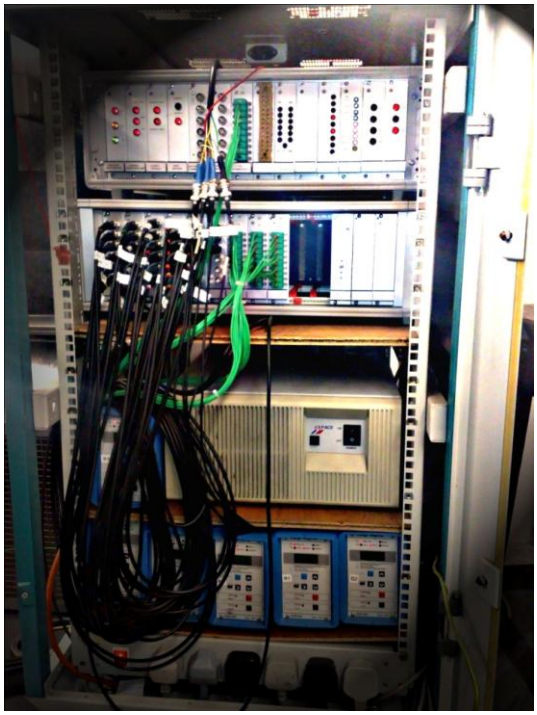

Figure 3.7 The dSPACE Simulator Control Tower

The key specification of the dSPACE for this test bench is shown in Table 3.3 (Misztal 2008).

Table 3.3 The Key Specification of the dSPACE Control Tower

Boards	Board No.	Functions	Main Technological Properties and Parameters
Processor Board	DS1005	It performs calculations in real time and provides an interface to the I/O boards as well as to the host PC.	32-bit synchronous I/O bus. 64 PHS bus interruptions. 20 processor boards are able to connect to Parallel Processing.
Multi-Channel A/D Board	DS2003	It is able to transfer the analogue signals to digital signals; due to the digital signals having stronger anti-interference ability.	32 A/D channels. 2 independent A/D converters. 16-bit resolution. An external trigger input to start A/D conversion.
Multi-Channel D/A Board	DS2103	The board provides digital-to-analogue signal conversion.	32 parallel D/A channels. 14-bit resolution. Typical build time: 10 µs
Multi-I/O Board	DS2201	The board provides a space-saving solution for applications requiring a lot of I/O.	8 timing I/O lines can be used as capture/compare channels and up to 6 of these lines can be used to generate PWM signals.
Direct Digital Synthesis Board	DS2302	It is a waveform generator with 6 DSPs. The DS2302 C function allow you to exchange data between your main application and an application running on one of the 6 DSPs.	6 channels. 6 digital I/O lines in every channel. It computes each signal sample just-in-time and outputs it immediately.
Timing and Digital I/O Board	DS4002	This board is able to measure digital signal parameters under signal record mode and generate digital waveforms (especially square-wave and PWM signals) under pulse generate mode.	8 channels. 30-bit/200ns time radix. 32-bit additional digital I/O lines (TTL).
Digital I/O Board	DS4003	It is used to receive single input signal, and generate control signal.	96 TTL compatible I/O lines. Every 8 bit a group and the direction is programmable. 3 synchronous lines are used to communicate with external devices.
Serial Interface Board	DS4201-S	The board allows serial communication between dSPACE and external devices.	It supports RS232-C, RS422 and RS485 asynchronous communication on 4 channels. 16-bit transmitter/receiver FIFO.

3.4.1 The dSPACE Hardware Arrangement

A brief sketch of the test cell wiring arrangement between PC, dSPACE and interface boxes is shown in Figure 3.8.

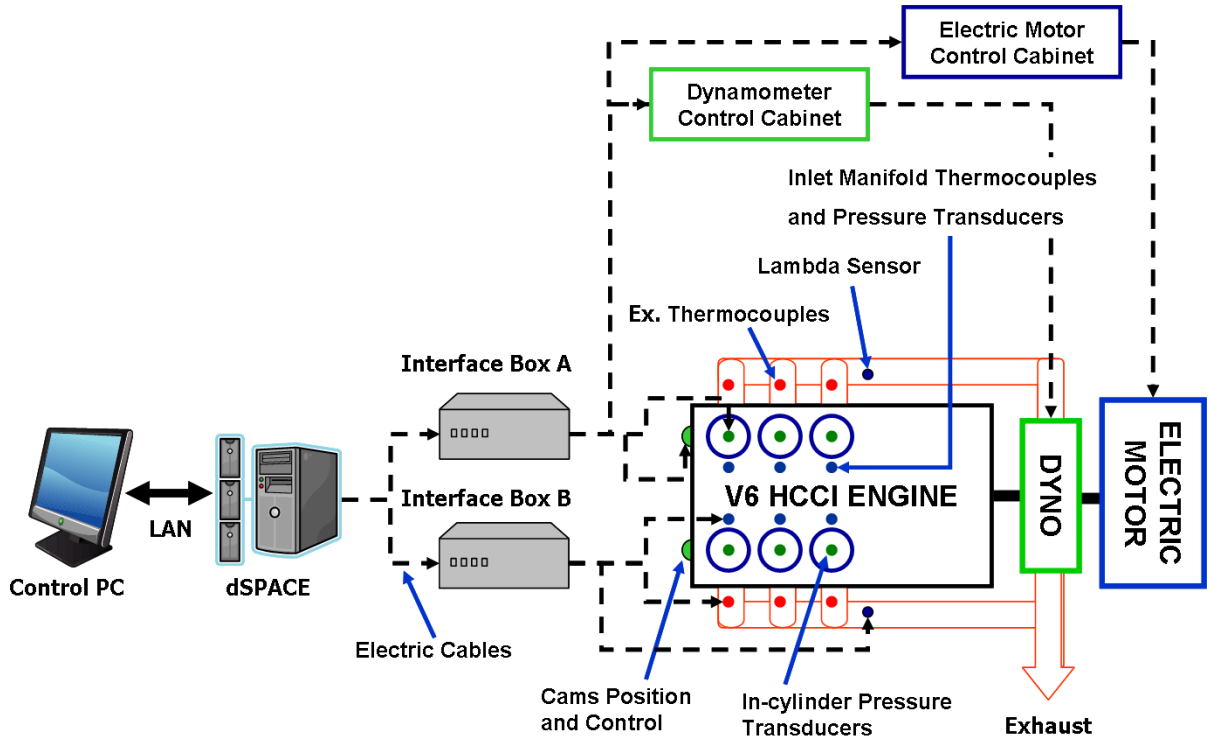

Figure 3.8 The Test Cell Arrangement and Wiring

As it shows in Figure 3.8, the dSPACE is connected with two interface boxes “A” and “B”. The interface box A is in charge of processing in-cylinder pressure signals, cam position signals etc. from the sensors. The interface box B is responsible for the signals from the thermocouples, pressure sensors in the inlet and exhaust manifold, lambda sensors, humidity sensor, torque and engine speed readings etc.

3.4.2 The dSPACE Controller Model and Control desk

The dSPACE Simulink controller model which is shown in Figure 3.9 is used to implement RCP control.

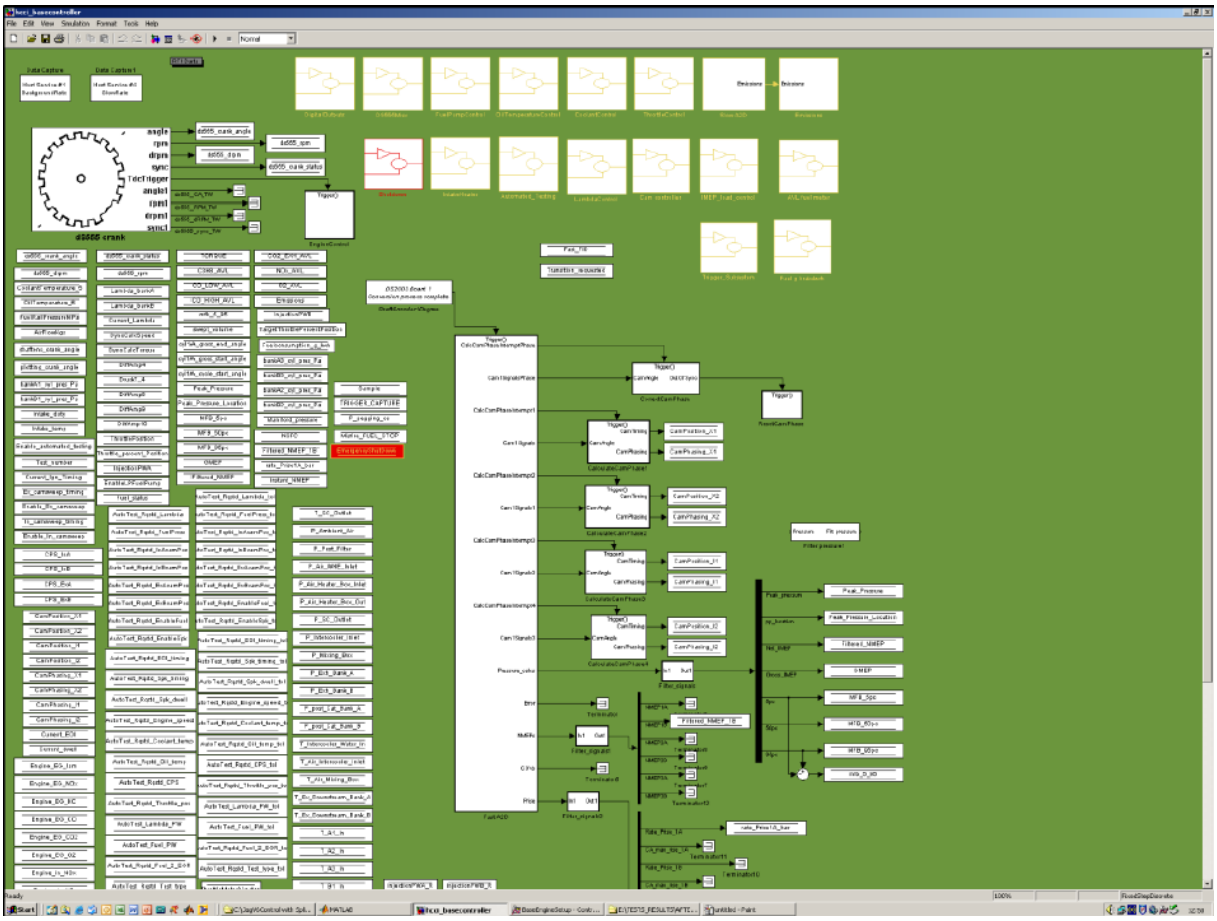

Figure 3.9 Simulink Engine Controller Model

The Simulink controller model is divided into four parts: fast analogue inputs, slow analogue inputs, digital outputs and fast digital outputs. Most of the engine parameters are controlled through PID controllers.

In order to implement experimental tests for model validation in transient status and the HCCI self-stabilisation study, the author developed a transient controller by Simulink (Figure 3.10) and embedded it into the engine controller model.

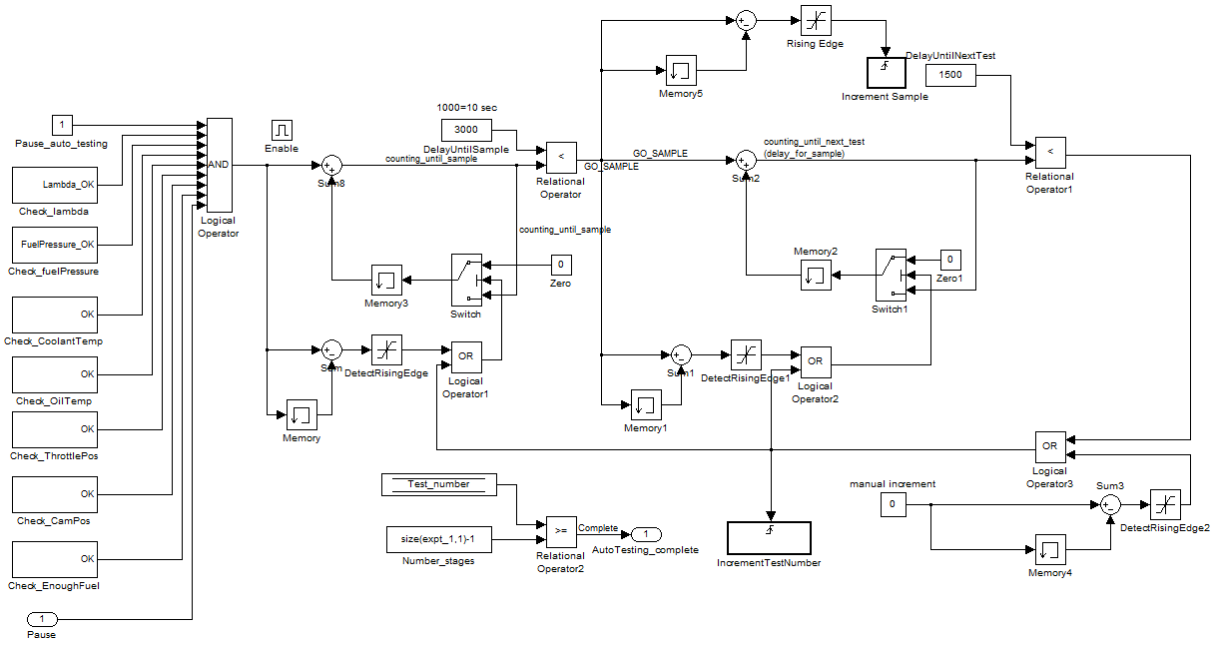

Figure 3.10 The Transient Experimental Test Controller

The developed controller lets the dSPACE automatically run the predesigned experimental tests order with different engine parameter settings, such as throttle position (for SI comparisons), IVO, EVC, λ and engine speed. The predesigned experimental tests order is able to be programmed in an M file in Matlab, and the tests will be ready to run after uploading the controller model to dSPACE.

Figure 3.11 shows the main tab of the dSPACE control desk panel. The most frequently used controllers and indicators are shown in the main tab, such as cam shaft controllers, throttle

position controller, load and engine speed meters etc. The controllers and indicators which are seldom used are put in the other tabs.

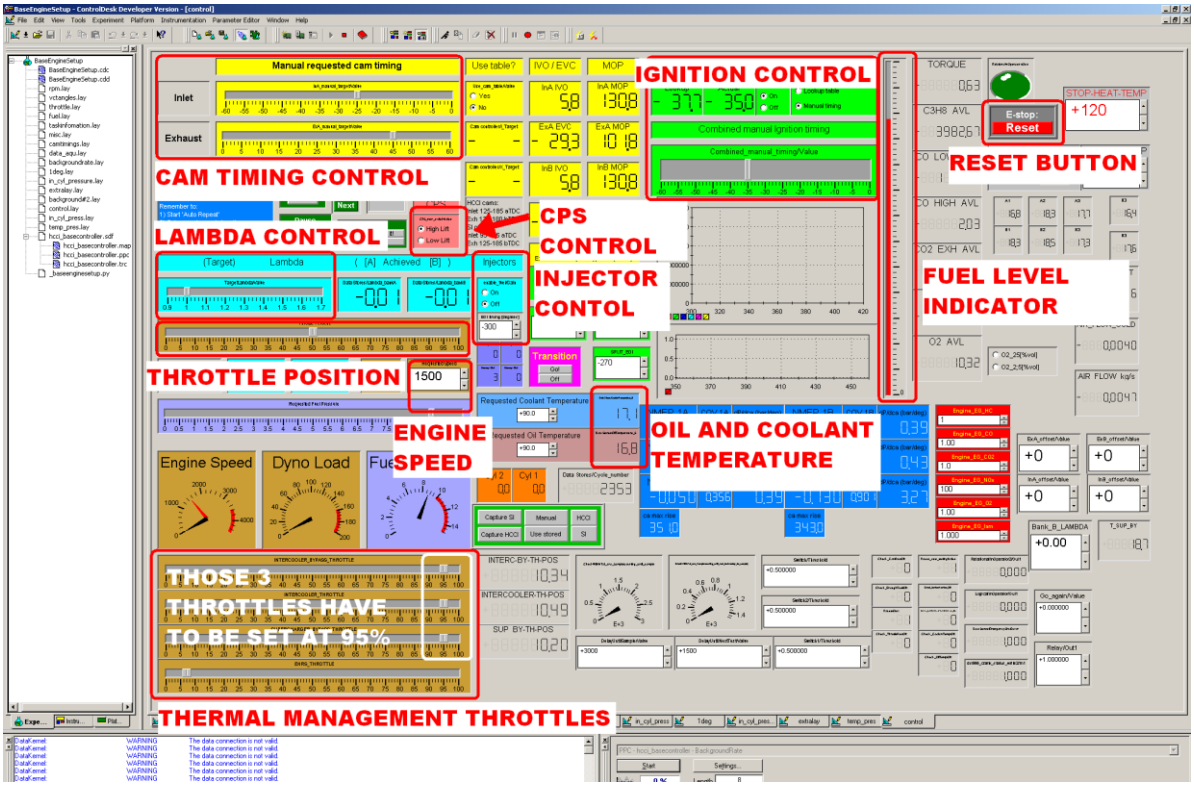

Figure 3.11 **dSPACE Control Desk Panel – Interface for the Simulink Engine Controller Model**

3.5 Engine Performance Measurements

In order to capture the engine performance data and to develop the engine model, there is a great deal of equipment installed and used. All of this performance measurement equipment was calibrated before the experiments.

3.5.1 The In-cylinder Pressure Sensor

There are six Kistler 6052B pressure sensors fitted in the head of each cylinder to measure the in-cylinder pressure with one crank angle resolution (Kistler 2007). Fundamentally, the pressure sensor is based on the piezoelectric effect. The charge outputs to the charge amplifiers and converts to proportional voltage consequently. The brief circuit diagram of the wiring between the pressure sensor and charge amplifier is shown in Figure 3.12. In order to minimise the capacitance influence from the cable and sensor, the open loop gain A should be set to high enough. Therefore, the output voltage U_0 depends on output charge Q and the capacitor of charge amplifier C_r only. The wiring between the pressure sensor and charge amplifier is shown in Figure 3.13.

$$U_0 = -\frac{Q}{C_r}$$

Figure 3.12 The Kistler 6052B Pressure Sensor and 5011B Charge Amplifier

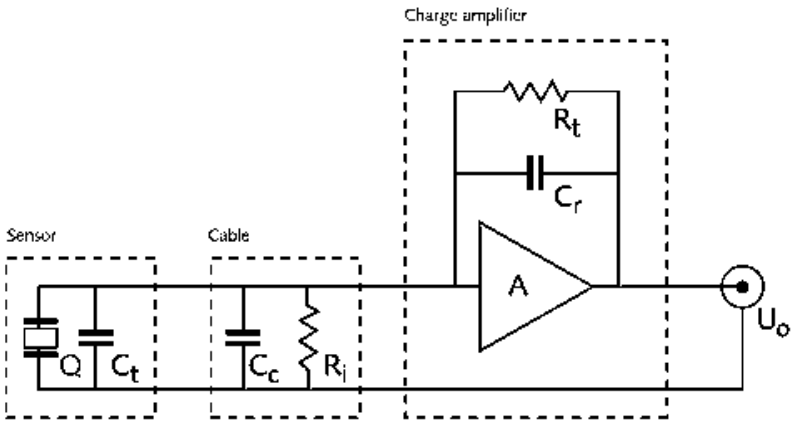

Figure 3.13 The Wiring between Pressure Sensor and Charge Amplifier

The sensitivity of the pressure sensor has been given as 20pC/bar. The linearity errors were measured by the manufacturer and are smaller than ±0.4% FSO (Full Scale Output).

3.5.2 The Fuel Supply and Consumption Measurement System

An AVL 7131-06 fuel meter (or fuel balance) is used for measuring the fuel consumption during a period of specific engine running cycle number. The principle of the measurement approach is shown in Figure 3.14. Basically, it has a balance scales structure, and the capacitive sensor will provide the continuous signal outputs depending on the fuel consumption rate in real-time.

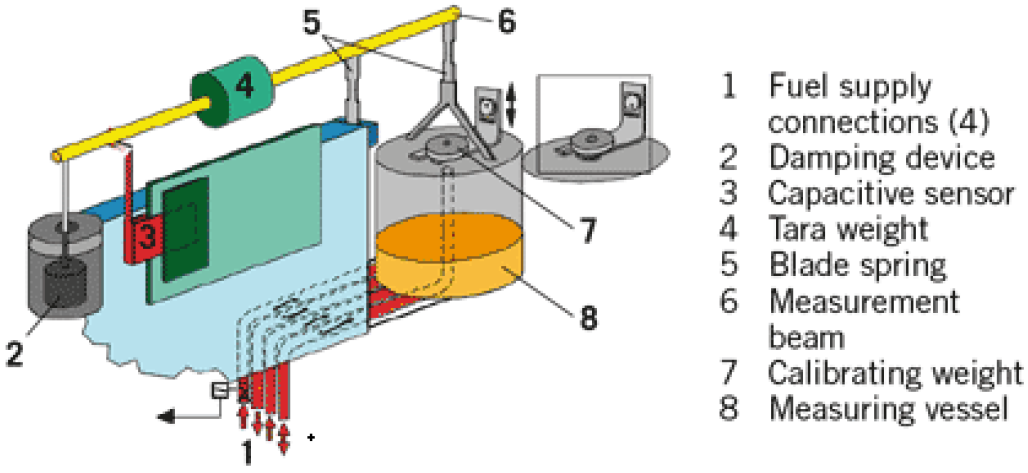

Figure 3.14 The AVL fuel Balance Measurement Principle

The fuel level value outputs to the interface box A of dSPACE system. The gasoline in the fuel meter is supplied by an external fuel line with ambient pressure. The low pressure electric fuel pump can boost the fuel pressure from ambient pressure in the output port of the fuel balance to 3-5 bar. Then the fuel goes through the pressure regulator to control the fuel pressure reaching the threshold to provide enough fuel pressure to the high pressure fuel pump. The high pressure fuel pump is driven by a cam shaft as a mechanical pump and is able to provide up to 120 bar injection pressure. The rest of the fuel will go back to the fuel tank through the pressure relief valve. The fuel supply circle is shown in Figure 3.15. Based on the calibration results of the fuel measurement system, the accuracy of fuel mass consumed and pendulum mass is ±0.12% and ±0.005% respectively.

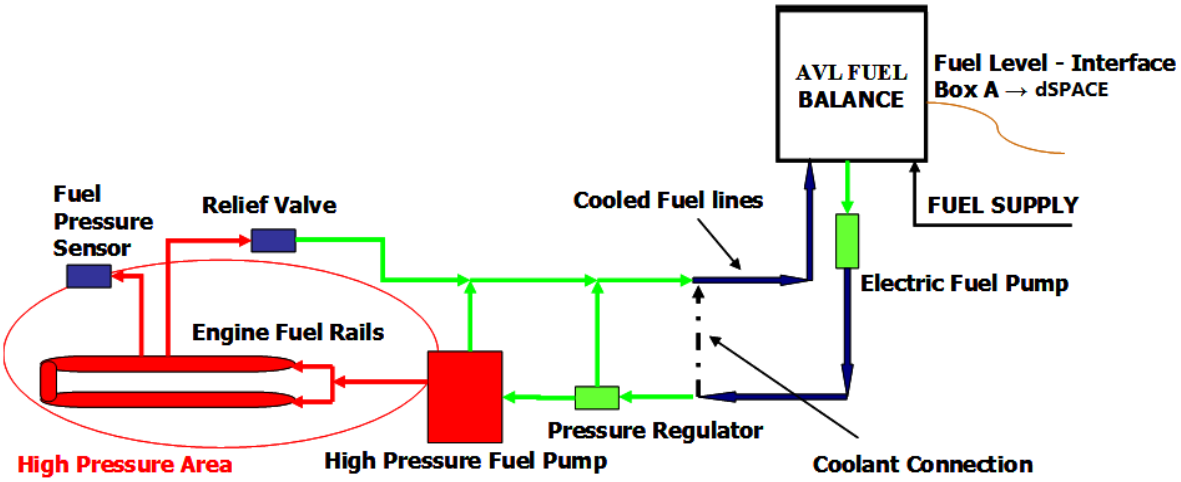

Figure 3.15 Sketch of Fuel System on the Research Engine

3.5.3 Emissions Measurements

Depending on the purposes, the engine emissions are measured by different objectives and equipment. For SI combustion mode, owing to the utilization of a three-way catalyst and the stoichiometric combustion, the HC, CO and NO_x emissions were not tested. However, as this engine is equipped with GDI injectors, PM concentration and weight levels are tested. On the other hand, for HCCI combustion mode, the λ can be higher, to implement lean combustion, and the three-way catalyst cannot work properly. Therefore, the HC emissions' level with different operating conditions was captured.

3.5.3.1 THE HORIBA MEXA-7100DEGR GAS TOWER

The Horiba MEXA-7100DEGR gas tower which was used for this study is shown in Figure 3.16.

Figure 3.16 Horiba Mexa-7100DEGR Gas Tower

The engine emissions were sampled near the exhaust port and went through a filter and heat line to maintain the temperature at around 190^{o}C. It is necessary to purge the Horiba sample line for around 10 minutes to avoid contamination before each experiment, and the Horiba must be calibrated at the beginning by calibration gases. The analyzer specification is shown in Table 3.4.

Table 3.4 The Horiba Analyzer Specification

Analyzer	Components	Principle	Range	T10-90	Noise
AIA-260	CO-L	NDIR (250 mm cell)	100-3K ppm	3.5 s	±1.0 % FS
	CO-H	NDIR (10 mm cell)	1-10 % vol	2.0 s	±1.0 % FS
	CO2	NDIR (10 mm cell)	1-16 % vol	2.0 s	±1.0 % FS
FCA-266	THC	Hot-FID	100-20K ppmC	2.0 s	±1.0 % FS
	NOx	CLD (atmospheric)	100-5K ppm	3.5 s	±1.0 % FS
IMA-262	O2	MPD	10-25 % vol	2.5 s	±1.0 % FS
	EGR-CO2	NDIR (10 mm cell)	1-10 % vol	2.0 s	±1.0 % FS

In order to process the emissions data from the HORIBA efficiently, a MATLAB script was written by the author.

3.5.3.2 THE DMS500 FAST PARTICLE ANALYZER

The DMS500 was used for measuring the PM emissions' size and concentration to provide data to calibrate the emissions' model of the SI engine; the equipment is shown in Figure 3.17.

Figure 3.17 The DMS500 Fast Particle Analyzer

DMS stands for Differential Mobility Spectrometer, which is able to provide a size/number spectrum for particles between 5nm and 1000nm. A classifier column is utilized to separate the charged particles according to their electrical mobility. The sample is surrounded by clean air and travels around a central high voltage electrode, which classifies the sample flow from the electrometer rings. The schematic of the classifier is shown in Figure 3.18 (Cambustion 2011).

A plug-in excel tool is used for data processing, which is developed by the COMBUSTION company. For all the data output, the DMS500 calculates the concentration with a standard temperature and pressure (0^{o}C and 100kPa). In addition, the author developed a MATLAB script to process the data for model development.

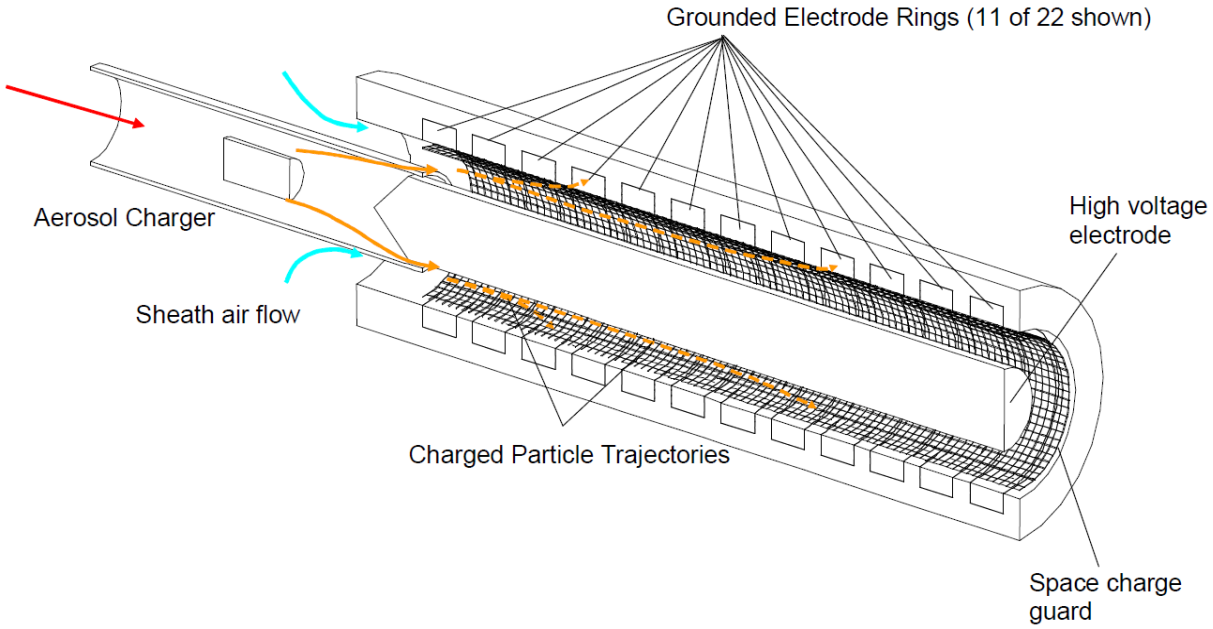

Figure 3.18 The DMS500 Classifier

3.6 Raw Experimental Data Processing

In order to have reliable and repeatable experimental results, each steady status operating point was sampled for 3 times and each time includes 100 engine cycles. For the purpose of processing the experimental data efficiently, a MATLAB script programme was developed by the author and Dr. Jacek Misztal. There are three main functions of the programme:

1. to average the captured steady status experimental data,
2. to normalize the averaged experimental results,
3. to calculate the required engine performance parameters.

Moreover, as it is not possible to ignore the cylinder-to-cylinder and cycle-to-cycle variations for this V6 engine, the coefficient of the variations (COV) of IMEP for SI and HCCI mode experiments are kept lower than 5% and 3% respectively, for the purpose of guaranteeing the reliability of the captured experimental data. The COV values for SI and HCCI are shown in Figure 3.19 and Figure 3.20.

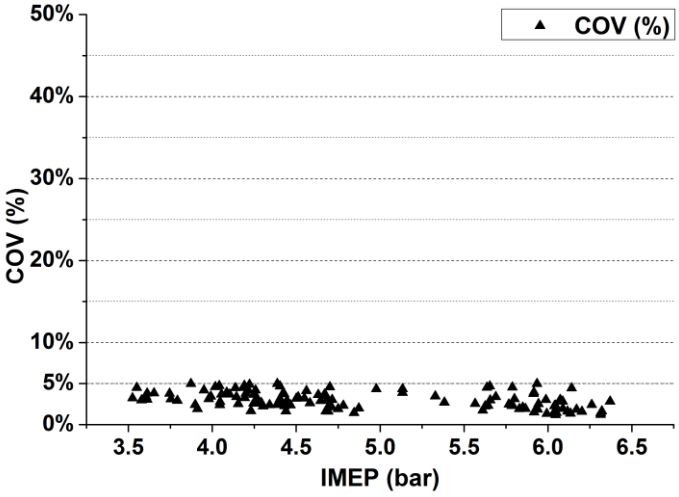

Figure 3.19 The COV of SI

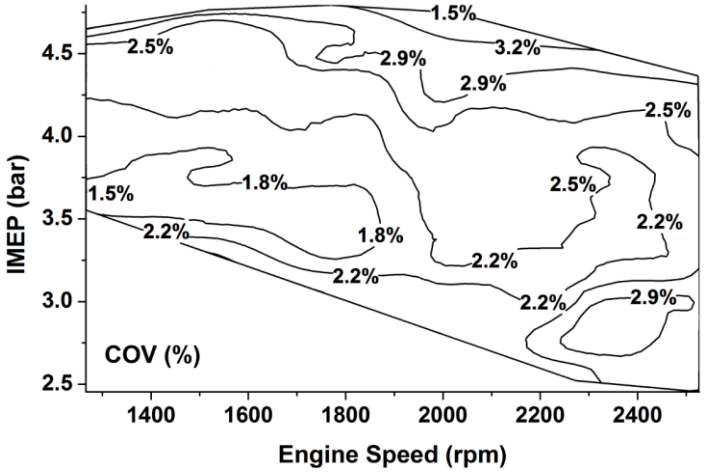

Figure 3.20 The COV of HCCI

Some of the most important equations in the script to evaluate the engine performance will be given afterwards. The Matlab script was developed by Mr. Jacek Misztal initially and complemented by the author.

Heat Release Rate (HRR): in the script, the net HRR ($dQ_n/d\theta$) is calculated by an equation described by Stone in his book, and which is given by (Heywood 1988):

$$\frac{dQ_n}{d\theta} = \frac{\gamma}{\gamma - 1} P \frac{dV}{d\theta} + \frac{1}{\gamma - 1} V \frac{dP}{d\theta} \ ,$$

where Q_n is the net heat release; θ is the crank angle; γ is the heat capacity ratio; V is the in-cylinder volume; P is the in-cylinder pressure. $dV/d\theta$ and $dP/d\theta$ indicate the changes of in-cylinder volume and pressure when the crank angle is changed. The calculation method of HRR is based on the first law of thermodynamics and the assumption of fully mixed in-cylinder mixtures.

Mass Fraction Burned (MFB): in the script, the MFB is calculated by the method of Rassweiler and Withrow (1938), which is given by:

$$MFB = \sum_{0}^{i} \Delta P \Big/ \sum_{0}^{N} \Delta P \ ,$$

where i is the current crank angle; ΔP is the in-cylinder pressure change; N is the crank angle when the combustion ends.

3.7 Summary

In summary, this chapter is mainly focused on experimental facilities and data processing. A Jaguar SI/HCCI dual mode V6 engine test bench was used for all the experiments. Owing to the CPS system, the engine is able to transfer between SI mode and HCCI mode smoothly. The test bench is also equipped with VVT and a GDI system, which allows researchers to change the valve timing and injection timing flexibly. The dSPACE control system is in charge of test bench control and hardware in-the-loop simulation.

As the engine test bench was unused for quite a long time before the author started to do the experimental tests, the engine test bench and dSPACE control system went through a series of re-configuration, re-calibration, components failure fixing and renovation works by the author, with technical supports from Dr. Jacek Misztal. The author also updated the previous MATLAB data processing script and developed a new programme to process and normalize the engine's HC, CO, NO_x and PM emissions efficiently.

Chapter 4 Engine Model Development and Multi-objective Optimal Feedback Control Strategy

In this chapter, the detailed descriptions of SI and HCCI engine modelling methodology and corresponding multi-objective optimal feedback control strategy are introduced. Because the differences between single cylinder engine modelling and V6 engine modelling are very limited in this study, the modelling of one cylinder of the V6 engine is mainly introduced in this chapter. The V6 engine model is very easy to be derived as long as the single cylinder engine model is established, just take the influences from different intake air flow and the operating phases in each cylinder into account. The detailed methodology of the multi-objective optimal feedback control strategy for optimising SI and HCCI engine performance is presented afterwards.

4.1 Descriptions of the SI Engine Modelling

Based on the analysis and comparisons results in chapter 2, the zero-dimensional single-zone Wiebe function based modelling strategy was used for developing the SI engine model. The

detailed modelling approaches of the second cylinder in bank B of the V6 engine will be introduced in the followed sub-sections.

4.1.1 SI Engine Model Outline

The real-time control oriented SI engine model is developed by Simulink with fixed simulation step. With the aim of designing multi-objective optimal feedback control strategy, the throttle position, the spark timing, the injection timing, the phases of the Intake Valves Opening (IVO) and Exhaust Valves Closing (EVC) are designated as variables in the model. The model consists of four major parts: 1. the engine geometry model, 2. the gas exchange model, 3. the combustion and emissions model, 4. the engine performance evaluation model.

In general, as shown in Figure 4.1, one conventional engine working cycle includes 4 strokes: the intake stroke, the compression stroke, the power stroke and the exhaust stroke. In this model, one SI engine simulation cycle is divided into three periodic steps:

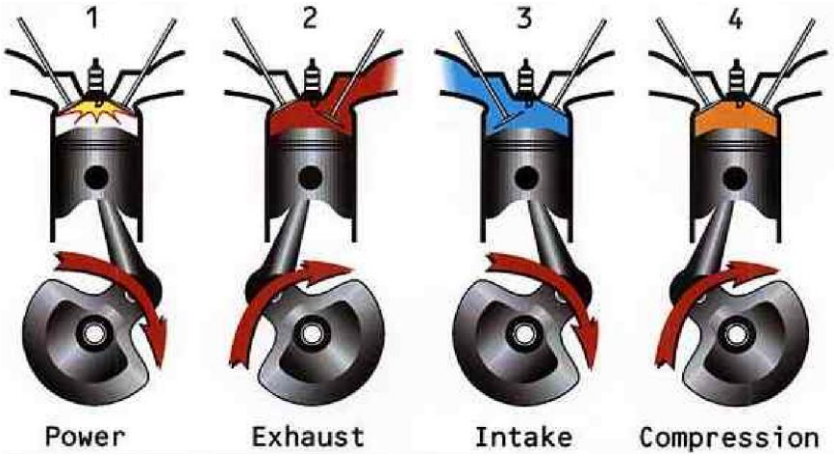

Figure 4.1 The 4 Strokes of Conventional SI Engines

1. The adiabatic compression. This period lasts from IVC to ignition timing. For model simplification, the cylinder leakage affection is ignored in this study, and the duration of heat transfer from cylinder wall is very short, the cylinder is considered as an adiabatic and confined space during this process. Therefore, the in-cylinder pressure and temperature are able to be predicted by the adiabatic compression formulae, which are given by:

$$P_1 {V_1}^{\gamma} = P_2 {V_2}^{\gamma}$$

$${P_1}^{1-\gamma} {T_1}^{\gamma} = {P_2}^{1-\gamma} {T_2}^{\gamma}$$

The whole simulation starts from this process, the in-cylinder pressure and temperature are able to be roughly given as 0.5bar and 430K at the end of intake process, i.e. IVC position.

2. The combustion. The combustion process starts after the spark ignition and ends at EVO. The in-cylinder pressure change is due to two factors: combustion and in-cylinder volume change. The in-cylinder pressure $P(\theta)$ during the combustion duration is able to be calculated by:

$$P(\theta) = \Delta P_c + P(\theta - 1) \cdot \left[\frac{V(\theta - 1)}{V(\theta)} \right]^{\gamma},$$

Equation 4.1 The in-cylinder Pressure Calculation

where ΔP_c indicates the pressure change due to combustion. The fuel MFB is derived from Wiebe function. As a result, HRR and ΔP_c is able to be calculated consequently. In this model, the spark timing is able to be adjusted from 15CAD bTDC to 25CAD bTDC.

3. The Gas exchange phase. This process is defined as the duration from EVO to IVC. The combustion residual gas is exhausted through the exhaust valves during EVO and EVC. In general, in order to exhaust the residual gas completely, the intake valves are needed to be opened a little bit earlier, i.e. positive valves overlap (PVO). For the port fuel injection (PFI) SI engines, the mixture of fresh air and fuel is inhaled into cylinder during intake stroke. In this case, the GDI technology is equipped with the V6 engine. Therefore, only air can be inhaled into the cylinder, thereby higher charging efficiency can be achieved. In order to have the homogeneous in-cylinder air-fuel mixture for guaranteeing stable combustion, the injection timing always is set during the intake stroke and before the bottom dead centre (BDC).

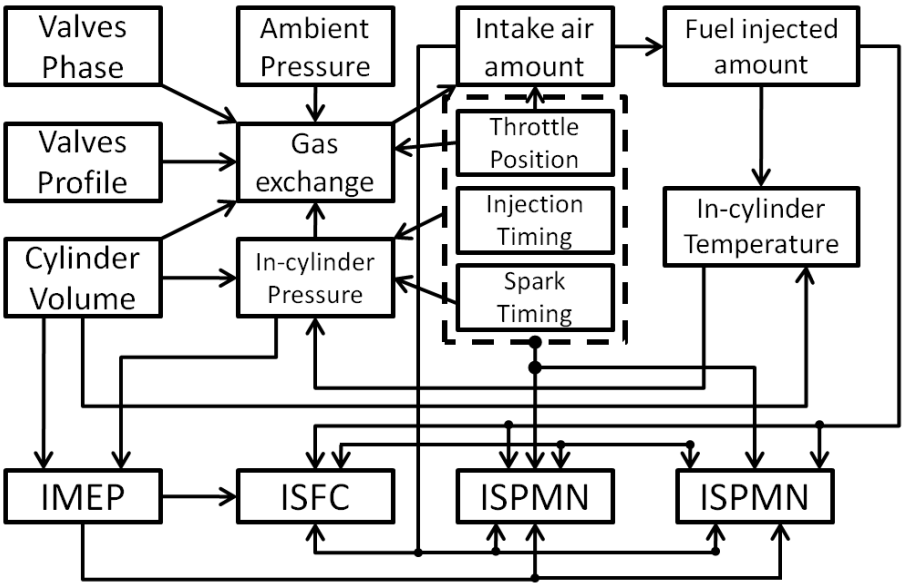

Figure 4.2 The Block Diagram of the SI Engine Model

Figure 4.2 gives the flow chart of the whole SI engine model structure, which indicates the relationships between different engine parameters or modules. The whole model is a highly intercoupling system, with many relationship networks mutually coupled with each other. For instance, the gas exchange model is influenced by in-cylinder pressure, which in turn is influenced by in-cylinder temperature. If we track this circle back to the end, it is able to find that the in-cylinder pressure is a function of intake air flow, which in turn is affected by gas exchange model. Therefore, it should be very careful to link each part of the model together when developing the model. The adjustable ranges of each engine parameters in SI model are given in Table 4.1.

Table 4.1 The Adjustable Ranges of Each Engine Parameters in SI Model

	Throttle Position (deg)	Spark Timing (bTDC)	Injection Timing (bTDC)	EVC (bTDC)	IVO (aTDC)
Min	10^{o}	15CAD	250CAD	-55CAD	-25CAD
Max	15^{o}	25CAD	350CAD	5CAD	35CAD

The detailed descriptions of each main module are given in the following sub-sections.

4.1.2 Model Overview

The control oriented SI model is developed by the author from start to finish. Since the HCCI engine model was developed before the SI model, the development time of the SI engine model is much shorter.

This model is developed by Simulink 7.6 and run with acceleration mode. The detailed model configurations are given in Table 4.2.

Table 4.2 The Detailed Model Configurations of the SI Engine Simulink Model

Model Size	527 KB	**Fixed step size**	1
Block Number	4370	**Solver**	Ode1 (Euler)
Subsystem Number	276	**Start Time**	IVC-719
Type	Fixed step	**Stop Time**	IVC-719+RunningCycles*720-1

The *RunningCycles* item of *Stop Time* indicates the expected simulation engine cycles. Therefore, the model is able to be operated with expected engine cycle number, which benefits the calculation of averaged engine performance parameters. The wiring diagram of the SI Simulink model is shown in Figure 4.3.

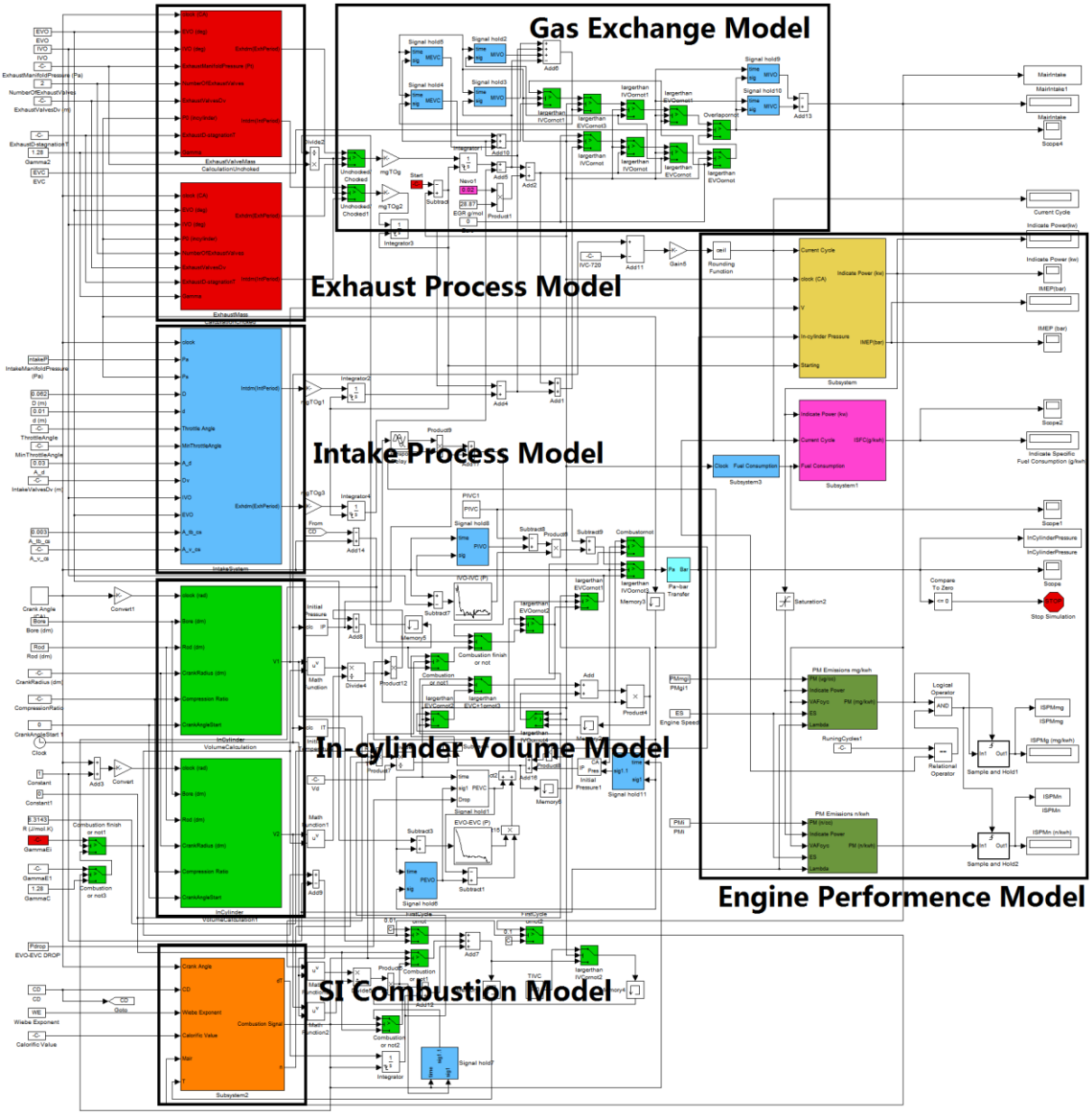

Figure 4.3 The Wiring Diagram of the SI Simulink Model

4.1.3 The Engine Volume Model

As shown in Figure 4.2, the in-cylinder volume directly influences the gas exchange module, in-cylinder pressure module, in-cylinder temperature module and the calculation of IMEP. Therefore, the accurate simulation of in-cylinder volume is critical to the entire engine model. Considering the compression ratio is fixed for this engine, the in-cylinder volume is a periodic function of crank angle and engine geometry parameters only. The dynamic in-cylinder volume is equal to the sum of displacement volume V_d and clearance volume V_c, and which is given by (Stone 1999):

$$V = V_d + V_c = \frac{\pi B^2}{4} \cdot \left[R \cdot (1 - \cos\theta) + L \cdot \left(1 - \sqrt{1 - \left(\frac{R \sin\theta}{L} \right)^2} \right) \right] + \frac{\pi B^2 R}{2(r_c - 1)} \quad ,$$

where V_d is the displacement volume; V_c is the clearance volume; θ is the current crank angle (CAD); B is the bore diameter; R is the crank radius; L is the rod and r_c is the compression ratio. The engine volume model was developed by Simulink and given in Figure 4.4.

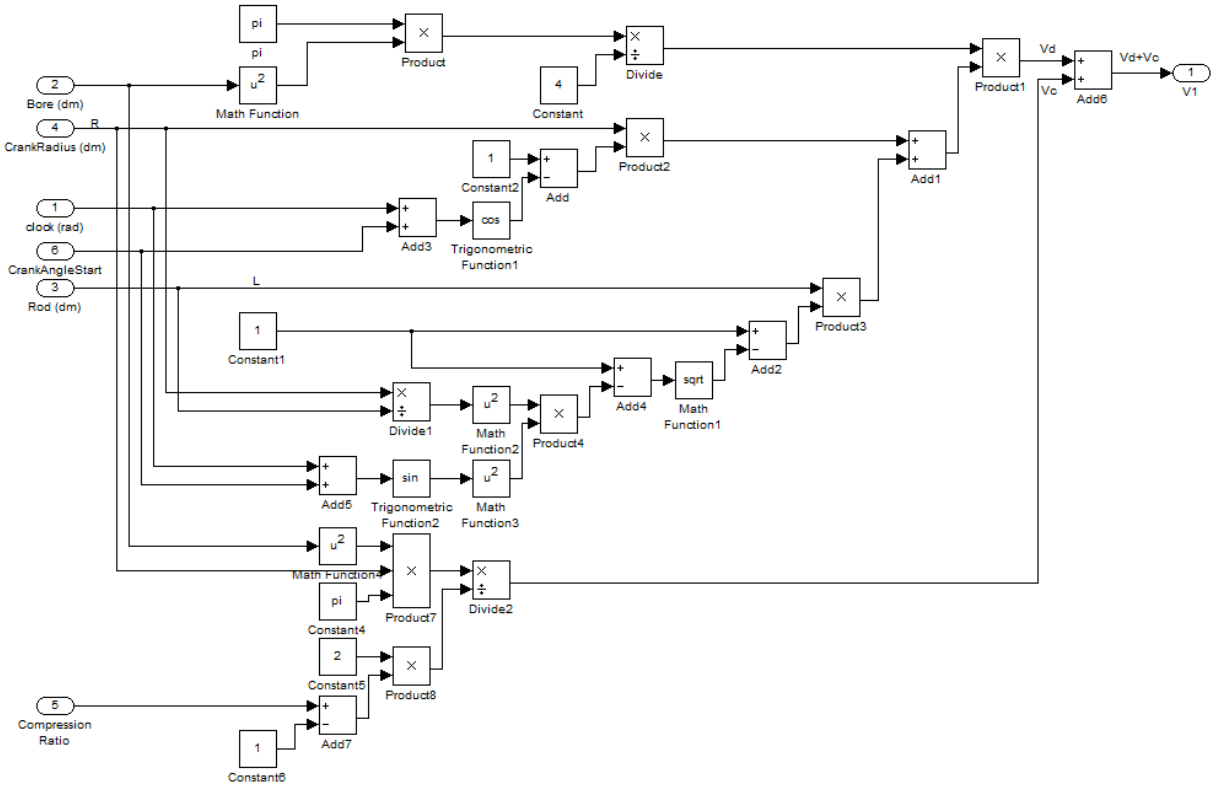

Figure 4.4 The Engine Volume Model

4.1.4 The Gas Exchange Model

From Figure 4.2, it can be found that the gas exchange model plays a very important role in the engine model, which has strong connections with combustion model and engine geometry model etc. The whole gas exchange model includes three parts, i.e. throttle, intake and exhaust valves. The modelling of the air flow through the throttle body is based on one-dimensional, steady, isentropic, compressible ideal gas flow theory. The mass flow through the throttle $\dot{m}_t$ is given by the equation (Karmiggelt 1998):

$$\dot{m}_t = \begin{cases} C_d \cdot A(\phi) \dfrac{P_0}{\sqrt{RT_0}} \cdot \sqrt{\gamma \cdot \left(\dfrac{2}{\gamma+1}\right)^{\frac{\gamma+1}{\gamma-1}}} & \gamma_t \le 1 \\ C_d \cdot A(\phi) \cdot \dfrac{P_0}{\sqrt{RT_0}} \cdot \sqrt{\gamma \cdot \left(\dfrac{2}{\gamma+1}\right)^{\frac{\gamma+1}{\gamma-1}} \cdot h(\gamma_t)} & \gamma_t > 1 \end{cases},$$

where C_d is the discharge coefficient; P_0 and T_0 is the upstream air pressure and temperature, i.e. ambient pressure (1bar) and temperature (300K); $A(\phi)$ is the efficient throttle open area and which is a function of the throttle angle ϕ, and which is given by:

$$A(\phi) = \frac{\pi}{4} \cdot D^2 \cdot \left(1 - \frac{\cos(\phi + \phi_0)}{\cos(\phi_0)}\right),$$

where D is the throttle diameter; and ϕ_0 is the angle of the throttle plate when it is closed.

The $h(\gamma_t)$ accounts for the pressure influence in subsonic flow and which is given by:

$$h(\gamma_t) = \sqrt{\frac{\gamma+1}{\gamma-1}} \cdot \sqrt{\gamma_t^{2/\gamma} - \left(\frac{2}{\gamma+1}\right) \cdot \gamma_t^{\frac{\gamma+1}{\gamma}}},$$

where γ_t is the parameter indicates the change of the pressure after and before the throttle plate, and which is given by:

$$\gamma_t = \frac{P_t}{P_0} \cdot \left(\frac{\gamma+1}{2}\right)^{\frac{\gamma}{\gamma-1}},$$

where P_t is the downstream air pressure.

The mass flow through the intake and exhaust valves $\dot{m}_v$ during the intake and exhaust strokes are given by the formulae (Heywood 1988):

$$\dot{m}_v = \frac{C_D A_R P_0}{\sqrt{RT_0}} \cdot \left(\frac{P_T}{P_0}\right)^{1/\gamma} \cdot \left[\frac{2\gamma}{\gamma - 1} \cdot \left[1 - \left(\frac{P_T}{P_0}\right)^{(\gamma-1)/\gamma}\right]\right]^{1/2},$$

For unchoked flow,

$$\frac{P_T}{P_0} > \left[\frac{2}{\gamma + 1}\right]^{\gamma/(\gamma-1)},$$

and

$$\dot{m}_v = \frac{C_D A_R P_0}{\sqrt{RT_0}} \cdot \sqrt{\gamma} \cdot \left[\frac{2}{\gamma + 1}\right]^{(\gamma+1)/2(\gamma-1)},$$

For choked flow,

$$\frac{P_T}{P_0} \leq \left[\frac{2}{\gamma + 1}\right]^{\gamma/(\gamma-1)},$$

where A_R is the effective open area of the valves; P_0 is the upstream stagnation pressure; T_0 is the downstream stagnation temperature and P_T is the downstream stagnation pressure; C_D is the discharge coefficient; R is gas constant and γ is specific heat ratio. The SI engine intake and exhaust system model was developed by Simulink and given in Figure 4.5 and Figure 4.6.

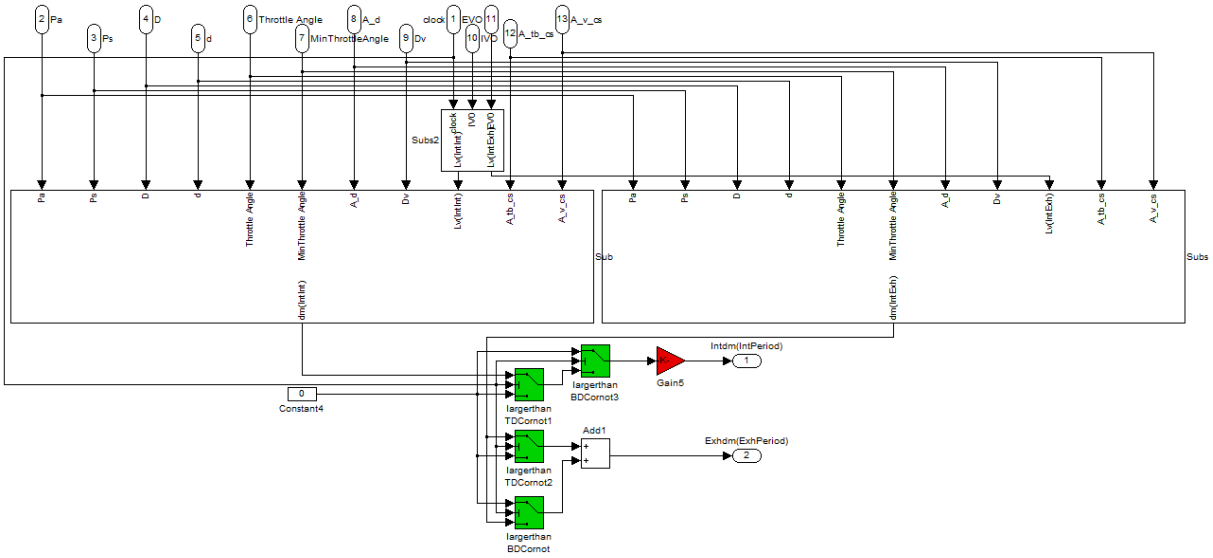

Figure 4.5 The Intake System Model of the SI Engine

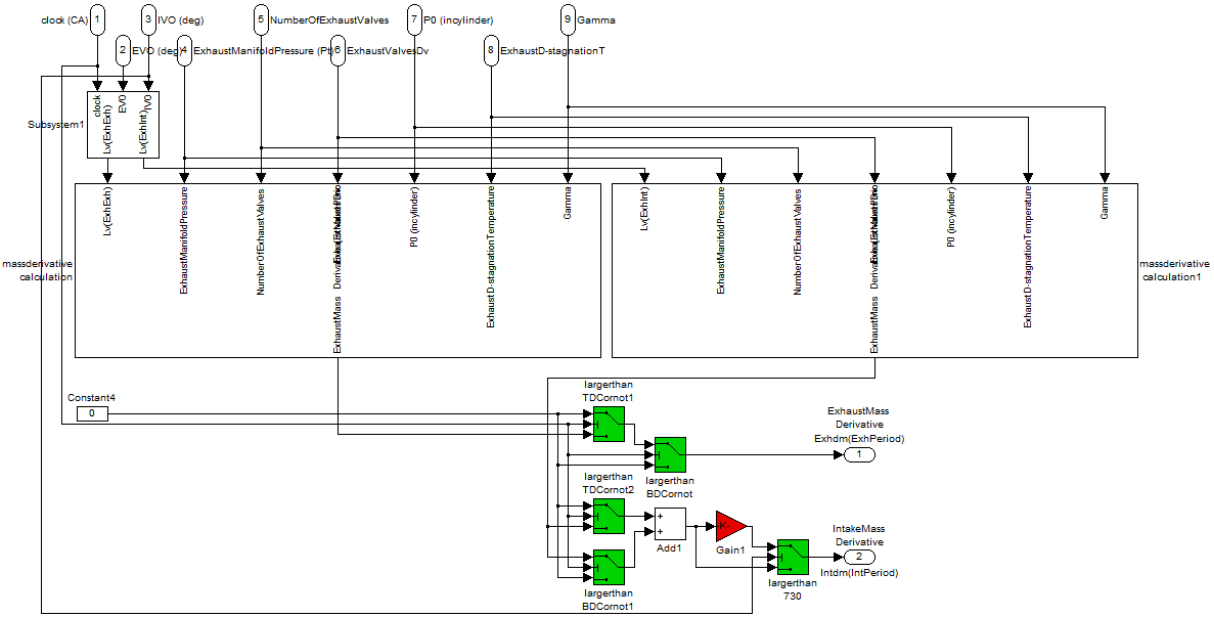

Figure 4.6 The Exhaust System Model of the SI Engine

It is able to find that the gas exchange modelling is not only needed to consider the intake and exhaust system, but also is requested to couple the affection from the piston movement. Both of them determine the pressure and temperature difference between the inside and outside of the cylinder, which is the most important indicator of gas exchange process.

In order to build the experimental data base to develop the engine model, three different settings of IVO and EVC are given in Figure 4.7. In other words, the adjustable range of IVO and EVC in this model is 25CAD bTDC to 35CAD aTDC and 55CAD aTDC to 5CAD bTDC respectively.

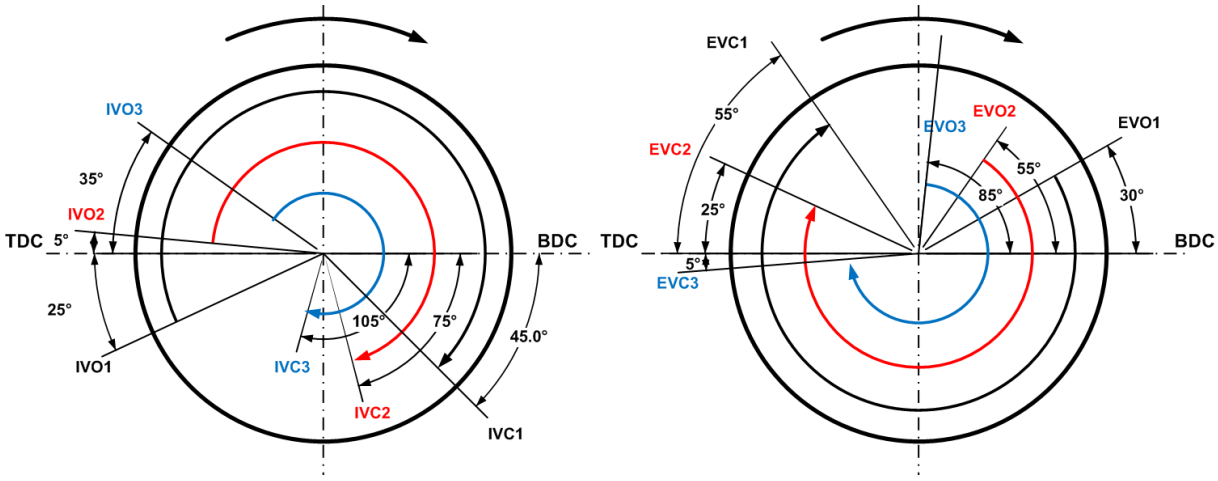

Figure 4.7 The Schematic of Tested Valves Timing for SI Engine Model Development

With different throttle position, IVO and EVC, the intake efficiency, exhaust efficiency and efficient compression ratio are different as well. The thermal efficiency and emissions performances can be optimised with different valves timing combinations.

4.1.5 The SI Combustion Model

For real-time control oriented engine modelling, the combustion model cannot involve detailed chemistry reactions due to the high time consumptions. As it discussed in chapter 2, the zero-dimensional single-zone Wiebe model was used for developing the SI engine

combustion module of this model. The end of combustion is defined as the position where the MFB reaches 99%. The applied Wiebe function is given by (Wiebe 1962, Ghojel 2010):

$$X_{MFB} = 1 - e^{-4.6052((\theta-\theta_0)/\Delta\theta_b)^{m+1}} \quad ,$$

where, X_{MFB} is the mass fraction burned; θ is the crank angle; θ_0 is the crank angle when the combustion starts; $\Delta\theta_b$ is the combustion duration; m is the combustion characteristic exponent. m is also the shape factor of the S-shape MFB curve to indicate the combustion rates during the different combustion periods, and $\Delta\theta_b$ is the combustion duration which presents the average combustion velocity, their values are influenced by throttle position, spark timing, fuel injection timing, IVO and EVC position. Therefore, in order to have the value of m and $\Delta\theta_b$ with different engine parameter combinations efficiently, the second order polynomial curve fitting method is adopted and given by:

$$\begin{cases} m = p_1 + p_2x_1 + p_3{x_1}^2 + p_4x_2 + p_5{x_2}^2 + p_6x_3 + p_7{x_3}^2 + p_8x_4 + p_9{x_4}^2 + p_{10}x_5 + p_{11}{x_5}^2 \\ \Delta\theta_b = q_1 + q_2x_1 + q_3{x_1}^2 + q_4x_2 + q_5{x_2}^2 + q_6x_3 + q_7{x_3}^2 + q_8x_4 + q_9{x_4}^2 + q_{10}x_5 + q_{11}{x_5}^2 \end{cases} ,$$

here, x_1 indicates the throttle position in degree; x_2 is the spark timing bTDC in CAD; x_3 is the fuel injection timing bTDC in CAD; x_4 presents EVC position aTDC in CAD; x_5 is on behalf of IVO position bTDC in CAD; p_1 to p_{11} and q_1 to q_{11} are corresponding coefficients of different engine parameters which are derived from curve fitting results and the values are given in Table 4.3.

Table 4.3 The Fitting Values of p and q

p_1	p_2	p_3	p_4	p_5	p_6	p_7	p_8	p_9	p_{10}	p_{11}
8.86E+00	-4.26E-01	1.64E-02	-3.86E-01	7.92E-03	-1.66E-03	2.05E-05	2.08E-03	-3.17E-05	6.09E-04	2.91E-05
q_1	q_2	q_3	q_4	q_5	q_6	q_7	q_8	q_9	q_{10}	q_{11}
3.05E+00	1.32E+01	-5.54E-01	-3.10E+00	5.60E-02	-4.25E-02	6.18E-04	-2.36E-02	2.87E-03	2.09E-02	2.69E-03

The development and evaluation of curve fitting were implemented by a Matlab programme. The author tested many different curve fitting function formations. The adopted second order polynomial function has the best compromise of performance between accuracy and complexity. The correlation coefficients R of m and $\Delta\theta_b$ curve fitting results are 0.829 and 0.903, which indicate that the curve fitting results are reliable. As long as the MFB is obtained, the heat release rate and in-cylinder pressure rise are able to be predicted correspondingly. The in-cylinder pressure rise is due to two factors, i.e. combustion and volume change. The equation to calculate in-cylinder pressure is given by Equation 4.1. The SI engine combustion model was developed by Simulink and given in Figure 4.8.

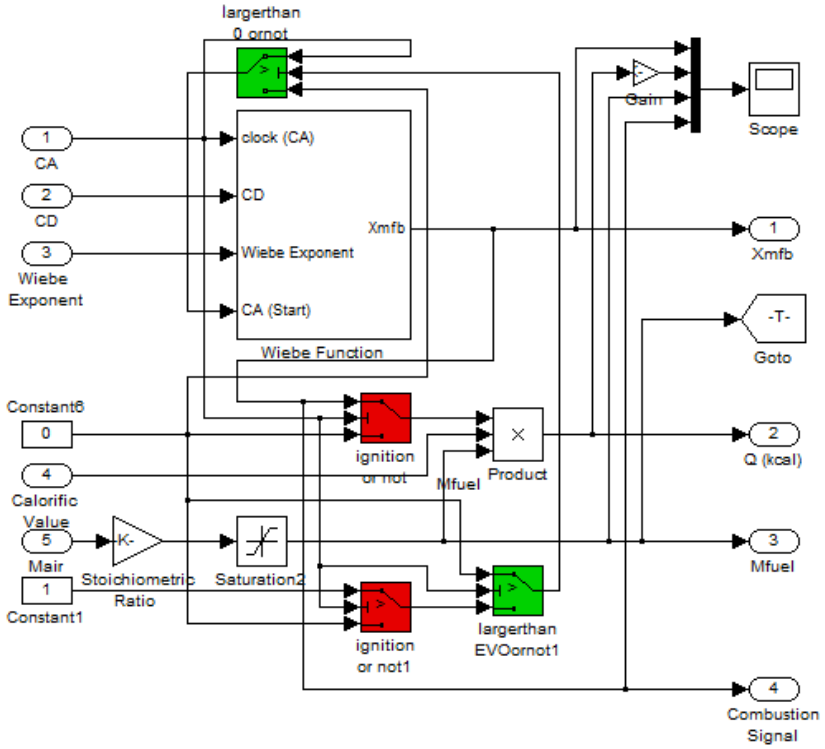

Figure 4.8 The Engine Combustion Model

4.1.6 The SI Engine Performance and Emissions Evaluation Model

Considering that the purpose to build this engine model is to build a virtual test bench for controller design, as a result, the objectives which need to be optimised should be defined. For this case, beside fuel consumption, the GDI technology is adopted in this engine to reduce the PM size and concentration levels are interested as well. Owing to the application of the three-way catalyst and stoichiometric combustion, the NO_x, HC and CO emissions were negligible. Furthermore, in order to have comparability, it is necessary to normalize the fuel consumption and PM emissions values by engine power outputs, i.e. *ISFC*, *ISPMM* and *ISPMN*. The equations which used for calculating ISFC are given by (Heywood 1988):

$$ISFC = \frac{FC}{P_i},$$

Equation 4.2 The Equation to Calculate ISFC

where FC is fuel consumption per hour, which is given by:

$$FC = 30 \cdot fc \cdot N \ ,$$

The ISFC calculation model was developed by Simulink and given in Figure 4.9.

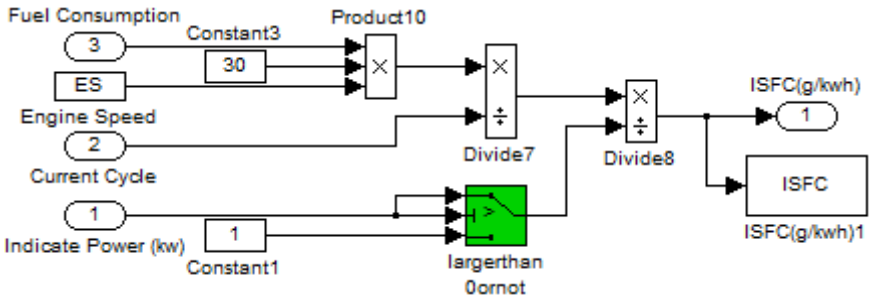

Figure 4.9 The ISFC Calculation Model

N is the engine speed in rpm; fc is the fuel consumptions per engine cycle, and which is obtained from the air intake amount derived from gas exchange model. It is based on the assumption that all the fuel is consumed during the combustion process with stoichiometric ratio, i.e. 14.7. P_i is the engine indicated power, and which is given by (Heywood 1988):

$$P_i = \frac{IMEP \cdot V_d \cdot N}{120} \quad ,$$

$IMEP$ stands for indicated mean effective pressure, and which is obtained from in-cylinder pressure simulation results. The calculation equation is (Heywood 1988):

$$IMEP = \frac{\oint pdV}{V_d} \, .$$

Equation 4.3 The Equation to Calculate IMEP

The equations for calculating $ISPMM$ and $ISPMN$ are given by:

$$ISPMM = \frac{CAM \cdot 10^{-6} \cdot 10^3 \cdot (MFF + MAF) \cdot 60}{P_i \cdot MMEx/22.7\ L/mol} \quad ,$$

$$ISPMN = \frac{AMC \cdot 10^3 \cdot (MFF + MAF) \cdot 60}{P_i \cdot MMEx/22.7\ L/mol} \, .$$

$ISPMM$ stands for indicated specific particulate matter by mass in g/kWh; $ISPMN$ stands for indicated specific particulate matter by number in n/kWh ; CAM stands for concentration accumulation mode weighted by mass with unit of $\mu g/cc$; AMC presents the accumulation mode concentration in n/cc; MFF and MAF are the fuel and air mass flow rate in g/min; $MMEx$ is the molar mass of emissions in g/mol.

Because the emission model is used for controller design purposes, a compromise between accuracy and complexity is required. In this case, the predictions of CAM and AMC are obtained from a 5-dimensional linear interpolation model. This is mainly because that CAM and AMC are very sensitive to some engine parameters. It is very hard to find a fitting function to predict PM emissions. The five dimensions are throttle angle, spark timing, injection timing, IVO and EVC position respectively. The detailed modelling codes of the 5-dimensional linear interpolation are presented in Appendix.

4.1.7 The Testing Matrix

The tests matrix was used to provide experimental data to develop the SI engine combustion and PM emissions model is shown in Table 4.4. The units of throttle, spark timing, injection timing, IVO and EVC are degree, CAD bTDCc, CAD bTDCc, CAD aTDC and CAD bTDC respectively. The main reason to design the testing matrix like this is to cover the stable operating window as much as possible.

It is able to find that the tests matrix includes 108 groups of experimental data which include engine and PM emissions performance. The tests matrix covered a wide possible combinations range of different engine variables with a fixed engine speed- 1500 rpm. It is able to provide enough parameters to fit the combustion characteristic exponent m and combustion duration $\Delta\theta_b$ in a very wide engine operating range. Thanks to the high flexibility of the dSPACE control system, the different combinations of engine parameters are easy to be implemented on the test bench and the engine calibration maps do not need to modify. In addition, the experimental data of PM emissions are utilized to build the PM emissions interpolation model. Furthermore, the design of the test matrix is based on the compromise between experimental groups' number and model accuracy. Otherwise, it is more like a look-up table model. Altogether, it is desired to have a simple test matrix for obtaining accurate simulation results. This principle applies to the design of the test matrix for HCCI model.

Table 4.4 The Testing Matrix of SI Engine Experiments (Engine Speed = 1500rpm)

Throttle	Spark	Injection	IVO	EVC	Number
10	15	250	-25	-55	1
				-25	2
				5	3
			5	-55	4
				-25	5
				5	6
			35	-55	7
				-25	8
				5	9
		300	-25	-55	10
				-25	11
				5	12
			5	-55	13
				-25	14
				5	15
			35	-55	16
				-25	17
				5	18
		350	-25	-55	19
				-25	20
				5	21
			5	-55	22
				-25	23
				5	24
			35	-55	25
				-25	26
				5	27

Throttle	Spark	Injection	IVO	EVC	Number
10	25	250	-25	-55	28
				-25	29
				5	30
			5	-55	31
				-25	32
				5	33
			35	-55	34
				-25	35
				5	36
		300	-25	-55	37
				-25	38
				5	39
			5	-55	40
				-25	41
				5	42
			35	-55	43
				-25	44
				5	45
		350	-25	-55	46
				-25	47
				5	48
			5	-55	49
				-25	50
				5	51
			35	-55	52
				-25	53
				5	54

Throttle	Spark	Injection	IVO	EVC	Number
15	15	250	-25	-55	55
				-25	56
				5	57
			5	-55	58
				-25	59
				5	60
			35	-55	61
				-25	62
				5	63
		300	-25	-55	64
				-25	65
				5	66
			5	-55	67
				-25	68
				5	69
			35	-55	70
				-25	71
				5	72
		350	-25	-55	73
				-25	74
				5	75
			5	-55	76
				-25	77
				5	78
			35	-55	79
				-25	80
				5	81

Throttle	Spark	Injection	IVO	EVC	Number
15	25	250	-25	-55	82
				-25	83
				5	84
			5	-55	85
				-25	86
				5	87
			35	-55	88
				-25	89
				5	90
		300	-25	-55	91
				-25	92
				5	93
			5	-55	94
				-25	95
				5	96
			35	-55	97
				-25	98
				5	99
		350	-25	-55	100
				-25	101
				5	102
			5	-55	103
				-25	104
				5	105
			35	-55	106
				-25	107
				5	108

4.2 Descriptions of the HCCI Engine Modelling

From the discussion in chapter 2, the *AFBR* approach is utilized to simulate the HCCI combustion process. Because the combustion modes and implement approaches of HCCI and SI engines are totally different, the modelling steps and principles are different too. Basically, the HCCI model is more complex than the SI model. The detailed modelling approaches for each module are given in the following sub-sections.

4.2.1 The HCCI Engine Model Outline

For the HCCI model described in this study, the Negative Valve Overlap (NVO) strategy is used for trapping the residual gas, which provides heat of the residual gas to promote the HCCI combustion for the next cycle (Wilson, Xu et al. 2006). One HCCI engine cycle is divided into six periodic steps which are shown in Figure 4.10.

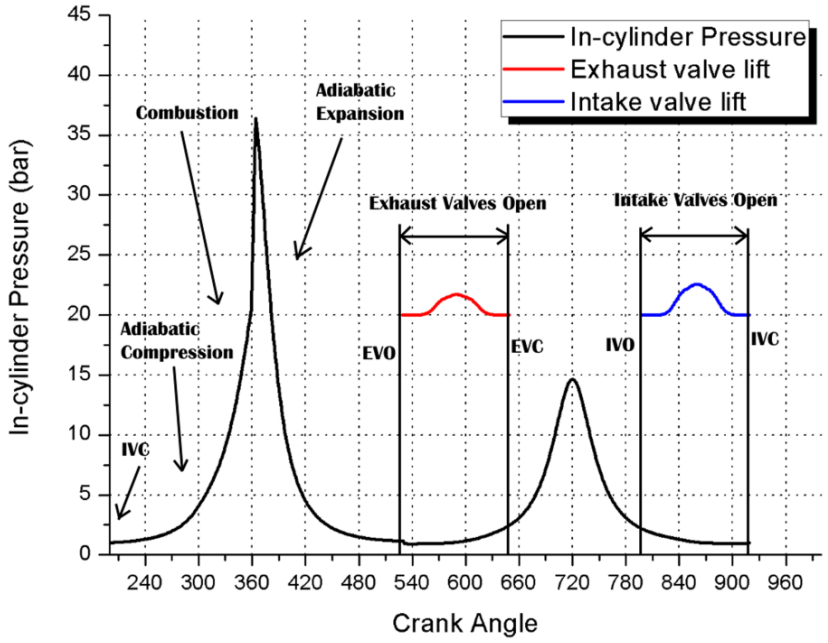

Figure 4.10 In-cylinder Pressure with NVO Strategy

1. The adiabatic compression. The model starts from this process. This step lasts between the IVC and the start phase of auto-ignition. The in-cylinder pressure and temperature are approximately equal to 1bar and 430K respectively when the intake valves are closed. As a result, the initial conditions are obtained. This step is finished when auto-ignition occurs.

2. The combustion. When the in-cylinder temperature, pressure and components reach the ignition conditions, HCCI combustion occurs. The auto-ignition position, combustion duration and mass fraction burned are given by curve fitting results and empirical functions in this model.

3. The adiabatic expansion. After the combustion process finishes, adiabatic expansion occurs until exhaust valve opens; the high pressure of in-cylinder gas does positive work on the piston.

4. The exhaust phase. This is the period between Exhaust Valves Open (EVO) and Exhaust Valves Close (EVC). The residual gas exits through the exhaust valves. Because the EVC is prior to IVO for the NVO based HCCI engine, the exhaust phase and intake phase are two independent processes and are separated by the recompression process, which is one of the most important differences from SI engines.

5. The recompression. This is the period between Exhaust Valves Close (EVC) and Intake Valves Open (IVO).The residual gas is trapped during this process, in which the high temperature of burned gas is to promote the auto-ignition for the next cycle.

6. The intake phase. This is the period between Intake Valves Open (IVO) and Intake Valves Close (IVC). The intake air and trapped residual gas will be mixed with each other during this phase. The intake air amount and effective compression ratio are determined by the residual gas ratio and the timing of the IVO.

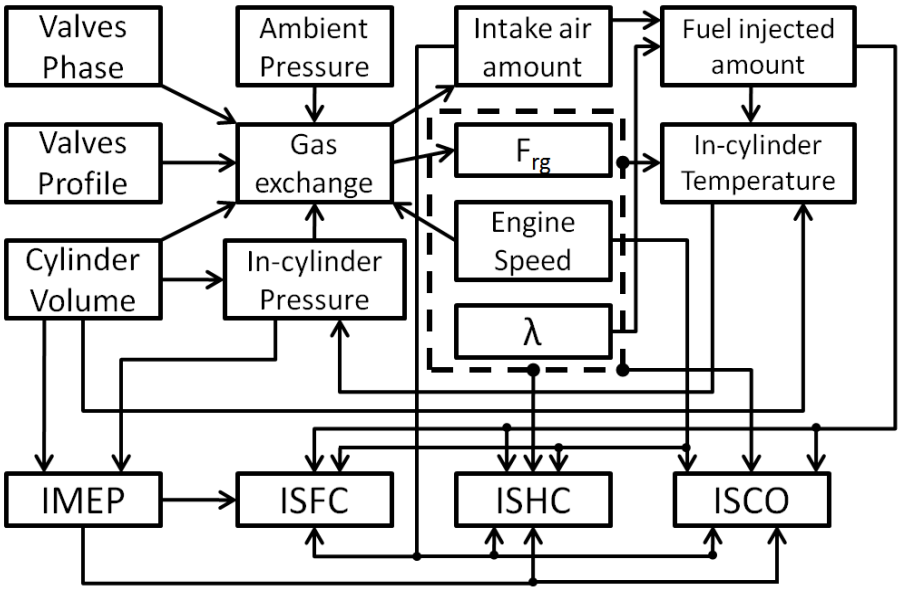

Figure 4.11 The Block Diagram of the HCCI Engine Model

The block diagram of the HCCI engine model is shown in Figure 4.11. Again, it is able to find that the gas exchange module and combustion module played a very important role in the engine model. As one of the most important parameters, the in-cylinder temperature is used to calculate the in-cylinder pressure. The main steps to simulate the in-cylinder temperature of this HCCI engine model are shown in Figure 4.12.

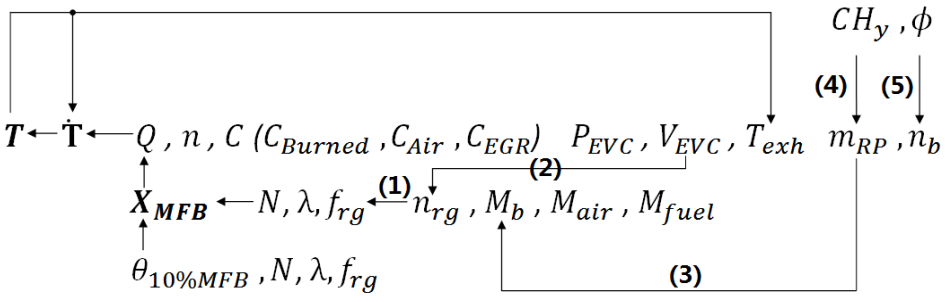

Figure 4.12 The Relationship between the Heat Release Amount and Other Related Parameters

The calculation steps are given by (Qin, Xie et al. 2005):

$$f_{rg} = \frac{n_{rg} \cdot M_b}{n_{rg} \cdot M_b + M_{air} + M_{fuel}}$$

$$n_{rg} = \frac{P_{EVC} \cdot V_{EVC}}{R \cdot T_{exh}}$$

$$M_b = \frac{m_{RP}}{n_b}$$

$$m_{RP} = 32 + 4\phi\left(1 + 2 \times \frac{4}{4+y}\right) + 28.16 \times 3.773$$

$$n_b = \left(1 - \frac{4}{4+y}\right) \times \phi + 1 + 3.773$$

Where $\dot{T}$ is the heat release rate; C is the specific heat; X_{MFB} and $\theta_{10\%MFB}$ is the mass fraction burned and MFB10 position, which are derived from N, λ and f_{rg}; N is engine speed; f_{rg} is the mass fraction of residual gas; n_{rg} is the mole number of residual gas; M_b is the molecular weight of the burned mixture; M_{air} is the mass of air; M_{fuel} is the mass of fuel; m_{RP} is the mass of mixture (burned or unburned); n_b is the number of moles of burned mixture; ϕ is the fuel/air equivalence ratio; CH_y is the formula of gasoline; and y is the atom number ratio of H and C of gasoline. For calculating heat release rate, the calorific value of gasoline is assumed equal to $4.6 \times 10^7 J/kg$. The ratio of N_2 and O_2 in air is 3.773. Equations 1 to 5 are used to calculate the parameters above. The adjustable ranges of each engine parameters in HCCI mode are given in Table 4.5.

Table 4.5 The Adjustable Ranges of Each Engine Parameters in HCCI Mode

	Engine Speed	EVC (bTDC)	IVO (aTDC)	λ
Min	1250	75	60	1.0
Max	2500	95	80	1.2

The detailed descriptions of each main module are given in the following sub-sections.

4.2.2 Model Overview

This model is developed by the author from start to finish like the SI engine model. The simulation tool is Simulink 7.6, and all the applied blocks come from the basic block library. The detailed model configurations are given in Table 4.6.

Table 4.6 The Detailed Model Configurations of the HCCI Engine Simulink Model

Model Size	598 KB	**Fixed step size**	1
Block Number	5083	**Solver**	Ode1 (Euler)
Subsystem Number	127	**Start Time**	IVC-719
Type	Fixed step	**Stop Time**	IVC-719+RunningCycles*720-1

The wiring diagram of the HCCI Simulink model is shown in Figure 4.13.

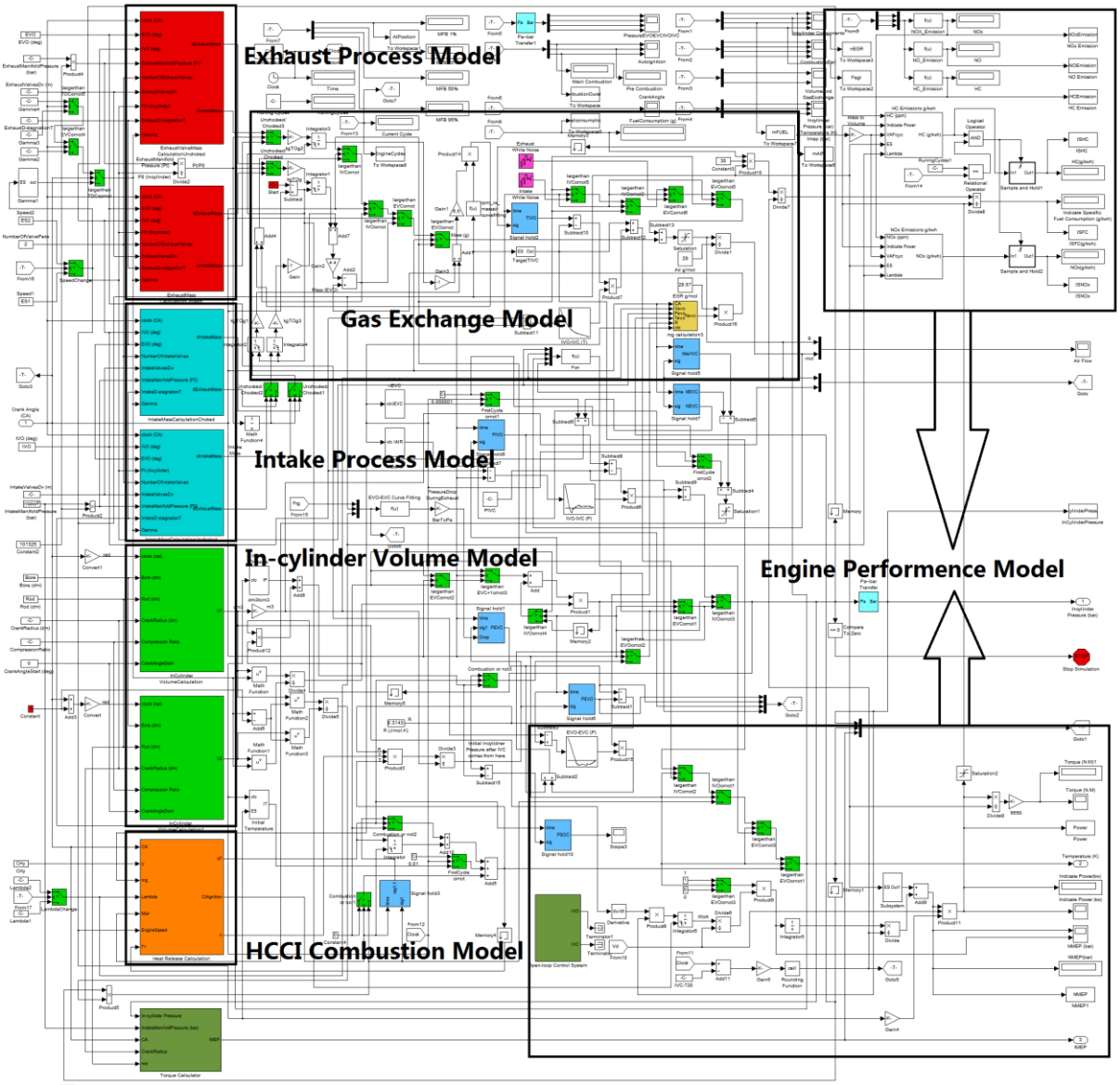

Figure 4.13 The Wiring Diagram of the HCCI Simulink Model

4.2.3 The Gas Exchange Model

The differences of the gas exchange processes between SI combustion mode and HCCI combustion mode are remarkable. In the first place, in order to inhale more air into the

cylinder, the throttle plate will be fully opened for NVO based HCCI engine. Therefore, it is unnecessary to involve the throttle model in the engine model. Secondly, the NVO strategy is used in the HCCI combustion mode. The intake process and exhaust process are separated by the recompression phase. The mass of residual gas at EVC and IVO are the key connectors between these three phases. The recompression phase is considered as adiabatic compression and expansion process. The equations which used to simulate the HCCI intake and exhaust process through intake and exhaust valves are similar with SI engine and given in the pre-section.

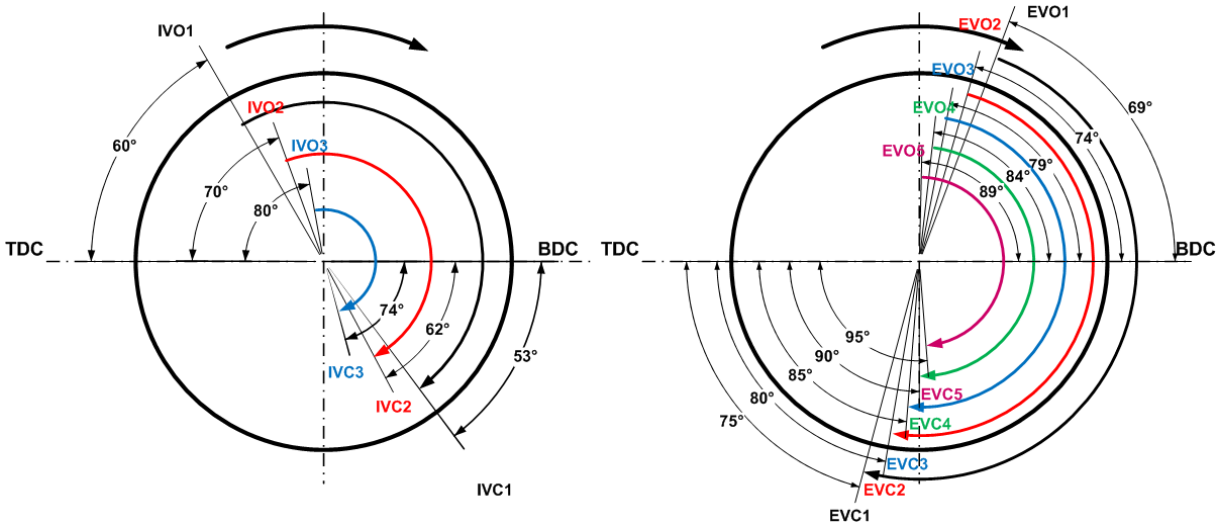

Figure 4.14 The Schematic of Tested Valves Timing for HCCI Engine Model Development

In this case, the adjustable range of IVO and EVC which allows stable HCCI combustion without misfire or large cycle-to-cycle variation are 60-80CAD aTDC and 75-95CAD bTDC respectively. With the aim to build the experimental database for model development, there are 3 and 5 different settings of IVO and EVC respectively. Because the EVC position mainly determines the trapped internal EGR fraction and thereby affecting power output, the

sampling interval for EVC is only 5 CAD. The detailed settings of IVO and EVC are given in Figure 4.14.

4.2.4 The HCCI Combustion Model

The combustion model is the most important part of the HCCI engine model and it influences the simulation results and computation time remarkably. Since HCCI combustion combines the features of SI (homogeneous) and CI (compression ignition), a modified Watson *AFBR* (statistical model) was used in this model to describe the HCCI combustion. Following a detailed analysis of HCCI combustion process, the combustion process was separated into two stages: the pre-combustion process (1-10% MFB) and the main-combustion process (10-90% MFB). The equations used to calculate the pre-combustion process are given by:

$$X_{\mathrm{MFB-Pre}} = C_{\mathrm{p1-pre}} \cdot \exp(C_{\mathrm{p2-pre}}\theta) \ ,$$

whereas the following equations were used to calculate the main-combustion process,

$$X_{\mathrm{MFB\text{-}Main}} = 1-(1-\tau^{C_{\mathrm{p1-main}}})^{C_{\mathrm{p2-main}}},$$

$$\tau = \frac{\theta - \theta_{10\%\mathrm{MFB}}}{\Delta\theta_b} \ ,$$

$$C_p = a_1 + a_2 F_{rg} + a_3 {F_{rg}}^2 + a_4 {F_{rg}}^3 + a_5 N + a_6 N^2 + a_7 N^3 + a_8 \lambda + a_9 \lambda^2 + a_{10} \lambda^3 \ ,$$

where C_{p1} and C_{p2} are shape factors and described as functions of EGR fraction F_{rg}; engine

speed N; and the ratio of actual AFR to stoichiometric for a given mixture λ, which are three of the most important parameters effecting HCCI combustion; $\theta_{10\%MFB}$ is the angle when 10% MFB occurs; $\Delta\theta_b$ is the combustion duration. The calculation approach for F_{rg} was given by Qin. The equation for calculation of the main-combustion process MFB was transformed from the Watson *AFBR* by letting the proportionality factor of flame propagation equal to zero, which was aimed to omit the effect of diffusion combustion. The MFB was calculated by twice curve fitting, i.e. (1) Experimental data of MFB and τ was used to determine the shape factors C_{p1} and C_{p2} by curve fitting, (2) Using these values, the constants of the curve fitting equations were then derived from the experimental data of the engine speeds, EGR fractions and λ. There were 90 groups of experimental data used for the curve fittings (Table 4.8). In order to implement the HCCI engine simulation within a wide engine operating range, the ranges of engine speed, λ, IVO and EVC were set as 1250-2500 rpm, 1.0-1.2, 60-80CAD aTDC and 75-95CAD bTDC respectively.

The auto-ignition process of HCCI combustion is mainly controlled by the in-cylinder conditions, including temperature, chemistry components and concentrations. However, these three in-cylinder parameters are very difficult to calculate in real-time accurately for model development. On the other hand, these three in-cylinder parameters are strongly related to internal EGR fraction, engine speed and λ. Therefore, in order to assure the high simulation speed and acceptable model accuracy, the combustion duration (10%-90%) and auto ignition position (MFB 10%) were calculated by curve fitting and described as a function of F_{rg}, N and λ. The curve fitting matrices are given by:

$$\begin{bmatrix} C_{\mathrm{p1-pre}} \\ C_{\mathrm{p2-pre}} \\ C_{\mathrm{p1-main}} \\ C_{\mathrm{p2-main}} \\ \Delta\theta \\ AIP \end{bmatrix} = A_{ij} \begin{bmatrix} 1 \\ F_{rg} \\ F_{rg}^2 \\ F_{rg}^3 \\ N \\ N^2 \\ N^3 \\ \lambda \\ \lambda^2 \\ \lambda^3 \end{bmatrix},$$

$$A_{ij} = \begin{bmatrix} 1.953 & -0.135 & 0.271 & -0.165 & -0.00026 & 1.36E-07 & -2.29E-11 & -4.761 & 4.296 & -1.287 \\ -183.314 & -25.827 & 55.691 & -40.538 & -0.0112 & 6.40E-06 & -1.10E-09 & 533.706 & -485.145 & 146.606 \\ -142.518 & 6.353 & -10.347 & 4.849 & 0.004 & -2.25E-06 & 3.90E-10 & 377.983 & -339.083 & 101.180 \\ 838.106 & -127.956 & 342.439 & -275.044 & 0.099 & -0.00005 & 9.67E-09 & -2423.467 & 2220.023 & -674.407 \\ 9687.199 & 290.938 & -654.481 & 559.120 & 0.217 & -0.00011 & 2.09E-08 & -26777.426 & 24195.269 & -7263.688 \\ 8170.285 & 719.314 & -1616.278 & 1199.123 & 0.064 & -0.00003 & 6.88E-09 & -21613.764 & 19540.247 & -5871.618 \end{bmatrix},$$

where AIP is the Auto-Ignition Position; A_{ij} is the correlation coefficients matrix. In order to evaluate the curve fitting results, the correlation coefficients R for each fitting are calculated and given by Table 4.7.

Table 4.7 The Correlation Coefficients R for Each Fitting

	C_{p1-pre}	C_{p2-pre}	$C_{p1-main}$	$C_{p2-main}$	$\Delta\theta$	AIP
R	0.81	0.83	0.85	0.83	0.80	0.81

It is found that the correlation coefficients R for each fitting equation are larger than or equal to 0.8, and this suggests that the curve fitting results are with acceptable accuracy. The SI engine combustion model was developed by Simulink and given in Figure 4.15.

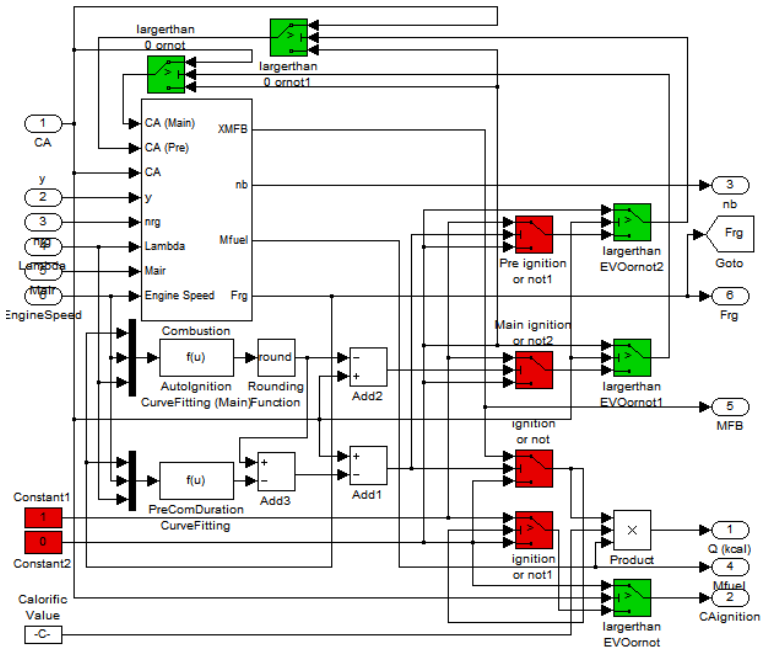

Figure 4.15 The Combustion Model of the HCCI Engine

It should be noticed that, as curve-fitting is a statistical modelling method, which limits the model application domain. Therefore, this curve-fitting only applies to simulate the similar engine or provide the main features which can be used for real-time feedback control purposes.

4.2.5 The HCCI Engine Performance Evaluation Model

The equations used to calculate the IMEP, P_i and ISFC for the HCCI engine are similar to the equations used for the SI engine. Owing to the low temperature and lean combustion features of HCCI combustion, the NO_x emissions are negligible. However, the HC emissions

will be higher for the same reasons. Therefore, prediction of ISHC is considered as a control objective and the calculation equation is given by:

$$ISHC = \frac{(12B_x + B_y + 16B_z) \cdot (HC \cdot 10^{-6}) \cdot (MAF + MFF) \cdot 60 \cdot 1000}{P_i \cdot MMEx},$$

where B_x, B_y and B_z are atom number of carbon, hydrogen and oxygen of fuel and derived from the data sheet of Shell company; HC is the simulation results of hydrocarbon emissions performances in ppm. In addition, the HC emission was calculated in real-time by a similar curve fitting method. Based on the experimental data, it was observed that HC emissions were strongly affected by λ and engine load and slightly influenced by engine speed. The curve fitting matrices are given by:

$$HC = B_{ij} \begin{bmatrix} 1 \\ F_{rg} \\ F_{rg}^2 \\ F_{rg}^3 \\ N \\ N^2 \\ N^3 \\ \lambda \\ \lambda^2 \\ \lambda^3 \end{bmatrix},$$

$$B_{ij} = [391450.169 \quad 78244.339 \quad -155918.270 \quad 115153.727 \quad 11.915 \quad -0.007 \quad 0.000001 \quad -1089364.125 \quad 966379.015 \quad -284617.016],$$

where HC emissions are in ppm (parts per million); B_{ij} is the corresponding correlation coefficients matrix. The correlation coefficients R for HC curve fittings are equal to 0.88, which means the curve fitting results are acceptable.

4.2.6 The Testing Matrix

The experimental testing matrix used to provide experimental data to develop the HCCI engine combustion and HC emission models is shown in Table 4.8.

It is able to find that there were 90 groups of HCCI in-cylinder and HC emissions experimental data were used to develop the engine model. Compared with the SI cases, it only needs 30 groups of experimental data to build the model for each engine speed. This is mainly because the adjustable engine parameters of the HCCI engine are less than SI engine. In addition, since the engine speed has more significant effect on the HCCI than SI, more engine speeds (1500 rpm, 2000 rpm and 2500 rpm) of HCCI are used in the testing matrix.

Table 4.8 The Testing Matrix of HCCI Engine Experiments

ES	λ	IVO	EVC	Number
1500	1.0	60	75	1
			80	2
			85	3
			90	4
			95	5
		70	75	6
			80	7
			85	8
			90	9
			95	10
		80	75	11
			80	12
			85	13
			90	14
			95	15
	1.2	60	75	16
			80	17
			85	18
			90	19
			95	20
		70	75	21
			80	22
			85	23
			90	24
			95	25
		80	75	26
			80	27
			85	28
			90	29
			95	30

ES	λ	IVO	EVC	Number
2000	1.0	60	75	31
			80	32
			85	33
			90	34
			95	35
		70	75	36
			80	37
			85	38
			90	39
			95	40
		80	75	41
			80	42
			85	43
			90	44
			95	45
	1.2	60	75	46
			80	47
			85	48
			90	49
			95	50
		70	75	51
			80	52
			85	53
			90	54
			95	55
		80	75	56
			80	57
			85	58
			90	59
			95	60

ES	λ	IVO	EVC	Number
2500	1.0	60	75	61
			80	62
			85	63
			90	64
			95	65
		70	75	66
			80	67
			85	68
			90	69
			95	70
		80	75	71
			80	72
			85	73
			90	74
			95	75
	1.2	60	75	76
			80	77
			85	78
			90	79
			95	80
		70	75	81
			80	82
			85	83
			90	84
			95	85
		80	75	86
			80	87
			85	88
			90	89
			95	90

4.3 The Compatibility of the Models

Because the SI and HCCI models which introduced above are developed for a specific engine, i.e. the Jaguar V6 SI/HCCI dual mode engine at the University of Birmingham, it is essential to discuss the compatibility of the models for other engines. In order to let the models simulate the operating process for other engines and let environmental conditions have higher compatibility, the author let the variable model parameters as much as possible at the beginning of model development. The variable model parameters and invariable model parameters are shown in Table 4.9.

Table 4.9 The Variable Model Parameters and Invariable Model Parameters

Model parameters	Variable	Invariable
Bore	√	
Rod	√	
Crank Radius	√	
Compression Ratio	√	
Fuel Calorific Value	√	
Intake Pressure	√	
Intake Temperature	√	
Intake/Exhaust Valves Radius	√	
Intake/Exhaust Valves Profile	√	
Correlation Coefficients Matrix for Combustion Model		√
Correlation Coefficients Matrix for Emissions Model		√

It indicates that the model is very easy to change the parameters to match a different engine. Although the correlation coefficients matrix for combustion model and emissions model is needed to update each time based on the experimental data, the fitting function formation are not needed to be changed. The matrixes are easy to be obtained by a Matlab programme based on the experimental data.

4.4 The Engine Multi-objective Optimal Feedback Controller

Because many new technologies are applied to modern engines, such as VVT, GDI, multi-injection, two stages supercharging, etc, the amount of adjustable variables for SI engines are increased considerably. As degrees of freedom for engine optimisation and the number of the calibration parameters are increasing, the classic off-board manual engine-bed based dynamometer calibration mapping method is reaching its limit. The classic calibration approach is becoming more complicated, expensive and time consuming with the increasing complexity of engines, and the combinatorial explosion of the parameter space. Moreover, since the classic engine calibration cannot self-adapt as engines age, the fuel consumptions and emissions tend to increase. Therefore, the multi-objective fast on-board engine optimal control strategy is desired.

For implementing the expectation above, an EA based multi-objective engine optimisation controller is developed by author, and the specific implementation methodology will be given in this section. With a fast, reliable model of the engine in place which is introduced in this chapter, it is possible to implement multi-objective optimal feedback control for operating optimal points for many operating condition. A huge variety of algorithms based on evolutionary search (Evolutionary Algorithms, EA) have been developed. Because SPEA2

has been shown in comparison with other MOEA to perform generally better, it is a good starting point to use it to explore the novel engine optimisation control strategy.

In SPEA and its variations, the dominance ordering is converted into a single performance value, which is then used for selection. To do this, it first computes a strength value for all parents and offspring: a count of all other individuals dominated by this individual. In a second step, the raw fitness of an individual is the sum of the strength values for all other individuals that dominate this individual. All non-dominated individuals have a fitness of 0, for all other individuals the fitness is higher (worse). The more they are dominated by other individuals, the stronger those other individuals are.

In order to encourage the population to cover the entire surface of the Pareto front of solutions, the algorithm also contains a fitness sharing method. Here, the raw fitness is scaled by a measure of the density of individuals in a particular area of the search space. For the next generation, SPEA first tries to preserve all non-dominated individuals. If there are more non-dominated IV than the population (archive) size, a clustering algorithm selectively removes individuals. On the other hand, if the number of non-dominated IV is smaller than the archive size, dominated individuals are added depending on their scaled fitness. The Parent selection in SPEA is simply a tournament selection, based on the scaled strength fitness.

4.4.1 Overview of the JAVA SPEA2 Code

The JAVA code was initially developed by Dr. Thorsten Schnier, a research fellow in the department of computer science in the University of Birmingham, and updated and complemented by the author afterwards. The updates include upgrading of the initial SOP to MOP, and the interface coding between the JAVA code and SIMULINK engine model. The main structure of SPEA2 JAVA code is shown in Figure 4.16.

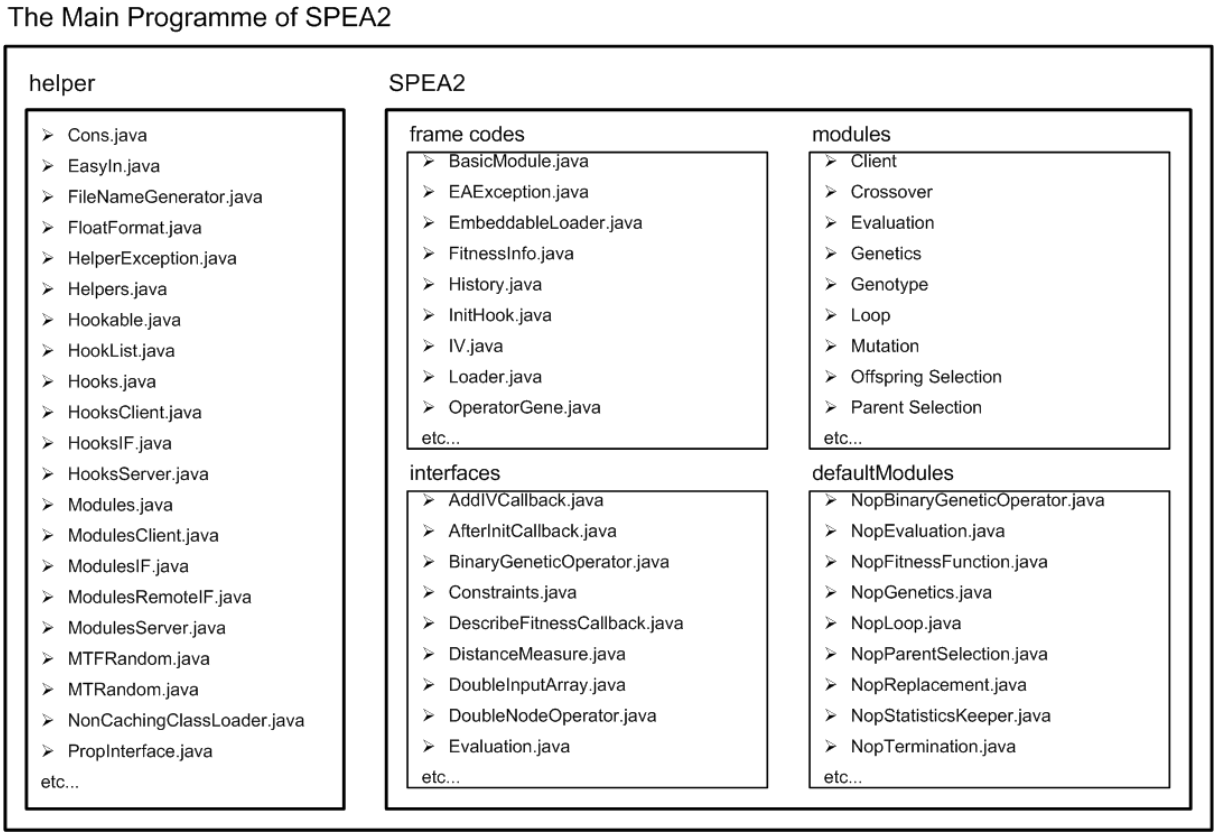

Figure 4.16 The Main Structure of SPEA2 JAVA Code

The main programme of SPEA2 JAVA code includes two packages, '*helper*' and '*SPEA2*'. The '*helper*' package contents some operations that are common to a couple of classes. The

'*SPEA2*' package has four sub-packages, which are *frame codes*, *modules*, *interfaces* and *defaultModules*. The contained classes of each sub-package are shown in Figure 4.16. The '*modules*' sub-package is the core of the code, which includes the SPEA2 control strategy and genetic operations. The SPEA2 is represented in the *Offspring Selection* class of the '*modules*' sub-package. Based on the Equation 2.1, the strength value of SPEA2 is defined by programme:

```
strengths = new double [allCandidates.length],
```

the fitness value of individual is equal to the sum of the strength values of all the individuals which dominates the individual i (Zitzler, Laumanns et al. 2001), the detailed programme code is given by:

```
%%
private void computeRawFitness (IV[] individuals, double[] strengths,
                    boolean[][] dominations, double[]fitnesses)
{
    for (int ivIndex1=0; ivIndex1<individuals.length-1; ivIndex1++)
    {
        for (int ivIndex2=ivIndex1+1; ivIndex2<individuals.length;
ivIndex2++)
{
        if (dominations [ivIndex1][ivIndex2])
{
            fitnesses[ivIndex1] += strengths[ivIndex2];
        }
        if (dominations [ivIndex2][ivIndex1])
{
            fitnesses[ivIndex2] += strengths[ivIndex1];
        }
        }
}
}.
%%
```

Because JAVA is a single inheritance language, it is very inconvenient to add new functions to an existing supertype with OCP principle, which needs the programmer to modify all the classes in the hierarchy. In order to improve the programme performance, the 'interfaces'

module is used to declare a series of method, which only includes the public method features and do not have the specific implementation method. The '*default Modules'* sub-package is used for configuring the JAVA default modules.

4.4.2 Implementation Details of the Co-simulation Controller

The controllers are set up to optimise engine controllable parameters. For SI case, they are throttle position, spark timing, injection timing, IVO and EVC. For HCCI case, they are IVO, EVC and λ respectively. With respect to the EA, they represent these values by a 5/3-element floating point vector, with each value restricted to the range of 0 to 1. These 'raw' values are scaled into the working ranges which were specified in Table 4.4 and Table 4.8. Furthermore, IVO and EVC are discretized into all crank angle values. This is necessary as the model is implemented with a discrete time solver, with one-degree crank angle step. Therefore, the population sizes for SI and HCCI mode can be obtained by Combination formula based on Table 4.1 and Table 4.5. The maximum possible individual evaluations of SI and HCCI engine multi-objective optimisation problem in this case is shown in Table 4.10.

Table 4.10 The Maximum Possible Individual Evaluations of SI and HCCI Engine Multi-objective Optimisation Problem in This Case

	The Maximum Possible Individual Evaluations
SI Mode	24804186
HCCI Mode	2205

Since the representation is based on a floating point vector with a uniform range over all elements, we can use a simple Euclidean distance as distance measure for the fitness sharing

used in SPEA2. A simple one-point crossover, applied to 24804186 (SI mode) and 2205 (HCCI mode) of all individuals is used, together with a Cauchy mutation.

In the experiments reported in this thesis, three and two fitness values are computed by the model for SI and HCCI modes respectively: ISFC, ISPMM and ISPMN for SI mode, and the ISFC and ISHC for HCCI mode. Not all combinations of parameters lead to stable operation of the engine. For conditions that lead to unstable engine operations the controller will exit early and return an indication that the output values are invalid.

The engine model is set up with a fixed, pre-defined speed, but variable power outputs. In addition to the primary optimisation objectives, the model produces an additional output value: the engine's output power at the operating point. In order for the optimisation to be useful in real-world situations, it needs to be able to target a specific output power. The optimisation therefore becomes a constraint optimisation problem: minimize objectives ISFC, ISPMM and ISPMN for SI mode, and the ISFC and ISHC for HCCI mode subject to:

$$IMEP\_min < IMEP < IMEP\_max \quad .$$

It modifies the SPEA2 to incorporate both constraints and individuals with invalid fitness values (engine stall), such that:

1. An invalid individual never dominates another individual, and a valid individual with an output power constraint violation will never dominate an individual that does not violate the power constraint.

2. The archive is first filled with non-dominated individuals, then with dominated individuals without constraint violation, then with individuals with constraint violation. If spaces remain, they are filled out with invalid individuals.
3. In the tournaments used in parent selection, individuals not violating the power constraint always win against those that do, and valid individuals always win against invalid individuals.

The dendrogram of implementation of the engine multi-objective optimal feedback controller is shown in Figure 4.17. The *Operation Module* includes the main programme file, i.e. *ea_frame.m*, which is the programme to call all other functions. The SPEA2 control strategy and genetic operations are included in the *GA_Package.jar* file, and which is connected with the *Operation Module* by *Optimizer.java* in the *Connector Module*. The *Optimizer.java* is a class to implement the skeleton of the EA. Its main functions are:

1. load the parameter file in the *Operation Module*,
2. demand-load the modules,
3. have the modules register their hooks,
4. call start up hooks (like data from an interrupted run),
5. kick off the EA.

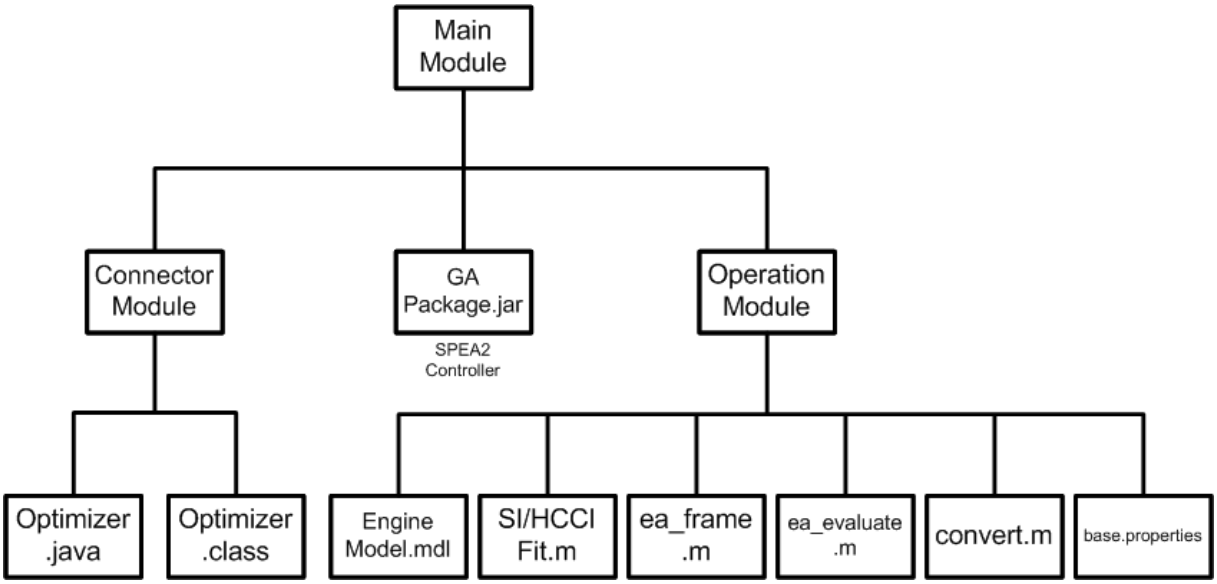

Figure 4.17 The Dendrogram of Implementation of the Engine Multi-objective Optimal Feedback Controller

The SPEA2 optimal controller is implemented in Java, while the engine simulation uses SIMULINK. Thanks to the fact that Java is supported directly in Matlab, linking the two is possible. However, as Matlab functions cannot be called from Java (only the reverse is supported), a slightly more complex interaction is required. The EA loop remains in the Matlab domain, and it calls Java to perform the genetic operations and SPEA2 selection. The population is stored in the Java domain, and then Matlab reads the genotypes and writes back fitness values. Figure 4.18 shows the flowchart for one engine multi-objective optimal feedback control case.

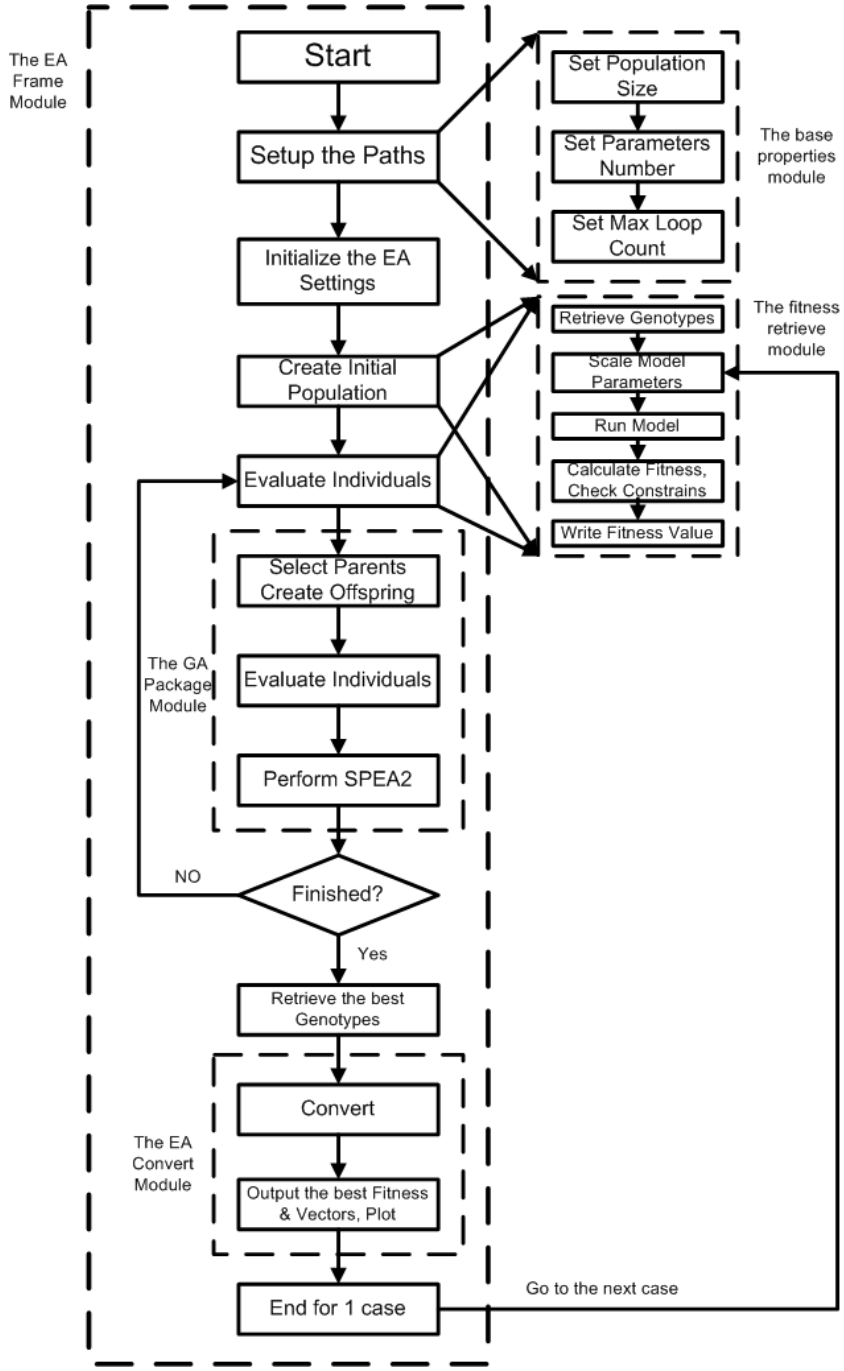

Figure 4.18 The Flowchart for One Engine Multi-objective Optimal Feedback Control Case

In Figure 4.18, the "fitnesses" are the values of the control objectives, for SI, they are ISFC, ISPMN and ISPMM, for HCCI, they are ISFC and ISHC. The "genotypes" are the variables which are used for scaling engine model parameters, i.e. individuals, for SI, they are throttle position, spark timing, injection timing, IVO and EVC, for HCCI, they are IVO, EVC and λ. The

genotype values are four decimal places between 0 and 1. The convert relationship between genotypes and engine parameters for SI and HCCI are given by:

For SI,

```
values = zeros (length (genotypes), 5);

for k=1:length(genotypes)
    X = genotypes (k,:);

    IVO = round (695 + X(1) * 60);
    EVC = round (715 + X(2) * 60);
    SparkTiming = round (15 + X(3) * 10);
    InjTiming =10 * (round (25 + X(4) * 10));
    ThrottleAngle = round (10 + X(5) * 5);

    values (k,:) = [IVO EVC SparkTiming InjTiming ThrottleAngle];
end
```

for HCCI,

```
values = zeros (length (genotypes), 3);

for k=1:length(genotypes)
    X = genotypes (k,:);
    IVO = round (780 + X(1) * 20);
    EVC = round (625 + X(2) * 20);
    Lambda = round(10 + 2 * X(3))/10;
    values (k,:) = [IVO EVC Lambda];
end
```

where “X” stands for the genotypes, i.e. individuals. The SPEA2 utilize these individuals to generate population and archive and thereby to optimise the control objectives.

The parents individuals come from the external archive A_{t+1} and population P_{t+1} by binary tournament selection method and put into the mating pool to generate the offspring. The

new offspring points are generated by operations of “crossover” and “mutation”. The concepts of “crossover” and “mutation” are shown in Figure 4.19 and Figure 4.20.

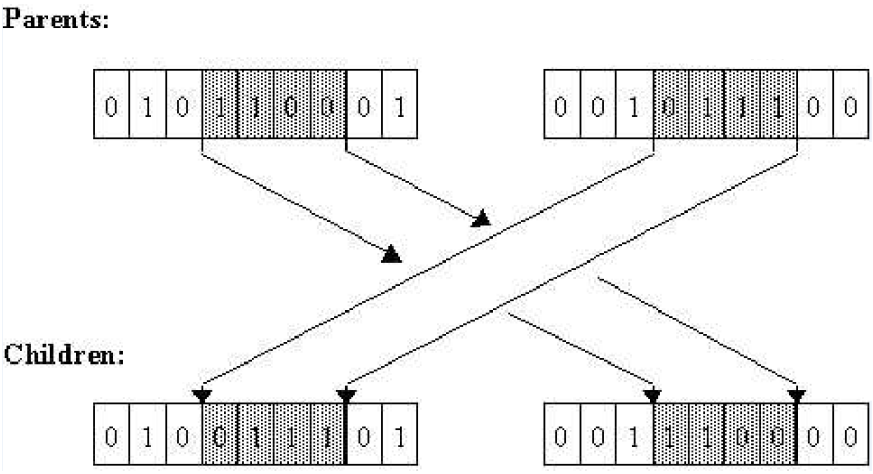

Figure 4.19 Crossover Operation

The crossover points are determined randomly. Then the different parts of parents are combined to generate two new offspring points. These new offspring points are new search points.

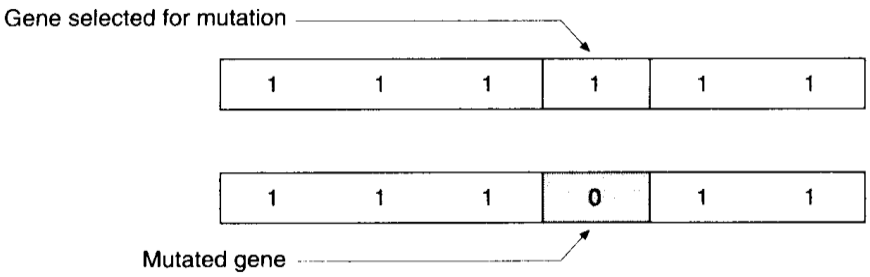

Figure 4.20 Mutation Operation

In the mutation operation, a certain bit of individual is chosen randomly. When this bit is equal 1, it is changed into 0. This operation also generates a new search point.

As long as the SPEA2 running loops reach the maximum, the optimisation process will be ended and outputs the external archive A_{t+1} (engine parameters) as well as the fitnesses (control objectives values).

The population size and parameters number are needed to be set in the *base.properties* file to configure the controller. The specific settings of them for SI and HCCI cases are given in Table 4.11.

Table 4.11 The Specific Settings of the Base Properties Module for SI and HCCI Cases

	Population Size	Parameters Number	Max Loop Count
SI Cases	50	5	200
HCCI Cases	20	3	40

As it shown in Table 4.11, the population size and max loop count of HCCI cases are smaller than SI cases. This is because the maximum possible individual evaluations of HCCI cases are less than SI cases, in other words, the search space is much smaller. Thus, in order to let the controller has higher efficiency and shorter time consumption, after a series tests and comparisons, the population size of SI cases and HCCI cases are set to 50 and 20 respectively, and the max loops of SI cases and HCCI cases are 200 and 40 respectively.

In addition, the model parameters are rescaled with the improved and retrieved genotype values in the fitness retrieve module. The Simulink model will be operated with the rescaled engine parameters and write the fitness values for the SPEA2 evaluation of the current loop. However, the settings of engine speed and load ranges must to be defined at first and will

not be changed during the whole engine multi-objective optimal feedback control process for one case.

Compared with other real-world optimisation problems, the actual optimisation is fairly easy for the EA: only three parameters are needed to be optimised for HCCI cases, and the fitness landscape is well behaved. As a result, a small population and a small number of generations are sufficient for the optimisation. Together with the fast model, run time in the order of a short time can be achieved. Further optimisations would be possible. By starting from random individuals, the algorithm first needs to find valid points in the search space, then move to the points in the correct IMEP range, and only then can search for the optimal points. However, it would be more efficient to seed the population from the points used in the calibration of the model. While there would be only very few points within any particular power range, these points could provide a good starting point for the algorithm.

4.5 Summary

In order to implement the engine multi-objective optimal feedback control, it is necessary to have a reliable and efficiency engine model at the first place. As long as the engine model has been developed, the co-simulation between the Simulink model and JAVA code are able to be implemented to test the engine multi-objective optimal feedback control strategy.

In this chapter, the detailed modelling methodologies for each important module of SI and HCCI engine mode are introduced. The curve fitting technology is applied to calculate the required parameters in combustion model and HCCI mode emissions model (statistical model). In order to evaluate the reliability of curve fitting functions, the correlation coefficients R of each fitting are calculated, and the calculation results are all larger than 0.8 which implies that the curve fitting results are reliable. In addition, in order to provide experimental data to implement curve fitting and cover a wide operating range, the tests matrixes of SI and HCCI mode are designed and presented.

The model is very easy to change the parameters to match a different engine. Although the correlation coefficients matrixes for combustion model and emissions model are needed to update each time based on the experimental data, the fitting function formation are not needed to be changed. The matrixes are easy to be obtained by a Matlab programme based on the experimental data.

On the other hand, for the implementation of the engine multi-objective optimal feedback control strategy, the detailed methodology is given, which includes the JAVA programme of SPEA2 and the implementation details of the co-simulation controller.

The validation results of SI and HCCI engine modelling and the engine multi-objective optimal feedback controller are presented in chapter 5 and 6.

Chapter 5 Validation of the Control Oriented Engine Models

5.1 Introduction

The validation of the control oriented SI and HCCI engine model will be presented and discussed in this chapter. The validation includes in-cylinder volume, MFB, in-cylinder pressure, IMEP, ISFC and normalized emissions of SI and HCCI engines under steady operation condition. In addition, the validations of HCCI engine model under transient status are also presented. In order to prove that the engine model can be run in real-time, the simulation speeds of SI and HCCI engines are presented. A computer with 1.6G Hz processor and 2GB RAM was used to run the simulation.

5.2 SI Engine Modelling

The described methodology in chapter 4 was implemented for the SI engine simulation model by SIMULINK, and the simulation results validation and discussions are presented in this section. In addition, the simulation speed of the SI engine model will be given afterwards.

5.2.1 Validation and Results Discussion

The validation and results discussion of the SI engine model will be given here.

5.2.1.1 MFB & IN-CYLINDER PRESSURE

There are 16 groups of simulated MFB results captured to compare with the experimental data with different engine parameters (spark timing, injection timing, IVO and EVC) at fixed engine speed (1500 rpm) and throttle (12^{o}) as given in Table 5.1.

Table 5.1 The SI Engine Input Parameters for Different Test Cases

Case No.	**1**	**2**	**3**	**4**	**5**	**6**	**7**	**8**	**9**	**10**	**11**	**12**	**13**	**14**	**15**	**16**
Throttle	12	12	12	12	12	12	12	12	12	12	12	12	12	12	12	12
Spark Timing (bTDC)	18	18	18	18	18	18	18	18	23	23	23	23	23	23	23	23
Injection Timing (bTDC)	280	280	280	280	320	320	320	320	280	280	280	280	320	320	320	320
IVO (aTDC)	-36	-11	-36	-11	-36	-11	-36	-11	-36	-11	-36	-11	-36	-11	-36	-11
EVC (bTDC)	-10	-10	-20	-20	-10	-10	-20	-20	-10	-10	-20	-20	-10	-10	-20	-20

The engine parameters were selected to be different from those used for developing the model. The experimental data were obtained from the test engine shown in Figure 3.2.

Thanks to the high flexibility of the dSPACE control system, the different combinations of engine parameters are easy to be implemented on the current test bench and do not need to modify the engine calibration maps. Although the throttle position can be adjusted from 10-15 degree in the model, the difference of intake air amount between 1 or 2 degree different throttle positions is very limited. Therefore, the author fixed the throttle position at "12^{o}" for the different cases in the validation tests. The comparison results between experimental data and simulation results of MFB are shown in Figure 5.1 and Table 5.2.

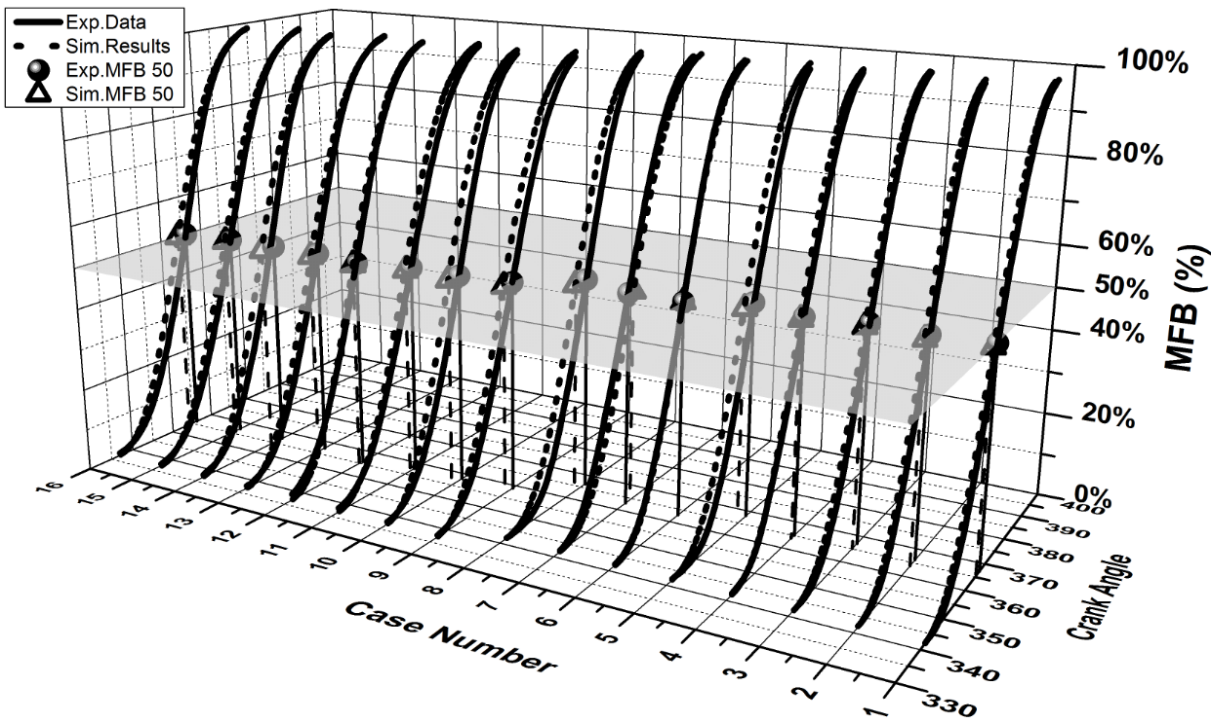

Figure 5.1 MFB Validation Results for Different Cases

Table 5.2 Comparison of the Experimental and Modelling Results for Different engine operating cases of SI engines

Case No.		**1**	**2**	**3**	**4**	**5**	**6**	**7**	**8**
MFB50 (CAD)	Exp.	367.2	366.2	367.1	365.1	368.2	363	363	366.5
	Sim.	365.2	363.8	365.1	363.8	364.8	363	364.5	363
Combustion Duration (CAD)	Exp.	31	40	31	41	40	39	40	38
	Sim.	34	38	29	43	42	37	43	38
Case No.		**9**	**10**	**11**	**12**	**13**	**14**	**15**	**16**

MFB50 (CAD)	Exp.	359	358	358.1	355.8	357.5	357.4	357.2	356.2
	Sim.	356.6	355	356.5	354.9	355.7	354.4	355.8	354.3
Combustion Duration (CAD)	Exp.	43	40	44	41	40	38	40	37
	Sim.	44	42	41	42	42	35	40	38

It can be seen that the simulation results and experimental data are very close to each other for all of these 16 different cases. The errors in MFB50 and combustion duration are within 3.4 CAD and 3 CAD respectively. For some cases, such as case 4, 6, 12 and 15, the experimental MFB curves are almost the same as the simulation results. In addition, it can be seen that almost all the simulated MFB50 positions are earlier than the experimental data. The reason is that the curve fitting function of the combustion characteristic exponent m in the Wiebe function always tends to give a smaller value than the practical value, and this has made the gradient of the forepart of the MFB curve steeper than the measured case. This bug is able to be improved by updating the curve fitting function in the future.

As one of the most important references, the validation result of in-cylinder pressure is the indicator evaluating the global performance of the engine model. Moreover, the in-cylinder pressure is always considered as an important control objective for controller development. Last but not least, a reliable in-cylinder pressure prediction is critical for predicting the IMEP, and other corresponding normalized engine performance indicators. The results of the comparison between the simulation results and experimental data of in-cylinder pressure in different cases, given in Table 5.1, are shown in Figure 5.2. Both of them are averaged results from 100 continuous engine cycles.

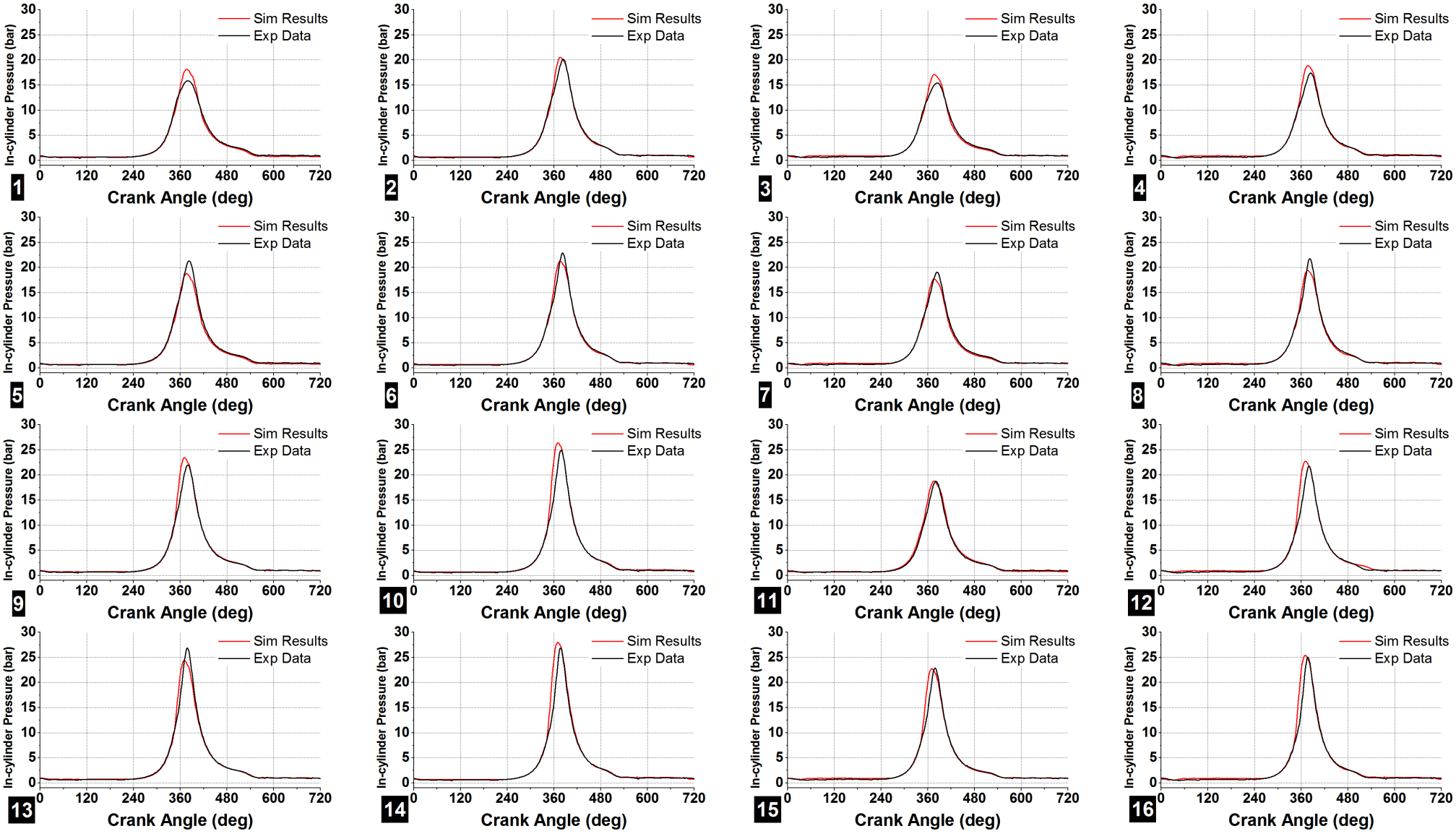

Figure 5.2 The Validation Results of In-cylinder Pressure for SI Mode

The Figure 5.2 shows a fair agreement between the simulation results and experimental data of all the 16 cases. It can be seen that the in-cylinder pressure traces are simulated very well by the engine model. The discrepancy is mainly associated with the combustion duration. As it is mentioned before, this part is very complex and impossible to obtain accurate simulation results by using a single-zone engine model. The current model is developed for control strategy development purpose, and the validation results show it is able to predict the main features and trends of the in-cylinder pressure of the SI engine successfully. In addition, it is observed that the simulated in-cylinder pressure rise rate during the forepart of combustion process is steeper than the experimental data in most cases. This is because the in-cylinder pressure is calculated from MFB in the model, and the foreparts of the simulated MFB results are steeper than the experimental data as it discussed before.

The location and magnitude of the in-cylinder peak pressure are very important control objects for avoiding knock in SI engine control. The comparisons of peak pressure and peak pressure position between simulation results and experimental data of the 16 different SI cases are shown in Figure 5.3.

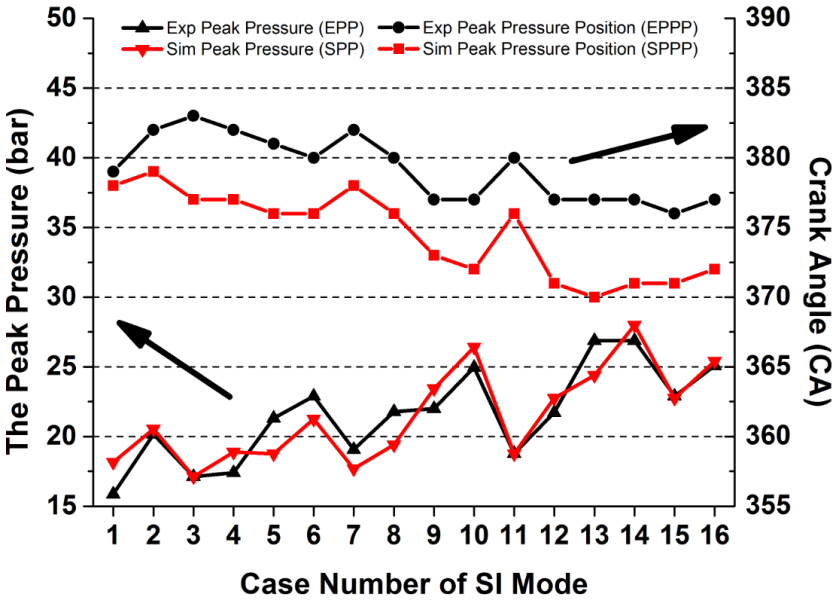

Figure 5.3 The Validation of Peak Pressure and Peak Pressure Position (SI)

It can be seen that the model is able to capture the main trends of peak pressure and peak pressure position with different engine parameter settings. The SPPP line is under the EPPP symbol line and this is mainly because the predicted MFB is early. On the other hand, the SPP line is very close to the EPP line, a good indicator for a useful model.

5.2.1.2 IMEP

IMEP is a very important engine parameter to indicate the engine operating condition or load. Moreover, according to the modelling of engine power and other power normalized engine performance parameters are based on the IMEP, accurate prediction of IMEP is critical. Because IMEP is calculated from in-cylinder pressure of an entire engine cycle, as shown in Equation 4.3, the validation results of IMEP are also considered as an indicator of

the accuracy of in-cylinder pressure prediction. The IMEP percentage errors for the 16 different engine parameter settings are calculated and given in Figure 5.4.

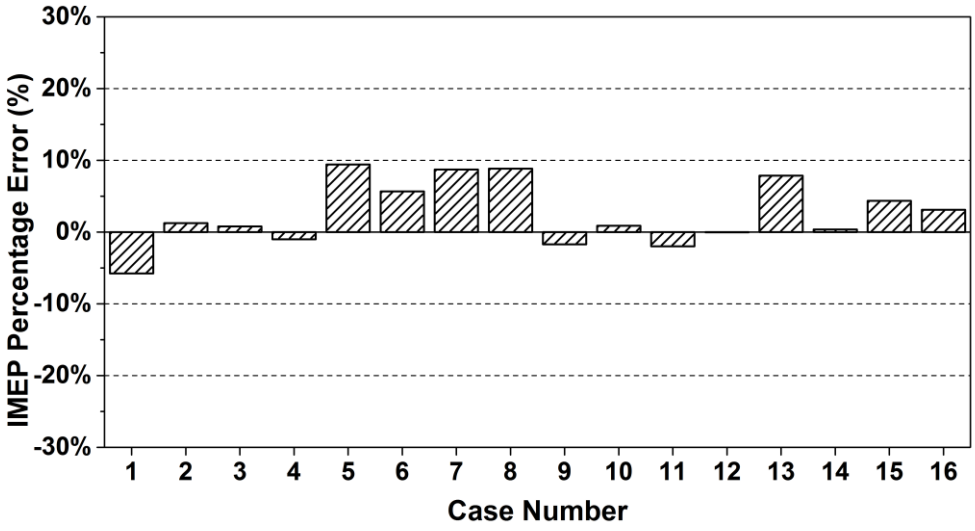

Figure 5.4 The Percentage Error of IMEP

From Figure 5.4, it shows that the percentage errors of IMEP for these 16 cases are within -5% to 10%, and 11 of them are with in ±5%.

5.2.1.3 ISFC

As one of the most important control objectives, ISFC is the indicator of engine thermal efficiency. The accuracy of ISFC simulation results affects the performance of the engine multi-objective optimal feedback controller directly. Equation 4.2 is used for modelling the ISFC value of SI engines. The percentage errors of ISFC for the 16 different SI cases are shown in Figure 5.5.

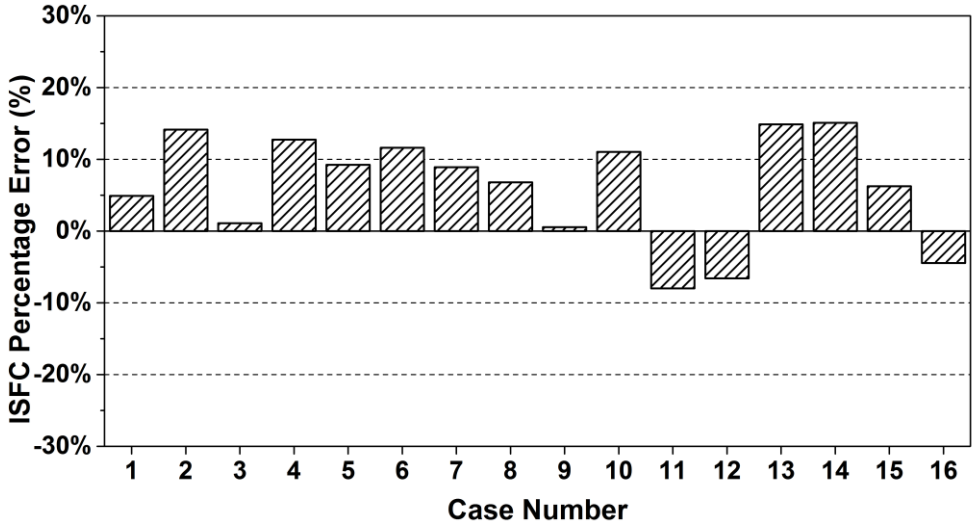

Figure 5.5 The Percentage Error of ISFC

The Figure 5.5 shows a fair agreement between the experimental data and simulation results, and the ISFC percentage errors are constrained within -9% to 15%.

5.2.1.4 ISPMN & ISPMM

The application of three-way catalyst and GDI technology on SI engine has allowed researchers to transfer their attention from controlling HC and NO_x to PM concentration and weight. Modelling of AMC and CAM is implemented by a 5-dimensional linear interpolation model. Again, the accuracy of ISPMN and ISPMM simulation results influence the engine multi-objective optimal feedback control a lot directly. The percentage errors of ISPMN and ISPMM for the 16 different SI cases are shown in Figure 5.6 and Figure 5.7.

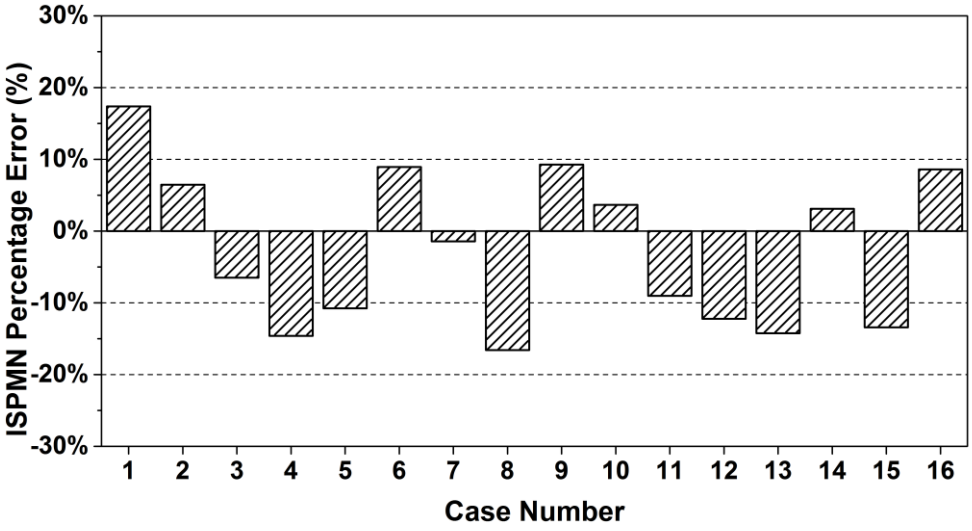

Figure 5.6 The Percentage Error of ISPMN

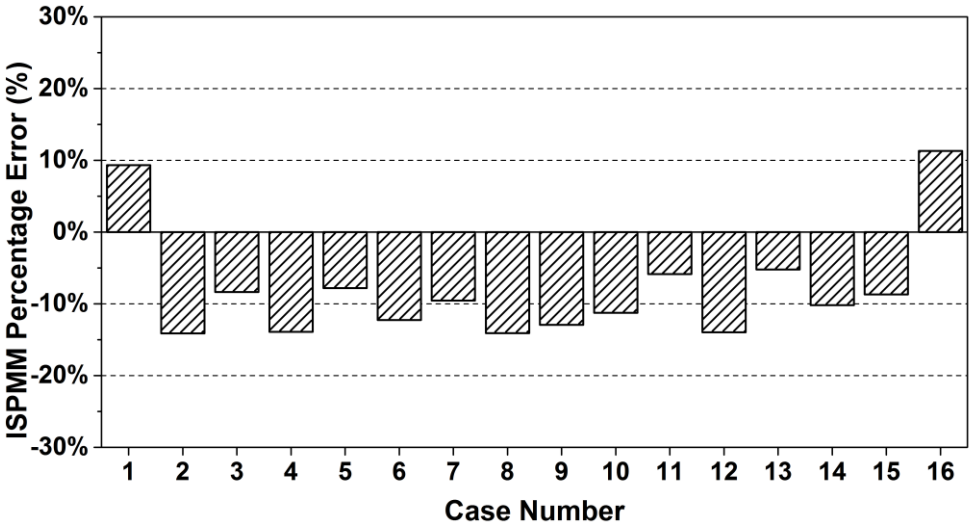

Figure 5.7 The Percentage Error of ISPMM

Figure 5.6 and Figure 5.7 show the fair agreement of ISPMN and ISPMM between the experimental data and simulation results respectively. The percentage errors of ISPMN and ISPMM are within -16% to 11% and -14% to 11% respectively.

5.2.2 Simulation Speed

In order to validate the control oriented SI engine model is able to be operated in real-time, the time consumption for 100 continuous engine cycles are recorded and compared with practical engine running time, and the results are given in Figure 5.8.

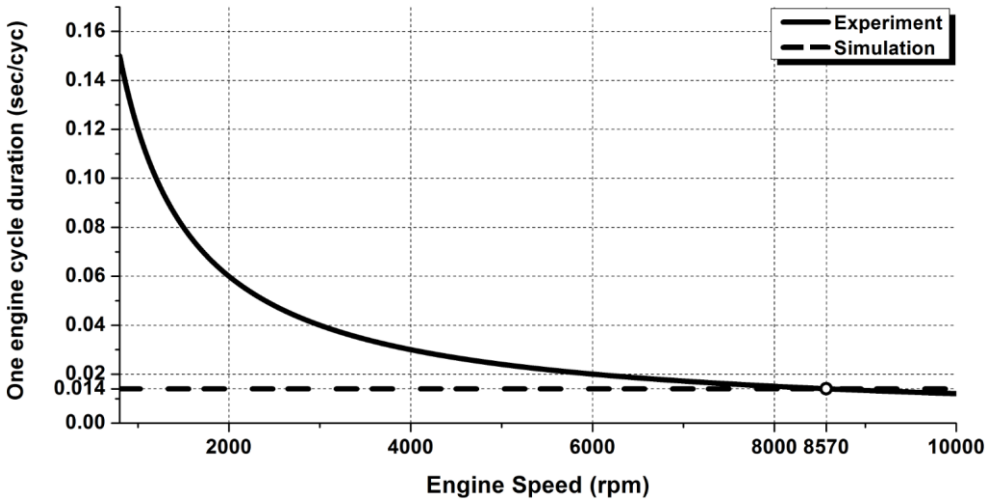

Figure 5.8 The Simulation Speed of SI

It can be seen from Figure 5.8 that it takes 0.014 seconds to simulate one engine cycle with a 1.6G Hz processor and 2GB RAM computer for any engine speed. The practice running time of one engine cycle is longer than simulation time consumption when the engine speed is below 8570 rpm. In other words, the SI engine model is sufficiently fast for real-time simulation below 8570 rpm with any engine parameter setting.

5.3 HCCI Engine Modelling

The described methodology in chapter 4 was implemented for the HCCI engine simulation model by SIMULINK, and the simulation results validation and discussions are presented here. In addition, the simulation speed of the HCCI engine model will be given afterwards.

In order to adjust the engine parameters in real-time when the simulation is operating, a GUI interface programme was developed by the author based on Matlab. The HCCI model control interface is shown in Figure 5.9. The engine parameters are able to be adjusted by typing in the blanks or dragging the sliders. The in-cylinder pressure and in-cylinder temperature are able to be observed in real-time in the right hand side of the interface.

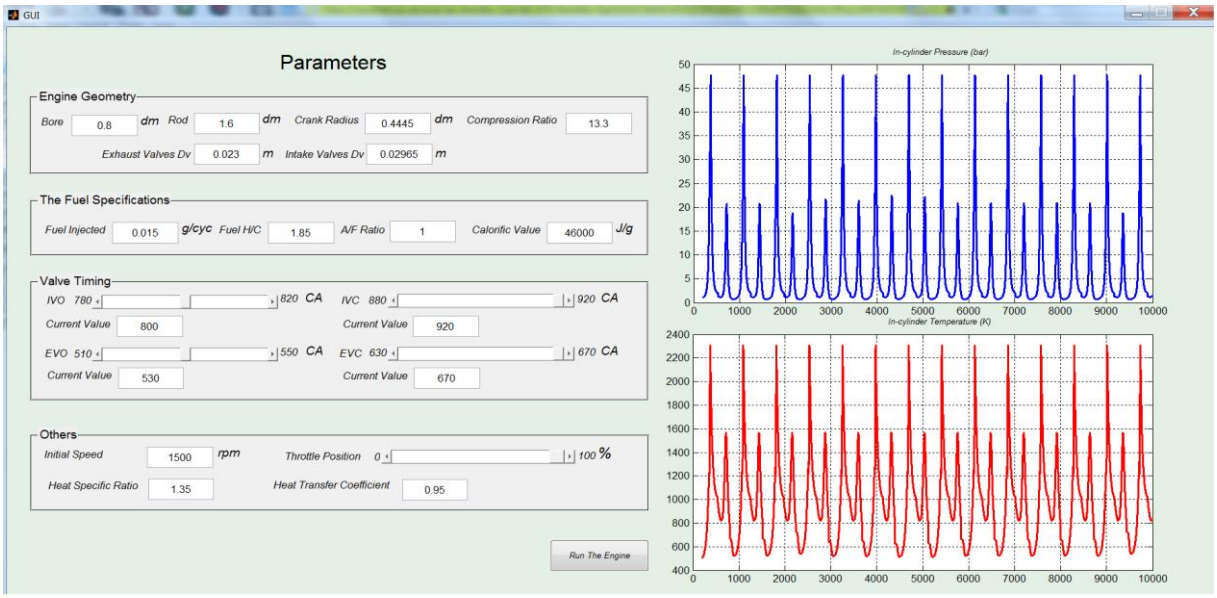

Figure 5.9 The GUI Control Interface of the HCCI Engine Model

5.3.1 Validation and Results Discussion

The validation results and discussions of the HCCI engine model will be given here.

5.3.1.1 MFB & INSYLINDER PRESSURE

The simulation errors contour maps of control oriented HCCI model for Auto-ignition Position (AIP) and Combustion duration with the engine operation range at 1250-2500 rpm and 2.5-4.8 bar IMEP are shown in Figure 5.10 and Figure 5.11. The data used for the comparisons were different than the data used for developing the model.

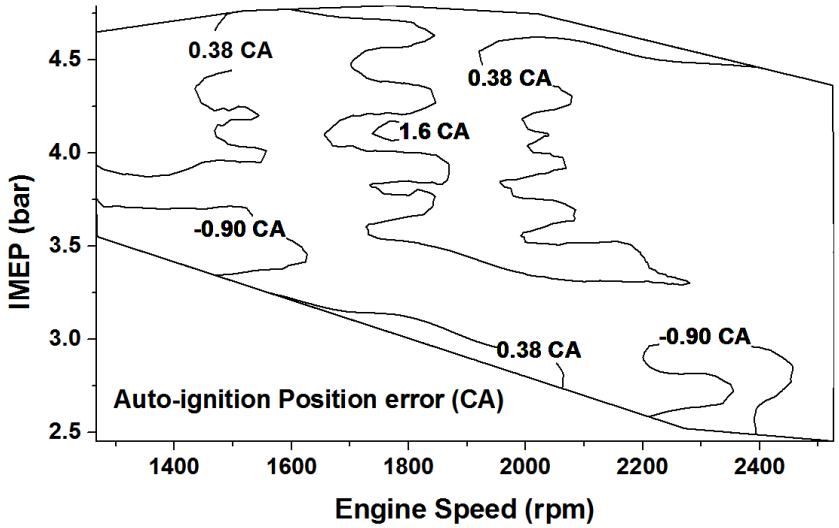

Figure 5.10 The Error of Auto-ignition Position

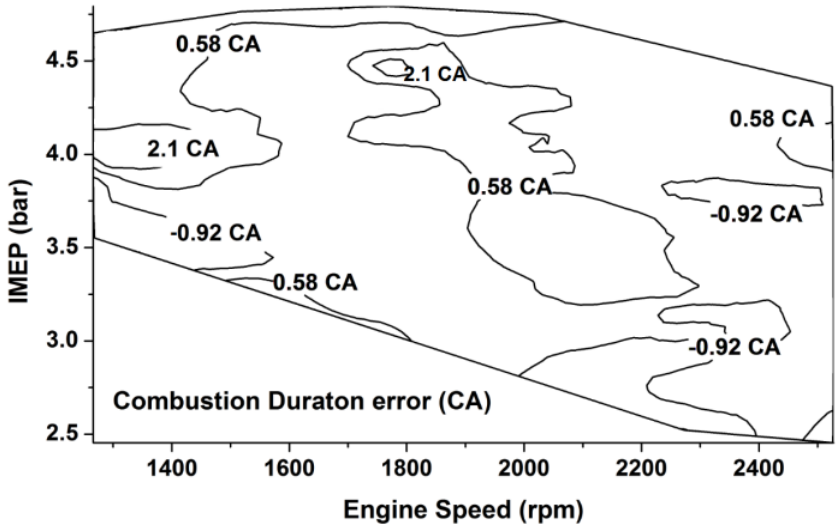

Figure 5.11 The Error of Combustion Duration

Figure 5.10 and Figure 5.11 indicate that the absolute simulation errors for AIP and combustion duration are kept within 1.6 CAD and 2.1 CAD respectively. The simulation errors increased when the engine speeds are around 1800 rpm.

The simulated MFB results were compared with the experimental data of different engine parameters (IVO, EVC and λ) at 1600 rpm and 2100 rpm as given in Table 5.3. The comparison results are shown in Figure 5.12 and Figure 5.13 and Table 5.4. The engine input parameters were selected to be different from those used for developing the model. The experimental data were obtained from the test engine shown in Figure 3.2.

Table 5.3 The HCCI Engine Input Parameters for Different Test Cases

Case No.	1	2	3	4	5	6	7	8	9	10	11	12	13	14	15	16
Speed	1600 rpm								2100 rpm							
λ	1.05				1.15				1.05				1.15			
IVO (aTDC)	63		72		63		72		63		72		63		72	
EVC (bTDC)	82	88	82	88	82	88	82	88	82	88	82	88	82	88	82	88

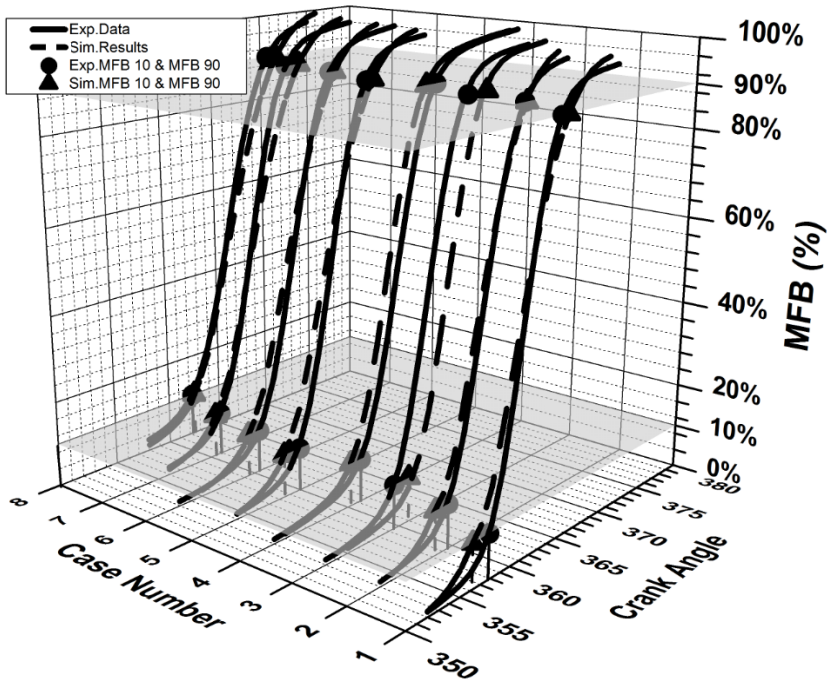

Figure 5.12 **MFB Validation Results for Different Cases at 1600 rpm**

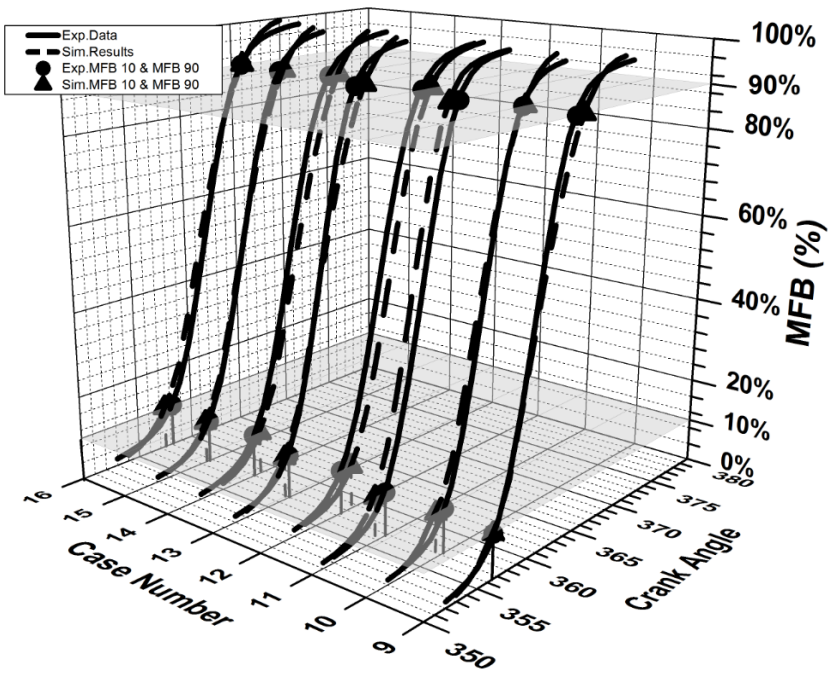

Figure 5.13 **MFB Validation Results for Different Cases at 2100 rpm**

Table 5.4 Comparison of the Experimental and Modelling Results for Different Engine Operating Cases of HCCI Engines

	Case No.		1	2	3	4	5	6	7	8
1600 rpm	MFB10 (CAD)	Exp.	357.8	359.5	359.9	361.3	360	360.5	361	362.3
		Sim.	356.2	358.2	361.2	360.3	358.5	359.5	360.5	362.5
	MFB10-90 (CAD)	Exp.	6.4	7	7	7.5	6.8	7.5	7.2	8.4
		Sim.	8.5	8.5	7.3	7.5	8.9	9	9	9.1
	Case No.		**9**	**10**	**11**	**12**	**13**	**14**	**15**	**16**
2100 rpm	MFB10 (CAD)	Exp.	356.5	357.3	356.8	357.4	357	358	357.8	358.2
		Sim.	356.5	356.5	355.8	358.4	356.6	358.6	357.5	357.5
	MFB10-90 (CAD)	Exp.	7.3	7.2	6.9	8.1	6.8	8	7.7	7.8
		Sim.	8.2	8.3	7	8.3	8.2	8.4	8.5	8.6

The simulation results and experimental data for different cases were in good agreements. It proves that the AFBR method is very reliable for modelling combustion process of HCCI engines. For most of the cases, the simulation results matched the experimental data very well, such as in cases 2, 6 and 7 at 1600 rpm and cases 9, 10 and 15 at 2100 rpm. However, for some cases, the small discrepancies can be observed such as in case 3 at 1600 rpm and case 11 at 2100 rpm. The simulation accuracy could be further improved by improving either the fitting equations or increasing the number of experimental data groups which were used to fit the curves.

The F_{rg} is a very important parameter of HCCI engines. This fraction determines the mass fraction burned, the heat release rate, the possibility of auto-ignition and other important parameters of HCCI combustion. Therefore, it is necessary to observe and analyze the simulation results of MFB with different F_{rg}. The simulation result of the relationship between the mass fraction burned X_{MFB} and combustion duration with different F_{rg} is showed in Figure 5.14. The different F_{rg} is achieved by the different EVC positions.

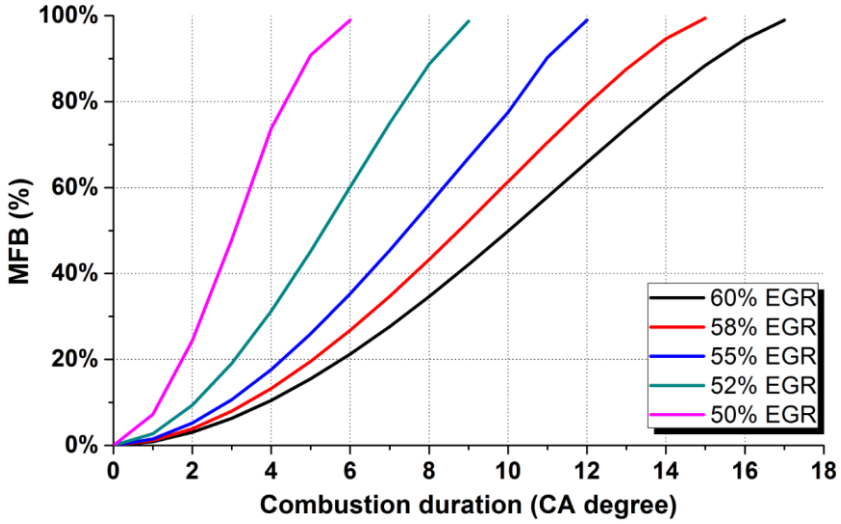

Figure 5.14 The Simulation Results of Mass Fraction Burned with Different EGR Fraction

Figure 5.14 shows that higher F_{rg} leads to longer combustion duration. For the 60% EGR case, the total combustion duration is almost 2 times longer than the 50% EGR case. This is due to the high F_{rg} restrains the in-cylinder combustion reactions and consequently a slower heat release rate. This also indicates that the model is able to simulate the trend of combustion duration when the F_{rg} is changed for control purposes.

The importance of the validation results of in-cylinder pressure has been discussed previously, and the validation results of in-cylinder pressure for different HCCI cases are given in Figure 5.15.

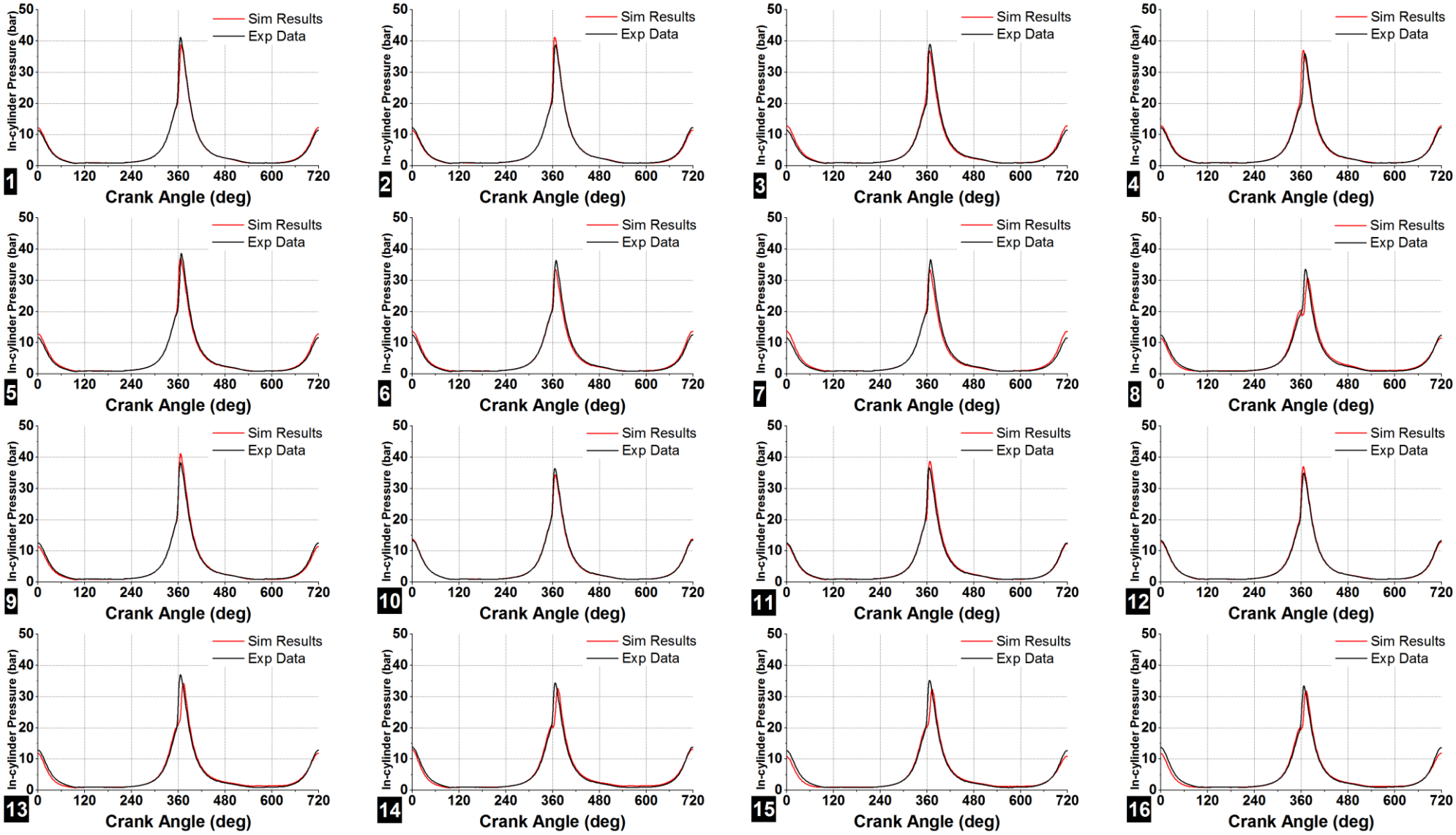

Figure 5.15 The Validation Results of In-cylinder Pressure for HCCI Mode

From Figure 5.15, it is clear that the developed HCCI engine model is able to capture the main features of HCCI in-cylinder pressure trace. Unlike SI engine simulation cases, the simulated combustion phases are not earlier than the experimental data, although they used the same type of curve fitting functions. The reason is that for HCCI combustion model, the ignition position must be predicted first, and then the MFB curve is used consequently. Therefore, MFB is not the only factor determine the simulated combustion phase, the error of auto-ignition position is a key factor also. The comparisons of peak pressure and peak pressure position between simulation results and experimental data of the 16 different HCCI cases are shown in Figure 5.16.

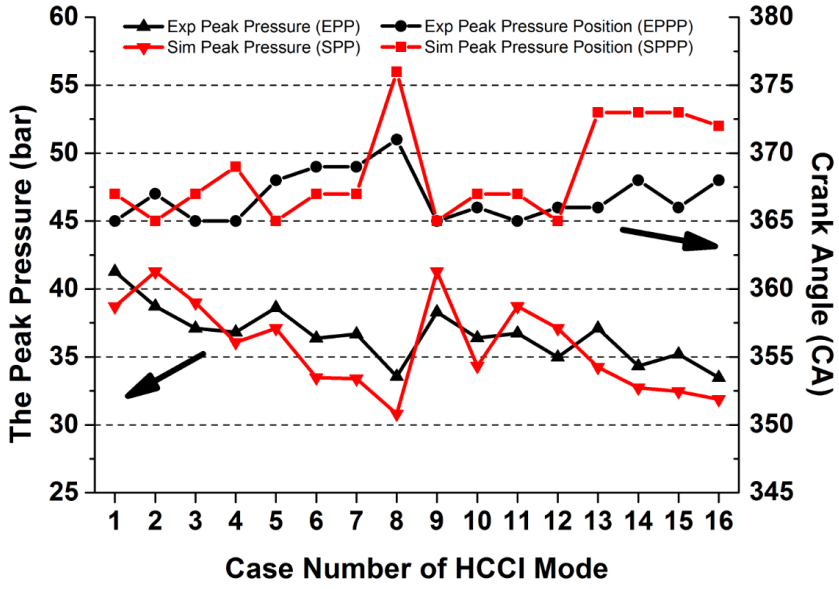

Figure 5.16 The Validation of Peak Pressure and Peak Pressure Position (HCCI)

Figure 5.16 shows a good agreement of peak pressure and peak pressure position between simulation results and experimental data. Compared the peak pressure position with the SI curve, it is to prove that the simulated combustion phase is affected not only by MFB curve but also by the auto ignition position prediction.

5.3.1.2 IMEP

The contour map of the IMEP percentage errors with different HCCI engine conditions is shown in Figure 5.17.

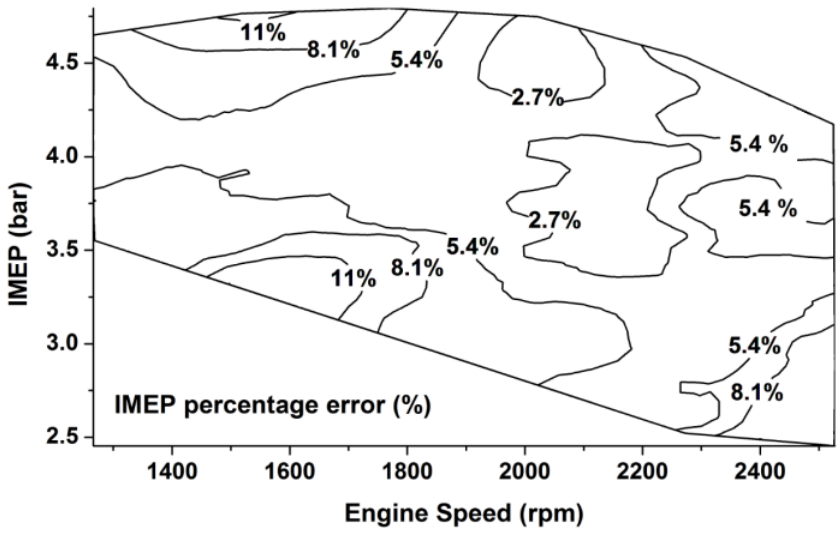

Figure 5.17 The Simulated and Experimental IMEP Percentage Error

It can be seen that the IMEP simulation percentage errors are kept within 11%. The simulation errors are mainly due to the limitation of single-zone combustion model, in which it was assumed that the mixture was fully homogeneous and the fuel was consumed completely during the combustion process. However, because of inhomogeneities under real operating conditions for low temperature combustion of HCCI engines, the fuel is not combusted in one single zone with a uniform heat release rate and the combustion is not completed due to low combustion temperature, as indicated by the relatively high hydrocarbon emissions. Since more fuel was assumed in the model than in real cases, the

IMEP percentage errors are all positive in value, i.e. the IMEP values predicted by the model are higher than the experimental data.

It is needed to point out that the data which are used to draw the contour maps of IMEP, ISFC and ISHC comes from the additional 60 groups of simulation results and experimental data to ensure the reliability of the maps.

5.3.1.3 ISFC

The contour map of ISFC percentage error with different HCCI engine condition is shown in Figure 5.18.

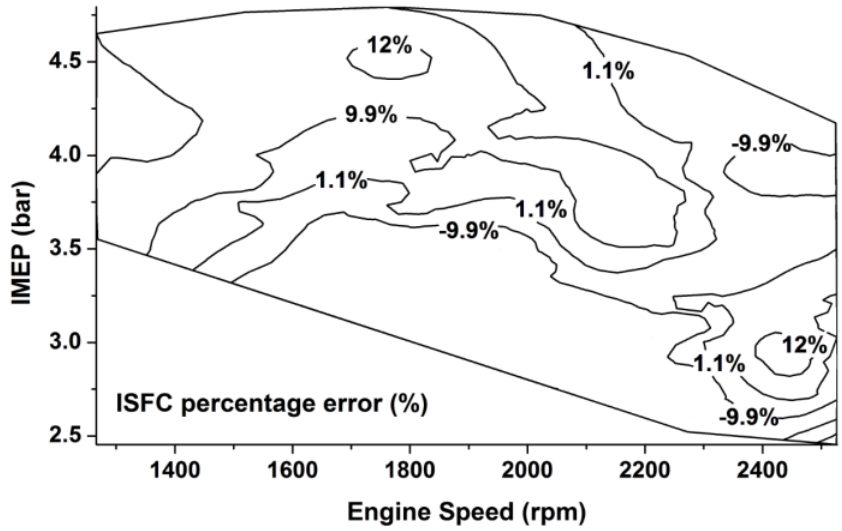

Figure 5.18 The Simulated and Experimental ISFC Percentage Error

Since fuel consumption was calculated based on the intake air amount in the model, the simulation percentage error of ISFC is a function of simulation error of intake air amount. Therefore, Figure 5.18 indicates the simulation accuracy of intake air amount indirectly.

5.3.1.4 ISHC

In order to control the HC emissions of HCCI engine based on the simulation results, the validation of ISHC is critical. The contour map of ISHC percentage error with different HCCI engine conditions is shown in Figure 5.19.

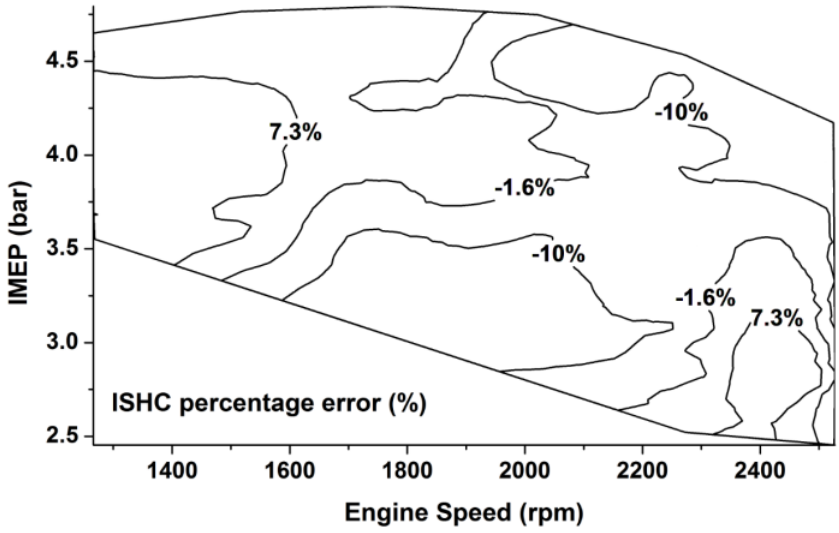

Figure 5.19 The Simulated and Experimental ISHC Percentage Error

ISHC is also a function of intake air amount. The simulation errors of IMEP at high-load-and-low-speed and low-load-and-high-speed domains are relatively larger as shown in Figure 5.17. The same pattern is observed for the validation maps of ISFC and ISHC, Figure 5.18 and Figure 5.19, since they are all functions of IMEP. The accurate calculations of these engine performance evaluation parameters are significant for future model-based control strategy development.

5.3.1.5 TRANSIENT STATUS

The transient performance responses of in-cylinder pressure, F_{rg}, M_{air} and M_{fuel} are shown in Figure 5.20 for engine speed or IMEP (or λ) change during simulation process. For transient performance responses comparison, 100 continuous engine cycles were used. The IMEP (or λ) change occurred at the 30^{th} engine cycle (from 1.0 to 1.2) with the fixed engine

speed, and the engine speed changed at the 70^{th} engine cycle (from 1500 rpm to 2000 rpm) with fixed λ. In order to validate the simulation results, the experimental data for the corresponding parameters with the same engine operating condition changes are shown in Figure 5.21.

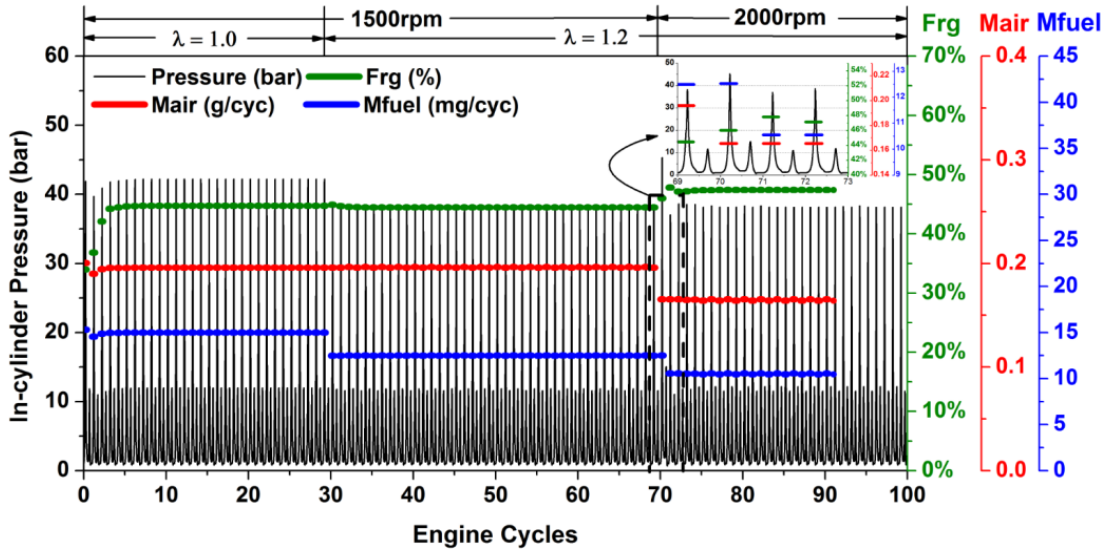

Figure 5.20 The Simulated Transient Performance Responses

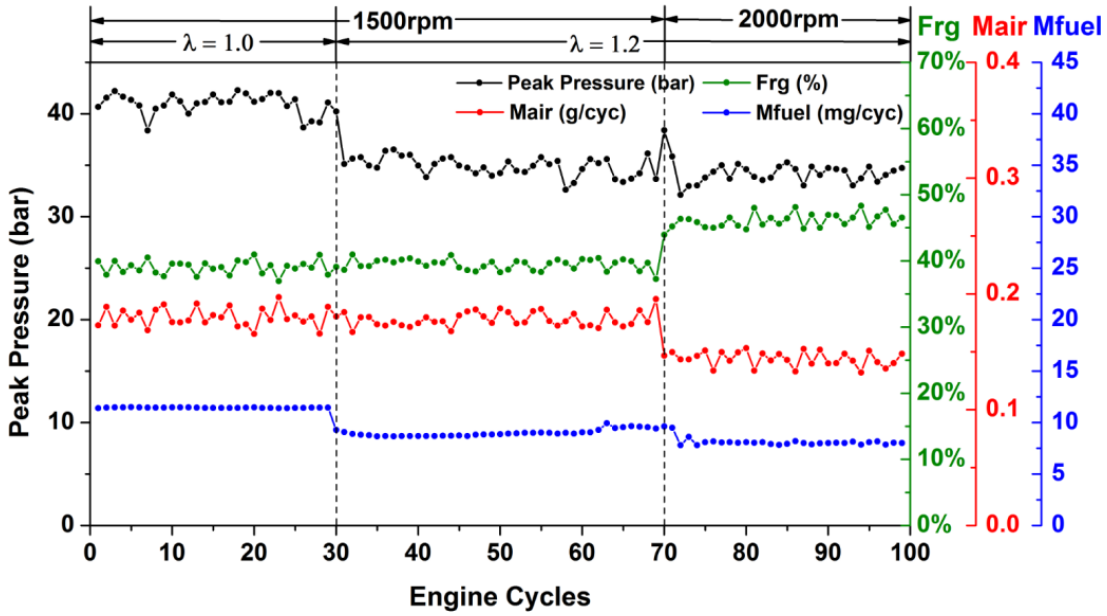

Figure 5.21 The Experimental Transient Performance Responses

According to the model used for controller design, the main target for transient response of this model is to capture the in-cylinder pressure, F_{rg}, M_{air} and M_{fuel} when the engine operating condition is changed. It assumes that the engine speed and λ are able to be adjusted and kept stable in one engine cycle as a step change. In order to remove the noise points, the experimental data presented in Figure 5.21 were chosen from every 3 data point in the database.

From Figure 5.20 and Figure 5.21, it can be seen that when λ changed from 1.0 to 1.2 at the 30^{th} engine cycle, the peak in-cylinder pressure decreased as the M_{fuel} decreased, and the F_{rg} and M_{air} did not change much.

When the engine speed increased from 1500 rpm to 2000 rpm at the 70^{th} engine cycle during the simulation process as it is shown in Figure 5.20, the peak in-cylinder pressure at the 70^{th} engine cycle increased to 46 bar suddenly and decreased to 38 bar at the 71^{st} engine cycle and became stable. This behaviour was confirmed in the experimental data shown in Figure 5.21. This phenomenon was mainly because of the air intake amount of the 70^{th} engine cycle was less than the 69^{th} cycle for the higher engine speed. Also, the timing of the fuel injection was at the TDC of the recompression process which was earlier than the air intake stroke, and the injected fuel amount was determined by the intake air amount of the 69^{th} engine cycle when the AFR was fixed. Thus, the in-cylinder mixture was richer during the 70^{th} engine cycle than others (see Figure 5.20), and it led to the abrupt increase

of peak in-cylinder pressure. After the 70^{th} engine cycle, the peak in-cylinder pressure decreased and became stable as the AFR went back to 1.2 and was kept stable. Although as the engine speed increased to 2000 rpm less fuel was injected, the auto-ignition position was advanced accordingly too which caused the peak in-cylinder pressure to remain apparently unchanged as compared with 1500 rpm.

The internal EGR fraction of the preceding cycle plays a very important role in the combustion of the next cycle, so it is a critical parameter in analyzing HCCI combustion and transient response. From Figure 5.20 and Figure 5.21, it is can be found that the model was able to predict the correct trend for F_{rg} during the transient speed change process (the 69^{th} to 72^{nd} engine cycle). At the 70^{th} engine cycle, due to the M_{air} being less than the 69^{th} engine cycle, the F_{rg} is apparently higher. Compared with the 70^{th} engine cycle, the M_{fuel} of the 71^{st} engine cycle was much less, and meanwhile M_{air} and internal EGR amount did not change too much, which led to higher F_{rg} than the 70^{th}. After the 71^{st} engine cycle, the M_{air} and M_{fuel} did not change too much. But because less fuel was burned in the 71^{st} engine cycle, the internal EGR amount of the 72^{nd} engine cycle decreased, and the F_{rg} was reduced slightly and became stable afterwards.

From the comparison between Figure 5.20 and Figure 5.21, it is concluded that the model can provide the correct trend with acceptable accuracy for in-cylinder pressure, F_{rg}, M_{air} and M_{fuel} during the transient speed or load change process. This model can be used

to control the cycle-to-cycle variations such as adjusting the fuel injected strategy in real-time during transient process.

5.3.2 Simulation Speed

As the model was developed for real-time oriented control and dynamic performance analysis, it was essential to test the simulation speed. The simulation took around 2.5 seconds to run 100 cycles, i.e. 0.025 sec/cycle. The potential real-time operation range of this model is shown in Figure 5.22.

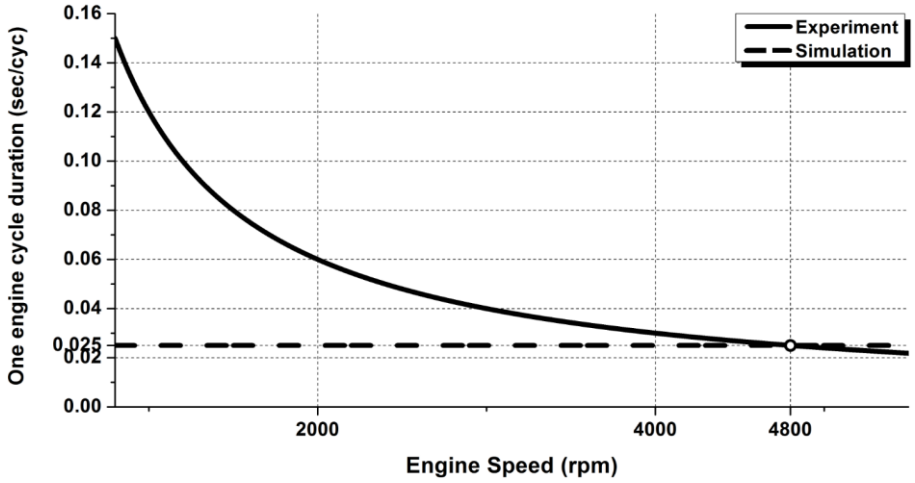

Figure 5.22 The Simulation Speed of HCCI

The simulation speed was quick enough to develop a real-time control strategy when the engine was operating below 4800 rpm, which currently covers the normal HCCI engines operating range. In addition, it needs around 6 seconds to run 100 engine cycles. If KIM is adopted for predicting the auto-ignition position which limits the real-time operating range

of the model to around 2000 rpm, and the simulation accuracy of AIP will not be improved too much.

5.4 Summary

The detailed SI and HCCI model validation results are given in this chapter. The real-time cycle-to-cycle control oriented gasoline fuelled SI and HCCI engine models were developed by using Simulink, which was validated by experimental data from a Jaguar V6 HCCI/SI dual mode engine. The SI engine model was validated with fixed engine speed (1500 rpm) and 16 different groups of engine parameter settings. On the other hand, the HCCI engine model was validated within a wide operating conditions (1250-2500 rpm and 2.5-4.8 bar IMEP). Based on the simulation and experimental results, the following conclusions were drawn:

1. The Wiebe function and AFBR method which are demonstrated in the chapter 4 are well suited to simulate the gasoline-fuelled SI and HCCI combustion process. The SI model is able to predict the MFB, combustion duration, in-cylinder pressure, peak pressure, peak pressure position, IMEP, ISFC, ISPMN and ISPMM with small errors. The HCCI model is able to calculate the HCCI MFB, AIP (MFB 10), combustion duration, in-cylinder pressure, peak pressure, peak pressure position, IMEP, ISFC and ISHC with sufficient accuracy. The simulated AIP error is within 1.6 CAD, and combustion duration error is within 2.1 CAD. IMEP, ISFC and ISHC errors were within 11%, 12% and 10% respectively.

2. The HCCI engine model is able to provide the correct trend of main features with acceptable accuracy for in-cylinder pressure, F_{rg}, M_{air} and M_{fuel} during the transient process.
3. The models can be used to run real-time cycle-to-cycle when the SI engine is operating below 8570 rpm and HCCI engine is operating below 4800 rpm, which allows engineers to design real-time control strategy based on these models for SI and HCCI engine control in the future.

Chapter 6 Engine Multi-objective Optimal Feedback Control

Following on from the development and validation of the control oriented SI and HCCI engine models which were introduced in the previous chapters, the validation of a developed SPEA2 based JAVA programme and a model-based engine multi-objective optimal feedback controller of the SI and HCCI engines are presented in this chapter. Moreover, a comparison between the SI controller and the HCCI controller will be discussed afterwards.

6.1 Introduction

As discussed before, the engine multi-objective optimal feedback control is a very useful and promising tool to replace conventional engine optimisation work. With this target, an engine multi-objective optimal feedback controller is developed using JAVA as it was introduced in chapter 4. The control strategy is based on SPEA2, which has been shown in comparison with other MOEA to generally perform better. Before implementing it in the real engine or in the engine model-based multi-objective optimal feedback control, a simulation study is essential. Because two validated engine models of SI and HCCI have been developed, the co-

simulation between the Simulink model and the JAVA controller is possible and implemented by the author. The block diagram of the engine multi-objective optimal feedback control strategy is shown in Figure 6.1.

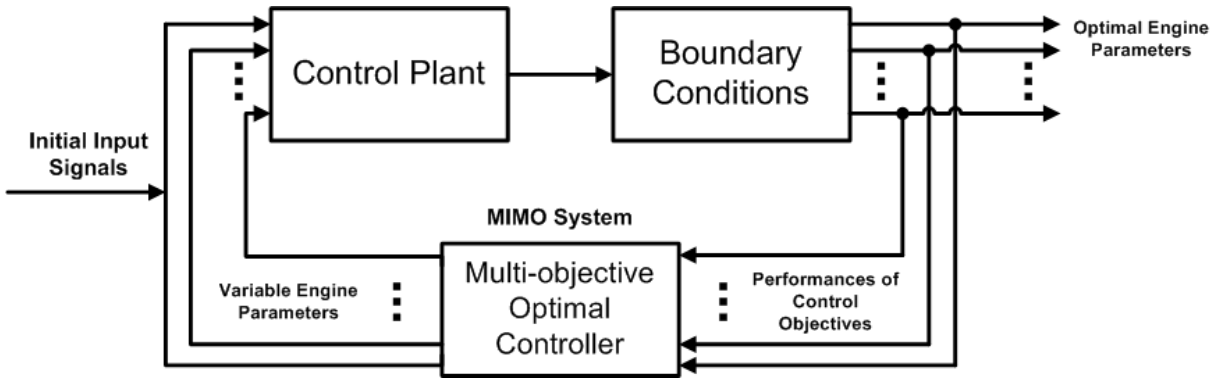

Figure 6.1 The Block Diagram of the Engine Multi-objective Optimal Feedback Control Strategy

In Figure 6.1, the control plant is the engine model, which operates in specified engine cycles with the engine parameters provided by the EA based optimal controller. The boundary conditions constrain the engine model operation within a specific IMEP range and outputs the corresponding performances of control objectives from the control plant. The multi-objective optimal feedback controller is a Multi-Input Multi-Output (MIMO) system, which processes the input control objectives' performances and outputs the optimised variable engine parameters. The initial input signals are generated by the initial EA population. A computer with 1.6G Hz processor and 2GB RAM was used to operate the control system.

6.2 The Validation of the SPEA2 Optimal Control Strategy

Although the performance of SPEA2 has been validated by E. Zitzler et al. in their papers, there is a need to validate the EA programme which has been developed by the author along with Thorsten. There are two MOPs which are used to validate the developed SPEA2 optimal control module, i.e. SCH and SRN. These are the classic MOPs to validate MOEA.

SCH and SRN are two equations groups with boundary conditions and constraint conditions, and there is no single point which is able to optimise all the objective equations to have the minimum values simultaneously.

6.2.1 SCH MOP Validation

SCH was designed for evaluating the MOEA (Schaffer 1984). As a Single-Input and Multiple-Output (SIMO) MOP, The MOP of SCH has one input (x) and two outputs (f_1 , f_2) which are given by:

$$SCH \quad \begin{cases} \min\ f_1(x) = x^2 \\ \min\ f_2(x) = (x-200)^2 \end{cases}$$

$$x \in \left[-10^3,\ \ 10^3\right]$$

For simplicity, the input x is considered as an integer. The optimal solutions of SCH MOP are shown in Figure 6.2.

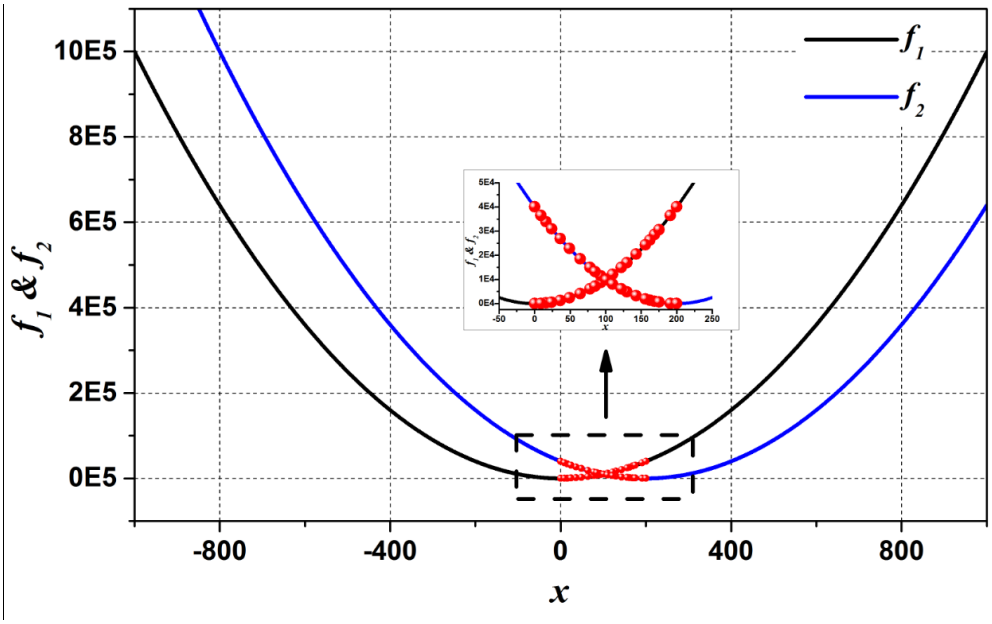

Figure 6.2 The Founded Optimal Solutions of SCH MOP

In Figure 6.2, the red balls are the optimal solutions and they are equally as good as each other. Moreover, it is found that all of the values of input x are within $[0, \ 200]$. This is logical since it is apparent that any x which is not within this range is worse than $x = 0 \ or \ 200$. The founded Pareto Front of SCH MOP is shown in Figure 6.3, which shows the solutions space and the optimal solutions.

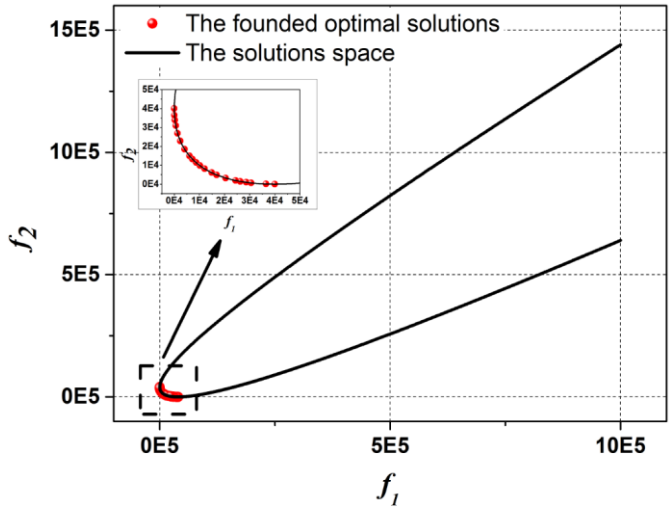

Figure 6.3 The Founded Pareto Front of SCH MOP

From Figure 6.3, it is found that the SPEA2 based MOEA is able to find the Pareto front of SCH MOP efficiently.

6.2.2 SRN MOP Validation

Because SCH is a single variable, unconstrained by MOP, it is relatively easy to solve in comparison to other complex test problems. As a result, another MOP SRN is introduced to validate the developed SPEA2 programme. As a MIMO MOP, the MOP of SRN has two inputs ($x,\quad y$) and two outputs (f_1 , f_2) which are given by (Chankong and Haimes 1983):

$$SRN \begin{cases} \min\ f_1(x,\quad y) = 2 + (x-2)^2 + (y-1)^2 \\ \min\quad f_2(x,\quad y) = 9x - (y-1)^2 \\ s.t.\qquad e_1(x,\quad y) = x^2 + y^2 \le 225 \\ \qquad e_2(x,\quad y) = x - 3y + 10 \le 0 \end{cases}$$

$$x\ \&\ y \in [-20,\quad 20]$$

For simplicity, the inputs ($x,\quad y$) are considered as integers as well. The 3-D map surfaces of f_1 and f_2 without constraint conditions are presented in Figure 6.4. The optimal solutions of SRN MOP are shown in Figure 6.5.

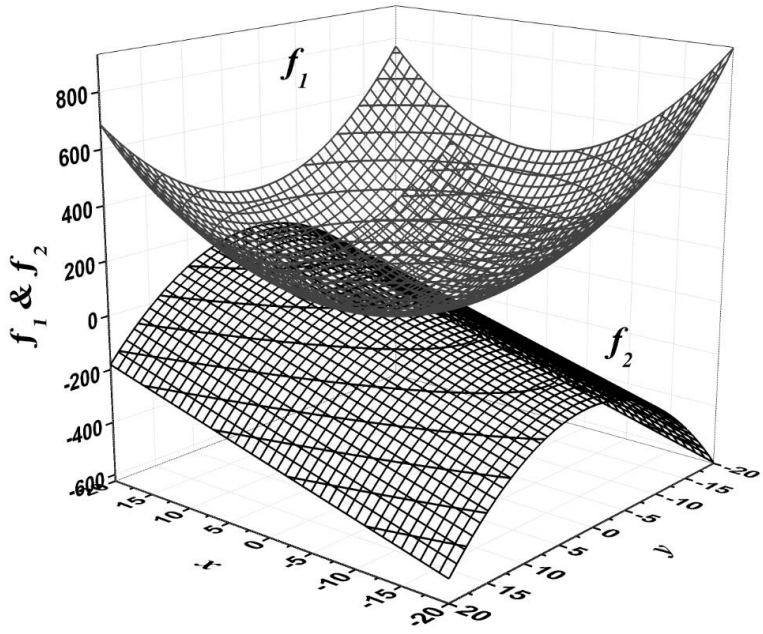

Figure 6.4 The Plots of f_1 and f_2 for SRN MOP

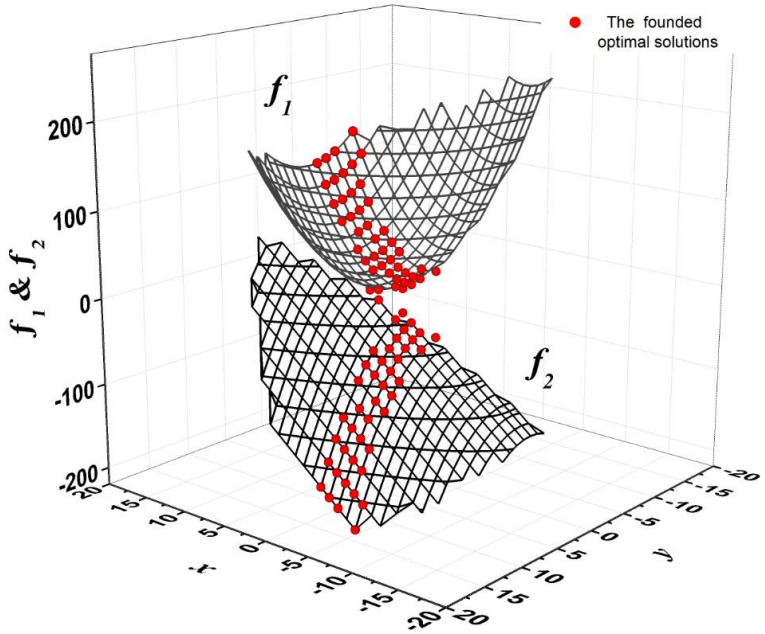

Figure 6.5 The Founded Optimal Solutions of SRN MOP

In Figure 6.5, the red points are the solutions which are found by the SPEA2 based JAVA programme which are also equally as good as the other solutions. The founded Pareto Front

of SCH MOP is shown in Figure 6.6, which shows the solutions space and the optimal solutions.

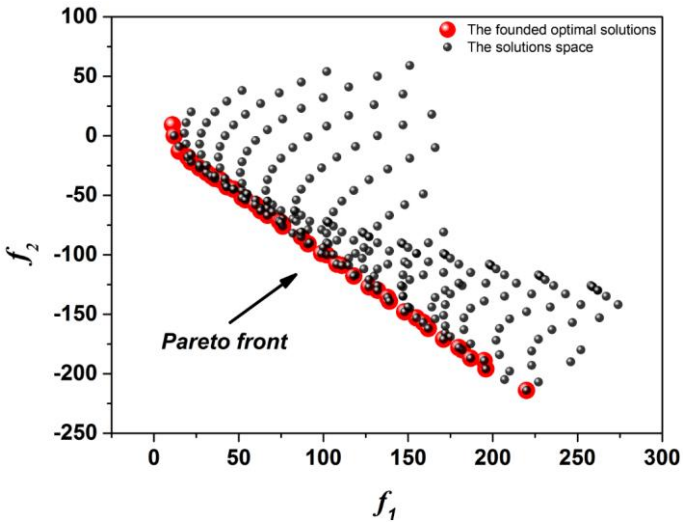

Figure 6.6 The Founded Pareto Front of SRN MOP

From Figure 6.3, it is recognized that the SPEA2 based MOEA is able to find the Pareto front of SCH MOP efficiently.

6.3 The Validation of SI Engine Multi-objective Optimal Feedback Control

Since the engine model and SPEA2 based optimal controller has been validated, it is time to validate the SI engine multi-objective optimal feedback control system by comparing the experimental data and co-simulation results.

6.3.1 Implementation Overview

In order to validate the SI engine multi-objective optimal feedback controller with different engine operating conditions, 6 different cases are defined for different IMEP ranges. The detailed information for the cases is given in Table 6.1.

Table 6.1 The Operating Conditions for Each SI Case

Case No.	**1**	**2**	**3**	**4**	**5**	**6**
Min IMEP (bar)	3.5	4.0	4.5	5.0	5.5	6.0
Max IMEP (bar)	4.0	4.5	5.0	5.5	6.0	6.5

Since the engine speed is fixed to 1500 rpm for the SI model as mentioned in chapter 4, the corresponding SI optimal controller validation has to be constrained to 1500 rpm. The controller needs to run 200 EA loops to find the optimal engine parameter settings.

6.3.2 Validation and Results Discussion

The validation includes three parts as described below:

1. Compare the experimental data which were used to develop the SI engine model with the optimal simulation results of control objectives, i.e. fuel consumption (ISFC), soot concentration (ISPMN) and soot mass (ISPMM).
2. Find out the three optimal engine parameter settings for each control objective, and implement them on the real engine test bench, and then compare the errors between the recorded experimental data and simulation results of the three control objectives.

3. Compare the difference between predicted experimental validation points for each control objective and the experimental data which used to develop the SI model. The performance improvements of the engine can be evaluated.

The validation results of different SI cases which are listed in Table 6.1 are given in Figure 6.7 to Figure 6.12.

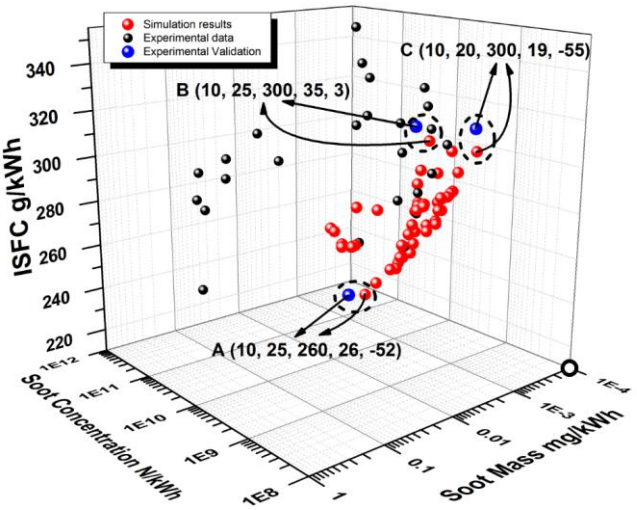

Figure 6.7 **Case 1 SI 3.5 to 4.0 bar**

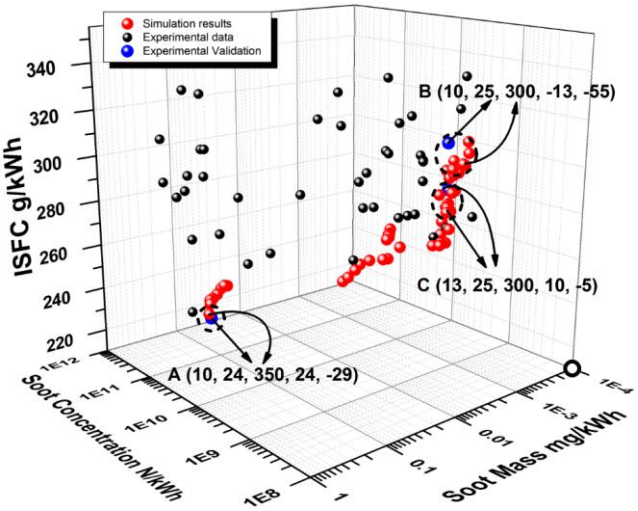

Figure 6.8 **Case 2 SI 4.0 to 4.5 bar**

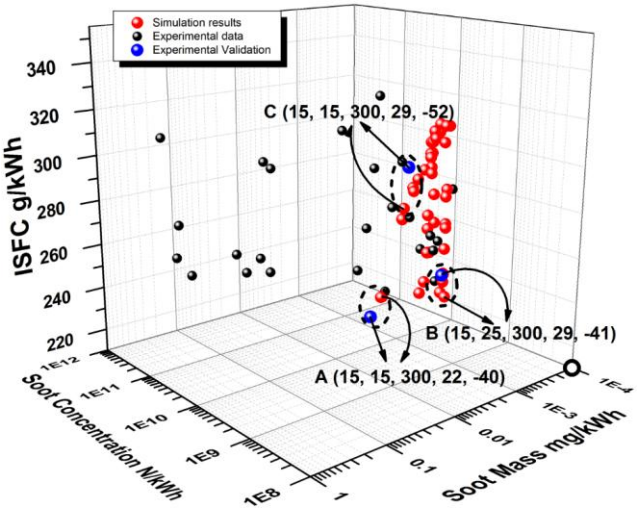

Figure 6.9 **Case 3 SI 4.5 to 5.0 bar**

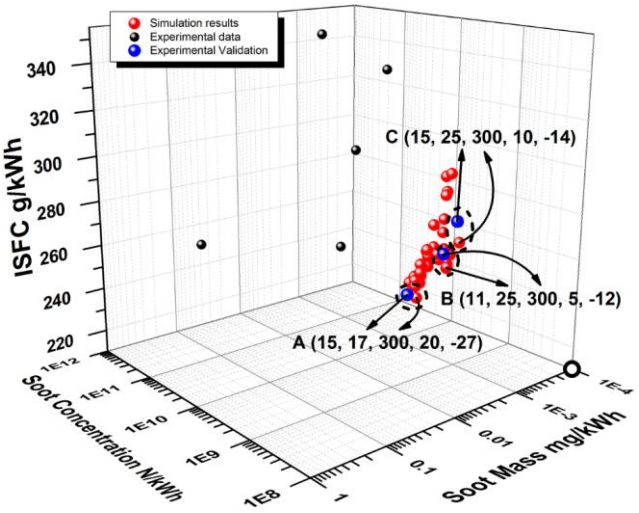

Figure 6.10 Case 4 SI 5.0 to 5.5 bar

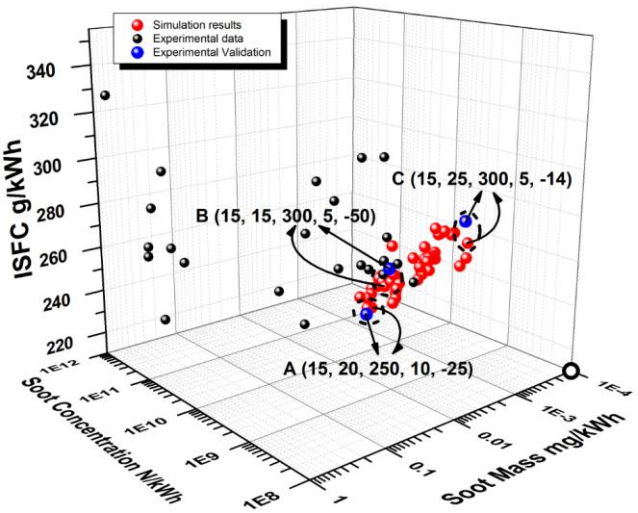

Figure 6.11 Case 5 SI 5.5 to 6.0 bar

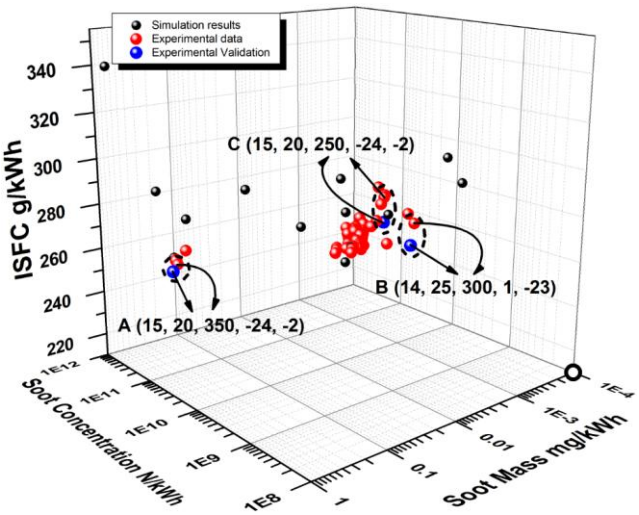

Figure 6.12 Case 6 SI 6.0 to 6.5 bar

Because there are three control objectives for the SI cases, i.e. fuel consumption (ISFC), soot concentration (ISPMN) and soot mass (ISPMM), the author has chosen to use 3-D figures to present the validation results. For the convenience of comparing and analysing the data, the scales of the three control objectives are unified for all six cases.

Before the analysis and discussion, it is needed to give a description of the figures above. In Figure 6.7 to Figure 6.12, the small black points are experimental data which were used to develop the SI engine model and named as experimental data points; the red points are obtained by the multi-objective optimal feedback controller as simulation result points, and the blue points are the experimental validation points which were obtained by implementing the predicted optimal engine parameter settings in the real engine bench test. The small black circles at the right bottom corner of each figure are the zero points. The closer to the zero point the better the result. In addition, the experimental data and simulation result for the optimal engine parameter setting of each case and objective are encompassed by small dashed circles. The values in the brackets stand for the engine parameter settings of the particular point in the order of throttle position, spark timing, injection timing, IVO and EVC.

From the figures above, it can be seen that all the red points are closer to the zero point than the black points. This means that the multi-objective optimal feedback controller is able to improve the engine performances of ISFC, ISPMN and ISPMM simultaneously based on the established control oriented SI engine model and limited experimental data. Additionally, it is observed that many red points are optimal solutions. From the point of view of multi-

objective control strategy, all of these points are equally as good as each other on the Pareto optimal surfaces with different engine operating conditions because they are all non-dominated solutions and none of them are dominated by others. It is impossible to evaluate which point is the best or which points are better than others. However, engine designers are able to find the best point from these existing and limited optimal candidate points, based on the specific engine design requirements.

The predicted optimal points (A, B, C) for three control objectives (ISFC, ISPMN and ISPMM) and the corresponding experimental data points (the blue ones) are encompassed by dashed circles for every case. By comparing the circled red points and blue points, it is found that they are very close to each other in the figures. Moreover, it is clear that the performances of the blue points are all better than the black points. The detailed numerical analysis is given in Table 6.2.

Table 6.2 The Numerical Analyses of the Validation for Different Cases

	Case No.	**1**	**2**	**3**	**4**	**5**	**6**
A ***ISFC***	Conditions (red & blue)	10,25,260, 26,-52	10,24,350, 24,-29	15,15,300, 22,-40	15,17,300, 20,-27	15,20,250, 10,-25	15,20,350, -24,-2
	Sim (red)	238	230	234	240	228	254
	Exp (black)	245	235	235	261	230	258
	Exp opt. (blue)	240	228	226	243	226	251
	Improvement	**2.0%**	**2.9%**	**3.8%**	**6.9%**	**1.1%**	**2.7%**
B ***ISPMN***	Conditions (red & blue)	10,25,300, 35,3	10,25,300, -13,-55	15,25,300, 29,-41	11.25,300, 5,-12	15,15,300, 5,-50	14,25,300, 1,-23
	Sim (red)	9.29e8	6.63e8	8.80e8	1.75e9	1.99e9	2.94e9
	Exp (black)	1.48e9	1.24e9	1.47e9	2.75e9	1.89e9	3.22e9
	Exp opt. (blue)	8.99e8	6.73e8	9.00e8	1.79e9	1.52e9	3.14e9
	Improvement	**39.26%**	**45.73%**	**38.78%**	**34.91%**	**19.58%**	**2.48%**
C	Conditions	10,20,300,	13,25,300,	15,15,300,	15,25,300,	15,25,300,	15,20,250,

ISPMM	(red & blue)	19,-55	10,-5	29,-52	10,-14	5,-14	-24,-2
	Sim (red)	5.24e-4	5.00e-4	2.76e-4	2.25e-4	1.59e-4	1.89e-4
	Exp (black)	8.21e-4	6.01e-4	3.25e-4	3.21e-4	2.26e-4	2.64e-4
	Exp opt. (blue)	5.64e-4	4.89e-4	2.96e-4	2.36e-4	1.36e-4	2.19e-4
	Improvement	**31.30%**	**18.64%**	**8.92%**	**26.48%**	**39.82%**	**17.05%**

In Table 6.2, the red and black points which have the best performance for each control objective are listed. The "improvement" indicates the percentage improvement comparing the blue point with the black point. It is observed that all the blue points are better than the black points, which means the controller is able to find better points based on the limited experimental data. In other words, the Pareto optimal front is able to cover the boundary points for each control objective. On the other hand, from the comparisons between black points and blue points, up to 6.9%, 45.73% and 39.82% improvements over the given experimental data can be achieved by the controller for ISFC, ISPMN and ISPMM respectively.

As discussed before, all the red points are equally as good as each other. The blue points can only prove that the multi-objective optimal feedback controller is able to find boundary points based on the limited experimental data. The best points can be determined by engine designers from the non-dominated solutions based on the particular compromise requirements.

It is also found that for lower PM emissions, the controller turns to keep the injection timing as late as possible. In a real engine using direct injection, the earlier the fuel is injected into

the cylinder, the more fuel will hit on the piston head, which may cause poor PM performance.

6.3.3 Optimisation Speed

As one of the most important indicators for the controller performance, the average time consumptions of different EA loops are recorded and shown in Figure 6.13. In general, the time required for a particular EA parameters setting for different engine operating cases are almost the same.

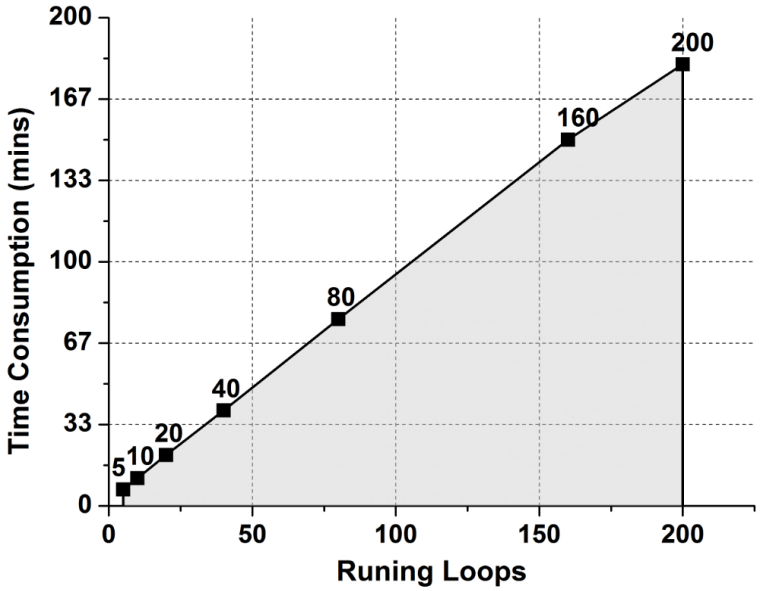

Figure 6.13 EA Optimisation Speed for SI

In Figure 6.13, it shows that the time consumptions linearly increase as the EA running loops increase. The time consumption is counted by “tic” and “toc” commands in Matlab. For the SI engine multi-objective optimal feedback control cases above, 200 loops are applied for

each case. Therefore, it means the SI engine multi-objective optimal feedback control process needs around 3 hours to optimise the engine performances for one case. Compared with traditional engine calibration approach, 3 hours for optimising one operating condition is very fast.

6.4 The Validation of HCCI Engine Multi-objective Optimal Feedback Control

The validation results of HCCI engine multi-objective optimal feedback control are given in the following sections.

6.4.1 Implementation Overview

In order to test the controller within a wide range, the HCCI engine multi-objective optimal feedback controller is validated by 8 HCCI cases with different engine speeds and IMEP. The conditions for these cases are given in Table 6.3 below.

Table 6.3 The Operating Conditions for Each HCCI Case

Case No.	**1**	**2**	**3**	**4**	**5**	**6**	**7**	**8**
Engine Speed	1500		1750		2000			2250
Min IMEP (bar)	3.5	4.0	3.5	4.0	3.0	3.5	4.0	3.0
Max IMEP (bar)	4.0	4.5	4.0	4.5	3.5	4.0	4.5	3.5

The controller needs to run 40 EA loops in order to find the optimal engine parameter settings.

6.4.2 Validation and Results Discussion

The validation results of the 8 different HCCI cases are shown in the 4-D Figure 6.14 to Figure 6.29. There are two figures for each case to display the validation results; one figure is coloured by the ISFC map and the other one is coloured by the ISHC map. The surface in each figure is the map of all the HCCI engine parameter settings (IVO, EVC and λ) which operates within the current engine speed and IMEP range. The 4^{th} dimension of the figure is the different colour on the surface, which indicates a different ISFC or ISHC value. The corresponding values of ISFC and ISHC can be read from the colour scale bar beside the figures. The best performance region is in the dark area. The ISFC and ISHC maps are derived from experimental data when the HCCI engine operates with different engine parameter settings. The red points are the predicted optimal results (non-dominated solutions) which were founded by the HCCI engine multi-objective optimal feedback controller.

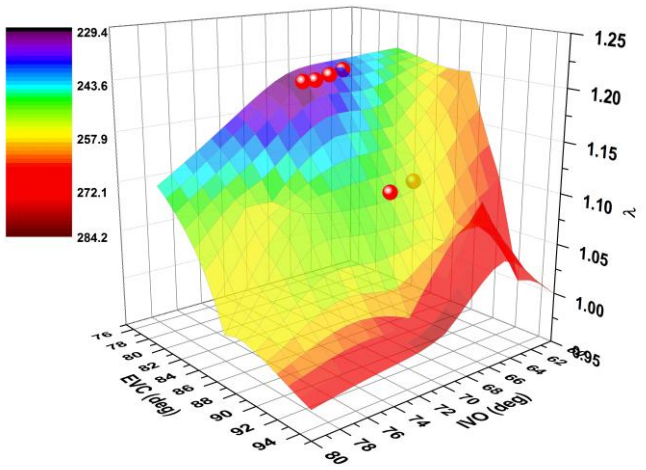

Figure 6.14 Case 1 1500 rpm 3.5_4.0 bar_ISFC (g/kWh)

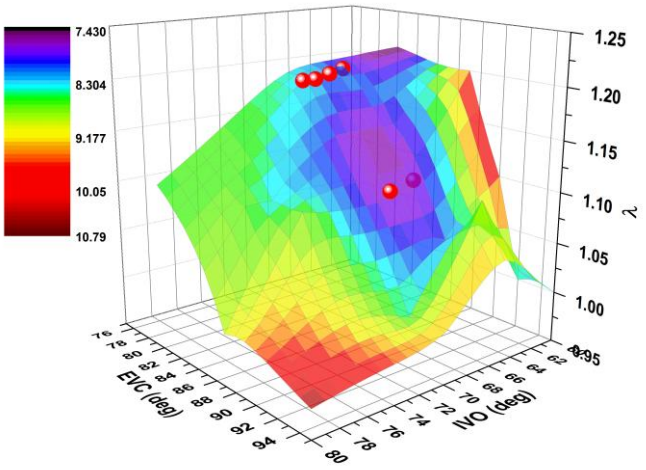

Figure 6.15 Case 1 1500 rpm 3.5_4.0 bar_ISHC (g/kWh)

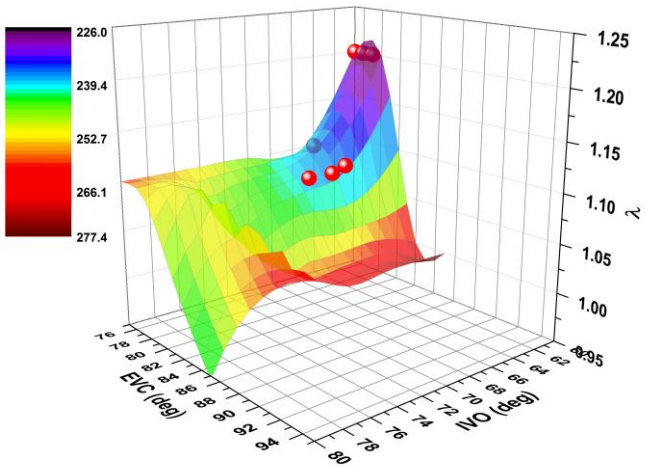

Figure 6.16 Case 2 1500 rpm 4.0_4.5 bar_ISFC (g/kWh)

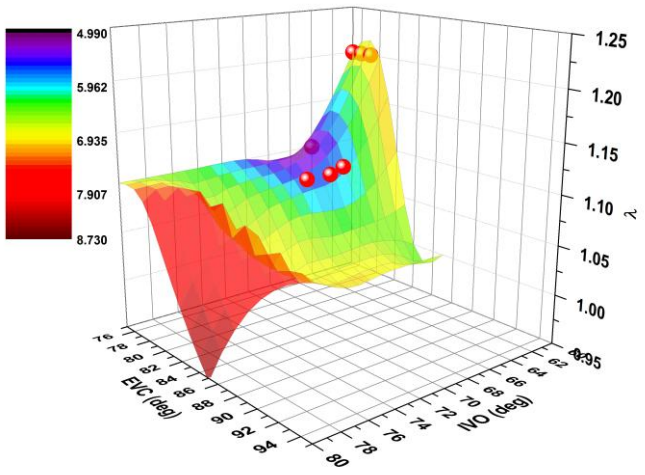

Figure 6.17 **Case 2 1500 rpm 4.0_4.5 bar_ISHC (g/kWh)**

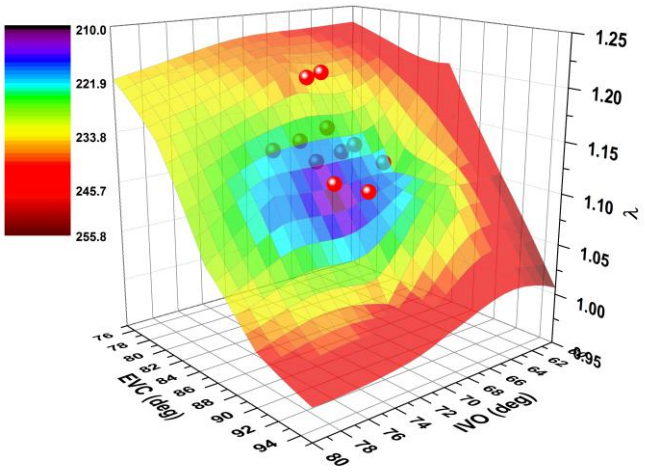

Figure 6.18 **Case 3 1750 rpm 3.5_4.0 bar_ISFC (g/kWh)**

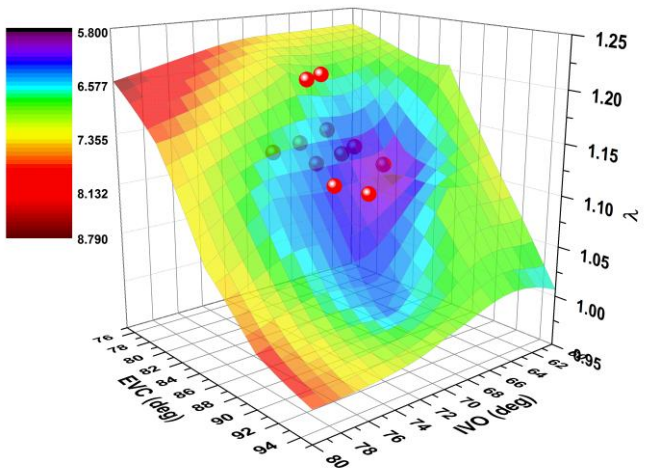

Figure 6.19 **Case 3 1750 rpm 3.5_4.0 bar_ISHC (g/kWh)**

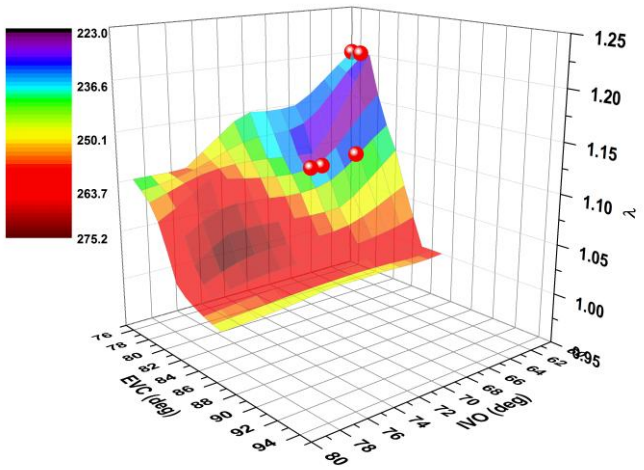

Figure 6.20 Case 4 1750 rpm 4.0_4.5 bar_ISFC (g/kWh)

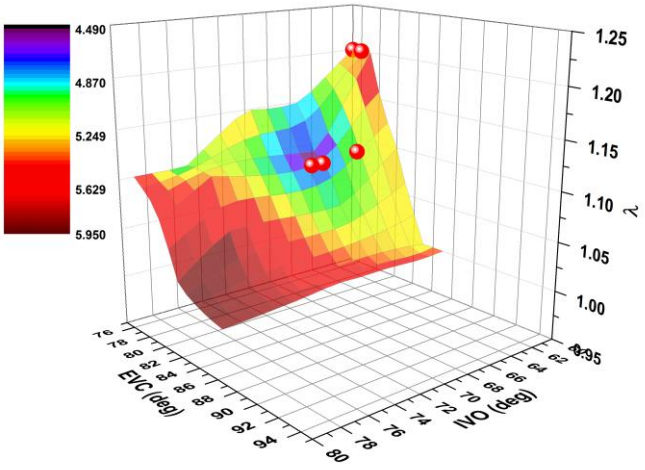

Figure 6.21 Case 4 1750 rpm 4.0_4.5 bar_ISHC (g/kWh)

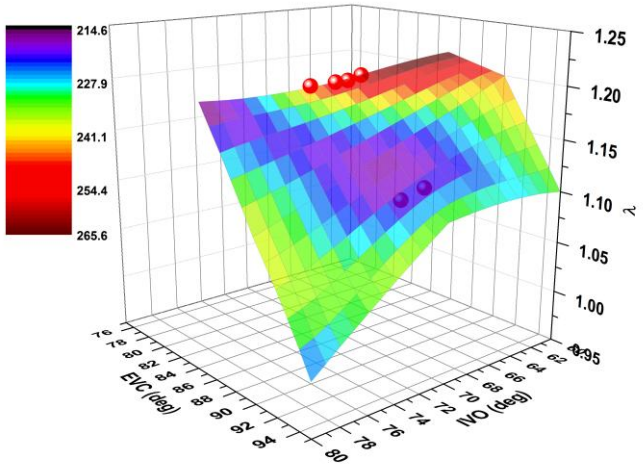

Figure 6.22 Case 5 2000 rpm 3.0_3.5 bar_ISFC (g/kWh)

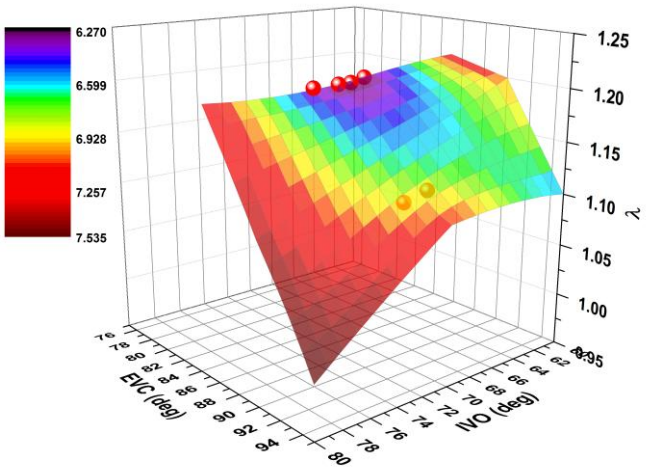

Figure 6.23 **Case 5 2000 rpm 3.0_3.5 bar_ISHC (g/kWh)**

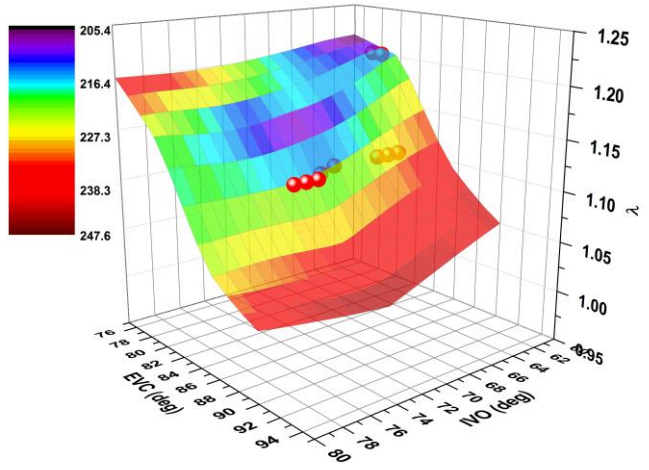

Figure 6.24 **Case 6 2000 rpm 3.5_4.0 bar_ISFC (g/kWh)**

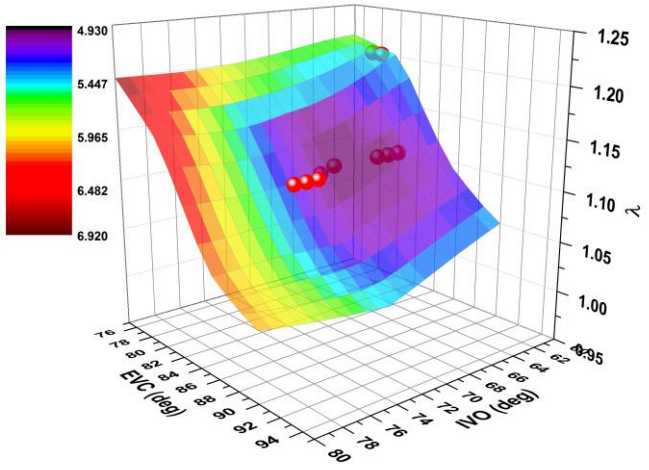

Figure 6.25 **Case 6 2000 rpm 3.5_4.0 bar_ISHC (g/kWh)**

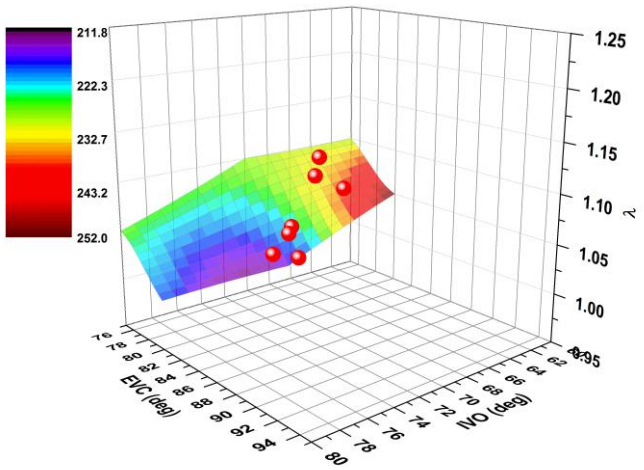

Figure 6.26 Case 7 2000 rpm 4.0_4.5 bar_ISFC (g/kWh)

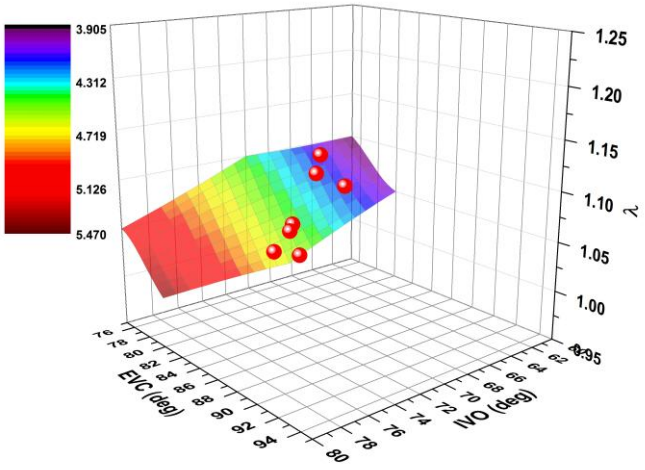

Figure 6.27 Case 7 2000 rpm 4.0_4.5 bar_ISHC (g/kWh)

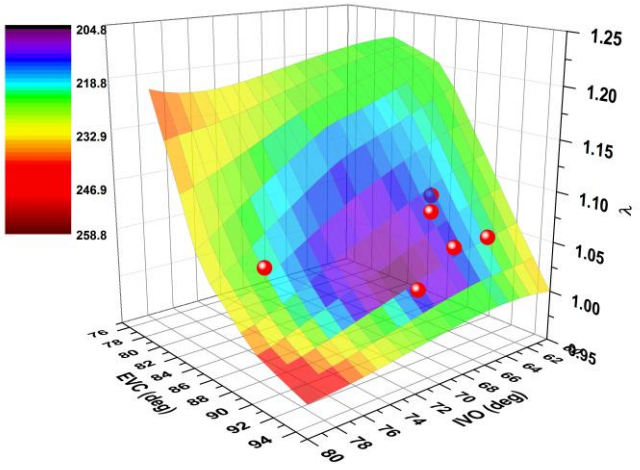

Figure 6.28 Case 8 2250 rpm 3.0_3.5 bar_ISFC (g/kWh)

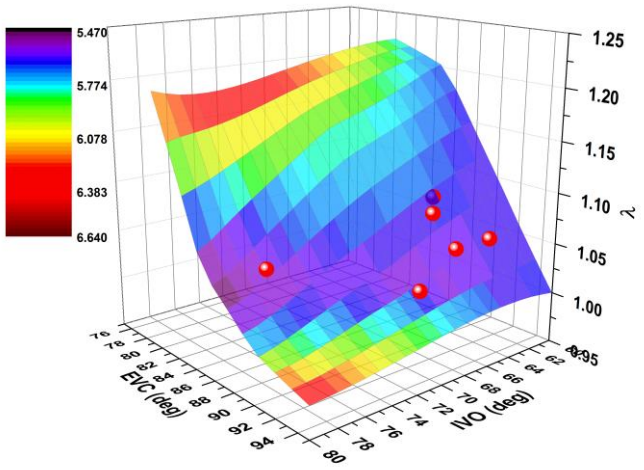

Figure 6.29 Case 8 2250 rpm 3.0_3.5 bar_ISHC (g/kWh)

From the validation results in the figures above, it is observed that most of the red points are located in the purple or blue areas. This implies that the HCCI engine multi-objective optimal feedback controller is able to control the HCCI engine for obtaining the best engine performance in terms of ISFC and ISHC simultaneously. As for the SI cases, these red points are equally good, from the EA based optimal control point of view. For these points, some have better fuel consumption performance, some have better HC emissions performance and some are the compromise results between ISFC and ISHC. Engine designers need to determine which point is the best solution based on the particular design requirements.

In some cases, the validation results are very good, where the red point is located at the centre of purple zone, such as cases 1, 2, 3, 4 and 6. For example, in case 1, the red points are evenly distributed in the purple zones of ISFC and ISHC surfaces. However, some of the cases do not show such good results, e.g. for cases 7 and 8. For case 8, it looks like the controller cannot find the best solution for each control objective and only found some

compromised points in the blue areas. This is mainly due to the simulation errors of the HCCI engine model. Another possible reason is that 40 EA loops are not enough to optimise the engine for achieving the best performance for this case. This case has a relatively wider surface than others which implies that there are more potential parameter settings for this case.

The comparisons between the optimised results and experimental data of case 1 and 2 are shown in Figure 6.30. The experimental points are derived from the experimental data which were used for developing the HCCI engine model.

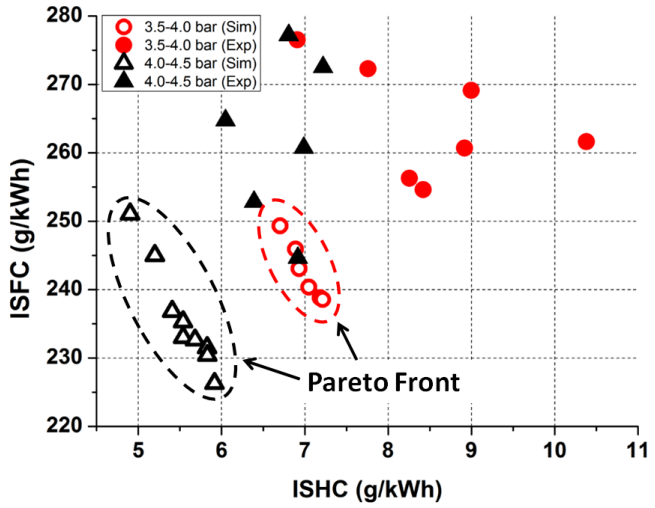

Figure 6.30 Comparisons between the Simulation and Experimental Data (1500 rpm)

From Figure 6.30, the Pareto front indicates the Pareto optimal solutions. It is found that the optimised results for both ISFC and ISHC are better than the experimental results. It means the controller is able to optimise the engine parameters with limited experimental data, but the experimental data should be captured with a wide parameter settings range. The Pareto front of case 1 and case 2 are encompassed by dashes in Figure 6.30. The points in the

Pareto front have the best fitness values for each case, i.e. at least one solution can be found which has lower ISHC and ISFC than a given experimental data point.

Furthermore, the SPEA2 based multi-objective optimisation process can be observed in Figure 6.31 and Figure 6.32. Case 1 is used as an example.

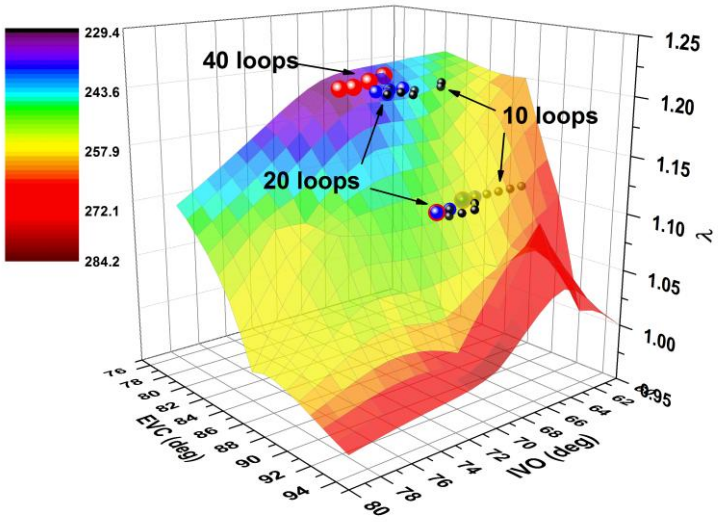

Figure 6.31 1500 rpm 3.5_4.0 bar_ISFC (g/kWh)

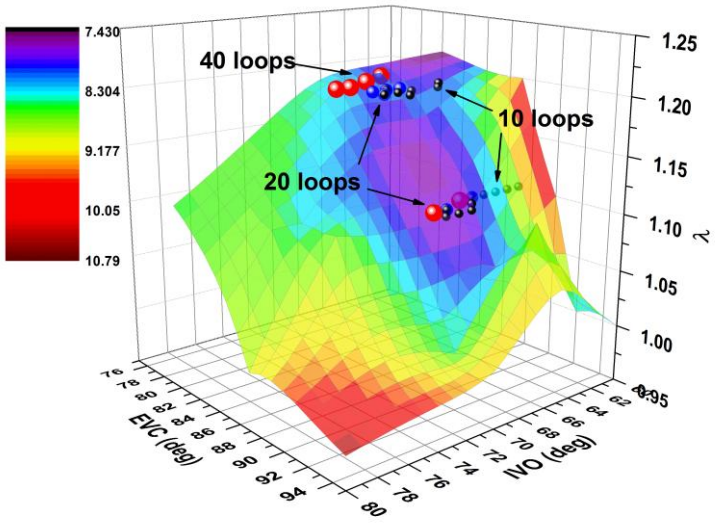

Figure 6.32 1500 rpm 3.5_4.0 bar_ISHC (g/kWh)

In Figure 6.31 and Figure 6.32, the small black points, medium red points and big red points represent 10, 20 and 40 loops of Pareto optimal results respectively. It is found that as the EA running loops increase, the optimal points will "climb" to the practical optimal zone gradually. For the cases with 10 loops, the Pareto optimal points (black) are located somewhere around the practical optimal zone, and some of them even appear in the green and yellow zones in the figure. However, after 20 loops, most of the Pareto optimal points (blue) are found in the blue zones. After 40 optimisation loops, all the Pareto optimal points (red) are located in the practical optimal zones (purple). However, the time consumption of 40 loops is twice as long as that of 20 loops. Therefore, a compromise between optimisation accuracy and time consumption is needed for any engine type or operating conditions. Additionally, it is found some points are overlapped by the Pareto surface of different running loops. The reason is that these points' fitness values were so good that the SPEA2 controller chose to keep them for even more loops.

6.4.3 Optimisation Speed

The average time consumption of the HCCI engine in the multi-objective optimal feedback control case 1 is shown in Figure 6.33. These cases have different EA running loops and the corresponding average engine performances improvements.

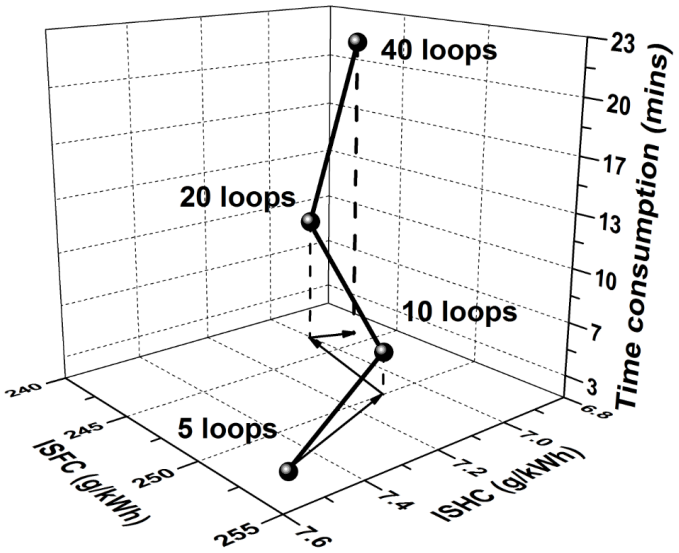

Figure 6.33 Time Consumption for Different Loops

From this figure, it is found that a remarkable improvement is made when the EA running loops increase from 5 to 10. Although it is not as large as before, a considerable improvement is still achieved when the EA running loop number increases from 10 to 20. After 20 loops, the improvement is small. In the foreseeable future, the improvements could be very limited with higher EA running loops. This implies that the improvement amplitude will decrease as the EA running loops increase. In general, no further improvement can be

observed after 100 loops. As a compromise result between optimisation standard and time consumption, the 40 EA running loops setting of HCCI cases is reasonable. It takes around 20 minutes to optimise one HCCI case.

6.5 Comparisons between HCCI EA and SI EA

In order to compare the differences of the multi-objective optimal feedback control system between the SI and HCCI case, a radar figure is created and demonstrated in Figure 6.34.

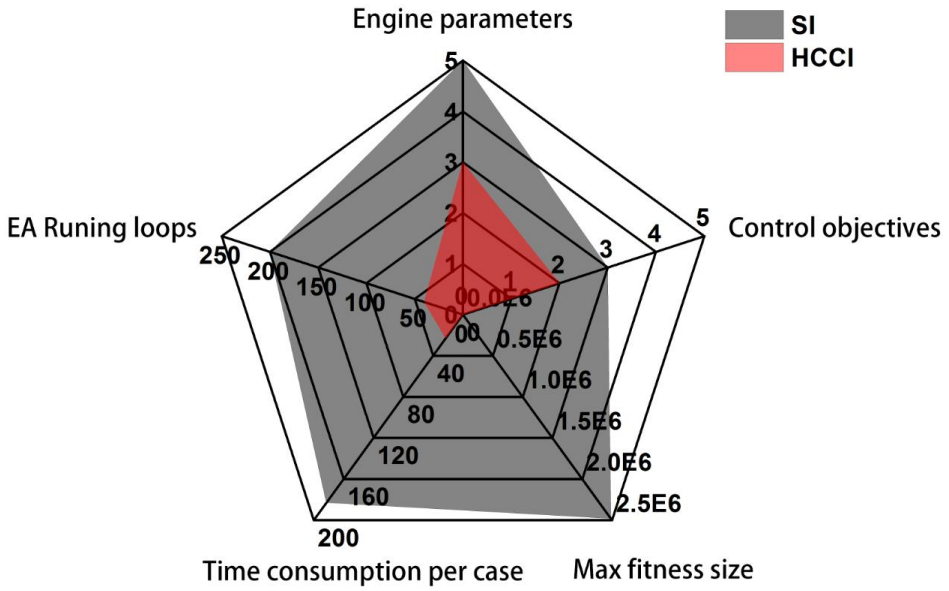

Figure 6.34 SI HCCI EA Comparisons

In Figure 6.34, it is very obvious that the SI cases are much more complex than the HCCI cases. This is mainly because more engine parameters and control objectives were introduced in the SI optimal control cases.

In theory, there is no limitation of the parameter input number and control objectives of the developed multi-objective optimal feedback controller. However, if there are too many different control objectives, the time consumption could be significantly longer and the points pound maybe of no use. This is because it is impossible to optimise all the control objectives simultaneously so it has to sacrifice some objectives to improve others. The improved amplitude for single objective optimal control is definitely larger than multi-objective optimal feedback control. Too many control objectives will lead the controller to find some “common performance” points, which are of no use. A weighting factor needs to be introduced into the controller to determine the priority for every control objective. Therefore, it is necessary to first carefully determine the control objectives; principally to choose the most important control objectives.

6.6 Summary

In this chapter, a novel method of optimising engine operating conditions under given objectives has been developed. The validation results of the developed SI/HCCI engine multi-objective optimal feedback controller are given. There are 6 and 8 different operating cases which are tested for the SI and HCCI engine respectively. The results showed very good control performance. The SI engine controller needs around 3 hours to obtain the best

engine performance points for one case. The HCCI engine controller needs around 20 minutes to obtain the best engine performance points for one case.

For the SI engine cases, there are up to 6.9%, 45.73% and 39.82% improvements over the given experimental data which can be achieved for ISFC, ISPMN and ISPMM respectively by the developed controller. For the HCCI cases, after 40 optimisation loops, all the Pareto optimal points are located in the practical optimal zones. It means the controller is able to find better performance points based on the limited experimental data.

It should be noticed that it is first necessary to carefully determine the control objectives. Otherwise, the time consumption could be significantly longer and the points found maybe of no use.

Chapter 7 Self-stabilisation Feature of HCCI Combustion

The combustion timing, work output and in-cylinder peak pressure for HCCI engines often converge to a stable equilibrium point, which implies that the HCCI combustion may have a self-stabilisation feature. It is thought that this behaviour is due to the competing residual-induced heating and dilution of the reactant gas. In this chapter, the self-stabilisation feature of HCCI combustion is discussed by experimental studies. The experimental studies are mainly focused on the change of COVs. Detailed analysis and discussion will be given.

7.1 Introduction

The self-stabilisation feature of HCCI combustion had been observed by many researchers and mentioned in some publications previously. However, there is no report to analyse this phenomenon from the view of system control. Because all or most of the fuel is injected into the cylinder during the NVO process and spark plug is not used for ignition in HCCI engines, there is no direct dominating control of the ignition, although a spark can be used to affect the ignition timing. The experimental or numerical validation of this feature will give control engineers confidence to control the HCCI combustion reliably and efficiently.

Moreover, from the study of the HCCI engine multi-objective optimal feedback control system which was presented in the previous chapter, it is found that the engine parameter settings are varied very frequently when the controller is operating. The self-stabilisation behaviour of HCCI engines will bring great benefit to the multi-objective optimal feedback control system to give the controller better efficiency and reliability when the control strategy is used in a real HCCI engine. It is considered that DoE can be a useful tool for the study of the HCCI engine multi-objective optimal feedback control. Therefore, it is very useful to study the self-stabilisation feature of HCCI combustion, so that some guide lines can be obtained.

To study the HCCI self-stabilisation behaviour experimentally, the experimental data for COVs of cylinder B2 in the HCCI engine is used. Transient responses with different operating condition changes are utilized as indicators of stability. The change of COV indicates how the engine is stabilized from one relatively stable point to another.

7.2 Experimental Study and Discussions

For testing the HCCI self-stabilisation behaviour, different types of transient experiments were designed. Firstly, the comparisons of COVs between different engine speeds (1500 rpm

and 2000 rpm) are presented when the IMEP is changed with different amplitudes. Secondly, the comparisons of HCCI self-stabilisation features with different IMEP change amplitudes are made. Also, the comparisons between SI and HCCI are discussed. For each case, the experiments take 2 minutes to record the COV change, and the IMEP transient at 0 point. In order to remove the noise points, the COV symbols in the figures below are all extracted from the raw data every 0.2 seconds. Moreover, for the HCCI transient process of each case, one step change of EVC is the unique approach to change the IMEP. For the SI cases, although the changing of throttle position is the most commonly used approach to change engine IMEP, it is implemented by one step change of spark timing in this case. There is no special method used to smooth the transient process for the HCCI and SI experiments.

Because there are many engine parameters which can affect engine IMEP, such as throttle position (for SI engines), spark timing, air fuel ratio (for HCCI engines), valves timing and injection timing, it is essential to choose a unique approach from them for both SI and HCCI to change the operating condition. Because the dSPACE control system and the new developed transient test model are implemented in the study, which are introduced in Chapter 3, the engine parameters can be changed and programmed independently. For this particular study, in order to enable the transient efficiency to be as high as possible for SI and HCCI conditions, spark timing and EVC phasing are used for changing the IMEP for the SI and HCCI engine respectively. The detailed transient approaches are shown as Table 7.1. The spark timing can be adjusted within one engine cycle, and the EVC phasing can be adjusted in 0.4-1 seconds, i.e. 5-10 engine cycles.

Table 7.1 The Detailed Approaches for SI and HCCI IMEP Transitions

		SI						HCCI					
		High-to-low			Low-to-High			High-to-low			Low-to-High		
1500 rpm	Range (bar)	4.2-4.0	4.6-4.0	4.9-4.0	4.0-4.3	4.0-4.6	4.0-4.9	4.2-4.0	4.6-4.0	4.9-4.0	4.0-4.3	4.0-4.6	4.0-4.9
	EVC (bTDC)							15-10	25-10	35-10	10-15	10-25	10-35
	Spark Timing (bTDC)	15-12	20-12	25-12	12-15	12-20	12-25						
2000 rpm	Range (bar)	4.0-3.5	4.3-3.5	4.5-3.5	4.8-3.5	4.0-4.3	4.0-4.5	4.0-4.7	4.0-4.9	4.0-3.5	4.3-3.5	4.5-3.5	4.8-3.5	4.0-4.3	4.0-4.5	4.0-4.7	4.0-4.9
	EVC (bTDC)									16-8	20-8	25-8	32-8	10-15	10-25	10-35	10-40
	Spark Timing (bTDC)	12-8	18-8	22-8	30-8	12-15	12-20	12-25	12-30								

7.2.1 Comparisons of IMEP Change at Different Speeds for the HCCI Engine

The comparisons of COVs between different engine speeds (1500 rpm and 2000 rpm) are presented in Figure 7.1 to Figure 7.6, when the IMEP is changed resulting in different amplitudes which include IMEP increases and decreases. In the figures, the final value for the averaged response of each case and the corresponding time are indicated by dash lines. It is needed to mention that the COV and IMEP have different time scale.

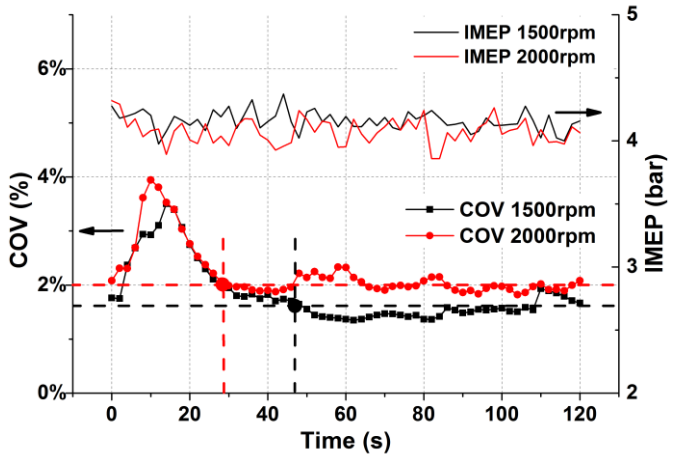

Figure 7.1 **Case 1 HCCI Transient for High-to-Low IMEP**

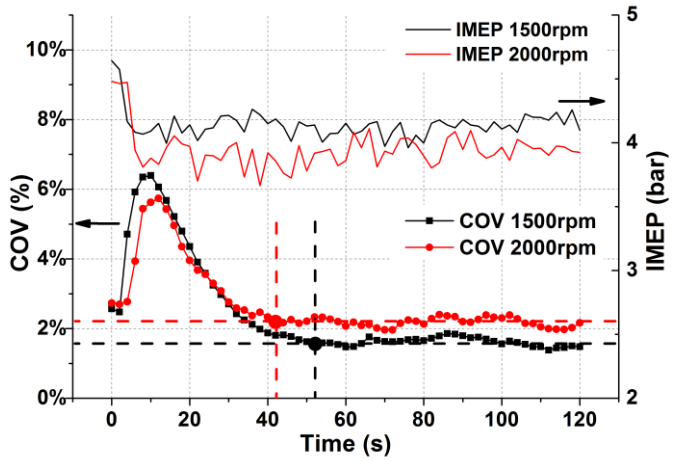

Figure 7.2 **Case 2 HCCI Transient for High-to-Low IMEP**

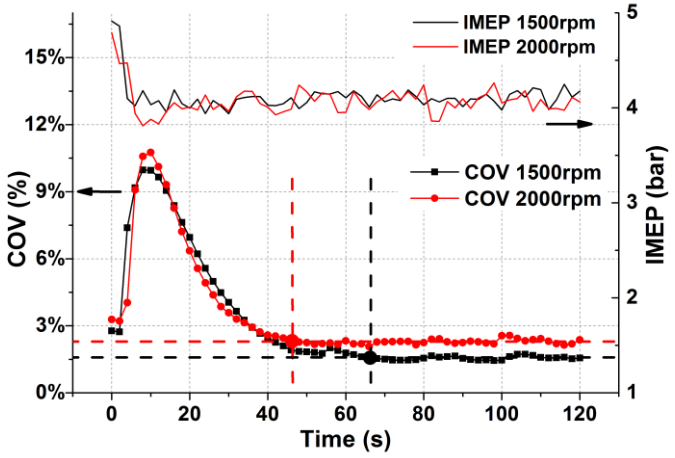

Figure 7.3 **Case 3 HCCI Transient for High-to-Low IMEP**

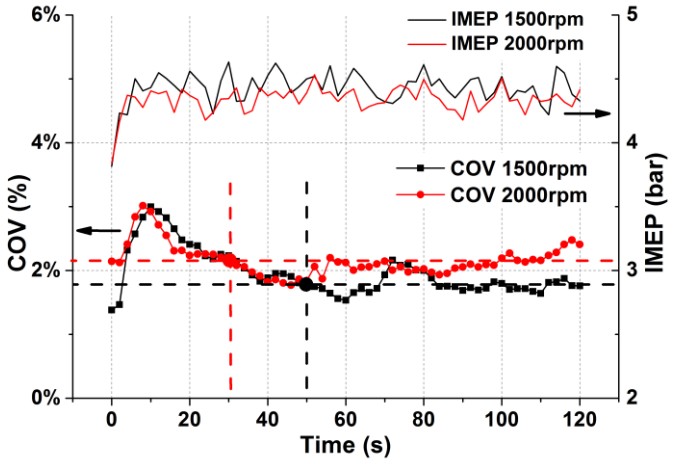

Figure 7.4 **Case 4 HCCI Transient for Low-to-High IMEP**

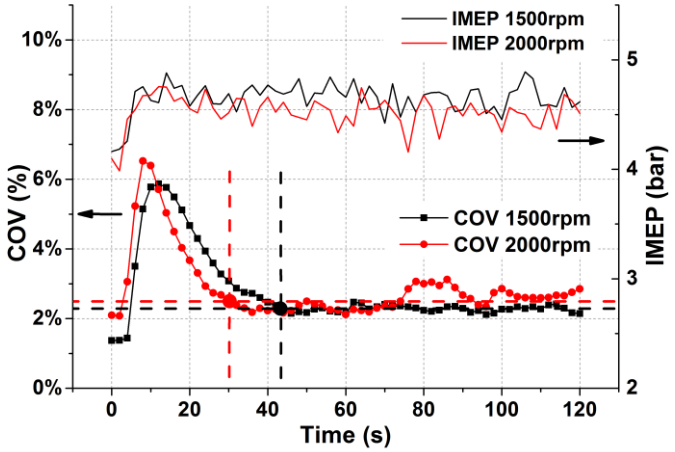

Figure 7.5 **Case 5 HCCI Transient for Low-to-High IMEP**

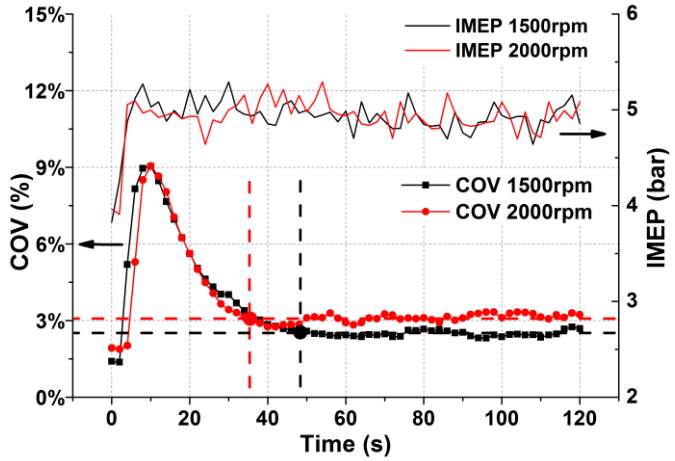

Figure 7.6 **Case 6 HCCI Transient for Low-to-High IMEP at 1500 rpm and 2000 rpm**

From Figure 7.1 to Figure 7.6, there are two features of HCCI engines which can be observed directly. Firstly, during the transient process, the higher engine speed leads to faster self-stabilisation speed. This is mainly because the time duration for each engine cycle is short for higher engine speed cases, which have relatively more engine cycles to stabilisation during the transient period. Secondly, higher engine speed leads to higher COVs. The reason is that the shorter engine cycle duration allows the HCCI combustion phase to retard greatly, which causes the combustion reactions to be incomplete. As a result, the combustion is not as stable as the low engine speed cases.

In order to analyse the HCCI self-stabilisation behaviour further, the COV percentage overshoot ($P.O.$) of each case is calculated by Equation 7.1 and given in Table 7.2. Here, M_{P_t} is response peak value; fv is the response final-value (Dorf and Bishop 2001).

$$P.O. = \frac{M_{P_t} - fv}{fv} \times 100\%$$

Equation 7.1 The Equitation to Calculate P.O.

Table 7.2 The Calculation Results of M_{P_t}, fv and $P.O.$ for Each Case

Case No.	1		2		3		4		5		6	
Speed (rpm)	1500	2000	1500	2000	1500	2000	1500	2000	1500	2000	1500	2000
M_{P_t}(%)	3.5	3.9	6.4	5.7	9.9	10.8	3.0	3.0	5.8	6.5	9.0	9.0
fv (%)	1.5	1.9	1.6	2.1	1.5	2.3	1.8	2.1	2.3	2.6	2.5	3.2
$P.O.$ (%)	133.33	105.26	300.00	171.43	560.00	369.57	66.67	42.86	152.17	150.00	260.00	181.25

From Table 7.2, it is found that higher engine speeds present smaller $P.O.$. This implies that the transient process for higher speeds is smoother than for lower speeds with same IMEP change amplitude.

7.2.2 Comparisons of IMEP Change at Same Speeds for the HCCI Engine

The comparisons of COVs between different IMEP changes amplitudes at 1500 rpm and 2000 rpm are presented in Figure 7.7 to Figure 7.10.

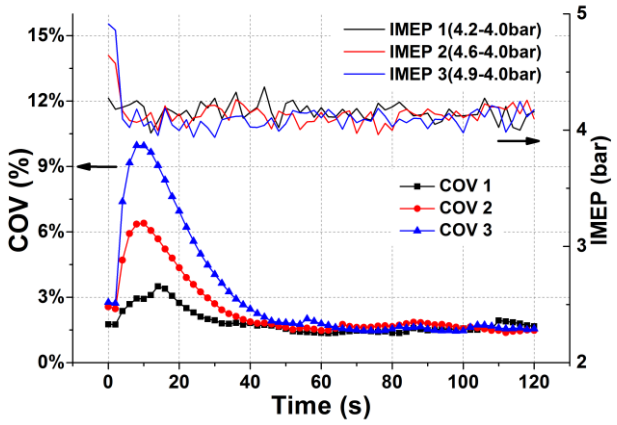

Figure 7.7 HCCI Transient for High-to-Low IMEP at 1500 rpm

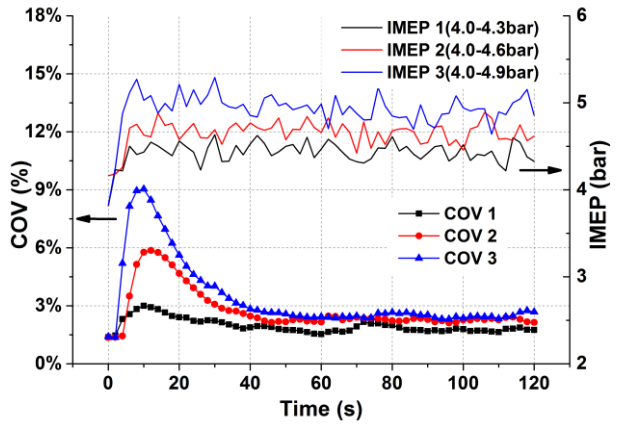

Figure 7.8 HCCI Transient for Low-to-High IMEP at 1500 rpm

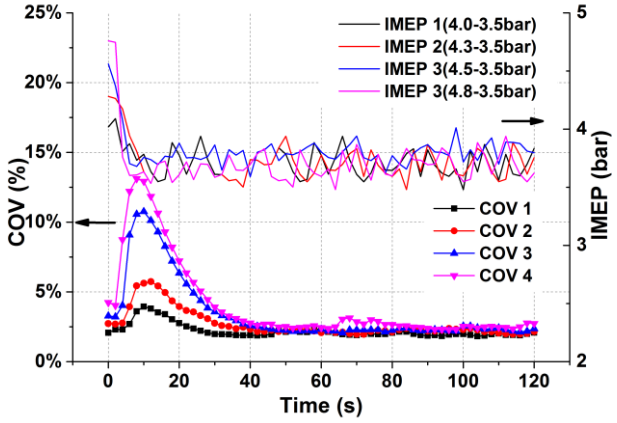

Figure 7.9 HCCI Transient for High-to-Low IMEP at 2000 rpm

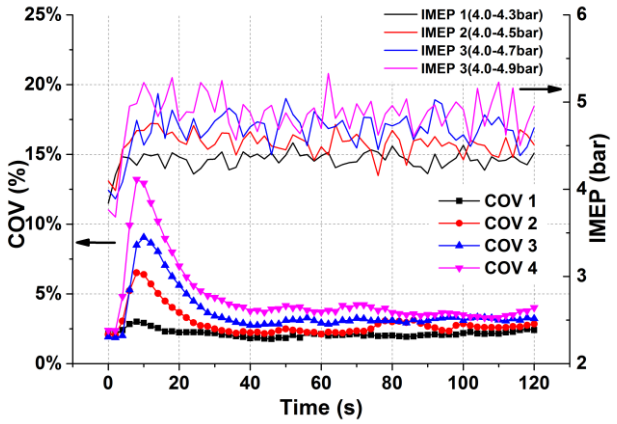

Figure 7.10 HCCI Transient for Low-to-High IMEP at 2000 rpm

From Figure 7.7 to Figure 7.10, it is found that during the transient process a larger IMEP change amplitude leads to higher overshoot, i.e. a more severe transient process. Also, it is observed that for HCCI combustion, higher IMEP leads to higher COVs.

7.2.3 Comparisons of SI and HCCI Engines

In order to compare the HCCI self-stabilisation behaviour with conventional SI engines, the COVs of different IMEP change amplitudes at different engine speeds in SI and HCCI mode are recorded and shown in Figure 7.11 to Figure 7.24. To facilitate the analysis, the marked blue lines with symbols indicate the average COV value per 20 seconds.

1500 rpm low-to-high IMEP transitions:

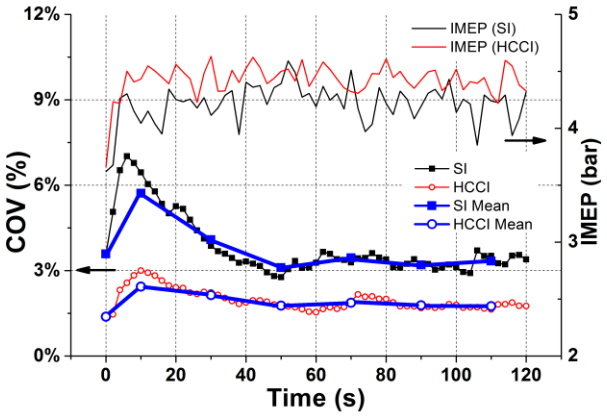

Figure 7.11 Case 1 IMEP Transient from 4.0 to 4.3 bar at 1500 rpm

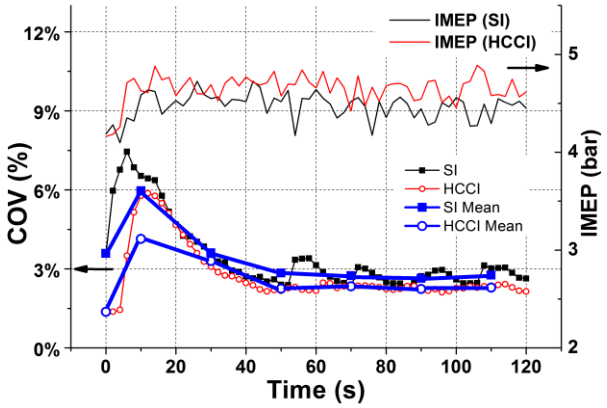

Figure 7.12 Case 2 IMEP Transient from 4.0 to 4.6 bar at 1500 rpm

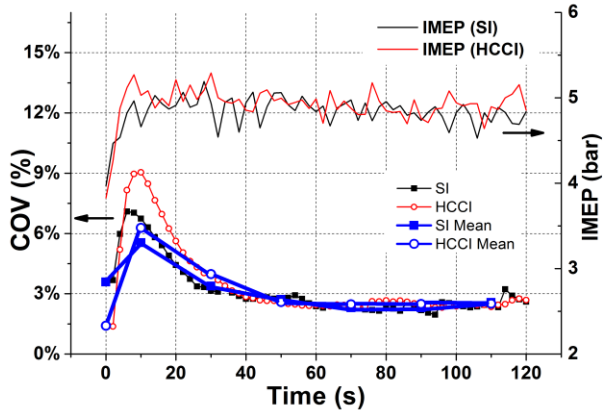

Figure 7.13 Case 3 IMEP Transient from 4.0 to 4.9 bar at 1500 rpm

1500 rpm high-to-low IMEP transitions:

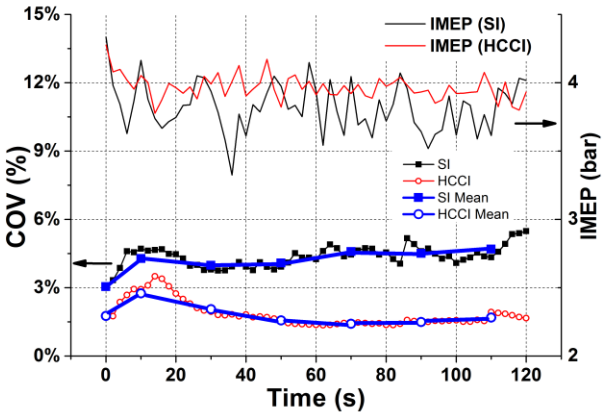

Figure 7.14 **Case 4 IMEP Transient from 4.2 to 4.0 bar at 1500 rpm**

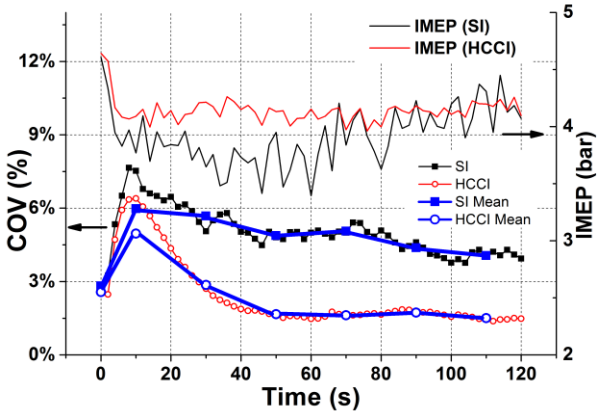

Figure 7.15 **Case 5 IMEP Transient from 4.6 to 4.0 bar at 1500 rpm**

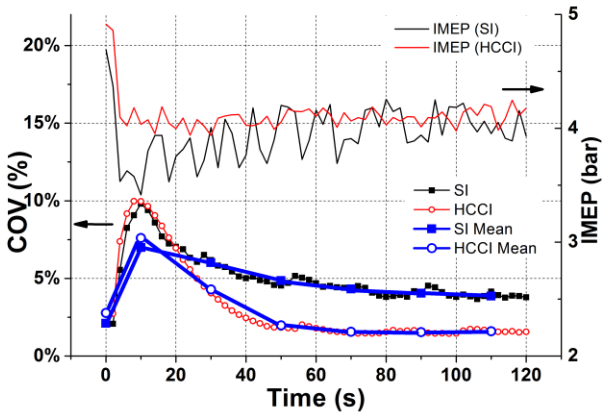

Figure 7.16 **Case 6 IMEP Transient from 4.9 to 4.0 bar at 1500 rpm**

2000 rpm low-to-high IMEP transitions:

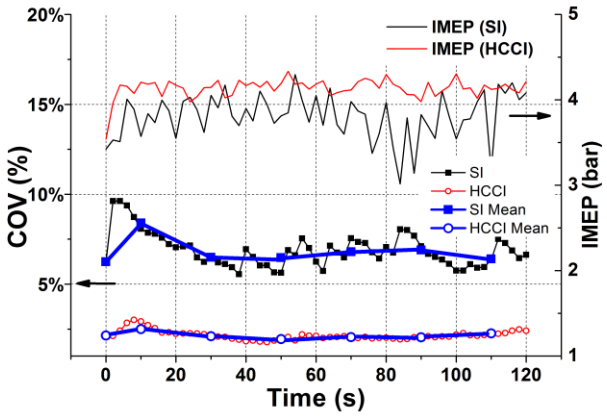

Figure 7.17 Case 7 IMEP Transient from 4.0 to 4.3 bar at 2000 rpm

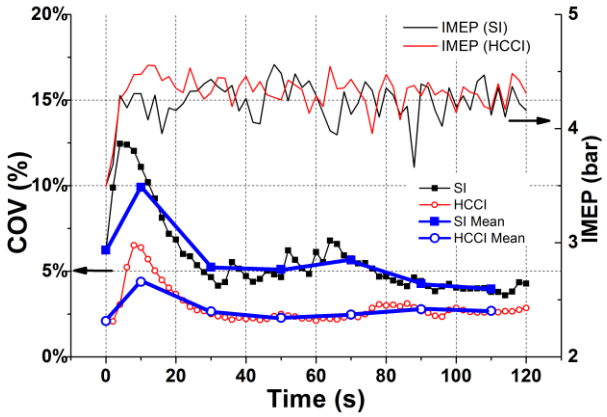

Figure 7.18 Case 8 IMEP Transient from 4.0 to 4.5 bar at 2000 rpm

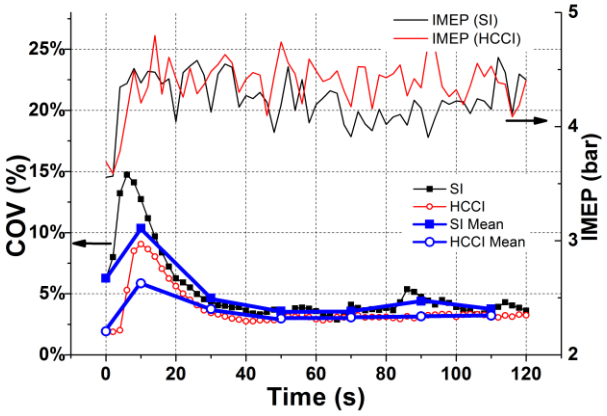

Figure 7.19 Case 9 IMEP Transient from 4.0 to 4.7 bar at 2000 rpm

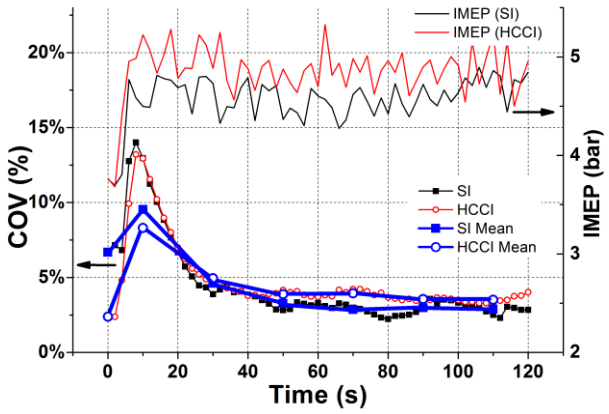

Figure 7.20 Case 10 IMEP Transient from 4.0 to 4.9 bar at 2000 rpm

2000 rpm high- to-low IMEP transitions:

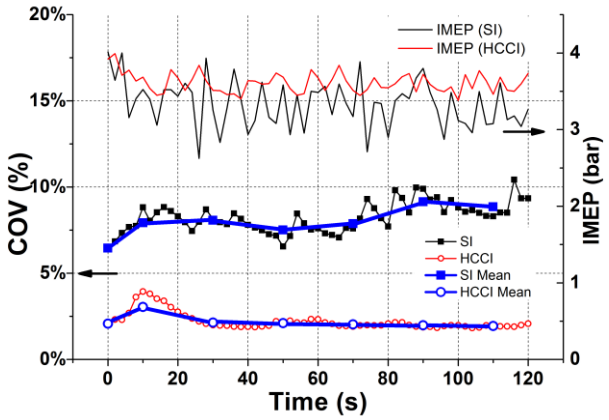

Figure 7.21 Case 11 IMEP Transient from 4.0 to 3.5 bar at 2000 rpm

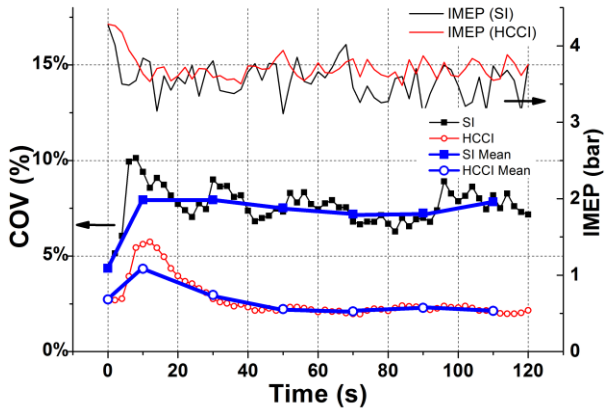

Figure 7.22 Case 12 IMEP Transient from 4.3 to 3.5 bar at 2000 rpm

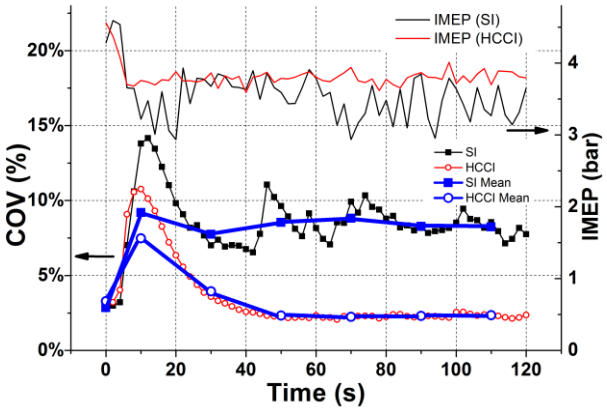

Figure 7.23 Case 13 IMEP Transient from 4.5 to 3.5 bar at 2000 rpm

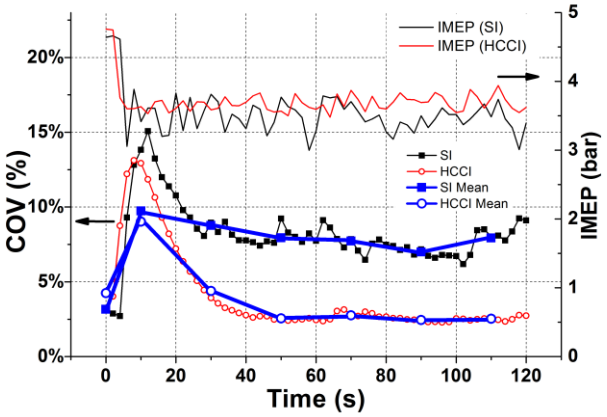

Figure 7.24 Case 14 IMEP Transient from 4.8 to 3.5 bar at 2000 rpm

From Figure 7.11 to Figure 7.24, it is clear that the SI combustion has higher COVs than HCCI combustion. For some of the SI cases above, they are not stable even after 2 minutes, such as case 4, 5, 6, 8, 11, 12, 13 and 14. It is believed that these unstable cases are not due to the operating condition transition, but rather that these conditions can never achieve stability. In this study the definition of stability is the COV converging to the final-value for 30 seconds with a maximum error of $\pm 10\%$. It implies that the HCCI combustion has better stability, although there is no direct control approach to control HCCI combustion. The numerical study analyses of the figures above are given in Table 7.3, where, T_s is stable time read from the blue symbol lines.

Table 7.3 Calculation Results of M_{P_t}, fv, $P.O.$ and T_S

Case No.	1		2		3		4		5		6		7		8		9		10		11		12		13		14	
Mode	SI	HCCI	SI	HCCI	SI	HCCI	SI	HCCI	SI	HCCI	SI	HCCI	SI	HCCI	SI	HCCI	SI	HCCI	SI	HCCI	SI	HCCI	SI	HCCI	SI	HCCI	SI	HCCI
M_{P_t}(%)	7.0	2.9	7.4	5.8	7.1	9.0	NA	3.5	NA	6.4	NA	9.9	9.6	3.0	NA	6.5	14.7	9.1	14	13	NA	3.9	NA	5.7	NA	10.7	NA	13.1
fv (%)	3.3	1.8	2.7	2.3	2.4	2.5	NA	1.9	NA	1.5	NA	1.5	6.7	2.2	NA	2.7	3.9	3.2	2.9	4.2	NA	2.2	NA	2.2	NA	2.3	NA	2.8
$P.O.$(%)	112	61	174	152	195	260	NA	84	NA	326	NA	560	43	36	NA	140	276	184	382	209	NA	77	NA	159	NA	365	NA	367
T_S (s)	70	50	50	50	50	40	NA	50	NA	50	NA	70	30	30	NA	50	50	40	70	50	NA	30	NA	50	NA	50	NA	50

From Table 7.3, for most of the cases, the $P.O.$ values of HCCI are smaller than SI. This implies that the HCCI combustion has smoother performance when the engine operating condition is changed. The stability of SI is not as good as HCCI. It is also found that the stable time T_S of HCCI are all equal to or shorter than SI, despite there being no direct approach to control HCCI combustion.

In order to analyse this HCCI combustion feature further, case 1 is subjected to further analysis. Case 1 compares the stability of the transient process for SI and HCCI conditions. The engine speed was fixed at 1500 rpm, and the IMEP was increased from 4.0 to 4.3 bar. Although the COVs comparisons of case 1 have been shown in Figure 7.11 and Table 7.3, it is still necessary to compare the peak pressure and MFB50 location of the SI and HCCI engines. The peak pressure and MFB50 location comparison of the first 900 engine cycles, i.e. the first 72 seconds, of case 1 is shown in Figure 7.25 and Figure 7.26.

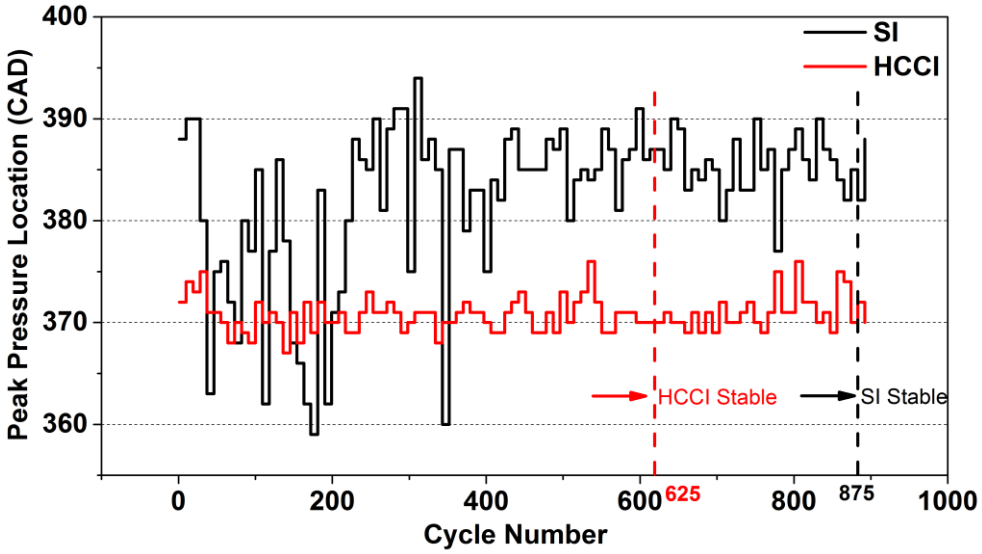

Figure 7.25 The Peak Pressure Location of Case 1

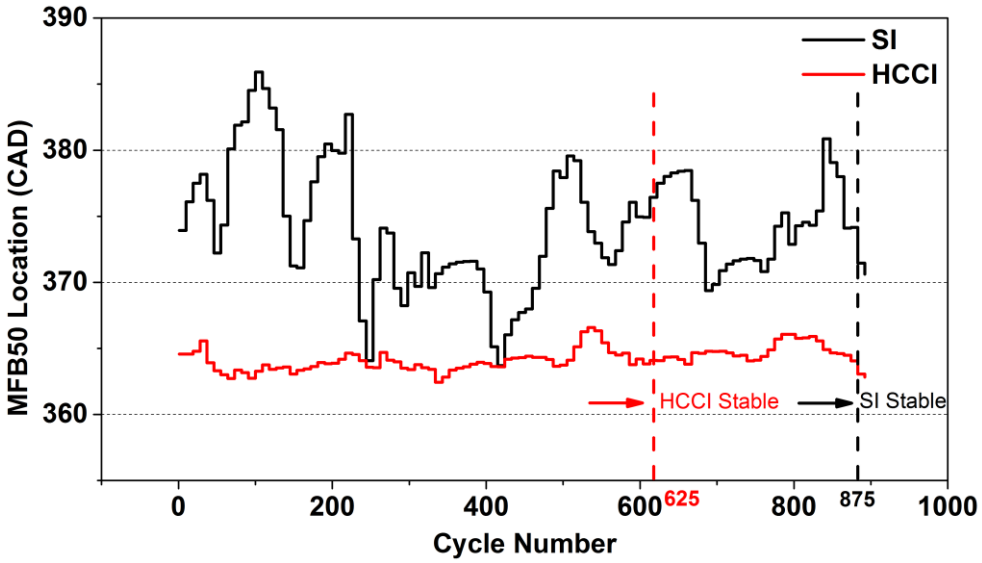

Figure 7.26 The MFB50 Location of Case 1

Compared with SI combustion, the peak pressure and MFB50 location fluctuation of HCCI combustion is much smaller. For HCCI combustion, the fluctuation amplitude of peak pressure and MFB50 locations before HCCI stable timing is similar to the fluctuation amplitude after the HCCI stable timing, which is very different from SI combustion. For SI combustion, the fluctuation amplitude of peak pressure and MFB50 locations are very large,

as shown in Figure 7.25 and Figure 7.26. It indicates that the HCCI combustion phase will not change remarkably even during the transition period compared with SI combustion.

For the auto-ignition of HCCI combustion, the most important factors are in-cylinder pressure, temperature and concentration. For concentration, it is mainly determined by the internal EGR fraction which is mainly affected by the preceding engine cycle, something that is very different from SI combustion. This explains why HCCI combustion has better stability than SI combustion without any direct control approach during the transient process i.e. the HCCI combustion is a continuous cycle-based self-tuning process; the combustion performance of the current engine cycle is affected by the preceding engine cycle and will affect the following engine cycle. Therefore, it is able to consider the in-cylinder conditions as cycle-based enabling the continuous control of the HCCI combustion. Comparatively, the spark ignition control signal for SI engines is too robust.

The self-stabilisation behaviour of HCCI combustion is also a considerable benefit to the DoE of EA based engine multi-object optimisation control. This is because HCCI has a more efficient transition response performance, which is able to finish the same testing loops within a much shorter timeframe.

7.3 Summary

In this chapter, the self-stabilisation features of HCCI combustion during IMEP and speed transitions are experimentally studied. The conclusions of experimental results can be summarized as:

1. For HCCI engines, during the transient process, the higher engine speed leads to faster stabilisation, and higher speed leads to higher COVs. Moreover, the transient process at higher engine speeds is smoother than at lower engine speeds with the same IMEP change amplitude.
2. For HCCI engines, during the transient process, larger IMEP change amplitudes leads to higher overshoot, i.e. a more severe transient process. Also, it is observed that for higher IMEP the COVs are higher.
3. The HCCI combustion has a smoother performance than that of SI engines when the engine operating condition is changed. Additionally, the stability times T_s of HCCI are all equal to or shorter than SI, despite there being no direct control approach for HCCI combustion.
4. Compared with SI combustion, the peak pressure and MFB50 location fluctuation of HCCI combustion is much smaller. For HCCI combustion, the fluctuation amplitude of peak pressure and MFB50 locations before HCCI stability timing are similar to the fluctuation amplitude after the HCCI stability timing.

The HCCI combustion is a continuous cycle-based self-tuning process; the combustion performance of the current engine cycle is affected by the preceding engine cycle and will affect the following engine cycle. Therefore, it is able to consider the in-cylinder conditions

as cycle-based continuous control signals. As one of the most important features of HCCI combustion, the summarized findings are useful to the DoE of HCCI engine multi-objective optimal feedback control.

Chapter 8 Conclusions and Future Work

The main target of this thesis is to study and develop a novel multi-objective optimal feedback control strategy for SI and HCCI engine, which is based on the real-time control oriented SI/HCCI cycle-to-cycle statistical model and a SPEA2 based multi-objective optimal feedback controller. The main conclusions of this thesis are presented in this chapter and followed by suggestions for future work.

8.1 Conclusions

The conclusions are divided by three parts and shown below.

8.1.1 Studies on Control Oriented SI & HCCI Engine Modelling

A control oriented SI and HCCI engine model have been developed, and the referenced key parameters in the model have been obtained by using statistical modelling approach based

on limited experimental data. The detailed conclusions of the models can be summarized as follows:

1. The Wiebe function and AFBR method (statistical model) demonstrated in the chapter 4 are well suited to simulate the gasoline-fuelled SI and HCCI combustion process. The SI model is able to predict the MFB, combustion duration, in-cylinder pressure, peak pressure, peak pressure position, IMEP, ISFC, ISPMN and ISPMM with acceptable errors. The HCCI model is able to calculate the HCCI MFB, AIP (MFB 10), combustion duration, in-cylinder pressure, peak pressure, peak pressure position, IMEP, ISFC and ISHC with sufficient accuracy. The simulated AIP error is within 1.6 CAD, and the combustion duration error is within 2.1 CAD. IMEP, ISFC and ISHC errors were within 11%, 12% and 10% respectively.
2. The HCCI engine model can provide the correct main features with acceptable accuracy for in-cylinder pressure, F_{rg}, M_{air} and M_{fuel} during the transient process.
3. The models can be used to run cycle-to-cycle in real-time when the SI engine is operated below 8570 rpm or the HCCI engine is operated below 4800 rpm, which allows engineers to design real-time control strategy based on these models for SI and HCCI engine control in the future.
4. The model is very easy to change the parameters to match a different engine. Although the correlation coefficients matrixes for combustion model and emissions model are needed to update each time based on the experimental data, the fitting function formation are not needed to be changed. The matrixes are easy to be obtained by a Matlab programme based on the experimental data.

8.1.2 The SI/HCCI Engine Multi-objective Optimal Feedback Control

The SPEA2 based multi-objective optimal feedback controller is successfully used for model-based engine control. The calculated results from the developed SI/HCCI engine multi-objective optimal feedback controller have been validated. This includes 6 and 8 different operating cases tested for SI and HCCI engine respectively. The results showed very good control performance. The SI engine controller needs around 3 hours to obtain the best engine performance points for one case. The HCCI engine controller needs around 20 minutes to have the best engine performance points for one case. Compared with traditional engine calibration approach, this is very fast.

For the SI engine cases, there are up to 6.9%, 45.73% and 39.82% improvements over the given experimental data could be achieved for ISFC, ISPMN and ISPMM respectively by the developed controller. For HCCI cases, after 40 optimisation loops, all the Pareto optimal points are located in the practical optimal zones. It means the controller is able to find better performance points based on the limited given experimental data.

It should be noticed that it is necessary to carefully choose the control objectives at the first. Otherwise, the time consumption could be considerable and the founded points maybe of

no use. Otherwise, it is needed to introduce weighting factor into the controller to determine the priority for every control objective.

8.1.3 Studies on the HCCI Self-stabilisation Features

For testing the HCCI self-stabilisation behaviour, different types of transient experiments were designed. Firstly, the comparisons of COVs between different engine speeds (1500 rpm and 2000 rpm) in HCCI mode are presented when the IMEP is changed with different amplitudes. Secondly, the comparisons of HCCI self-stabilisation features with different IMEP change amplitudes are made. Finally, the comparisons between SI and HCCI are taken. The conclusions of the experimental study of the HCCI self-stabilisation features are summarized as follows:

1. For HCCI engines, during the transient process, the higher engine speed leads to faster stabilisation, and higher speed leads to higher COVs. Moreover, the transient process at higher engine speeds is smoother than at lower engine speeds with the same IMEP change amplitude.
2. For HCCI engines, during the transient process, larger IMEP change amplitudes leads to higher overshoot, i.e. a more severe transient process. Also, it is observed that for higher IMEP the COVs are higher.
3. The HCCI combustion has a smoother performance than that of SI engines when the engine operating condition is changed. Additionally, the stability times T_s of HCCI are all

equal to or shorter than SI, despite there being no direct control approach for HCCI combustion.

4. Compared with SI combustion, the peak pressure and MFB50 location fluctuation of HCCI combustion is much smaller. For HCCI combustion, the fluctuation amplitude of peak pressure and MFB50 locations before HCCI stability timing are similar to the fluctuation amplitude after the HCCI stability timing.

The HCCI combustion is a continuous cycle-based self-tuning process; the combustion performance of the current engine cycle is affected by the preceding engine cycle and will affect the following engine cycle. Therefore, it is able to consider the in-cylinder conditions as cycle-based continuous control signals. As one of the most important features of HCCI combustion, the summarized findings are useful to the DoE of HCCI engine multi-objective optimal feedback control.

8.2 Future Work

The research presented in this thesis is a preliminary exploration of a new EPSRC funded project “New Control Methodology for the Next Generation of Engine Management Systems (EP/J00930X/1)”. Further work will be done based on my research for this project in the future. The author has outlined some recommendations for future work as follows:

Steady status multi-objective engine optimisation control:

1. For engine modelling to be used for accurate control, it is required to have a more accurate combustion model and guarantee the simulation time consumption can be kept in a very low standard meanwhile. This is because the success of model-based engine optimal control has close association with model accuracy. As one of the potential solutions, it is able to utilize the multi-objective optimal feedback EA strategy to optimal the coefficients of curve-fitting functions which are used to develop the combustion model or emissions model in the future.
2. It is required to further reduce the number of experimental data group which are used for engine model development. Meanwhile, the multi-objective optimal feedback control performance should be kept in a good status. The less the experimental data are needed, the better control efficiency is achieved.
3. It will be critical to implement the hardware in-the-loop control of the multi-objective optimal feedback controller in the real engine test bench by dSPACE, and test the controller performance in order to optimise and implemented the control strategy.
4. It is useful to prove the HCCI self-stabilisation behaviour mathematically, which will need to find a way to descript the HCCI engine process by a mathematical function at the first. And it will possible to utilized the control theory and mathematical way, such as Lyapunov approach, to prove the HCCI self-stabilisation behaviour.
5. The HCCI self-stabilisation behaviour can be used to further optimise the HCCI engine multi-objective optimal feedback control system, through the DoE process.

Transient status multi-objective engine optimisation control:

1. For model-based transient control strategy development and tests, it is essential to develop an engine model which can simulate the transient process with acceptable accuracy. The experimental tests and model verification is needed by then.
2. As long as the transient model have been developed, it is possible to combine the developed steady status engine model and the transient status engine model. The new engine model will be able to simulate the engine operation both in steady status and transient status. The NEDC cycle based MOEA controller will be tested off-line and on-line HIL simulation.
3. In order for validating the new personalized control strategy, it is needed to spent some time on DoE to test more types of driving cycles rather than NEDC cycle. The controller should be able to continually being updated and optimise the engine performances with different driving cycles.
4. A new MOEA will be developed for this project to let the controller has the best performances.
5. Practical on-line evaluation of the whole control strategy will be tested on a new engine test bed in the University of Birmingham by RCP. The controller model will be uploaded to dSPACE control system to validate the controller in different driving cycles and environmental conditions. The time consumption of optimisation process for one particular driving cycle type should be very short compared with traditional calibration approaches.

Appendix

The Main Modelling Codes of PM emissions from SI Engine.

```
%Build the 5-dimensional grid
[IVO1,EVC1,SparkTiming1,InjTiming1,ThrottleAngle1]=ndgrid(695:30:755,715:30
:775,15:5:25,250:50:350,10:5:15);

%Table of PMN
PMN(:,:,1,1,1)=[1543968.81371353,1317886.24554622,349811.69997191;1460518.9
0880319,1023324.69846821,796211.59020202;1807247.39915642,1408432.86244041,
1070177.17680357];
PMN(:,:,2,1,1)=[3305411.95648253,1138542.66975718,402358.391413238;2739083.
7569392,2054344.77002068,929459.569047618;1388343.00663309,1813500.8601005,
1361690.29241026];
PMN(:,:,3,1,1)=[2158459.27411957,2862242.38096154,624638.289723404;3261487.
00321637,2690749.49175573,3880689.82930175;3887708.76146268,4161326.5402167
2,2377888.01298137];
PMN(:,:,1,2,1)=[632806.017548543,813598.949611994,152711.387784783;528568.8
94958402,615115.808687846,529110.645;365119.380886599,395824.021346154,1663
58.94997153];
PMN(:,:,2,2,1)=[871881.835949368,448703.998286445,163558.680689223;400564.7
10586011,456074.045167464,294565.126464187;231182.44639201,401826.455857988
,153597.165685792];
PM(:,:,3,2,1)=[556455.979132791,776624.954444445,129433.084031746;427857.02
8918919,448983.662444444,221769.935115596;202424.971364161,433247.468407643
,433247.468407643];
PMN(:,:,1,3,1)=[53048783.5408654,24036553.565097,2852934.64047619;31628001.
2739496,34789005.719084,12172150.8882667;20249538.157424,21761914.0896328,1
0944415.0666667];
PMN(:,:,2,3,1)=[43339690.4420063,23471020.0338028,3404740.2281768;28248904.
4061625,27143487.2299578,15536316.4174757;19713536.3359788,20353167.5326877
,14376876.0823389];
PMN(:,:,3,3,1)=[38248475.6987448,24089688.0841424,3119339.7458891;38054490.
7768116,37582302.0162933,20842269.7198582;25653340.4423077,30350582.352,181
18581.5570248];
PMN(:,:,1,1,2)=[3873276.60884354,3811975.33245614,1591801.48488608;2157715.
33754941,2449585.4771223,2262137.91697733;2488862.34987539,2651473.69156334
,2835157.59898462];
PMN(:,:,2,1,2)=[3712731.61814815,3517560.3042654,1322702.15399003;3276392.9
6242236,3724418.70439024,1557770.14131222;3503387.73383562,4664143.96390041
,2759375.82233129];
PMN(:,:,3,1,2)=[3539816.69931507,4413634.88423913,1461797.49256262;2422083.
55746032,3486901.69769231,2908667.71648718;2652884.9145,3205719.91479401,36
13354.09041523];
PMN(:,:,1,2,2)=[1072942.41608856,1581557.34284153,2920101.070378;3051848.13
564132,991759.540064103,442776.896666667;1409731.35748744,451812.239440299,
192284.847662429];
```

```
PMN(:,:,2,2,2)=[854789.082969697,1065790.10490521,447970.065277045;606536.2
32093023,725874.318949275,1216831.96380841;1462222.70619529,448954.06311653
1,345723.823231198];
PMN(:,:,3,2,2)=[1048583.75409253,1732405.01473088,1356117.27908537;740481.6
62418605,773251.119873949,5121186.14808602;2368491.36476793,1227875.3342732
6,4781238.27020642];
PMN(:,:,1,3,2)=[64496836.6925859,46861427.6300813,10400128.0683938;56765396
.9303571,58559738.8239278,39501404.0679095;41199229.7119114,39095417.943847
7,14954206.6535185];
PMN(:,:,2,3,2)=[56396269.7284483,46507781.6305419,11510225.5693498;50384679
.7075472,57861245.7225434,37793444.3407407;38430215.1904762,39184485.406040
3,22896923.8689139];
PMN(:,:,3,3,2)=[76982918.1489362,87344063.6130178,12388117.8855263;64585726
.2434457,86058126.7606557,37960113.0223048;44126097.320132,41370858.2146119
,25419514.7985866];

%Table of PMM
PMM(:,:,1,1,1)=[0.000597680500425532,0.000432406980518934,0.000624311135830
986;0.000470175716053333,0.000338751369304348,0.000199488292532389;0.000293
15121457423,0.000200603908212987,0.000088674340495524 4];
PMM(:,:,2,1,1)=[0.00163984260588036,0.000501561315752213,0.0003682617796580
13;0.00114791131786989,0.000907685717184265,0.000299077428408488;0.00023559
813115625,0.00029281967968262,0.000153243516956309];
PMM(:,:,3,1,1)=[0.00128410999869423,0.00147317209667736,0.00261071575986567
;0.0016022329297654,0.00875017637984694,0.00128798813549313;0.0006151673047
92793,0.000706939414456522,0.001307442810591 9];
PMM(:,:,1,2,1)=[0.00236769750266129,0.000627809750547704,0.0009156427793289
75;0.000469353028899999,0.000560112142946058,0.000360646943520694;0.0002478
84183695563,0.00043626708593068,0.000120398939767857];
PMM(:,:,2,2,1)=[0.00081247325606599,0.000443727844282051,0.0004601973569346
73;0.000421130267935606,0.000563684888776979,0.000144809954324138;0.0282298
735031399,0.000418823510671937,0.000114416466671233];
PMM(:,:,3,2,1)=[0.000156252330339674,0.000593605307202479,0.000324754800478
088;0.000100822826091525,0.000484767420804795,0.000355900818308824;0.000794
482395771188,0.000575408500607028,0.00068];
PMM(:,:,1,3,1)=[0.0368466842262334,0.0131011427059639,0.00155456161813842;0
.0304399537239057,0.0315108013119266,0.00509303556925134;0.0215312297634409
,0.0189186444122162,0.00312871794148607];
PMM(:,:,2,3,1)=[0.0690758832798742,0.0144911643497175,0.00211084118168975;0
.0640528014101124,0.0598995182177589,0.00794836864415584;0.0471510865198939
,0.0493942613325243,0.00529637941674642];
PMM(:,:,3,3,1)=[0.0302195103907563,0.0183396062529221,0.00127598252764368;0
.0568577733517442,0.0623180085510204,0.0153660418758523;0.0491112863629344,
0.051921544480962,0.0146787141473029];
PMM(:,:,1,1,2)=[0.00367043577730376,0.0021139300729912,0.00620905316522843;
0.000393422806015873,0.000497908212924188,0.00337141167820707;0.00034178347
6176875,0.000404235637072973,0.0012038988658642];
PMM(:,:,2,1,2)=[0.000385595249702602,0.000345246118647619,0.003278114253925
;0.000350541353218069,0.000760645449568627,0.00203060121345455;0.0005038870
40771167,0.00062283428433195,0.000839631929264616];
PMM(:,:,3,1,2)=[0.00174990020590389,0.0065738774792643,0.00200161736297297;
0.0010294029063535,0.00238108770489985,0.0105195629944216;0.000369110460623
656,0.000518097555417293,0.000443135670770833];
PMM(:,:,1,2,2)=[0.00128927162683333,0.00309843737356712,0.0354698001886207;
0.00730058648971591,0.00131820280599679,0.00166309719322266;0.0004077027620
65491,0.000464832010561798,0.000250603427752475];
PMM(:,:,2,2,2)=[0.00394470865597297,0.00394470865597297,0.00217408856428572
;0.000744848267372093,0.000443451200098182,0.00132197810716628;0.0002399971
57695946,0.000124731534815217,0.000346045642234637];
```

```
PMM(:,:,3,2,2)=[0.00334729100172727,0.00334729100172727,0.00451917361308232
;0.0000523233033084112,0.0000744855630506329,0.0000634;0.000174966876183932
,0.000143907896329446,0.000159437];
PMM(:,:,1,3,2)=[0.123845175155797,0.00712942418553971,0.00808243578701298;0
.131422236100179,0.168655068412429,0.0402775273093333;0.101320413394444,0.1
00247316573669,0.00830783963951762];
PMM(:,:,2,3,2)=[0.0805192713203463,0.0539569292574258,0.00935046584192546;0
.0885144087488152,0.108190935942029,0.0726382280185874;0.0707584500440368,0
.0767835954949495,0.0303516146804511];
PMM(:,:,3,3,2)=[0.202227686219512,0.248719885402844,0.0115911047927393;0.15
3149124473684,0.265724839572369,0.106574805518657;0.091500626,0.08806069672
01835,0.0349487851134752];
```

References

Abido, M. A. (2003). "A niched Pareto genetic algorithm for multiobjective environmental/economic dispatch." International Journal of Electrical Power & Energy Systems 25(2): 97-105.

AVL. (2012). "AVL CAMEO™." from https://www.avl.com/cameo. Last access: 06.06.2013.

BOSCH, R. (2006). Gasoline-Engine Management, Robert Bosch GmbH; 3 Updated edition (1 Sep 2006),ISBN:978-0837613901.

Cambustion, L. o. (2011). "DMS500 Fast Particulate Spectrometer with Heated Sample Line High Ratio Diluter User Manual." User Manual.

Catania, A. E., D. Misul, A. Mittica and E. Spessa (2003). "A refined two-zone heat release model for combustion analysis in SI engines." Jsme International Journal Series B-Fluids And Thermal Engineering 46(1): 75-85,DOI: Doi 10.1299/Jsmeb.46.75.

Chang, K., A. Babajimopoulos, G. A. Lavoie, Z. S. Filipi and D. N. Assanis (2006). "Analysis of Load and Speed Transitions in an HCCI Engine Using 1-D Cycle Simulation and Thermal Networks." SAE Paper 2006-01-1087.

Chankong, V. and Y. Y. Haimes (1983). Multiobjective Decision Making Theory and Methodology, Dover Publications (February 4, 2008),ISBN:0486462897.

Chiang, C.-J. and A. G. Stefanopoulou (2007). "Stability Analysis in Homogeneous Charge Compression Ignition (HCCI) Engines With High Dilution." IEEE Transactions on Control Systems Technology 15(2): 209 - 219

Chiang, C. J. and A. G. Stefanopoulou (2004). Steady-state multiplicity and stability of thermal equilibria in homogeneous charge compression ignition (HCCI) engines. 43rd IEEE Conference on Decision and Control, 2004. CDC., MI, USA, 0-7803-8682-5, 1676 - 1681 Vol.1672.

Choi, Y. and J.-Y. Chen (2005). "Fast prediction of start-of-combustion in HCCI with combined artificial neural networks and ignition delay model." Proceedings of the Combustion Institute 30: 2711-2718.

Corne, D. W., J. D. Knowles and M. J. Oates (2000,Last access date:06.06.2013). The Pareto Envelope-Based Selection Algorithm for Multiobjective Optimization. from http://www.macs.hw.ac.uk/~dwcorne/pesa.pdf.

Deb, K. and T. Goel (2001). "Controlled Elitist Non-dominated Sorting Genetic Algorithms for Better Convergence." Evolutionary Multi-Criterion Optimization Lecture Notes in Computer Science 1993, 2001: 67-81.

Deb, K., A. Pratap, S. Agarwal and T. Meyarivan (2002). "A fast and elitist multiobjective genetic algorithm: NSGA-II." Ieee Transactions on Evolutionary Computation 6(2): 182-197,DOI: Doi 10.1109/4235.996017.

Dorf, R. C. and R. H. Bishop (2001). Modern Control Systems, Prentice Hall; 9 edition (3 Aug 2000),ISBN:0130306606.

Embouazza, M., D. Haworth and N. Darabiha (2002). "Implementation of Detailed Chemical Mechanisms into Multidimensional CFD Using in situ Adaptive Tabulation: Application to HCCI Engines." SAE Paper 2002-01-2773.

Embouazza, M., D. C. Haworth and N. Darabiha (2002). "Implementation of Detailed Chemical Mechanisms into Multidimensional CFD Using in situ Adaptive Tabulation: Application to HCCI Engines." SAE Paper 2002-01-2773.

ETAS. (2012). "INCA Software Products." from http://www.etas.com/en/products/inca_software_products.php. Last access: 06.06.2013.

FEV. (2012). "TOPexpert." from http://www.fev.com/what-we-do/methods-tools-and-products/calibration-methods-topexpert/. Last access: 06.06.2013.

Fiveland, S. and D. Assanis (2001). "Development of a two-zone HCCI combustion model accounting for boundary layer effects." SAE paper 2001-01-1028.

Flowers, D. L., S. M. Aceves, J. Martinez-Frias and R. W. Dibble (2002). "Prediction of carbon monoxide and hydrocarbon emissions in iso-octane HCCI engine combustion using multizone simulations." Proceedings Of the Combustion Institute 29: 687-694,DOI: Doi 10.1016/S1540-7489(02)80088-8.

Fonseca, C. M. and P. J. Fleming (1993). Genetic Algorithms for Multiobjective Optimization - Formulation, Discussion And Generalization. Proceedings Of the Fifth International Conference on Genetic Algorithms, San Mateo, 416-423.

Fonsecay, C. M. and P. J. Flemingz (1993). Genetic Algorithms for Multiobjective Optimization: Formulation, Discussion and Generalization. Genetic Algorithms: Proceedings of the Fifth International Conference.

Ghojel, J. I. (2010). "Review of the development and applications of the Wiebe function: a tribute to the contribution of Ivan Wiebe to engine research." International Journal Of Engine Research 11(4): 297-312,DOI: Doi 10.1243/14680874jer06510.

Gieré, R. and P. Stille (2004). Energy, waste and the environment : a geochemical perspective. London, Geological Society,ISBN:186239167X.

Guriaa, C., P. K. Bhattacharyab and S. K. Guptab (2005). "Multi-objective optimization of reverse osmosis desalination units using different adaptations of the non-dominated sorting genetic algorithm (NSGA)." Computers & Chemical Engineering 29(9).

Gurney, A., H. Ahammad and M. Ford (2009). "The economics of greenhouse gas mitigation: Insights from illustrative global abatement scenarios modelling." Energy Economics 31: S174-S186,DOI: DOI 10.1016/j.eneco.2009.08.016.

Heywood, J. B. (1988). Internal combustion engine fundamentals. McGraw-Hill series in mechanical engineering. New York, McGraw-Hill: xxix, 930 p., 932 p. of plates.

Hiroyasu, T., M. Miki, J. Kamiura and S. Watanabe (2002). "Multi-Objective Optimization of Diesel Engine Emissions and Fuel Economy using Genetic Algorithms and Phenomenological Model." SAE Paper 2002-01-2778.

Horn, J., N. Nafpliotis and D. E. Goldberg (1994). Multiobjective optimization using the niched pareto genetic algorithm. Proceeding of the 1st IEEE Conference on Computation, NJ, USA.

Horn, J., N. Nafpliotis and D. E. Goldberg (1994). A niched Pareto genetic algorithm for multiobjective optimization. Proceedings of the First IEEE Conference on Evolutionary Computation, NJ, USA.

International-Limited-of-China-Yuchai (2007,Last access date:06.06.2013). The common rail diesel engine calibration manual. from http://wenku.baidu.com/view/3241b6232f60ddccda38a014.html. Last access: 06.06.2013.

Ishibuchi, H. (1998). "A multi-objective genetic local search algorithm and its application to flowshop scheduling." Systems, Man, and Cybernetics, Part C: Applications and Reviews, IEEE Transactions 28(3).

Jasak, H., A. D. Gosman, J. Y. Luo, B. Kaludercic and etc. (1999). "Rapid CFD Simulation of Internal Combustion Engines." Retrieved 06.06.2013, from http://citeseerx.ist.psu.edu/viewdoc/download?doi=10.1.1.31.3240&rep=rep1&type=pdf.

Jia, M. and M. Z. Xie (2006). "A chemical kinetics model of iso-octane oxidation for HCCI engines." Fuel 85(17-18): 2593-2604,DOI: DOI 10.1016/j.fuel.2006.02.018.

Jia, N. (2007). HCCI Engine Modeling for Real-Time Implementation and Control Development. Ph.D, University of Liverpool, Liverpool.

Jia, N., J. Wang, K. Nuttall, J. Wei, H. Xu, M. L. Wyszynski, J. Qiao and M. J. Richardson (2007). "HCCI engine Modeling for real-time implementation and control development." Ieee-Asme Transactions on Mechatronics 12(6): 581-589,DOI: Doi 10.1109/Tmech.2007.910045.

Jurgen, R. K. (2004). Electronic engine control technologies. Warrendale, PA, Society of Automotive Engineers,ISBN:0768013399.

Karmiggelt, R. (1998). Mean value modelling of a S.I. engine, EUT, Department of Mechanical Engineering, Eindhoven University of Technology.

Kesgin, U. (2004). "Genetic algorithm and artificial neural network for engine optimisation of efficiency and NOx emission." Fuel 83(7-8): 885-895,DOI: DOI 10.1016/j.fuel.2003.10.025.

Kim, M., T. Hiroyasu, M. Miki and S. Watanabe (2004,Last access date:06.06.2013). SPEA2+: Improving the Performance of the Strength Pareto Evolutionary Algorithm 2. from http://mis.doshisha.ac.jp/academic/papers/pdf/04/200409_kim.pdf.

Kistler. (2007). "High-Temperature Pressure Sensor." from http://www.intertechnology.com/Kistler/pdfs/Pressure_Model_6052B1.pdf. Last access: 06.06.2013.

Knowles, J. D. and D. W. Corne (2000). "Approximating the Nondominated Front Using the Pareto Archived Evolution Strategy." Evolutionary Computation 8(2): 149-172,DOI: Doi 10.1162/106365600568167.

Kong, S. C. and R. D. Reitz (2002). "Application of detailed chemistry and CFD for predicting direct injection HCCI engine combustion and emissions." Proceedings Of the Combustion Institute 29: 663-669,DOI: Doi 10.1016/S1540-7489(02)80085-2.

Kong, S. C. and R. D. Reitz (2003). "Numerical study of premixed HCCI engine combustion and its sensitivity to computational mesh and model uncertainties." Combustion Theory And Modelling 7(2): 417-433,DOI: Doi 10.1088/1364-7830/7/2/312.

Kuriakose, S. and M. S. Shunmugam (2005). "Multi-objective optimization of wire-electro discharge machining process by Non-Dominated Sorting Genetic Algorithm." Journal of Materials Processing Technology 170(1-2): 133-141.

Lee, Y. H., J. I. Lee and H. C. No (2010). "A point model for the design of a sulfur trioxide decomposer for the SI cycle and comparison with a CFD model." International Journal Of Hydrogen Energy 35(11): 5210-5219,DOI: DOI 10.1016/j.ijhydene.2010.02.088.

Lei, D. and X. Yan (2009). "Evolutionary Multi-objective Optimization Algorithms and Its Application(BOOK)."

Li, Y. (2012). EXPERIMENTAL STUDY ON SPRAY AND COMBUSTION CHARACTERISTICS OF DIESEL-LIKE FUELS. Ph.D, University of Birmingham, Birmingham.

Lu, X. C., Y. T. Shen, Y. B. Zhang, X. X. Zhou, L. B. Ji, Z. Yang and Z. Huang (2011). "Controlled three-stage heat release of stratified charge compression ignition (SCCI) combustion with a two-stage primary reference fuel supply." Fuel 90(5): 2026-2038,DOI: DOI 10.1016/j.fuel.2011.01.026.

M.A. Abido (2006). Multiobjective Optimal VAR Dispatch Using Strength Pareto Evolutionary Algorithm. Evolutionary Computation 2006. CEC 2006. IEEE Congress, Vancouver, BC, 0-7803-9487-9, 730-736.

Ma, F. H., S. F. Ding, Y. Wang, Y. F. Wang, J. J. Wang and S. L. Zhao (2008). "Study on combustion behaviors and cycle-by-cycle variations in a turbocharged lean burn natural gas SI engine with hydrogen enrichment." International Journal Of Hydrogen Energy 33(23): 7245-7255,DOI: DOI 10.1016/j.ijhydene.2008.09.016.

Ma, F. H., Y. Wang, M. Y. Wang, H. Q. Liu, J. J. Wang, S. F. Ding and S. L. Zhao (2008). "Development and validation of a quasi-dimensional combustion model for SI engines fuelled by HCNG with variable hydrogen fractions." International Journal Of Hydrogen Energy 33(18): 4863-4875,DOI: DOI 10.1016/j.ijhydene.2008.06.068.

Ma, H., H.-M. Xu and J.-H. Wang (2011). "Real-time Control Oriented HCCI Engine Cycle-to-cycle Dynamic Modelling." International Journal of Automation and Computing: 317-325.

Malikopoulos, A. A., D. N. Assanis and P. Y. Papalambros (2008). "Optimal Engine Calibration for Individual Driving Styles." SAE Paper 2008-01-1367.

Malikopoulos, A. A., D. N. Assanis and P. Y. Papalambros (2008). "Optimal Engine Calibration for Individual Driving Styles." SAE Paper 2008-01-1367.

Malikopoulos, A. A., D. N. Assanis and P. Y. Papalambros (2009). "Real-Time Self-Learning Optimization of Diesel Engine Calibration." Journal Of Engineering for Gas Turbines And Power-Transactions Of the Asme 131(2),DOI: Doi 10.1115/1.3019331.

Malikopoulos, A. A., P. Y. Papalambros and D. N. Assanis (2008). "A learning algorithm for optimal internal combustion engine calibration in real time." Proceedings Of the Asme International Design Engineering Technical Conferences And Computers And Information In Engineering Conference 2007, Vol 6, Pts a And B: 91-100.

Mancaruso, E., S. S. Merola and B. M. Vaglieco (2008). "Study of the multi-injection combustion process in a transparent direct injection common rail diesel engine by

means of optical techniques." International Journal Of Engine Research 9(6): 483-498,DOI: Doi 10.1243/14680874jer01308.

Maricq, M. M., J. J. Szente and K. Jahr (2012). "The Impact of Ethanol Fuel Blends on PM Emissions from a Light-Duty GDI Vehicle." Aerosol Science And Technology 46(5): 576-583,DOI: Doi 10.1080/02786826.2011.648780.

Millo, F., L. Rolando and M. Andreata (2011). "Numerical Simulation for Vehicle Powertrain Development." Numerical Analysis - Theory and Application.

Misztal, J. W. (2008). Study of Homogeneous Charge Compression Ignition (HCCI) Combustion and Emission Characteristics in a Multi-cylinder Engine. Ph.D, University of Birmingham, Birmingham.

Murata, T., H. Ishibuchi and H. Tanaka (1996). "Multi-objective genetic algorithm and its applications to flowshop scheduling." Computers & Industrial Engineering 30(4): 957-968.

Najt, P. M. and D. E. Foster (1983). "Compression ignited homogeneous charge combustion." SAE Paper 830264,DOI: 10.4271/830264.

Obodeh, O. and C. I. Ajuwa (2008). "Calibration of Aging Diesel Engine with Artificial Neural Networks." European Journal of Scientific Research Vol.24: 520-531.

Perini, F., F. Paltrinieri and E. Mattarelli (2010). "A quasi-dimensional combustion model for performance and emissions of SI engines running on hydrogen-methane blends." International Journal Of Hydrogen Energy 35(10): 4687-4701,DOI: DOI 10.1016/j.ijhydene.2010.02.083.

Pfiffner, R., F. Weber, A. Amstutz and L. Guzzella (1997). Modeling and model-based control of supercharged SI-engines for cars with minimal fuel consumption. Proceedings Of the 1997 American Control Conference, 0743-1619, 304-308.

Potrzebowski, A., J. Misztal, H. M. Xu, M. L. Wyszynski and J. Qiao (2009). "An autoignition combustion model for homogeneous charge compression ignition engine cycle simulations." Proceedings Of the Institution Of Mechanical Engineers Part D-Journal Of Automobile Engineering 223(D9): 1207-1221,DOI: Doi 10.1243/09544070jauto1005.

PRABHAKAR, R., S. J. CITRON and R. E. GOODSON (1977 Jan 01). "Optimization of Automotive Engine Fuel Economy and Emissions." Transactions, Series G-Journal of Dynamic Systems, Measurement, and Control. 99: 109-117,DOI: 10.1115/1.3427082.

Qin, J., H. Xie, Y. Zhang and H. Zhao (2005). "A Combustion Heat Release Correlation for CAI Combustion Simulation in 4-Stroke Gasoline Engines." SAE Paper 2005-01-0183.
Ramos, J. I. (1989). Internal combustion engine modeling. New York, Hemisphere Pub. Corp.,ISBN:0891161570.

Rausen, D. J., A. G. Stefanopoulou, J.-M. Kang, J. A. Eng and T.-W. Kuo (2005). "A Mean-Value Model for Control of Homogeneous Charge Compression Ignition (HCCI) Engines." Journal of Dynamic Systems, Measurement, and Control.

Richard, S., S. Bougrine, G. Font, F. A. Lafossas and F. Le Berr (2009). "On the Reduction of a 3D CFD Combustion Model to Build a Physical 0D Model for Simulating Heat Release, Knock and Pollutants in SI Engines." Oil & Gas Science And Technology-Revue D Ifp Energies Nouvelles 64(3): 223-242,DOI: Doi 10.2516/Ogst/2008055.

Schaffer, J. D. (1984). (Ph.D Thesis) Some experiments in machine learning using vector evaluated genetic algorithms (artificial intelligence, optimization, adaptation, pattern recognition). Ph.D, Vanderbilt University Nashville, TN, USA ©1984.

Schaffer, J. D. (1985). Multiple objective optimization with vector evaluated genetic algorithms. 1st international Conference on Genetic Algorithms, Hillsdale, NJ, USA, 0-8058-0426-9, 93-100.

Schaffer, J. D. (1985). Some experiments in machine learning using vector evaluated genetic algorithms.

Schoning, L.-C. and Y. Li (2011). Review electromagnetic field ignition system for Internal Combustion Engine. 17th International Conference on Automation and Computing (ICAC), 2011 306 - 309.

Shahbakhti, M. and C. R. Koch (2007). Control Oriented Modeling of Combustion Phasing for an HCCI Engine. Proceedings of the 2007 American Control Conference, New York, NY, 1-4244-0988-8, 3694 - 3699.

Shaver, G. M. (2009). "Stability analysis of residual-affected HCCI using convex optimization." Control EngineeringPractice 5: 487-492.

Shaver, G. M., J. C. Gerdes, M. J. Roelle, P. A. Caton and C. F. Edwards (2005). "Dynamic modeling of residual-affected homogeneous charge compression ignition engines with variable valve actuation." Journal Of Dynamic Systems Measurement And Control-Transactions Of the Asme 127(3): 374-381,DOI: Doi 10.1115/1.1979511.

Shaver, G. M., J.Christian and G. P. Jain (2003). Modeling for Control of HCCI Engines. Proceedings of me American Control Conference 2003, CA, USA, 0743-1619, 749 - 754 vol.741.

Shaver, G. M., M. J. Roelle and J. C. Gerdes (2006). "Modeling cycle-to-cycle dynamics and mode transition in HCCI engines with variable valve actuation." Control Engineering Practice 14.

Srinivas, N. and K. Deb (1994). "Muiltiobjective optimization using nondominated sorting in genetic algorithms." Evolutionary Computation 2(3): 221-248.

Stiesch, G. (2003). Modeling engine spray and combustion processes. Berlin ; New York, Springer,ISBN:3540006826 (alk. paper).

Stone, R. (1999). Introduction to internal combustion engines. Warrendale, Pa., Society of Automotive Engineers,ISBN:0768004950.

Suzuki, T. (1997). The romance of engines. Warrendale, PA, Society of Automotive Engineers,ISBN:1560919116 (hc).

Tanaka, S., F. Ayala and J. C. Keck (2003). "A reduced chemical kinetic model for HCCI combustion of primary reference fuels in a rapid compression machine." Combustion And Flame 133(4): 467-481,DOI: Doi 10.1016/S0010-2180(03)00057-9.

Tian, G. (2007). Research on Transient Process of Gasoline Direct Injection HCCI Combustion. Ph.D, Tsinghua University, Beijing.

Vector. (2012). "CANape - Measuring, Calibrating, Diagnosing and Flashing ECUs." from http://www.vector.com/vi_canape_en.html. Last access: 06.06.2013.

Vossoughi, G. R. and S. Rezazadeh (2-5 Sept. 2005). Optimization of the calibration for an internal combustion engine management system using multi-objective genetic algorithms. 2005 Ieee Congress on Evolutionary Computation, Vols 1-3, Proceedings, 0-7803-9363-5, 1254 - 1261 Vol. 1252.

Watson, H. C., A. Das, X. Ni and H. G. Rosenkranz (1998). A quasi-dimensional model applied to 4-valves per cylinder combustion in SI engines. International Conference on Combustion Engines And Hybrid Vehicles, IMechE. 1998: 271-286.

Watson, N. and A. D. Pilley (1980). "A Combustion Correlation for Diesel Engine Simulation." SAE Paper 800029,DOI: 10.4271/800029.

Wiebe, I. I. (1962). "Progress in engine cycle analysis: Combustion rate and cycle processes." Mashgiz, Ural-Siberia Branch.

Wikipedia. (2012). "European emission standards." from http://en.wikipedia.org/wiki/European_emission_standards. Last access: 06.06.2013.

Wilson, T. S., H. M. Xu, S. Richardson, M. L. Wyszynski and T. Megaritis (2006). "Optical study of flow and combustion in an HCCI engine with negative valve overlap." Journal of Physics 45: 94-103,DOI: Doi 10.1088/1742-6596/45/1/013.

Woollenweber, W. and E. Halimi (2000). Two-stage supercharging systems for internal combustion engines. US Patent 6,079,211.

Wu, B., R. G. Prucka and Z. S. Filipi (2006). "Cam-phasing Optimization Using Artificial Neural Networks as Surrogate Models-Fuel Consumption " SAE Paper 2006-01-1512.

Xie, H., J. Qin, Y. Zhang, H. Zhu and H. Zhao (2004). "A Combustion Correlation for CAI Combustion and Its Application to CAI Engine Simulation." Journal of Combustion Science and Technology Vol. 10 No. 6.

Xu, H., J. Wang and X. Yao. (2012). "Research Proposal of New Control Methodology for the Next Generation of Engine Management Systems." from http://gow.epsrc.ac.uk/NGBOViewGrant.aspx?GrantRef=EP/J00930X/1. Last access: 06.06.2013.

Yasar, H., H. S. Soyhan, H. Walmsley, B. Head and C. Sorusbay (2008). "Double-Wiebe function: An approach for single-zone HCCI engine modeling." Applied Thermal Engineering 28: 1284–1290.

Zhao, F. (2003). Homogeneous charge compression ignition (HCCI) engines : key research and development issues. Warrendale, PA, Society of Automotive Engineers,ISBN:076801123X.

Zitzler, E., M. Laumanns and L. Thiele (2001,Last access date:06.06.2013). SPEA2: Improving the strength Pareto evolutionary algorithm. from http://www.kddresearch.org/Courses/Spring-2007/CIS830/Handouts/P8.pdf.

Zitzler, E. and L. Thiele (1998). An evolutionary algorithm for multiobjective optimization: The strength pareto approach.

Zitzler, E. and L. Thiele (1999). "Multiobjective evolutionary algorithms: A comparative case study and the Strength Pareto approach." Ieee Transactions on Evolutionary Computation 3(4): 257-271,DOI: Doi 10.1109/4235.797969.